Absolute and Relative Orbit Determination for Satellite Constellations

Mao, Xinyuan

DOI
10.4233/uuid:37157458-338d-4aa9-98df-f0c32470d5d3

Publication date
2019

Document Version
Final published version

Citation (APA)
Mao, X. (2019). *Absolute and Relative Orbit Determination for Satellite Constellations*. [Dissertation (TU Delft), Delft University of Technology]. https://doi.org/10.4233/uuid:37157458-338d-4aa9-98df-f0c32470d5d3

Important note
To cite this publication, please use the final published version (if applicable).
Please check the document version above.

Absolute and Relative Orbit Determination for Satellite Constellations | Xinyuan MAO

Absolute and Relative Orbit Determination for Satellite Constellations

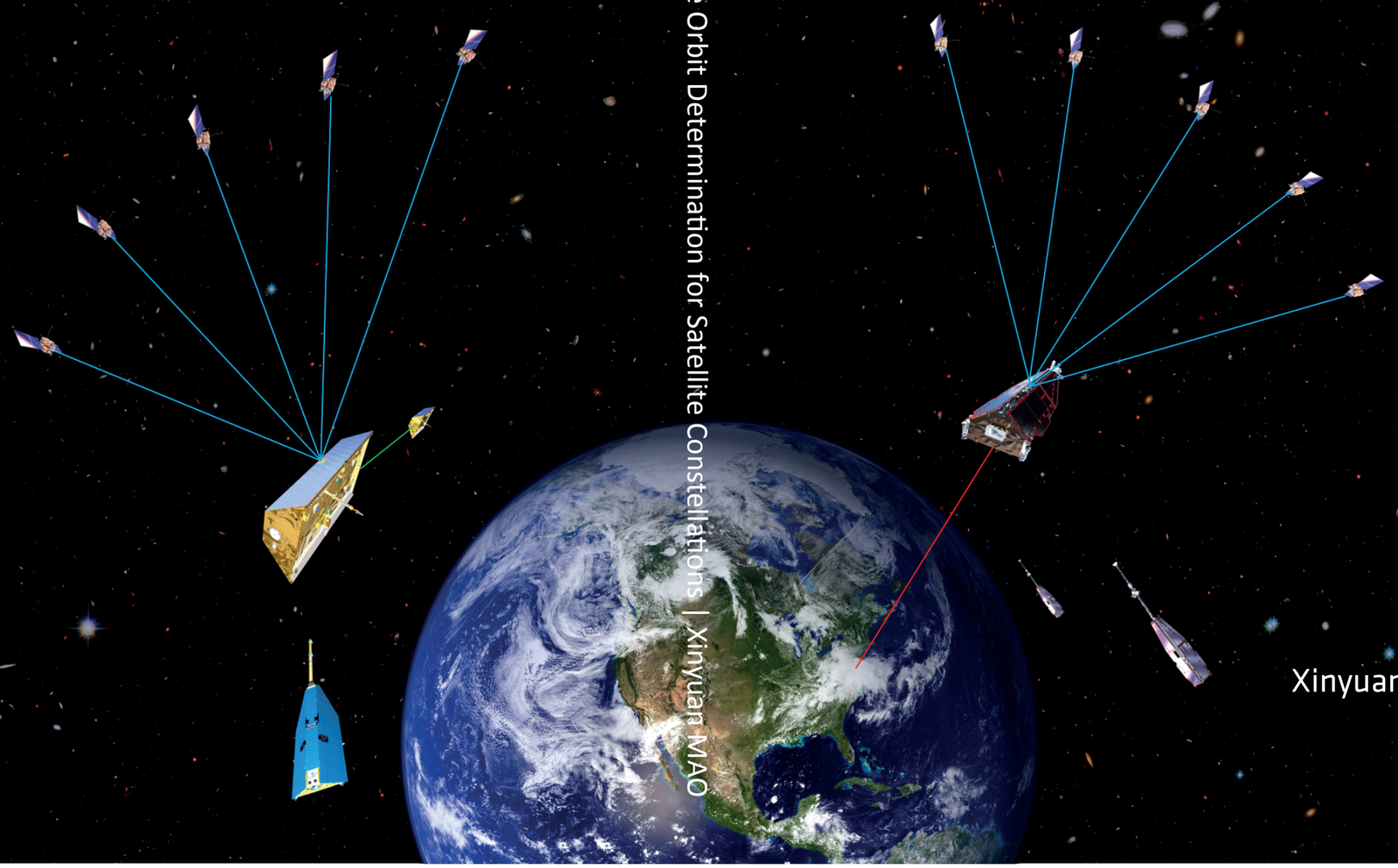

Xinyuan MAO

Invitation

You are cordially invited to attend the public defense of my PhD dissertation entitled

Absolute and Relative Orbit Determination for Satellite Constellations

On **Monday, 3rd of June, 2019** in the Science Centre Delft, Mijnbouwstraat 120, 2628 RX Delft

14:30 PM
Brief presentation

15:00 PM
Défense

16:30 PM
Reception

You are also welcomed to the party that will take place at **20:00** pm in

Boterhuis café, Markt 15-17a, 2611 GP Delft

Xinyuan MAO

531387-L-os-Mao

Processed on: 17-5-2019

Absolute and Relative
Orbit Determination for Satellite Constellations

Absolute and Relative
Orbit Determination for Satellite Constellations

Dissertation

for the purpose of obtaining the degree of doctor
at Delft University of Technology
by the authority of the Rector Magnificus prof. dr. ir. T. H. J. J. van der Hagen
chair of the Board for Doctorates
to be defended publicly on
Monday 3 June 2019 at 15:00 o'clock

by

Xinyuan MAO

Master of Engineering in Aeronautical & Astronautical Science & Technology
Beijing Institute of Technology, China
born in Zhumadian, China

This dissertation has been approved by the promotors:

Promotor: Prof. dr. ir. P. N. A. M. Visser
Copromotor: Dr. ir. J. van den IJssel

Composition of the doctoral committee:

Rector Magnificus,	chairperson
Prof. dr. ir. P. N. A. M. Visser	Delft University of Technology
Dr. ir. J. van den IJssel	Delft University of Technology

Independent members:

Prof. dr. E. K. A. Gill	Delft University of Technology
Prof. dr. ir. A. J. van der Veen	Delft University of Technology
Prof. dr. U. Hugentobler	Technical University of Munich, Germany
Dr. O. Montenbruck	German Aerospace Center, Germany
Dr. P. Willis	Institut national de l'information geographique et forestiere Institut de physique du globe de Paris, France
Prof. dr. L. L. A. Vermeersen	Delft University of Technology, reserve member

The realization of the dissertation was partially sponsored by The China Scholarship Council.

Keywords: Satellite Constellation; Antenna Pattern; GPS; Precise Orbit Determination; Precise Baseline Determination

Printed by: Ipskamp Printing

Cover by: Designed by Feifei Song, image credits: NASA, ESA/ATG medialab, GFZ, CSR.

ISBN 978-94-028-1555-9

An electronic version of this dissertation is available at
http://repository.tudelft.nl/.

Preface

Five years of my life fly just like low earth orbiters. It seems like they are close enough for you to grab, however you can never capture and hold. The best option is staying remotely and computing their precise orbits, then you will be amazed by the happiness of knowing the coordinates of satellites, and more importantly, the steps of your life. At this best moment of rendezvous and docking with my doctorate, I would like to say thanks to many of my "giant shoulders".

First and foremost, my sincerest appreciation goes to my promotor, Prof. Pieter Visser, for offering me an opportunity to pursue a PhD at TU Delft. We have had meetings on a weekly basis all through my PhD project. You have always been so kind to guide me, motivate me, and encourage me. Without your supervision, this dissertation would not have been completed at all. The largest asset that I obtained in The Netherlands is the attitude towards research and life, apparently it has been greatly influenced by you. I think I will benefit from it in the rest of my life. My special gratitude extends to my copromotor Dr. Jose van den IJssel. You taught me to be critical about research and keep an open eyesight about the state-of-the-art development in the field of orbit determination. Thank you so much for your efforts and support!

I would also express my appreciation to Prof. Boudewijn Ambrosius, who is retired and was my promotor in the first year. You still come to office once in a while. I really enjoy every conversation with you, particularly the mindful thoughts that I learned from you. Moreover, I want to say many thanks to Relly van Wingaarden. When I first arrived at Delft, shocks came from many aspects such as culture, language, and even food. However, you have been the one to bridge everything.

TU Delft is a great platform providing me opportunities of communicating with the "big guys" in this field. I would like to thank Dr. Oliver Montenbruck from the German Aerospace Center and Prof. Adrian Jäggi from the University of Bern, for sharing your research experience, ideas and orbit products with me. Besides, I gained so much from the conversations and email communications with Dr. Daniel Arnold, Dr. Stefan Hackel and Dr. Gerardo Allende-Alba, wish you all the best with your career! I also want to thank Dr. Jian Guo and Le Ren for many fruitful discussions!

I did some education-related work in the past years and I enjoyed these quite much. Thank you, Ernst, Wouter, Pieter, Jose, Erwin, Hans, Marc and Prem for giving me these opportunities. Ernst, also thanks for reading and helping to improve this dissertation. Our section, Astrodynamics and Space missions, is a warm and comfortable place to do research. Ron, Leonid, Francesco, Bert, Daphne, Bernhard, Imke, Eelco, Joao, Kevin, Stéphanie, Jeannette, Wim, Elisabetta, Yanli, Vidhya, Kartik, Löic, Marcel and Asrul, thank you for inspiring me through many of your thoughts about research and life.

In our faculty, the most wonderful place must be the student-run bar De Atmosfeer. At this place I Cheers! Ganbei! Proost! Prost! Santé! Salud! Salute! Saúde! with so many PhD students in our section. Jinglang, Hermes, Tatiana, Bart, Dominic, Haiyang, Zheng, Svenja, we enjoyed so much in space bar and we finally progressed to the moments of finishing our PhDs! More importantly, my sincere blessing also goes to Jacco, Tim, Günther, Teresa, Bas, Yuxin, Gourav, Marc and Jesse, I wish you all the best with your PhD progress! Special thanks to Tim, you were so kind to help me translating the summary into Dutch.

Although we often lost the beer drinking competitions between the 9th floor (our section) and 8th floor (section Space Systems Engineering), I still want to say thanks to our funny and interesting competitors. They are Eberhard, Mariëlle, Debby, Prem, Minghe, Zixuan, Linyu, Marsil, Adolfo, Dadui, Johan, Dennis, Fiona, Angelo and Mario. Many thanks!

My life in The Netherlands will never be so enjoyable without my close friends. Special thanks to the other four members of our band "Little Apple", Yongjia, Li, Zhijie and Yu. The diamond we won is still on my wedding ring! Zhijie and Yu, Li and Yixin, Long and Mengting, hold your hands forever! Qile and Dong, hope we can still enjoy many night-long fun in Shanghai!

Wanrong, thanks for the fresh berries and cool beers in your beautiful garden! Xiali, it was really nice experience tasting tea with you. Xiaoyu, Ke, Hao, Ping, Zhou, Haiqiang, Qingqing, Zi, Jia, Feijia, Yanqing, Anqi, Jingtang, Xiang and Yueting, you already started your new careers, I wish you all the best in making progress! Zhi, Wenbin, Ying and Xiao, I am looking forward to seeing your bright future! Shaokang, thanks for many fancy beer pictures!

People sometimes call me "Space Brewer" since I often brew my own beers and post articles about beers. The best reason can be attributed to our "Doctor Beer" group, which now consists of 16 members from all around the world. Chang, Li, Yongjia, I really enjoyed the experience of brewing different beer recipes with you! Lu, thanks for many wonderful beer trips in Beijing! Lizi, take care of your cute Hugo and always get better beers! Zhongyuan, thanks for many interesting discussions about politics! Xiao, please use your fancy potatoes in beer brewing, and Yongran, probably you can introduce tomatoes! Lijing, thank you for bringing beers from America and wish everything goes well with your PhD. Wei, congrats to be the first "Professor Beer" in our group! Thanks for many night-long talks with you whenever you flew back to The Netherlands, wish you and your "big and to-be-bigger" family all the best!

I also want to express my deep gratitude to friends who shared many unforgettable moments with me in ACSSNL-Delft. Qingyu Meng, YiWei Wang and Xiaoxiao Cheng, my sincere appreciation for so much help to Feifei and me! Jiakun, I enjoyed so many unforgettable moments with you, take care of Xiaoyan and Kanyun and enjoy your family life! Xuliang, Dichao, Wenjing, Zhe, Lizuo, Tianqi and Chenjie, wish you enjoy your new positions. Jiao, Fei, Ding, Chulin, Zhi, Yanbo and Jinyu, good luck with your future!

Everyone has a root, that is family. Thank you, my dear family, you have given such great patience, firm encouragement and endless love to me. I will use a better

me as a response to all of these. I love you all.

Ultimately, the person who stands behind me and supports my life is my beloved wife Feifei. No matter what happened to me in the past 10 years, from a weak me laying on the hospital bed to a strong me standing on the top of mountains, from a fragile me struggling with research to a motivated me striving for our bright future, she has always been there with warm smiles. This year you give me the best award for all my endeavours, our angel daughter, Songsong. The moment when I first heard her heart beating, my attitude towards life and everything was completely reshaped. That is the power of a new life, I never experienced this before however it simply feels like you locate the origin of gravity. I can not simply say thanks to you, I will use the rest of my life to prove a good husband and father. I love you!

Xinyuan MAO
Delft, January 2019

Summary

Precise absolute and relative orbit determination, referred to as Precise Orbit Determination (POD) and Precise Baseline Determination (PBD), are a prerequisite for the success of many Low Earth Orbit (LEO) satellite missions. With the spaceborne, high-quality, multi-channel, dual-frequency Global Positioning System (GPS) receivers, typically a precision of the order of a few cm is possible for single-satellite POD, and of a few mm for dual-satellite PBD of formation flying spacecraft with baselines up to hundreds of km. The research in this dissertation addresses and expands methods for computing reliable orbits for not only stable satellite formations such as the US/German GRACE (Gravity Recovery And Climate Experiment) and lower pair of the European Space Agency (ESA) Swarm missions, but also for satellite constellations that include rapidly varying baselines, such as all three Swarm satellites or the combination of the German CHAllenging Minisatellite Payload (CHAMP) and GRACE missions. The POD and PBD solutions are based on an Iterative Extended Kalman Filter (IEKF) that is capable of using relative spacecraft dynamics constraints for enhancing the robustness of the solutions. Moreover, the IEKF allows to iteratively fix the Double-Differenced (DD) carrier-phase integer ambiguities by the Least-squares AMBiguity Decorrelation Adjustment (LAMBDA) method. A subset fixing strategy allowing for partial ambiguity resolution was used instead of the full-set fixing which only accepts ambiguities when all integer ambiguities were fixed for certain epochs. The nominal products of the IEKF are reduced-dynamic POD and PBD solutions, but also include the possibility to derive kinematic PBD solutions afterwards. The internal consistency of the reduced-dynamic and kinematic solutions is used as a quality measure in addition to comparisons with POD and PBD solutions by other institutes.

The IEKF implementation used for the research described in this dissertation is capable of running in single-, dual-, and triple-satellite POD and PBD modes. The CHAMP single-satellite mission, the GRACE twin-satellite mission and the Swarm triple-identical-satellite mission were selected as test beds.

For LEO satellite GPS receivers, often a-priori Phase Center Variation (PCV) maps are obtained by pre-launch ground campaigns. However, it was found that in-flight frequency-dependent antenna calibration leads to superior PCV maps and thus tracking measurement corrections. A further improvement is obtained by including so-called Code Residual Variation (CRV) maps in absolute/Undifferenced (UD) POD and relative/DD PBD schemes. Orbit solutions have been produced for the CHAMP, GRACE and Swarm satellites for different test periods, allowing to evaluate the impact of using the in-flight PCV and CRV maps on POD and PBD precision. For the GRACE mission flying in tandem formation with a baseline length of around 220 km, computation for four months (August-November 2014) of orbits and baselines proved that CRV maps led to a significantly better initialization of the DD

carrier phase ambiguity fixing. The maps resulted also in a better consistency between kinematic and reduced-dynamic orbit solutions for especially the cross-track direction. The application of both PCV and CRV maps led to a slightly better consistency with independent Satellite Laser Ranging (SLR) and K-Band Ranging (KBR) low-low satellite-to-satellite tracking observations. The consistency improvements were largest for GRACE-B, where a *cross-talk* between the GPS main antenna and the occultation antenna yielded higher systematic observation residuals. This unfavorable influence of antenna *cross-talk* could be well compensated by CRV maps.

The three identical Swarm satellites have experienced a number of GPS receiver modifications and a GPS Receiver Independent Exchange Format (RINEX) converter update from October 2014 to August 2016. Moreover, the on-board GPS receiver performance was influenced by different levels of ionospheric scintillations. The impact of these factors was assessed for PBD of the pendulum formation flying Swarm-A and -C satellites with a varying baseline length between about 30 and 180 km. In total 30 months of data - from 15 July 2014 to the end of 2016 - were analyzed. The assessment included analysis of observation residuals, success rate of GPS carrier-phase integer ambiguity fixing, a consistency check between the kinematic and reduced-dynamic baseline solutions, and validations of orbits by comparing with SLR measurements. External baseline solutions from The German Space Operations Center (GSOC/DLR) and Astronomisches Institut - Universität Bern (AIUB) were also included in the comparisons. Results indicated that the GPS receiver modifications and RINEX converter update were effective to improve the baseline determination. Further improvement could be obtained when the half-cycle integer ambiguities (present in the original release of GPS RINEX data) were corrected to full-cycles and the RINEX converter was updated as well. Eventually, a consistency level of 9.3/4.9/3.0 mm between kinematic and reduced-dynamic baselines was possible in the radial/along-track/cross-track directions. On average 98.3% of the epochs had kinematic solutions. Moreover, consistency between solutions from this research and external reduced-dynamic baseline solutions was at a level of 1 mm in all directions when the same set of data was used.

A more challenging PBD occurs when baselines between two satellites change rapidly, which is the case when adding the third Swarm satellite B. This results in two so-called high-dynamic baselines, namely for the Swarm-B/A and Swarm-B/C satellite pair combinations. Swarm-B flies in a higher orbit, causing its orbital plane to slowly rotate with respect to those of Swarm-A and -C. This special geometry results in short periods when the Swarm-B satellite orbital plane is adjacent to the orbital planes of the other Swarm satellites. Ten 24-hr periods around such close encounters were selected for which the baseline lengths varied between 50 and 3500 km. Results showed that resolving the issue of half-cycle carrier-phase integer ambiguities and reducing the code observation noise by the converter update improved the consistency of kinematic and reduced-dynamic baseline solutions for the Swarm-A/C pendulum pair and other combinations of Swarm satellites. The single-, dual- and triple-satellite POD and PBD modes led to comparable consistencies between the computed orbit solutions and SLR observations at a level of 2 cm. In addition, the consistencies with single-satellite ambiguity fixed orbit solutions

provided by GSOC/DLR were at comparable levels for all the modes, with reduced-dynamic baseline consistency at a level of 1-3 mm for the pendulum Swarm-A/C formation and 3-5 mm for the high-dynamic Swarm-B/A and -B/C satellite pairs in the different directions.

The most complicated POD and PBD were done for a satellite constellation comprised of two different missions, the CHAMP satellite and the GRACE twin satellites. The orbital planes of these two missions aligned closely during March to May 2005, allowing PBD between the associated three satellites. The baselines between CHAMP and the GRACE tandem varied from about 100 to 7500 km during 24-hr orbital arcs centered around the point of closest approach. All three satellites were equipped with high-precision, dual-frequency BlackJack GPS receivers which however performed distinctly. This required a careful data pre-processing scheme to screen out data outliers such as irregular carrier-phase residual jumps. For the CHAMP/GRACE PBD, a number of factors needed to be dealt with, including the *cross-talk* between the CHAMP GPS main navigation and occultation antennas, the different levels of non-gravitational accelerations, and the rapidly changing geometry that complicated the fixing of integer ambiguities for the GPS carrier-phase observations. It was also assessed how the quality of especially the CHAMP/GRACE baselines depended on the orbit arc length around the point of closest approach, where this length was set from 2 to 24 hr. The longer the arc length, the less favorable the geometry became for ambiguity fixing for the CHAMP/GRACE PBD. Orbit solutions had an agreement of typically 2-3 cm with the SLR observations. Consistency between CHAMP/GRACE kinematic and reduced-dynamic baselines varied from 1 to 4 cm, where better consistency was obtained for shorter arcs. For GRACE, the kinematic/reduced-dynamic baseline consistency was typically below 1 cm, with an integer ambiguity fixing success rate of around 94%. The agreement with the KBR measurements was about 0.6 mm.

The results obtained indicate that further improvements are to be explored in terms of GPS data pre-processing and DD carrier phase ambiguity fixing. Moreover, it will be very interesting in the future to assess the capabilities of future spaceborne multi-GNSS receivers for POD and PBD. Last but not the least, it will be very interesting to further investigate the benefits of PBD solutions of satellite formations and constellations for e.g. global temporal gravity field retrieval.

Samenvatting

Precieze absolute en relatieve baanbepaling, ofwel Precise Orbit Determination (POD) en Precise Baseline Determination (PBD), zijn onmisbaar voor het succes van veel satellietmissies in een lage aardbaan (Low Earth Orbit, LEO). Met meerkanaals, *dual-frequency* Global Positioning System (GPS) ontvangers van hoge kwaliteit kan in de ruimte typisch een precisie in de orde grootte van enkele centimeters worden behaald bij POD voor enkele satellieten, en van enkele milimeters bij PBD voor satellieten die in formatie vliegen, tot enkele honderden kilometers afstand van elkaar. Het onderzoek in dit proefschrift omvat uitbreidingen voor de methodes waarmee betrouwbare baanberekeningen worden gedaan, zowel voor stabiele satellietformaties, zoals de Amerikaans–Duitse GRACE (Gravity Recovery And Climate Experiment) missie en het onderste paar Swarm satellieten van de Europese Ruimtevaartorganisatie (ESA), als voor satellietconstellaties met snel veranderende onderlinge afstanden, zoals de combinatie van de Duitse CHAllenging Minisatellite Payload (CHAMP) en GRACE missie, of het drietal Swarm satellieten. The POD en PBD oplossingen komen voort uit een Iterative Extended Kalman Filter (IEKF), dat gebruik maakt van begrenzingen op de relatieve satellietdynamica om tot robuustere oplossingen te komen. Bovendien is het IEKF in staat Double-Difference (DD) gehele draaggolffase ambiguïteiten iteratief op te lossen met de Kleinstekwadraten AMBiguity Decorrelation Adjustment (LAMBDA) methode. In plaats van een strategie te gebruiken die de complete verzameling aan ambiguïteiten oplost op voorwaarde dat alle ambiguïteiten in bepaalde tijdspannes zijn opgelost, werd een subset strategie toegepast waarbij een deel van ambiguïteiten wordt opgelost. Het resultaat van het IEKF bestaat uit *reduced-dynamic* POD en PBD oplossingen, maar de methode biedt ook de mogelijkheid om achteraf kinematische PBD oplossingen te berekenen. De mate van overeenkomst tussen de *reduced-dynamic* en kinematische oplossingen wordt gebruikt als maat voor de kwaliteit, naast de vergelijking tussen de POD en PBD oplossingen door andere instituten.

De IEKF implementatie die voor dit onderzoek is gebruikt, kan worden ingezet voor POD en PBD methodes in het geval van één, twee of drie satellieten. Om dit te demonstreren werden de CHAMP satelliet, het tweetal GRACE satellieten, en het drietal identieke Swarm satellieten als testcasussen gebruikt.

Voor GPS ontvangers aan boord van LEO satellieten worden vaak Phase Center Variation (PCV) patronen aangewend die vooraf worden geconstrueerd op basis van grondtests. Frequentie-afhankelijke antennecalibratie tijdens de vlucht blijkt echter tot betere PCV patronen te leiden, en daarmee tot betere correcties voor de GPS metingen. Het resultaat kan verder worden verbeterd door zogenaamde Code Residual Variation (CRV) patronen toe te voegen aan absolute/Undifferenced (UD) POD en relatieve/DD PBD algorithmes. Voor CHAMP, GRACE en Swarm zijn baanbepalingen uitgevoerd voor verschillende periodes, waarmee de invloed kon

worden bepaald van PCV en CRV patronen die tijdens de vlucht zijn gemaakt op de nauwkeurigheid van de POD en PBD oplossing. Op basis van baanberekeningen over een vier maanden durende test periode (augustus–november 2014) kon voor de twee GRACE satellieten, in tandem met een onderlinge afstand van ongeveer 220 km, worden aangetoond dat de CRV patronen leidden tot een beduidend betere initialisatie van de DD draaggolffaseambiguïteitsoplossing. De patronen zorgden bovendien voor betere consistentie tussen de kinematische en *reduced-dynamic* baanberekeningen, vooral in de dwarsrichting. Door zowel de PCV als CRV patronen te gebruiken, werd ook de consistentie met onafhankelijke laser-afstandsmetingen ofwel Satellite Laser Ranging (SLR) en K-Band Ranging (KBR) *low-low* satelliet-naar-satelliet afstandsbepaling ietwat verbeterd. De grootste verbetering werd behaald voor GRACE-B, die door interferentie tussen de hoofd GPS antenne en occultatieantenne hogere systematische observatie residuën produceerde. Deze onwenselijke interferentie kon door de CRV patronen goed worden gecompenseerd.

De drie identieke Swarm satellieten hebben enkele wijzigingen ondergaan aan de GPS ontvangers, alsmede een update in de GPS Receiver Independent Exchange Format (RINEX) omzetter van oktober 2014 tot augustus 2016. Bovendien werden de prestaties van de GPS ontvanger beïnvloed door ionosferische scintillatie van verschillende intensiteit. De impact van deze effecten is geanalyseerd voor de PBD van de Swarm-A en -C satellieten die in pendulum formatie vliegen, met een onderlinge afstand variërend van 30 to 180 km. In totaal zijn gegevens geanalyseerd verzameld over 30 maanden – van 15 juli 2014 tot eind 2016. Het onderzoek omvatte een analyse van de observatieresidueën, het aandeel juist geschatte draaggolfambiguïteiten, de consistentie tussen de kinematische en *reduced-dynamic* oplossingen voor de onderlinge afstand, en de validatie van baanoplossingen aan de hand van SLR metingen. De schattingen van de onderlinge afstand berekend door het Duitse Space Operations Center (GSOC/DLR) en het Astronomische Instituut van de Universiteit Bern (AIUB), werden ook gebruikt in de vergelijkingen. De resultaten van deze analyses lieten zien dat zowel de aanpassingen aan de GPS ontvanger als aan de RINEX omzetter de schatting van de onderlinge afstand verbeterden. De schattingen konden nog verder worden verbeterd door de halve-cyclus ambiguïteiten (meegeleverd met de originele GPS RINEX gegevens) te corrigeren naar volledige-cyclus en door ook de RINEX omzetter te updaten. Uiteindelijk is een consistentieniveau van 9.3/4.9/3.0 mm tussen de kinematische en *reduced-dynamic* oplossingen mogelijk in respectievelijk de radiale richting, de vliegrichting en de dwarsrichting. Voor gemiddeld 98.3% van de meetpunten waren kinematische oplossingen mogelijk. Bovendien waren de onderlinge afstanden berekend in dit onderzoek en die uit onderzoek van andere instituten consistent tot op 1 mm in alle richtingen, zolang dezelfde meetgegevens werden gebruikt.

PBD wordt uidagender als de onderlinge afstand tussen twee satellieten snel verandert, zoals het geval is wanneer de derde Swarm-B satelliet wordt toegevoegd. Dit zorgt voor twee zogenaamde hoog-dynamische satellietparen, namelijk Swarm-B/A en Swarm-B/C. Swarm-B vliegt in een hogere baan, waardoor zijn baanvlak langzaam draait ten opzichte van dat van Swarm-A en -C. Door deze geometrie komt het voor dat de baanvlakken van Swarm-B en de andere Swarm satellieten

voor korte tijd parallel liggen. Tien periodes van 24 uur rond zulke momenten werden geselecteerd, waarbij de onderlinge afstand variëerde tussen 50 en 3500 km. Uit de resultaten bleek dat het oplossen van de halve-cyclus draaggolffaseambiguïteiten en een reductie van de *code observation* ruis aan de hand van de omzetter updates, een verbetering teweegbracht van de kinematische en *reduced-dynamic* oplossingen voor de onderlinge afstand van alle Swarm paren. De POD en PBD methodes waarbij één, twee of drie satellieten werden gebruikt resulteerden in vergelijkbare consistentie tussen de berekende baanoplossingen en de SLR metingen, tot 2 cm nauwkeurig. Bovendien waren de baanoplossingen voor de individuele satellieten, inclusief correctie voor de draaggolfambiguïteiten, aangeleverd door GSOC/DLR, consistent tot op een vergelijkbaar niveau voor alle methodes. Voor de *reduced-dynamic* oplossing werd een consistentie van 1-3 mm gehaald voor het Swarm-A/C paar, en 3-5 mm voor de hoog-dynamische Swarm-B/A en Swarm-B/C paren in de verschillende richtingen.

De constellatie bestaande uit de CHAMP satelliet en de twee GRACE satellieten leidde tot de meest ingewikkelde POD en PBD bepaling. In de periode van maart tot mei 2005 lagen baanvlakken van deze missies vrijwel parallel, waardoor PBD mogelijk werd voor alle drie de satellieten. De onderlinge afstand tussen CHAMP en het GRACE paar variëerde tussen de 100 en 7500 km over het etmaal gecentreerd rond het moment van dichtste nadering. De satellieten waren alle drie uitgerust met zeer preciese *dual-frequency* BlackJack GPS ontvangers, al zij het met verschillende werking. Daarom was een zorgvuldige voorbereidende gegevensverwerking vereist om uitschieters te detecteren, zoals ongewone sprongen in het draaggolfresidu. Voor de PBD tussen CHAMP enerzijds en één van de GRACE satellieten anderzijds, moest rekening worden gehouden met een aantal factoren, waaronder interferentie tussen de GPS hoofdantennes en de occultatieantennes van CHAMP, de verschillen in niet-zwaartekrachtsgerelateerde versnellingen, en de snel veranderende geometrie die het oplossen van onderlinge ambiguïteiten in de GPS draaggolf bemoeilijkte. De invloed van de gekozen tijdsspanne rond het moment van dichtste nadering op de kwaliteit van de oplossing voor de onderlinge afstand tussen CHAMP en GRACE, werd beoordeeld door deze te variëren van 2 tot 24 uur. Hoe langer de tijdsspanne, hoe slechter de geometrie werd voor het oplossen van de ambiguïteiten in het CHAMP/GRACE PBD process. In het algemeen was het verschil tussen de baanoplossing en de SLR metingen 2-3 cm. Kinematische en *reduced-dynamic* oplossingen voor de onderlinge afstand kwamen overeen tot op 1 tot 4 cm, waarbij kortere tijdsspannes tot beter resultaten leidde. In het geval van GRACE kwamen de kinematische en *reduced-dynamic* oplossingen overeen tot op minder dan 1 cm, met 94% van de ambiguïteiten succesvol opgelost. Het verschil met de KBR metingen lag rond de 0.6 mm.

De behaalde resultaten geven een indicatie dat verdere verbeteringen mogen worden verwacht door verbeterde voorbereidende GPS gegevensverwerking en DD draaggolfambiguïteitsoplossing. Bovendien is het uiterst interessant om in de toekomst de mogelijkheden te onderzoeken van een combinatie van multi-GNSS ontvangers voor POD en PBD methodes. Als laatste is het zeer interessant om de voordelen van PBD oplossingen voor satellietformaties en -constellaties verder te

onderzoeken ten behoeve van, bijvoorbeeld, het meten van het wereldwijde, tijdsafhankelijke gravitatieveld.

Important Acronyms

Research Organizations

AIUB	Astronomisches Institut - Universität Bern
CODE	Center for Orbit Determination in Europe
CSR	Center for Space Research - The University of Texas at Austin
DLR	Deutsches Zentrum für Luft- und Raumfahrt
ESA	European Space Agency
GFZ	German Research Center for Geosciences
GSOC	German Space Operations Center - DLR
IERS	International Earth Rotation and Reference Systems Service
IGS	International GNSS Service
ILRS	International Laser Ranging Service
JPL	Jet Propulsion Laboratory

Satellite Missions

CHAMP	CHAllenging Minisatellite Payload
GOCE	Gravity Field and Steady-State Ocean Circulation Explorer
GRACE	Gravity Recovery and Climate Experiment
LEO	Low Earth Orbit
TerraSAR-X	Terra Synthetic Aperture Radar - X-band
TanDEM-X	TerraSAR-X add-on for Digital Elevation Measurement

Satellite Tracking System

GNSS	Global Navigation Satellite System
GPS	Global Positioning System
KBR	K-Band Ranging
SLR	Satellite Laser Ranging

Software and Algorithms

BERNESE	Bernese GNSS Software
GHOST	GPS High Precision Orbit Determination Software Tools
LAMBDA	Least-squares AMBiguity Decorrelation Adjustment
MODK	Multiple Orbit Determination using Kalman filtering

Miscellaneous

IEKF	Iterative Extended Kalman Filter
CRV	Code Residual Variations
DD	Double Differenced
GDOP	Geometric Dilution Of Precision
IF	Ionosphere Free
LSM	Least Squares Method
PBD	Precise Baseline Determination
PCV	Phase Center Variations
POD	Precise Orbit Determination
RINEX	Receiver Independent Exchange Format
RMS	Root Mean Square
SD	Single Differenced

Contents

1

Introduction

The modern era of space exploration originated with the launch of Sputnik-1 in 1957. During the ensuing decades, thousands of objects have been delivered into space and most of them can be referred to as artificial satellites. Depending on the specific applications, the greater part of those satellites are placed into so-called Low Earth Orbits (LEO) with altitudes lower than 1500 km (Montenbruck and Gill, 2012). Compared to the early days of spaceflight, when many satellites were of an experimental nature, today more and more satellites have designated commercial and/or research tasks. In addition, more and more use is made of satellite formations and constellations to meet certain mission objectives. This includes constellations in which the composing satellites fly in completely different orbital planes (Sabol et al., 2001). Based on their combined space-borne instrumental measurements, engineers and scientists further build up our knowledge about the Earth and its surroundings such as the gravity field (Tapley et al., 2004a), magnetic field (Friis-Christensen et al., 2006), topography (digital elevation maps) (Moreira et al., 2004), ionosphere (Hajj and Romans, 1998) and thermosphere (Doornbos, 2012), etc.

Orbit determination is a prerequisite to fulfill the objectives of almost each space mission (Schutz et al., 2004). A satellite has to be equipped with space-borne orbit determination equipment such as retro-reflector for acquiring Satellite Laser Ranging (SLR) observations (Degnan, 1993), phase Doppler shift tracking receiver for using the Doppler Orbitography and Radiopositioning Integrated by Satellite (DORIS) system (Schrama, 2018; Willis et al., 2010), and pseudo-range/carrier-phase tracking receiver for using Global Navigation Satellite Systems (GNSS) (Yunck et al., 1994), etc. The U.S. Global Positioning System (GPS), that was initially proposed for military applications, has become the most crucial system for single-satellite Precise Orbit Determination (POD) and dual-satellite Precise Baseline Determination (PBD), or in other words absolute and relative orbit determination (Jäggi et al., 2007).

Nowadays, GPS-based precise orbit solutions are recognized as essential prod-

ucts for several formation flying space missions (Friis-Christensen et al., 2008; Tapley et al., 2004a). The research described in this dissertation focuses on more robust POD and PBD solutions for satellite constellations which include longer and more rapidly varying (or high-dynamic) baselines. The following section will provide a historical overview of selected satellite missions flying with space-borne high-precision multi-channel dual-frequency GPS receivers. A brief review regarding the state-of-the-art POD and PBD methodologies is introduced, and this inspires the motivations of investigating into four research cases. Eventually this chapter concludes with an outline of the research and research questions.

1.1. GPS-based satellite orbit determination

This section provides examples of low flying satellites carrying high-quality GPS receivers (1.1.1), provides short descriptions of the associated GPS receivers (1.1.2), and briefly introduces existing orbit determination methods (1.1.3).

1.1.1. LEO satellites carrying high-quality GPS receivers

The first experiment with a space-borne GPS receiver dates back to the Landsat-4 satellite which was launched in 1982 (Yunck, 1996). Its on-the-fly navigation achieved a precision of merely 50 meters (Birmingham et al., 1983). This precision is insufficient for many scientific and operational applications for which a higher orbit precision at the level of a few centimeters is required. Subsequently, fundamental work was done for the TOPEX/POSEIDON oceanographic research satellite, which witnessed an unprecedented post-facto orbit precision of about 3 cm in the radial direction, better than the desired precision of about 10 cm before launch (Schutz et al., 1994; Tapley et al., 1994). Its successors Jason-1/-2/-3 continued to carry GPS receivers for determining orbits, providing orbit solutions with a precision of about 1 cm in the radial direction (Cerri et al., 2010; Haines et al., 2004). Later on, the mission CHAMP showed the tremendous possibilities for global gravity field recovery using high-quality tracking by GPS in combination with very precise space-borne accelerometers (Van den IJssel et al., 2003; Reigber et al., 2002a). High-quality GPS tracking also proved to be indispensable for the gravity field missions GRACE and GOCE (Kang et al., 2003; Visser et al., 2009). Currently, many different space missions such as the Swarm geomagnetic field mission (Van den IJssel et al., 2015), the Sentinel satellite series under the Copernicus Programme (Peter et al., 2017), the TerraSAR-X/TanDEM-X Synthetic Aperture Radar (SAR) mission (Hackel et al., 2017), and GRACE Follow-On (Sheard et al., 2012) are all equipped with space-borne GPS receivers. Many of these satellites are equipped with laser retro-reflectors for SLR tracking. This allows an independent way of validating GPS-based orbit solutions. Nowadays a typical orbit precision at a level of 2 cm in the line-of-sight direction - from an SLR ground station to a LEO satellite - is achievable for the mentioned satellites (Persson et al., 2009).

Satellite formations offer great opportunities for certain applications such as the observation of temporal gravity field variations and generation of precise digital elevation maps. Such formations require not only high-precision absolute position,

but also relative position solutions. The first test of GPS-based relative navigation for two approaching spacecraft, the Space Shuttle Endeavour and the Wake Shield Facility (WSF) free-flyer, was done during the Space Transportation System (STS)-69 mission. Errors of hundreds of meters were confirmed in this on-the-fly baseline determination experiment (Carpenter and Bishop, 1996). More tests were done during the rendezvous and docking operations between the International Space Station (ISS) and spacecraft such as the Space Shuttle (Goodman, 2006), the Automated Transfer Vehicle (ATV) (Pinard et al., 2007) and the Soyuz manned spacecraft (Zin et al., 2007). Hereafter, GPS-based PBD was applied to scientific missions demanding a higher baseline precision. A perfect test bed for GPS-based high precision PBD is the US/German GRACE in-line tandem formation, which maintains a stable distance of around 220 km (Tapley et al., 2004b). A μm precision level K-Band Ranging (KBR) system can be used to validate the GPS-based PBD. As for its GPS-based baselines, a precision of sub-mm can be achieved using different software packages (Gu et al., 2017; Jäggi et al., 2007; Kroes et al., 2005). Besides, PBD was done for the TerraSAR-X/TanDEM-X satellites flying in a side-by-side bistatic formation with a baseline length varying from hundreds of meters to a few km (Krieger et al., 2013). Consistency between its kinematic and reduced-dynamic baselines is at a level of a few mm (Allende-Alba and Montenbruck, 2016). Investigations for the recent European Space Agency (ESA) Swarm-A/C satellites (the lower pair of this triple-identical-satellite constellation (Friis-Christensen et al., 2008)) flying in a pendulum formation were done by Allende-Alba et al. (2017); Mao et al. (2018), indicating a consistency level of 5-40 mm in each individual direction between reduced-dynamic and kinematic baseline solutions.

1.1.2. Space-borne GPS receivers

Years of practical satellite POD applications confirmed the effectiveness of a few series of state-of-the-art space-borne GPS receivers. The BlackJack dual-frequency GPS receivers (or TurboRogue space receiver) and its follow-on Integrated GPS and Occultation Receiver (IGOR) have been developed by the Jet Propulsion Laboratory (JPL) (Kuang et al., 2001). They served for a large group of missions such as Oersted, CHAMP, SAC-C, ICESat, GRACE, Formosat-3/COSMIC, TerraSAR-X/TanDEM-X, Jason-1/-2/-3 and GRACE-FO. Their use for GPS radio occultation research is also exceedingly successful (Wickert et al., 2005). ESA has supervised a few space-borne GNSS receivers based upon the series of Advanced GPS/GLONASS ASIC (AGGA) correlators (Roselló et al., 2010). Three main types of GNSS receivers have been under continuous development in Europe. One is the GNSS Receiver for Atmospheric Sounding (GRAS) developed by SAAB Aerospace, Sweden, which flies successfully onboard METOP satellites (Loiselet et al., 2000). The second is the LAben GNSS Receiver for Advanced Navigation, Geodesy and Experiments (LAGRANGE) receiver developed by Laben, Italy, which has flown successfully onboard the COSMO/SkyMed, RadarSat-2 and GOCE satellites (Marradi et al., 2001). The third is the GPS navigation receiver developed by RUAG Space, Austria, which has flown - and is flying - successfully onboard the Swarm, ICESat-2, Sentinel-1A/1B/2A/2B/3A satellites (Zangerl et al., 2014).

Each GPS receiver normally comes along with at least one antenna, which is affected by unique phase center variations in its in-flight space environment. The acquired GPS signals will be advanced or delayed differently as a function of the viewing directions (Rothacher, 2001; Schmid and Rothacher, 2003). Multi-path reflections can be also exclusively caused by the surfaces of satellite. Besides, signal disturbances such as the so-called *cross-talk* between GPS navigation and radio occultation antennas (if switched on) possibly also impact such delays or advances (Montenbruck and Kroes, 2003). Therefore, full exploitation of GPS observations requires a precise modeling of - or correction for - Phase Center Variations (PCV). Much work has been done in the past for obtaining the best possible PCV maps and it is now standard procedure to include those maps in POD (Haines et al., 2004; Jäggi et al., 2009; Montenbruck et al., 2009). It has been shown that these antenna patterns are also crucial for PBD (Allende-Alba and Montenbruck, 2016; Mao et al., 2017). In addition, each GPS receiver performs distinctly in space, often requiring in-flight modifications (Van den IJssel et al., 2015). It is crucial to analyze GPS receiver in-flight data to properly model the above mentioned effects and assess the impact of receiver software modifications and updates.

1.1.3. Orbit determination methods

The availability of GPS has revolutionized independent POD of LEO satellites in that it provides in general continuous tracking of these LEO satellites by at least 4 GPS satellites. The use of code/pseudo-range observations, or preferably the combination of code and carrier-phase observations then enable the instantaneous computation of four parameters including three satellite position coordinates and one GPS receiver clock offset (Schutz et al., 2004). According to the primary design specification, each GPS satellite transmits signals on two independent frequencies (i.e. $f_1 = 1575.42\ MHz$, $f_2 = 1227.60\ MHz$). The GPS measurements are influenced by ionosphere differently on each frequency, and an ionosphere-free combination can be constructed to eliminate the first order ionospheric effect in the GPS observations (McDonald, 2002). For obtaining the best possible precision, POD and PBD primarily rely on the carrier-phase observations and the best precision is obtained when the so-called carrier-phase ambiguities can be fixed to integer values (Kaplan and Hegarty, 2005). Precisions at the cm level (absolute) and even mm level (relative) are a prerequisite for several terrestrial and space-based applications.

Currently, there are two main methods for single satellite GPS-based POD. On the one hand, the kinematic method solely relies on GPS observations, GPS satellite orbit/clock products and other associated products. The instantaneous GPS receiver position or - after correction for the antenna offset - satellite Center-of-Mass (CoM) coordinates are determined for each individual epoch (Yunck, 1996). It does not create solutions for epochs for which an insufficient number of GPS satellites is in view (in principle 4, but often 5 is defined as the minimum to have at least one redundant observation) or epochs with too many unreliable observations (outliers). On the other hand, the so-called reduced-dynamic method combines the strengths of the kinematic method (strong observation geometry) and dynamic orbit determination (high precision knowledge for force models) (Yunck et al., 1994).

Reduced-dynamic orbit determination includes the use of gravitational and non-gravitational force models, and so-called empirical accelerations for compensating errors in the force modeling (Montenbruck et al., 2005). For satellites equipped with accelerometers, the non-gravitational force models can be replaced by the associated observations typically leading to a reduced need for estimating empirical accelerations (Van Helleputte and Visser, 2008).

For satellites flying in close formation, for instance the GRACE tandem, it is interesting to realize that they experience predominantly similar perturbing forces, especially non-gravitational ones. This similarity is utilized to constrain the estimate of empirical accelerations such that the robustness and precision of PBD solutions can be improved (Kroes et al., 2005). More importantly, by forming a so-called Double-Differenced (DD) combination between two GPS satellites and two GPS receivers, errors such as GPS orbit/clock bias and receiver clock offsets are significantly mitigated, and the DD ambiguities take in principle integer values. These DD integer ambiguities can be fixed with higher possibility, which further improves the PBD precision. Two ambiguity resolution algorithms - the Least-squares Ambiguity De-correlation Adjustment (LAMBDA) (Teunissen, 1999) and Wide-Lane and Narrow-Lane (WL/NL) bootstrapping algorithm (Jäggi et al., 2007) - have been consistently developed for satellite formation PBD. The fixed integer ambiguities can be also fed into a kinematic PBD approach (Kroes, 2006; Mao et al., 2018). In addition, methods have been developed by other research groups and implemented to conduct so-called single receiver ambiguity fixed POD. Bertiger et al. (2010) make use of the ionosphere-free wide-lane model developed by Blewitt (1989), whereas Montenbruck et al. (2018b) adopt the wide-lane phase bias estimate products provided by Loyer et al. (2012). The associated Swarm solutions have served for quality assessments of the POD and PBD solutions described in this dissertation (Mao et al., 2019b; Montenbruck et al., 2018b).

1.2. Motivation and research questions

Achievable PBD precision for different satellite formations is dependent on the complexity of the satellite formation, such as distance and relative velocity between the satellites, and the difference in perturbing forces (Allende-Alba and Montenbruck, 2016). The quality of onboard GPS receiver hardware and software, GPS antenna and satellite platform characteristics also have an impact on satellite PBD (Mao et al., 2018). Present PBD investigations for satellite formations mostly focused on short and stable baselines whose lengths are normally in the scope of hundreds of meters to hundreds of kilometers (D'Amico et al., 2013; Jäggi et al., 2007; Montenbruck et al., 2011). However, several new satellite constellations with rapidly changing geometry are established or proposed for future space missions. For instance, the European Copernicus Program is leading to a constellation of diverse satellites functioning in different orbits in the upcoming decade (Butler et al., 2014). The Sentinel-1 component will already consist of two or even four radar imaging satellites flying in formations to provide continuous global data (Torres et al., 2012). The 66 satellites Iridium-next constellation will be completed by the end of 2018 (status November 2018). A simulation has shown that their GPS-based orbits have

the potential to recover large-scale gravity variations caused by e.g. large scale redistribution of continental water masses (Gunter et al., 2011). The next generation gravity field recovery satellite mission will probably consist of two separate formations flying in different orbital planes (Elsaka et al., 2014). Sharifi et al. (2007) showed that the qualitative differences in four respective formation flying baselines can be reflected in the recovered gravity fields. These mentioned applications all demand precise baseline solutions for different missions. However, more robust POD and PBD methods particularly for large satellite constellations are more challenging and need to be further investigated. This has resulted in the formulation of four main Research Questions (RQ) below.

RQ.1 What is the impact of GPS receiver antenna patterns on orbit determination precision, not only regarding GPS carrier-phase, but also code observations?

POD and PBD primarily rely on the GPS carrier-phase observations. The code observations are vital for initializing the estimates of the carrier-phase ambiguities. Although the influence of antenna carrier-phase pattern corrections for PBD has been widely analyzed, that of the code observations has not. Moreover multi-functional GPS receivers such as BlackJack series often makes use of multiple GPS antennas for e.g. both POD and radio occultation purposes, which typically results in systematic *cross-talk*. Therefore, it is worthwhile to evaluate corrections for code observations to account for not only this possible *cross-talk*, but also multipath. The CHAMP and GRACE missions both experienced certain periods when their occultation antennas were switched on and they can serve as ideal test platforms.

RQ.2 How is PBD influenced by the in-flight performance of GPS receivers and in conjunction with receiver settings?

Several GPS-relevant factors play a role regarding POD and PBD of low flying satellites and satellite formations or constellations. These factors include GPS receiver settings such as antenna tracking elevation cut-off angle, tracking loop bandwidth, carrier-phase counting, and pre-processing tasks such as outlier detection. In addition, acquisition and quality of Swarm GPS tracking observations can be affected by the level of ionospheric activity and scintillations leading to e.g. seasonal effects and a dependency on the 11-year solar cycle. A detailed assessment of these factors for especially the ESA Swarm-A/C satellites formed part of the research described in this dissertation. A rich data set is available and the impact of several receiver modifications can be assessed.

RQ.3 Can we get precise baseline estimates for satellite constellations with long and highly variable baselines?

This research question is based on **RQ.1** and **RQ.2** however calls for more challenging application of these methods. When forming more complicated satellite constellations such as the combination of CHAMP and GRACE or the three-satellite Swarm mission, the baseline lengths vary easily from tens to thousands of kilometers in short time. This differs significantly with the past research focusing on short and stable satellite baselines such as GRACE and TerraSAR-X/TanDEM-X. For very long baselines, the number of common GPS satellites in view by the two associated GPS receivers is reduced. Consequently, PBD becomes more challenging or even impossible. In addition, for long baselines integer ambiguity fixing becomes more troublesome. Moreover, LEO satellites flying in distinctly different orbits experience also distinctly different perturbing forces. A proper understanding of these is crucial for optimizing PBD for such satellite constellations. The ESA Swarm triple-identical-satellite mission will act as a convenient test bed to address this research question.

RQ.4 Can we have reliable PBD solutions for satellite constellations comprised of different satellite missions?

This research question can be seen as a sub-question of **RQ.3**. PBD for LEO satellite constellations comprised of multi-mission satellites is challenging as shown by Van Barneveld (2012). It will be more complicated to get precise baselines for this constellation due to its geometry. Van Barneveld (2012) produced POD and PBD solutions for the CHAMP/GRACE combination, but often with significantly degraded precision as compared to single-satellite POD. The procedures and methods for PBD of more complicated constellations need to be improved. An important aspect is that CHAMP and GRACE fly different BlackJack GPS receivers displaying different performance. The CHAMP GPS navigation receiver experienced strong *cross-talk* due to the activation of its occultation antenna. Besides, three satellites fly in distinct in-flight environment and experience different levels of non-gravitational perturbations. During the first half of 2005, the CHAMP and GRACE missions were flying in good in-view geometry when their orbital planes were closely aligned. For each close encounter, a rapidly changing geometry can be observed, which resulted in a challenging test bed to assess the performance of the proposed POD and PBD methods (Mao et al., 2019a).

1.3. Selected satellite missions

To address the research questions formulated in the previous section, data from the CHAMP, GRACE and Swarm missions are selected. This section introduces these missions and pays more attention to the associated GPS receivers.

1

1.3.1. CHAllenging Minisatellite Payload (CHAMP)

The CHAllenging Minisatellite Payload (CHAMP, Figure 1.1) is a cooperative geophysical research mission between The German Research Center for Geosciences (GFZ) and The German Space Operations Center (GSOC/DLR) (Reigber et al., 2002b). Its primary objectives included the mapping of global long-to-medium wavelength static Earth gravity field as well as its temporal variations, for which CHAMP was equipped with a high-precision, dual-frequency GPS receiver and a space-borne accelerometer. Its primary objectives also included the global observation of atmospheric quantities through radio occultation. All these objectives required very precise orbit solutions (both in terms of position and velocity). Finally, CHAMP aimed at observing the global geomagnetic field and its temporal variations. CHAMP was initially launched into a near-circular orbit with an altitude of 450 km on 15 July 2000. In 2005 its orbit altitude decayed to around 350 km. Therefore it experienced much stronger gravitational and non-gravitational perturbations than the other satellites selected for the research described in this dissertation. Eventually, this fruitful mission de-orbited on 19 September 2010.

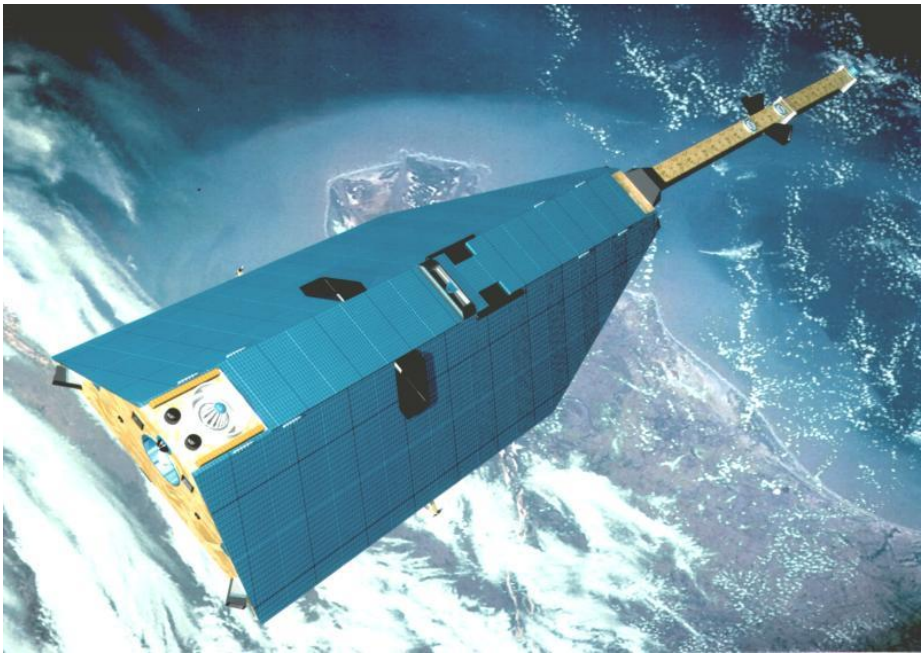

Figure 1.1: Artist's image of the CHAMP satellite (source: Astrium GmbH).

CHAMP carries a BlackJack GPS receiver with a pack of 4 GPS antennas. For most of its mission period only the zenith-installed prime POD antenna and the rear-side-installed radio occultation antenna were activated. The latter was found to affect the main POD antenna significantly, as it brings large systematic multi-path and *cross-talk* to the main GPS navigation antenna (Montenbruck and Kroes, 2003). CHAMP also carries a retro-reflector allowing SLR validations (Neubert et al., 1998).

1.3.2. Gravity Recovery And Climate Experiment (GRACE)

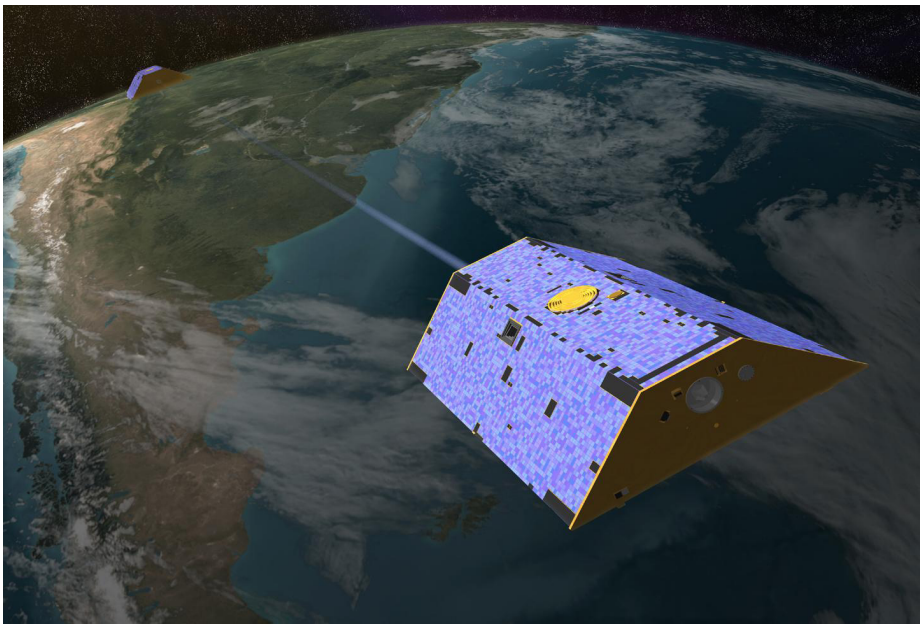

Figure 1.2: Artist's image of the GRACE twin satellites and their onboard KBR system (source: NASA/JPL-Caltech).

The Gravity Recovery And Climate Experiment (GRACE, Figure 1.2) is a US/German dual-satellite formation aiming at observing the global Earth gravity field and its temporal variations on a monthly basis. Its intended 5-year lifetime starting from 17 March 2002 was eventually extended to more than 15 years up to 27 October 2017. It has achieved unprecedented research outputs for the redistribution of ocean mass, melting of ice sheets and glaciers, and continental hydrology (Tapley et al., 2004a). The initial orbit for the two satellites was a near-circular polar orbit with an altitude of about 500 km. The two satellites fly in an in-line or along-track tandem formation maintaining a stable baseline length of around 220 km.

In its mission period, high quality GPS data have been collected by two space-borne BlackJack IGOR receivers, in combination with choke ring antennas (Montenbruck et al., 2006). Since 22 May 2006, the GPS observations for the trailing satellite collected by the main navigation antenna are characterized by larger systematic effects due to the switched-on GPS radio occultation antenna (Witkowski and Massmann, 2014). In addition to the retro-reflector for SLR, it carries ultra-precise accelerometers and a high-precision KBR system. The latter allows to validate the GPS-based baseline solutions. The GRACE follow-on mission, launched on 22 May, 2018, is now flying a similar orbit pattern (Flechtner et al., 2014). Both GRACE and its follow-on mission can be used as perfect platforms to test different PBD methods since they have quite stable baselines and a KBR system. In 2005,

1

GRACE and CHAMP experienced a good orbit alignment phase which provided the possibility to investigate PBD for a more complex multi-mission constellation.

1.3.3. Swarm triple-identical-satellite mission

The Swarm constellation (Figure 1.3), launched on 22 November 2013, is the fifth mission of the ESA living planet program. With three identical satellites, Swarm aims at unscrambling the Earth geomagnetic field and its temporal variations (Friis-Christensen et al., 2008). Its constellation geometry and associated maneuvers guarantee a comprehensive observation scheme of the Earth in high spatial and temporal resolution. After the early orbit commissioning phase, the Swarm-A and -C satellites fly in orbital planes with identical inclination but a difference of 1.5° in the right ascension of the ascending node and about $0.3^\circ - 0.9^\circ$ in argument of latitude. These differences manifest themselves as a pendulum like relative motion. Later on, Swarm-B maneuvered into a higher polar orbit which was about 80 km above the pendulum pair. In 2014, the Swarm constellation showed good orbit alignment and close encounters between Swarm-B and the other two satellites.

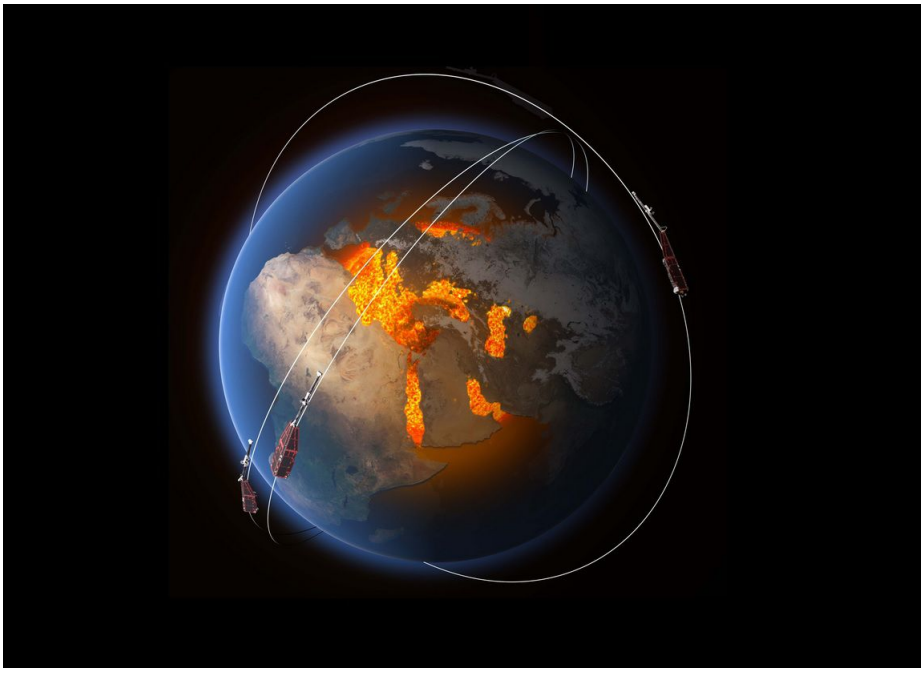

Figure 1.3: Artist's image of the three identical Swarm satellites (source: ESA/ATG Medialab).

Each Swarm satellite carries a *RUAG Space* GPS receiver (Zangerl et al., 2014). Ionospheric scintillations were proved to have a big impact on the performance of associated GPS receivers and consequently POD (Van den IJssel et al., 2016). To improve the GPS signal tracking performance in certain geographical areas experiencing strong ionospheric influences, a few modifications have been made to the

Swarm GPS receivers. In addition, carrier-phase integer ambiguity resolution was especially challenging because half-cycles were to be fixed due to the tracking problem with the Numerically Controlled Oscillator (NCO) (Allende-Alba et al., 2017). Systematic 180° phase rotation frequently happened during the tracking process, for more information please see in (Montenbruck et al., 2018b). A systematic GPS RINEX converter software issue also existed for code observations leading to higher code noise. Both these issues were eventually resolved, but it was very interesting to investigate the impact of these issues.

1.3.4. Satellite constellations

Time series of the evolution of the altitude of the selected LEO satellites are displayed in Figure 1.4. The CHAMP and GRACE missions have a long overlapping period of mission operations. For the artificial CHAMP/GRACE constellation, a period when the right ascension of the ascending nodes of two orbital planes are close enough could be identified during which the satellites closely approach each other and are in common view of GPS satellites. This was the case for March to May 2005.

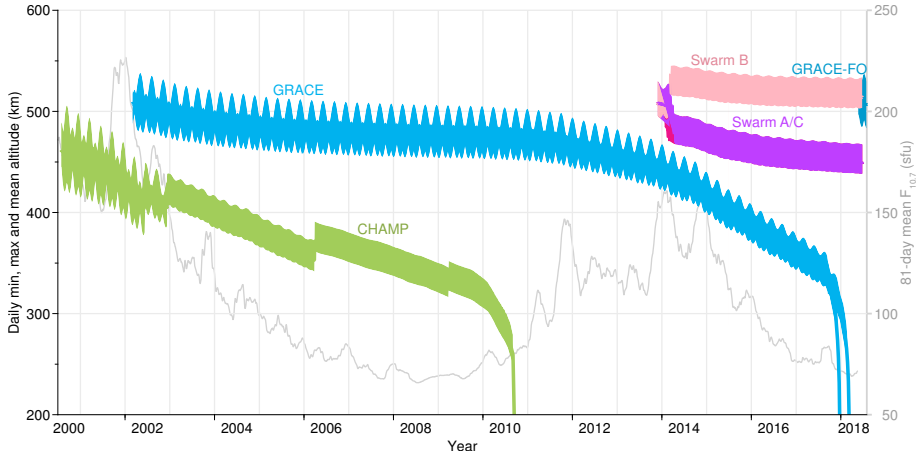

Figure 1.4: Evolution of the altitudes of the CHAMP, GRACE and Swarm satellites. In addition, the 81 day mean of F10.7 cm (the solar radio flux at 10.7 cm or at a frequency of 2800 MHz) is displayed which provides a measure of ionospheric activity (March et al., 2018).

The research described in this dissertation relies on data collected by the Swarm and CHAMP/GRACE constellations, for which different baseline evolution can be observed (Figure 1.5). For the Swarm constellation, Swarm-A/C satellites fly in a pendulum formation with a distance varying between 30 and 180 km. The high-dynamic Swarm-B/A and Swarm-B/C pairs fly in a high-low orbit geometry for which the baseline lengths can vary between 50 and 3500 km in 12-hr before and after a close encounter. The CHAMP and GRACE satellites form a constellation providing a stable GRACE-A/B baseline and two high-dynamic CHAMP/GRACE baselines, whose lengths vary from about 100 to 7500 km during 24-hours around an encounter.

1

For POD and PBD for these constellations, a number of important questions regarding the in-flight performance of different GPS receivers, different levels of (differential) orbit perturbations and DD ambiguity fixing for high-dynamic baseline have to be addressed in this dissertation. The eventual POD and PBD method should obtain a precise orbit solution for each satellite as well as a precise baseline solution for each satellite pair.

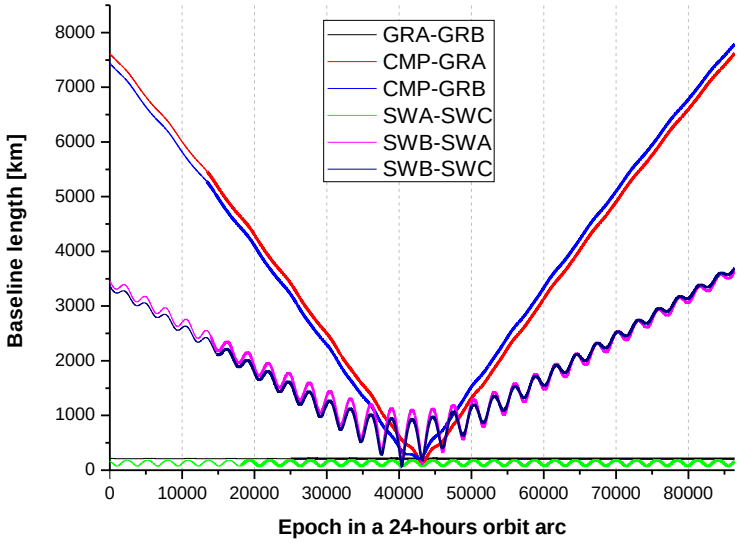

Figure 1.5: The length variations for six satellite baselines during a typical 24-hours orbit arc as analyzed in this research (the selected day for CHAMP/GRACE is Day-Of-Year (DOY) 093, 2005 and that for Swarm is DOY 198, 2014). Please note that the middle of the periods is the time of closest approach for the high-dynamic satellite pairs.

1.4. Outline

In this dissertation, POD and PBD for satellite constellations that gradually grow in complexity are addressed and investigated. Each chapter begins with a section about data analysis for relevant GPS receivers and data (pre)processing, followed by a description of produced POD and PBD solutions with a quality assessment.

Chapter 2 introduces the PBD investigation for the GRACE tandem formation. Absolute and relative orbit determinations are done for a four months test period (August to November 2014), demonstrating orbit determination improvements due to the use of different antenna patterns for correcting signal interference.

Chapter 3 presents the PBD investigation for the Swarm-A/C pendulum formation. In total 30 months of data - from 15 July 2014 to the end of 2016 - are used. The influences of GPS receiver modifications and ionospheric scintillations are assessed.

Chapter 4 introduces the PBD investigation for the whole Swarm constellation which provides three different baselines. Ten 24-hr orbital arcs are selected around the points of closest approach for the high-low satellites. Evaluations are done to check the applicability of PBD methods, particularly for the ambiguity fixing and the consistency between kinematic and reduced-dynamic baseline solutions.

Chapter 5 presents the PBD investigation for the complex CHAMP/GRACE constellation. It provides the most dynamic baselines and demands the investigations into many impact factors for a period of three months (March to May, 2005). The CHAMP satellite arouses many new questions due to its significantly different GPS receiver performance and stronger in-flight perturbations.

The conclusions and recommendations for future work are given in Chapter 6.

2

GRACE Formation Baseline Determination

RQ.1 What is the impact of GPS receiver antenna patterns on orbit determination precision, not only regarding GPS carrier-phase, but also code observations?

This chapter introduces the PBD investigation for the GRACE tandem formation. Absolute and relative orbit determinations are done for a four months test period (August to November 2014), demonstrating orbit determination improvements due to the use of different antenna patterns for correcting signal interference.

Impact of GPS antenna phase center and code residual variation maps on orbit and baseline determination of GRACE

2

Xinyuan Mao[a], *Pieter Visser*[a], *Jose van den IJssel*[a]

Published in *Advances in Space Research*, 59/12 (2017) 2987–3002,
doi:10.1016/j.asr.2017.03.019.

Precision Orbit Determination (POD) is a prerequisite for the success of many Low Earth Orbiting (LEO) satellite missions. With high-quality, dual-frequency Global Positioning System (GPS) receivers, typically precisions of the order of a few cm are possible for single-satellite POD, and of a few mm for relative POD of formation flying spacecraft with baselines up to hundreds of km. To achieve the best precision, the use of Phase Center Variation (PCV) maps is indispensable. For LEO GPS receivers, often a-priori PCV maps are obtained by a pre-launch ground campaign, which is not able to represent the real space-borne environment of satellites. Therefore, in-flight calibration of the GPS antenna is more widely conducted.

This paper shows that a further improvement is possible by including the so-called Code Residual Variation (CRV) maps in absolute/undifferenced and relative/Double-differenced (DD) POD schemes. Orbit solutions are produced for the GRACE satellite formation for a four months test period (August-November, 2014), demonstrating enhanced orbit precision after first using the in-flight PCV maps and a further improvement after including the CRV maps. The application of antenna maps leads to a better consistency with independent Satellite Laser Ranging (SLR) and K-band Ranging (KBR) low-low Satellite-to-Satellite Tracking (ll-SST) observations. The inclusion of the CRV maps results also in a much better consistency between reduced-dynamic and kinematic orbit solutions for especially the cross-track direction. The improvements are largest for GRACE-B, where a cross-talk between the GPS main antenna and the occultation antenna yields higher systematic observation residuals.

For high-precision relative POD which necessitates DD carrier-phase ambiguity fixing, in principle frequency-dependent PCV maps would be required. To this aim, use is made of an Extended Kalman Filter (EKF) that is capable of optimizing relative spacecraft dynamics and iteratively fixing the DD carrier-phase ambiguities. It is found that PCV maps significantly improve the baseline solution. CRV maps slightly enhance the baseline precision, more significantly they lead to a much better initialization of the ambiguity fixing. The GRACE single-satellite orbit solutions compare to within a few cm 3-dimensionally with state-of-the-art external orbit solutions and SLR obser-

(a): Delft University of Technology, The Netherlands

vations, whereas for the baseline a consistency of better than 0.7 mm with KBR observations is achieved.

Keywords: GRACE; Precision Orbit Determination (POD); Baseline determination; Code Residual Variation (CRV); Phase Center Variation (PCV); Antenna pattern

2.1. Introduction

Precision Orbit Determination (POD) is a prerequisite for the success of many Low Earth Orbiting (LEO) missions, such as CHAMP (Reigber et al., 2002b), GRACE (Tapley et al., 2004b), GOCE (Drinkwater et al., 2006; Visser et al., 2002), TanDEM-X/TerraSar-X (Montenbruck et al., 2009) and Swarm (Van den IJssel et al., 2015), whose GPS-based orbit precisions have reached the cm level. The great potential of using satellite-to-satellite tracking by the Global Positioning System (GPS) was demonstrated by the TOPEX/Poseidon altimeter mission in the nineties of the 20^{th} century (Yunck et al., 1994). Since then, GPS has become the prime system for POD of many LEO satellites.

High-precision GPS-based orbit solutions primarily rely on the carrier-phase observations (in the following referred to as phase observations), where the pseudo-range or code observations can be used to serve the initialization or estimation of the so-called phase ambiguities. Full exploitation of the phase observations requires a precise modeling of - or correction for - Phase Center Variation (PCV). Much work has been done in the past for obtaining the best possible PCV maps and it is now standard procedure to use those maps in POD (Bock et al., 2011; Haines et al., 2004; Van den IJssel et al., 2015; Jäggi et al., 2009; Montenbruck et al., 2009).

GPS receivers on LEO missions provide perfect test beds for assessing and showing the positive impact on orbit precision of PCV maps, in particular those derived from in-flight data. As for GRACE and TanDEM-X/TerraSAR-X, these in-flight data come from BlackJack and the Integrated GPS and Occultation Receiver (IGOR) receivers, respectively, in combination with a choke ring antenna. These receivers display typical phase noise levels of the order of 1 mm on each frequency or equivalently 2-3 mm after ionosphere-free combination (Montenbruck et al., 2006). PCV maps can basically be derived by two calibration methods: (1) by ground campaigns, or (2) by analysis of in-flight data. Research by several authors, *e.g.* Jäggi et al. (2009); Montenbruck et al. (2009), indicates that the second method leads to superior results, which can be explained by the fact that the setups for ground calibration can not accurately mimic the space environment. For the second calibration method, a further distinction can be made between the so-called *direct approach* and *residual approach*. In the *direct approach*, a PCV map consisting of an equiangular grid in azimuth and elevation is estimated directly in the POD process (Jäggi et al., 2009), or could be performed by estimating the coefficients of a spherical-harmonics expansion (Zehentner and Mayer-Gürr, 2016). In the *residual approach*, the PCV map is based on an averaging of phase residuals produced by the POD process. Whereas the first approach allows to take properly into account correlations between estimated orbital parameters and PCV map corrections, the second method is computationally much less demanding and easy to implement

(Montenbruck et al., 2009). Although not a complete PCV map can be recovered by the *residual approach* as its large-scale variations might be wrongly captured, it is concluded in (Jäggi et al., 2009) that the small-scale structures can be recovered well and good results have been obtained with this approach in the past (Montenbruck et al., 2009). Therefore, in this paper the *residual approach* is adopted, where the final PCV maps are obtained by iterations until convergence. For the Code Residual Variation (CRV) maps, an equivalent *residual approach* is adopted. For both antenna patterns, most of the changes occur in the first iteration.

The first objective of this paper is to investigate the impact of using not only PCV, but also CRV maps on the precision of undifferenced reduced-dynamic and especially kinematic POD. Haines et al. (2004) have proved that the modeling of LEO's antenna center for not only carrier phase, but also pseudo-range, results in 1 cm radial orbit precision for Jason-1. Zehentner and Mayer-Gürr (2016) show that kinematic POD could be enhanced by directly estimating Antenna Center Variations (ACV) for both GPS observation types. In fact, code observations are characterized by not only much higher noise levels, but also by larger systematic effects such as multipath and - in case of simultaneously operating antennas - cross-talk. In our undifferenced POD schemes, the code observations have a much lower weight than the phase observations and effectively serve to initialize or constrain the so-called phase float ambiguities. Systematic errors in the code observations may then lead to systematic orbit errors as well. Moreover, the code observations are required to discriminate between receiver clock offset correction estimates and the phase float ambiguities (Kroes, 2006). The impact of including CRV maps on orbit quality is assessed, among others, by a comparison of our orbit solutions with external orbit solutions, independent Satellite Laser Ranging (SLR) observations, and observations of the GRACE baseline through the K-band Ranging (KBR) measurements. Furthermore, internal consistency checks are conducted by comparing the kinematic with the reduced-dynamic orbit solutions.

The second objective of this paper is to assess if relative POD or baseline determination for GRACE can be improved as well by the adoption of not only PCV maps, but also CRV maps. To meet this objective, PCV maps that are only valid for ionosphere-free observations do not suffice. Frequency-dependent PCV and CRV maps need to be estimated in order to support a proper fixing of Double-differenced (DD) phase ambiguities, which are required to achieve the most precise baseline solutions (Kroes, 2006). In this paper frequency-dependent antenna patterns are estimated and evaluated in resolving DD integer phase ambiguities. An iterative Extended Kalman Filter (EKF) approach is designed to this aim.

The prime objective of this paper is to assess the impact of CRV maps on single-satellite and relative satellite precise orbit determination from GPS observations. The GRACE satellites will be used as test bed. The outline of this paper is as follows: first, a short description of the GPS antenna sensor system will be provided (Section 2.2.1). The iterative algorithm of generating antenna patterns is then briefly introduced in Section 2.2.2. Section 2.3 describes the reduced-dynamic and kinematic POD strategies as employed in this study, and specifies the adopted setup. The orbit solutions are described and discussed in Section 2.4. Finally, conclusions

are drawn in Section 2.5.

2.2. Antenna patterns

A description of the antenna sensor system and conventions used in our research is provided in Section 2.2.1, followed by an introduction of the algorithm of using in-flight data for generating PCV and CRV maps based on the *residual approach* in Section 2.2.2.

2.2.1. Antenna sensor system

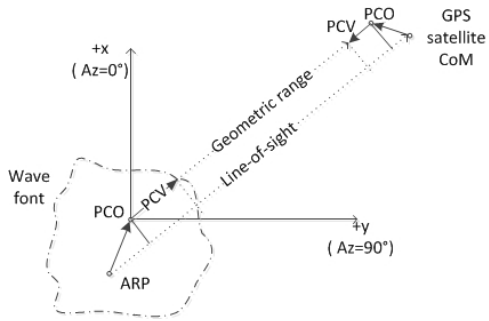

Figure 2.1: Schematic representation of ARP, PCO and PCV. The diagram is simplified to 2 dimensions and other range errors than PCV are excluded. In this research the *ARP* solution denotes a solution obtained by using the ARP and PCO information only.

Precisely modeling GPS observations is a prerequisite for any POD strategy. It is crucial to know as precisely as possible where the GPS signals leave the antenna of the GPS satellite (transmitting end) and enter the antenna of the LEO satellite (receiving end) with respect to the Center of Mass (CoM) of the satellites, since POD solutions are in general defined as providing the location of the CoM. For the GPS satellite antenna location with respect to the CoM, corrections are based on Phase Center Offset (PCO) locations and PCV maps provided by the International GNSS Service (IGS) (Schmid et al., 2016). For LEO satellites, it is assumed that the location of the so-called Antenna Reference Point (ARP) with respect to the CoM is well-defined and includes a-priori known PCO measured by ground experiments. In addition, a PCV map needs to be applied. Thus, the difference in location between the LEO antenna entry point and the ARP is composed of PCV corrections that are azimuth and elevation dependent. This scheme is illustrated in Figure 2.1. For the PCV maps, use will be made of the ANTEX (ANTenna EXchange) format (Rothacher and Schmid, 2006).

For several LEO satellites, antenna PCV maps have been produced before launch by a ground campaign. These maps are often significantly different from in-flight calibration. In general, corresponding maps are missing for code observations. To keep consistency in this research, PCV maps are estimated from scratch, *i.e.* the ground-based PCV maps are not used a-priori. This approach is similar to the

approach adopted for GOCE by Bock et al. (2011) and for Swarm by Van den IJssel et al. (2015). The same applies to the estimated CRV maps.

The GRACE antennas come with the identifier S67-1575-14+CRG. They are fixed to the upper surface of each GRACE satellite and include a choke ring. The PCV and CRV maps are defined in a right-handed North-East-Up (NEU) antenna-fixed reference system, for which the North axis coincides with the GRACE satellites body-fixed +X axis (0° azimuth), the Up and bore-sight axis coincides with the -Z axis, and the East axis completes the right-handed system. The location of the ARP is taken equal to the known location of the top surface center of the choke ring (Bettadpur, 2012).

Systematic code residual patterns were present in the early mission life of the GRACE twin satellites, as analyzed by (Kroes, 2006). Since 22 May, 2006, the patterns became much stronger for the trailing GRACE satellite as its occultation antenna had been switched on, and GRACE-B was the trailing satellite between the second swap maneuver (from 30 June to 28 July, 2014) and the third swap maneuver (from 15 December, 2014 to 15 January, 2015) for GRACE (Witkowski and Massmann, 2014). For this paper, data from August to November, 2014 (Day of Year (DOY) 213-334, for GRACE-B DOY 268 was excluded because of maintenance maneuvers) was selected for analyzing the impact of PCV and CRV maps, especially for GRACE-B. During this period, the orbital altitude of the GRACE satellites decreased from 427 to 415 km, and the baseline length was varying between 242 and 174 km, as indicated in Figure 2.2.

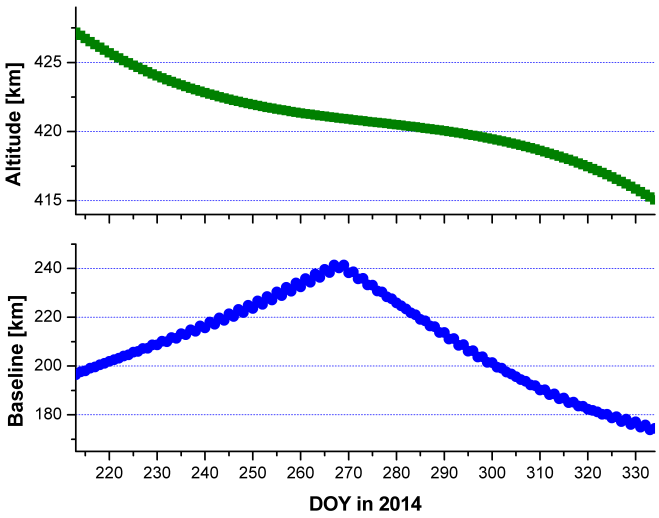

Figure 2.2: GRACE satellites orbital status: altitude (top) and baseline length (bottom) (DOY: 213-334, 2014).

2.2.2. In-flight data calibration algorithm

Generally, the antenna PCV and CRV maps display complicated patterns (see also in Figure 2.5 and 2.6). For obtaining the associated correction maps, the GPS observations which are processed simultaneously in the EKF, can be represented as:

$$\begin{aligned} P_m &= r + ion + PCV_{Em} + CRV_{Em} \\ L_m &= r - ion + PCV_{Em} + W - B \end{aligned} \tag{2.1}$$

where P_m and L_m represent the modeled pseudo-range and carrier-phase observations, respectively. It should be noticed that for single-satellite POD use of ionosphere-free combinations of GPS observations is made, while for relative POD the observations are modeled for each frequency, which facilitates integer ambiguity fixing of DD phase observations. The geometric distance between the GPS transmitter phase center (at departure time) and the LEO receiver ARP (at arrival time) is given by r. ion indicates the ionospheric influence on each frequency, which has opposite impact on phase and code. It is assumed that the observations are already corrected for relativistic and clock effects. B denotes the float ambiguities that are estimated in the POD process. Furthermore, a phase wind-up model W is used. Finally, the PCV and CRV map corrections are represented by PCV_{Em} and CRV_{Em}, (with Em indicating the maps are empirical). After converging the PCV_{Em} the CRV_{Em} is obtained accordingly. An iterative scheme is used to compute the PCV maps:

$$\begin{aligned} \Delta PCV(k) &= L_o - L_m \\ PCV_{Em}(k+1) &= PCV_{Em}(k) + \Delta PCV(k) \end{aligned} \tag{2.2}$$

where k is the index of iteration and L_o represents the phase observation. It is found that for the generation of PCV maps five iterations are sufficient to reach convergence after which no further improvement could be observed in *e.g.* fit of external SLR observations (*cf.* Jäggi et al. (2009); Van Barneveld (2012)). During this process, no CRV maps are computed. After the convergence of PCV maps, the CRV maps are computed using a similar iterative approach. The same five iterations are performed, leading to sufficient convergence.

2.3. Precise orbit determination

This research is accomplished using the GPS High precision Orbit determination Software Tools (GHOST), which is a POD software package developed by DLR/GSOC (German Space Operations Center) with support from TU Delft (Wermuth et al., 2010). In addition, use is made of a GHOST add-on tool for Multiple satellites Orbit Determination using Kalman filtering (MODK) (Van Barneveld, 2012). All approaches are implemented based on GPS transmitter antenna maps issued by IGS, and ionospheric maps, GPS orbits and 5s GPS clocks products issued by the Center of Orbit Determination in Europe (CODE) (Dach et al., 2016, 2015; Dow et al., 2009). The satellite dynamic modeling consists of three parts: (1) gravitational forces, including a mean gravity field of the Earth which is described by

the GOCO03S model (Mayer-Gürr et al., 2012), third body perturbations by the Moon and the Sun, and solid-Earth and ocean tides (Lyard et al., 2006), (2) non-gravitational forces, including atmospheric drag (Jacchia, 1977) and solar radiation pressure (each spacecraft is currently modeled as canon ball with a mass of 500 kg and cross-sectional area of 1.0 m^2), and (3) empirical accelerations. The drag coefficient C_D and solar radiation coefficient C_R are estimated to partly compensate for non-gravitational force model errors due to the simplified spacecraft model (Table 2.1). Empirical accelerations are part of the set of estimated parameters and will further compensate force model errors. In the EKF, the correlation time (τ), the a-priori values (σ_a) and the process noise (σ_p) of empirical accelerations have to be set. The employed models, parameters and preprocessing settings are summarized in Table 2.1.

For both the single-satellite absolute and dual-satellite relative POD schemes, three different solutions are generated to assess the cumulative impact of first including PCV maps and second CRV maps. Thus, first a solution is generated without the use of these maps (in the following referred to as *ARP*). Second, PCV maps are used (referred to as *+PCV*) and third CRV maps are included as well (referred to as *+CRV*).

2.3.1. Single-satellite absolute orbit determination

For single-satellite POD, two POD schemes are used: the kinematic and the reduced-dynamic methods. The geometric strength of the GPS tracking system allows a purely kinematic POD for LEO satellites. The GHOST implementation employs a weighted linearized Bayesian batch least squares estimator to process undifferenced GPS observations. Kinematic position estimates can be provided only for those epochs for which a sufficient number of satellites (≥ 4) is in view simultaneously. For high-quality kinematic orbit solutions, it is thus important to have a continuously working GPS receiver with no (big) data gaps. Spurious GPS observations are eliminated by applying the thresholds included in Table 2.1. Thresholds are defined for the signal to noise ratio, elevation cutoff angle and code/phase outliers. The estimated parameters are 3-dimensional position coordinates and clock corrections on an epoch-by-epoch basis and phase float ambiguities.

The reduced-dynamic POD is based on a weighted Bayesian batch least squares estimator with the same data editing scheme, where use is made of detailed force models and numerical integration to solve the equations of motion and variation. The estimated parameters include the position and velocity at the start of the orbital arc, a solar radiation coefficient, an atmospheric drag coefficient, epoch-wise clock corrections, empirical accelerations and phase float ambiguities, as summarized in Table 2.1. The reduced-dynamic POD is more robust and is better capable of handling data gaps (Visser and Van den IJssel, 2003).

The ionosphere-free PCV patterns are very persistent and stable over time (Jäggi et al., 2009). However a sufficiently long time span is required to accumulate an adequate number of observations in each grid cell or bin and to avoid bins that are empty. The latter might cause artefacts when in POD interpolations take place between those empty bins and bins that are filled. To ensure enough observations, for

Table 2.1: Overview of settings employed in the GHOST software package for POD of GRACE.

Spacecraft model	500 kg canon-ball with cross-section of 1.0 m^2	
Gravitational forces	GOCO03S 120×120 (selectable, maximum 250×250) static gravity field, plus linear trends for spherical harmonic degree 2 terms according to IERS2003 (McCarthy and Petit, 2004) Luni-Solar third body perturbations CSR ocean tides model based on TOPEX and GRACE data (use FES2004 as reference)	
Non-gravitational forces	Atmospheric drag: Cannon-ball model, Jacchia 71 density model Solar radiation pressure: cannon-ball model, conical Earth shadow, Sun flux data	
Earth parameters	Leap second data table of TAI-UTC IGS Earth rotation parameters, version 2.0	
GPS products	CODE GPS orbits and 5s GPS clocks IGS transmitter antenna phase center offsets and variations CODE ionospheric maps	
GPS data editing	Minimum signal to noise ratio : 5 Minimum cut-off elevation [deg] : 0 Code editing outliers [m] : 1.0 Phase editing outliers [m] : 0.015	
Orbit arc length	24 hours	
Settings	GHOST single-satellite absolute POD	MODK dual-satellites relative POD
Antenna patterns	Ionospheric-free combination patterns	Frequency-dependent patterns
Ambiguities	Float ambiguities	Integer ambiguities
Methodologies	Batch least squares	Iterative extended Kalman filter
C_D	1 per 24 hr, σ =2.3	1 per 24 hr, σ_a =1.3, σ_p =1.0
C_R	1 per 24 hr, σ =1.3	1 per 24 hr, σ_a =1.3, σ_p =0.5
Empirical acc.	Δt =600 s, σ =5/30/15 nm/s^2 Radial/Along-track/Cross-track	Radial: τ =600 s, σ_a =10 nm/s^2, σ_p =2 nm/s^2 Along-track: τ =600 s, σ_a =40 nm/s^2, σ_p =8 nm/s^2 Cross-track: τ =600 s, σ_a =20 nm/s^2, σ_p =4 nm/s^2
Differential empirical acc.		Radial : τ =600 s, σ_a =5 nm/s^2, σ_p =0.1 nm/s^2 Along-track: τ =600 s, σ_a =30 nm/s^2, σ_p =1 nm/s^2 Cross-track: τ =600 s, σ_a =10 nm/s^2, σ_p =0.3 nm/s^2
GPS data weighting	Code/Phase: 1.0/0.015 [m]	Frequency-dependent: Code/Phase: 0.3/0.015 [m] Single-difference : Code/Phase: 0.7/0.002 [m]
Amb. Validation		Probability test:99.9% Integer test:5% Discrimination test:5 Widelane test:5%,0.2 cycles Ionosphere free test:5%,0.01 m (Verhagen, 2005)

GRACE all GPS observations are used with the nominal time interval of 10 s between consecutive epochs. After preprocessing, on the average over 65 thousand code and phase observations are available for GRACE-A per day, and about 60 thousand for GRACE-B. When accumulating four months of data, the eventual numbers are more than sufficient to conduct reliable POD and antenna map estimations.

2.3.2. Dual-satellite and relative orbit determination

In the work by Kroes (2006), the orbit of the GRACE-A satellite is read from a reference orbit file and then kept fixed. The baseline between the GRACE satellites is determined by computing the orbit of the GRACE-B satellite relative to GRACE-A. In that case, only the relative empirical accelerations are estimated which can be constrained more than the absolute empirical accelerations, since it is assumed that mis- or unmodeled accelerations are largely the same for the two GRACE satellites. Therefore the precision of GRACE-B orbit is downgraded in terms of SLR validation. In the MODK tool developed by Van Barneveld (2012), which is used for our research, the absolute orbits of the two GRACE satellites are both estimated, where at the same time the highest possible precision for baseline determination is aimed at by fixing as many DD phase integer ambiguities as possible. Empirical accelerations are estimated for both GRACE satellites, where it is found to be crucial to also constrain the differences between these two sets of empirical accelerations, as indicated in Table 2.1.

An iterative EKF determining the baselines of multiple flying satellites is implemented in MODK. The same data editing scheme as for single-satellite POD applies to MODK, which models the GPS observations for both the f_1 and f_2 frequencies. Referring to the global ionospheric map which initializes the a priori values for the corresponding EKF matrix entries, the ionospheric delays between a tracked GPS satellite and a GRACE satellite are estimated on the first frequency. It is multiplied by the factor of $(f_1/f_2)^2$ to get the delays on the second frequency. The empirical accelerations are modeled as Gauss-Markov processes in an EKF estimation scheme.

It has been shown by *e.g.* Kroes (2006), Allende-Alba and Montenbruck (2016), and Jäggi et al. (2007) that the fixing of DD phase integer ambiguities is crucial for obtaining the best possible baseline solutions for GRACE from GPS observations. By forming DD GPS observations, errors such as GPS orbit/clock bias and receiver clock offsets are eliminated, and the DD ambiguities take in principle integer values. Over the years many strategies for resolving ambiguities have been developed, such as integer rounding, bootstrapping, or wide-lane/narrow-lane combination. The LAMBDA (Least-squares Ambiguity De-correlation Adjustment) method is proved to be highly successful for baseline determination (Teunissen, 1995), therefore it is used in this paper. The used EKF implementation allows multiple iterations, where each iteration consists of a forward and backward filter step, plus a smoother based on covariance information from both filter steps. The covariance information is fed to the LAMBDA algorithm together with the estimated float ambiguities in order to arrive at integer ambiguities.

To minimize the negative impact wrongly fixed ambiguities would have on the

precision of baseline solution, the used LAMBDA implementation adopts a sequence of very strict validations (Table 2.1, (Verhagen, 2005)). A partial fixing strategy is used to reorder the ambiguity sets: when the set of all ambiguities at one epoch can not be fully fixed, the least likely ambiguity will be taken out. This process repeats until the remaining ambiguities are fixed and pass the validation criteria. When the number of fixed ambiguities does not change significantly in three consecutive iterations, the EKF terminates and yields the converged satellite states. It has to be noted that the EKF implementation can also be used for single-satellite POD, where thus no use is made of DD phase observations. In this mode, the frequency-dependent antenna patterns could be determined.

2.4. Results and discussion

This section first briefly discusses the computed PCV and CRV maps (Section 2.4.1), followed by POD results. The discussion of results includes quality assessments through both internal consistency checks (Section 2.4.2) and external validations (Section 2.4.3).

2.4.1. Antenna patterns

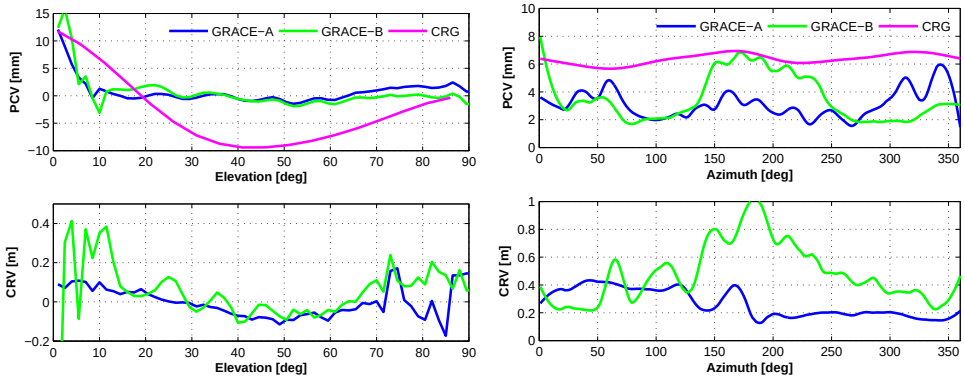

Figure 2.3: Mean (left) and RMS about mean (right) of ionosphere-free combined PCV and CRV map grid values as a function of elevation and azimuth for the GRACE-A/B antennas. The PCV map obtained by the ground campaign is indicated by CRG (analyzed period: DOY 213-334, 2014).

Characteristics of the GRACE PCV and CRV maps obtained by the *residual approach* are displayed in Figure 2.3. Please note that the maps are obtained with the EKF implementation in single-satellite mode. For each GPS frequency separate PCV and CRV maps are created, the ionosphere-free maps are then obtained by combining these maps with the associated multiplication factors. The maps consist of grids that are equiangular in azimuth and elevation with a cell or bin size of $1.5° \times 1.5°$. The average PCV and CRV map corrections are shown as a function of elevation (average statistics of all azimuth bins at same elevation), where for the PCV map the average corrections based on the ground campaign (CRG) (Garcia

and Montenbruck, 2007) are included for comparison. In addition, the Root-Mean-Square (RMS) about mean of the corrections as a function of azimuth are included. The latter reflects that along certain directions, the corrections are more variable.

It can be observed that the PCV maps are very different from the one obtained by the ground campaign (Figure 2.3), confirming the importance of using in-flight calibrations. In general, the phase residual level for GRACE-A is higher than for GRACE-B. However it can be observed in Figure 2.3 and Figure 2.6 that the code and phase corrections for August-November 2014 are larger for GRACE-B: much bigger phase and code residuals occur at low elevations (elevations between 5° and 15°), at azimuths especially between 120° and 240°, due to the cross-talk interference between the GRACE-B main POD antenna and the radio occultation antenna (located on the rear side of GRACE-B). The CRV map reaches to values of up to 1 m, showing that initial phase float ambiguity estimates can be seriously affected.

It has to be noted that the large values for the mean of the CRV maps for elevations close to 90° are caused by the small number of observations in the central grid cells or bins. It is interesting to note that more observations are collected at certain azimuth angles (indicated by the stripes in Figure 2.4), which illustrates the local horizon for GPS satellites in the different orbital planes as seen from the GRACE polar orbit (Jäggi, 2007). The GRACE-A/B PCV and CRV maps obtained by the *residual approach* are displayed in Figures 2.5-2.6. These Figures include the maps for the GPS L1 and L2 frequencies and the associated ionosphere-free combination.

When analyzing the CRV maps, it can be seen that the cross-talk interference between the GPS occultation and POD antenna strings lead to significantly larger CRV map values for GRACE-B in part of the pattern. The single frequency code residuals reach levels of up to 0.4 m, leading to up to 1.0 m for ionosphere-free combinations. These high values are most prominent at the antenna rear segment, which is closer to the occultation antenna. For GRACE-A, the CRV maps display much less pronounced and smaller patterns, which confirms that the associated radio occultation antenna is switched off. Noticeable is a cross-track asymmetry in the ionosphere-free CRV maps for both GRACE-A and -B (*e.g.* negative values for azimuths between 180° and 270°). It can be anticipated that this asymmetry will especially influence orbit solutions in the cross-track direction.

2.4.2. Internal consistency

This Section contains the results and quality assessments for the single-satellite absolute and dual-satellite relative POD, both in terms of absolute and relative orbit solutions.

Single-satellite orbit determination

As indicated above, three series of kinematic and reduced-dynamic single-satellite orbit solutions are generated, referred to as *ARP*, *+PCV* and *+CRV*, allowing to assess the impact of the cumulative addition of PCV and CRV maps. The internal consistency of these solutions is assessed by (1) analysis of observation residuals,

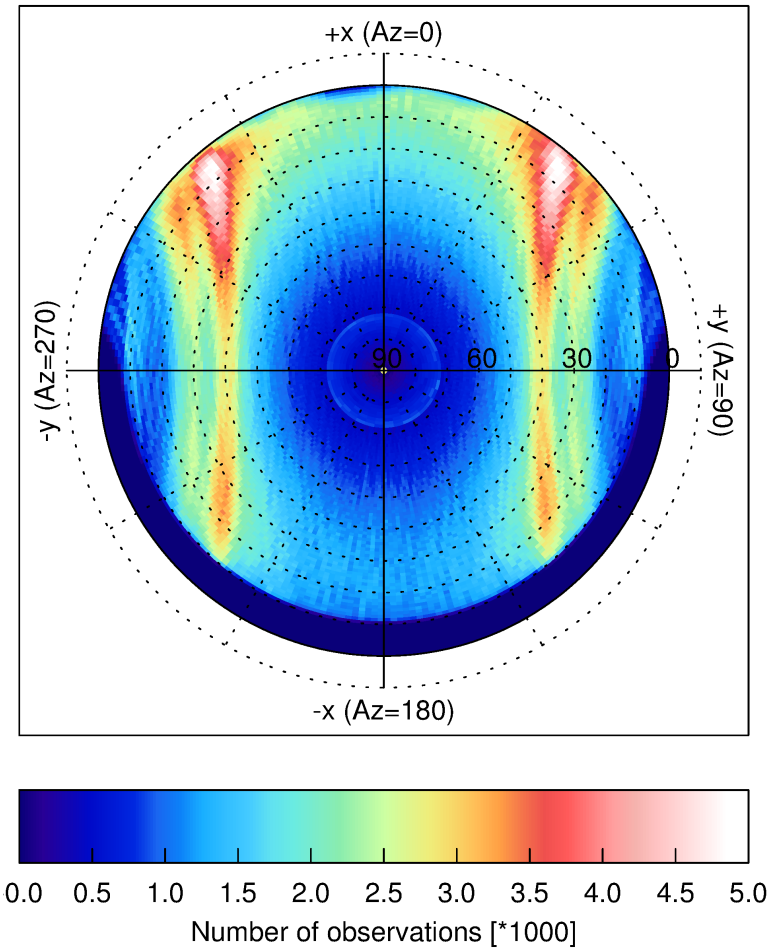

Figure 2.4: Number of observations collected by the POD antenna of the BlackJack receiver on board of GRACE-A (DOY 213-334, 2014).

(2) ephemeris comparison between the different orbit solutions and (3) the analysis of estimated empirical accelerations and non-gravitational force coefficients.

It is anticipated that the application of PCV and CRV maps will lead to lower observation residuals. In case of a proper implementation of the *residual approach*, this should in fact be the case. Ideally, the remaining residuals are caused by random observation noise and all systematic effects are eliminated. The RMS about mean of the ionosphere-free phase and code residuals is displayed in Table 2.2 for the different orbit solutions. It can be observed that the phase residuals are reduced significantly when including PCV maps (*+PCV vs.* ARP): for GRACE-A and -B from 5.27 to 4.55 mm and from 5.13 to 3.87 mm, respectively, for reduced-dynamic POD. Although GRACE-B experienced strong interference, its overall phase residual level

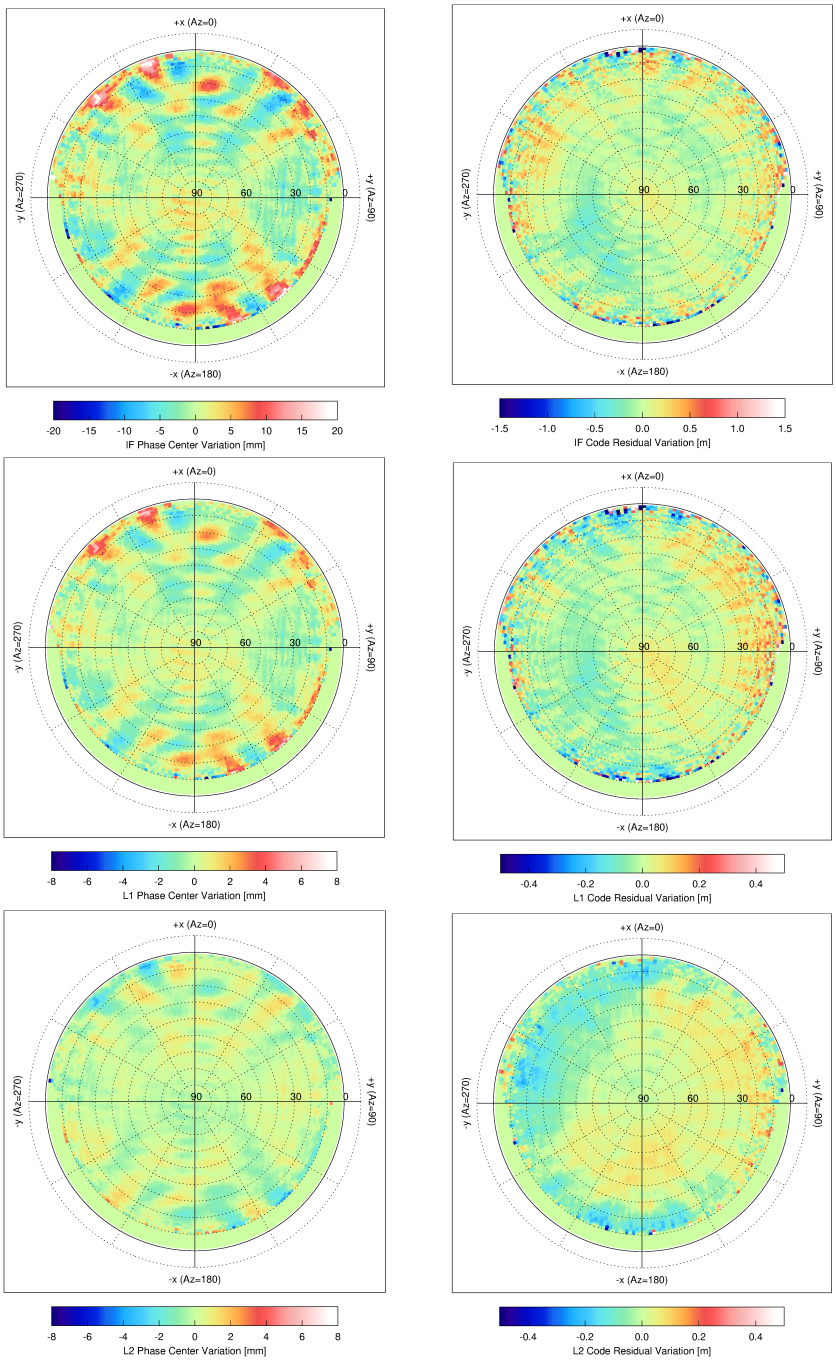

Figure 2.5: The in-flight PCV (left) and CRV (right) maps: ionosphere-free (top), f_1 frequency (middle) and f_2 frequency (bottom) for GRACE-A in the NEU reference frame. Please note that for GRACE-A the X-axis is opposite to the velocity vector. Note that each plotted bin represents the mean value of observation residuals as obtained by the *residual approach* (DOY: 213-334, 2014).

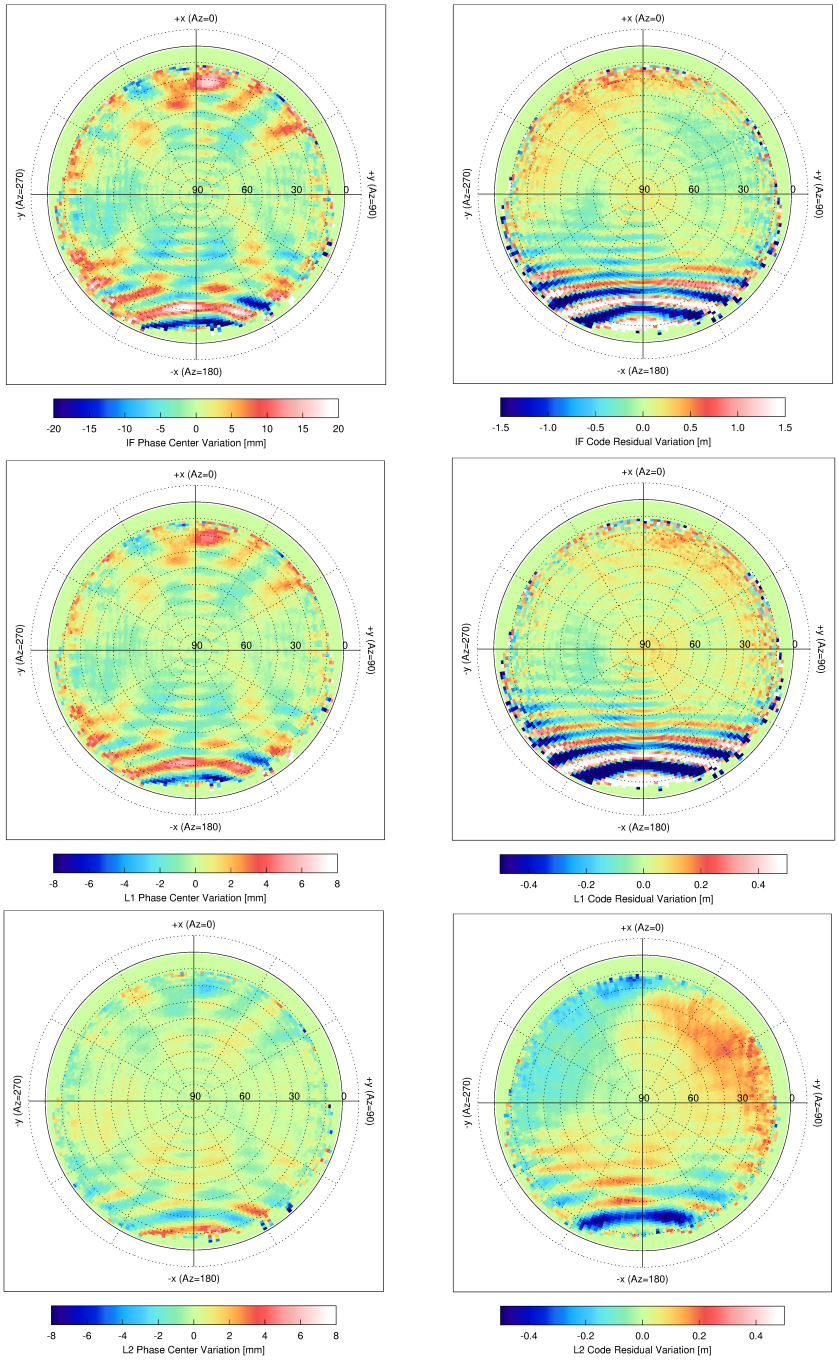

Figure 2.6: The in-flight PCV (left) and CRV (right) maps: ionosphere-free (top), f_1 frequency (middle) and f_2 frequency (bottom) for GRACE-B in the NEU reference frame. Please note that for GRACE-B the X-axis is in the direction of the velocity vector. Note that each plotted bin represents the mean value of observation residuals as obtained by the *residual approach* (DOY: 213-334, 2014).

Table 2.2: RMS of code and phase residuals of reduced-dynamic (RD) and kinematic (KIN) solutions for single-satellite POD of the GRACE twin satellites (DOY: 213-334, 2014).

Spacecraft	Pattern	Code[m]		Phase[mm]	
		RD	KIN	RD	KIN
GRACE-A	*ARP*	0.54	0.54	5.27	3.57
	+PCV	0.54	0.54	4.55	3.10
	+CRV	0.54	0.54	4.55	3.04
GRACE-B	*ARP*	0.55	0.54	5.13	3.36
	+PCV	0.55	0.54	3.87	2.53
	+CRV	0.45	0.45	3.87	2.49

Table 2.3: Mean and RMS about mean (cm) of orbit differences between reduced-dynamic (RD) and kinematic (KIN) single-satellite POD for GRACE-A and -B (DOY: 213-334, 2014).

Spacecraft	Pattern	Radial	Along-track	Cross-track
GRACE-A	*ARP*	0.1+/-3.4	0.1+/-2.4	-2.5+/-2.2
	+PCV	0.0+/-3.2	0.0+/-2.3	-3.3+/-2.0
	+CRV	0.0+/-2.9	0.0+/-2.1	-0.4+/-1.9
GRACE-B	*ARP*	0.5+/-3.5	0.0+/-2.3	3.1+/-2.1
	+PCV	0.1+/-3.0	0.0+/-2.1	2.6+/-1.9
	+CRV	0.1+/-3.0	0.0+/-2.0	0.4+/-1.9

is lower. For kinematic orbit determination, the reduction is less pronounced, which can be explained by the large number of epoch-wise kinematic position coordinates that are estimated. This large number of estimated parameters leads to a larger freedom for absorbing the (systematic) PCV (if uncorrected). These results are largely consistent with those reported in Montenbruck et al. (2009): differences can be explained by the choice of a different data period (27 September - 7 October, 2007), the use of shorter interval 5 s GPS clock products in this research and possibly the different data editing thresholds and dynamic models.

In order to reduce the risk of including artefacts due to outliers in the CRV maps, a rather aggressive code observation editing scheme is adopted as specified in Table 2.1. Moreover, several POD test runs with GHOST showed that the data weighting of the phase and code observations, especially the relative weighting, has a significant impact on the orbit solution quality. The applied uniform observation weights has been selected by a trial and error procedure using SLR observations for external validation (see also Section 2.4.3). The corresponding values are specified in Table 2.1.

The resulting CRV map leads to a reduction of the ionosphere-free code residuals from 55 to 45 cm for GRACE-B in terms of RMS about mean, whereas for GRACE-A hardly a reduction can be observed (Table 2.2). The effect of the cross-talk, and the intrinsically lower noise levels for GRACE-B, are thus again confirmed.

Second, the quality of orbit solutions is checked internally by comparing the kinematic and reduced-dynamic single-satellite orbit solutions with each other for the three different solutions *ARP*, *+PCV* and *+CRV*. The mean and RMS about mean of orbit differences are displayed in Table 2.3. It is interesting to note that the PCV maps result in a similar offset in the cross-track direction of around 0.8 and 0.5 cm for GRACE-A and -B, respectively. However, this PCV-induced cross-track orbit shift has a different sign for each satellite, reasoning that the X-axis of one antenna frame points along the flight direction while the other points to the opposite. When using the CRV maps as well, the coherence of the kinematic and the reduced-dynamic orbit solutions improves significantly, which is due to the much better consistency in the cross-track direction. The mean cross-track offset is reduced to 0.4 cm for both satellites, which can be explained by the asymmetry observed and mentioned earlier in Section 2.4.1 (see also Figures 2.5 and 2.6). Especially the kinematic orbit solutions turn out to be sensitive to the CRV map corrections. Figure 2.7 indicates the cross-track offsets of GRACE-B orbit solutions *+PCV* and *+CRV* in comparison with solution *ARP*. It can be seen that the CRV maps further shift both the reduced-dynamic orbit (0.5 cm) and especially the kinematic orbit (2.7 cm) in the cross-track direction.

Furthermore, the shift of RD orbit has a strong correlation with the beta angle, which is the angle between the satellite orbital plane and the direction to the Sun. When including PCV and CRV maps, the RD orbit is shifted according to the beta angle, emphasizing that the use of these maps compensates the mis-modeling of satellite dynamics, mostly the solar radiation pressure modeling.

It is interesting to look at the impact of the PCV and CRV maps on the estimated empirical accelerations, solar radiation coefficient (C_R) and drag coefficient (C_D), for which results are displayed in Figures 2.8 and 2.9. For GRACE-B, it can be observed that the mean of the radial empirical accelerations is reduced significantly when using PCV maps. The CRV maps then hardly change this mean. For the along-track direction, the impact is small, whereas for the cross-track direction the mean of the empirical accelerations is reduced significantly by using PCV maps and even - again significantly - more when also using CRV maps. In addition, it can be observed that the solar radiation coefficients are changed significantly by using PCV maps, and slightly more when using CRV maps as well.

For GRACE-B, the use of the PCV maps results in a mean shift of the empirical accelerations in the radial direction of 1.2 nm/s^2 (Figure 2.8), which is commensurate with the shift in terms of mean radial position of 1 mm (Table 2.5). When using the PCV and CRV maps, the estimate of the cross-track empirical accelerations is reduced from 4.1+/-19.7 nm/s^2 to 1.6+/-18.9 nm/s^2. It can thus be concluded that the use of not only the PCV, but also the CRV maps, not only increases the consistency between orbit solutions, but also compensates the mis-modeling of non-gravitational forces.

Dual-satellite orbit determination

For dual-satellite POD, which not just aims at the best precision possible for the single-satellite orbit solutions but more importantly for the baseline between the

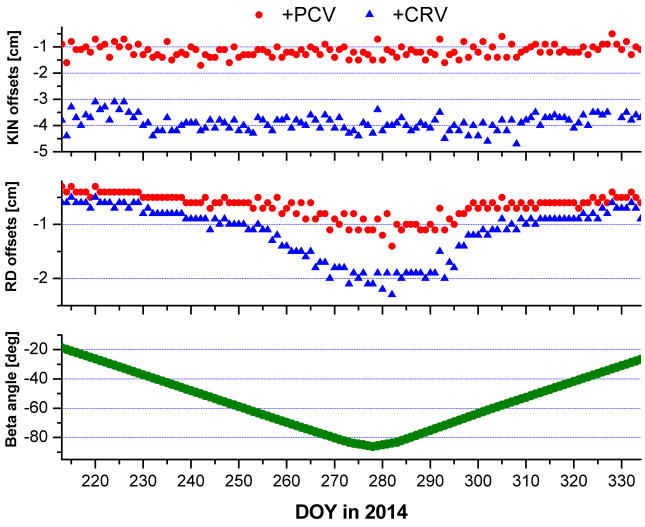

Figure 2.7: The GRACE-B cross-track orbital offsets for kinematic (top) and reduced-dynamic (middle) solutions when using different antenna maps in comparison with the reference *ARP* solution, the beta angle during this period is shown (bottom) (DOY: 213-334, 2014).

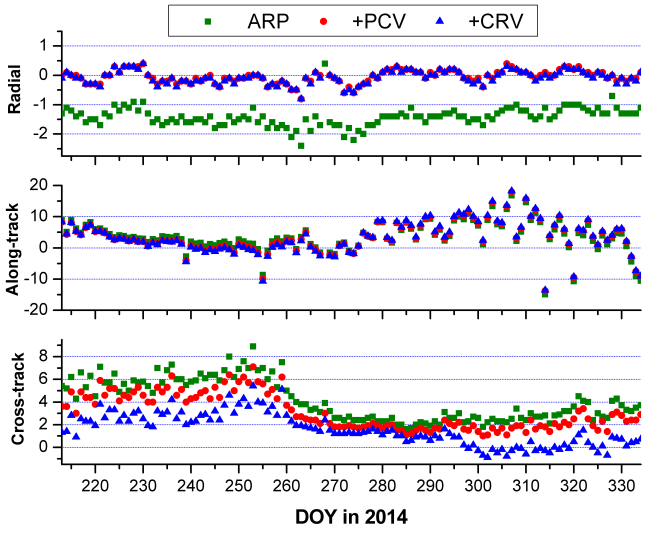

Figure 2.8: The mean of estimated empirical accelerations for GRACE-B reduced-dynamic POD (nm/s^2) when using different antenna maps (DOY: 213-334, 2014).

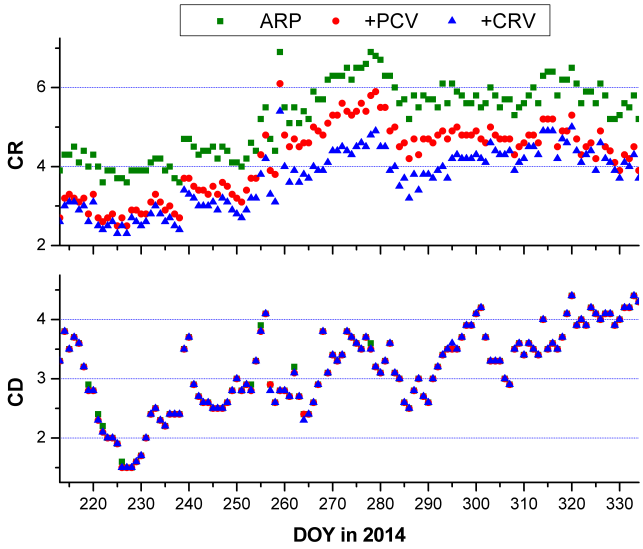

Figure 2.9: The GRACE-B estimated solar radiation (top) and drag (bottom) coefficients when using different antenna maps (DOY: 213-334, 2014).

Table 2.4: Frequency-dependent phase and code residual RMS for the two GRACE satellites based on EKF dual-satellite orbit determination (DOY: 213-334, 2014)

Index	GRACE-A			GRACE-B		
	ARP	+ PCV	+ CRV	ARP	+ PCV	+ CRV
Data [%]	88.0	88.0	88.4	93.1	93.1	94.0
C1W [m]	0.19	0.19	0.18	0.19	0.19	0.16
C2W [m]	0.17	0.17	0.17	0.16	0.16	0.12
L1 [mm]	2.25	2.11	2.05	2.15	1.96	1.89
L2 [mm]	1.52	1.44	1.37	1.47	1.31	1.22

two satellites, use is made of the EKF method as outlined in Section 2.3.2. In this method, GPS observations are modeled for each GPS frequency instead of ionosphere-free combinations. This means that for each frequency separate PCV and CRV maps are used. These separate maps are needed for properly assessing the impact on DD phase ambiguity resolution, which is indispensable for achieving the best baseline precision possible. GPS observations weights are according to Table 2.1, note that for single-differenced GPS observations more weight should be put on phase to better initialize ambiguities fixing.

Just as for the single-satellite POD, the PCV maps result in a significant reduction of the phase observation residuals, in this case for both frequencies (Table 2.4). These residuals are reduced slightly more when using also CRV maps. In total,

the reduction is from 2.25/1.52 to 2.05/1.37 mm for GRACE-A (L1/L2), and from 2.15/1.47 to 1.89/1.22 mm for GRACE-B (L1/L2), respectively. When using the CRV maps, the code residual RMS is reduced from 19/17 to 18/17 cm for GRACE-A (C1W/C2W), and from 19/16 to 16/12 cm for GRACE-B (C1W/C2W), respectively. It is, however, interesting to note that the use of CRV maps leads to - be it small - reductions of the RMS about mean of phase residuals. For GRACE-B clearly a bigger reduction is obtained for the code residual RMS (also after data processing, about 0.9% more of the observations are used in the POD process). Below, the question will be addressed how these reduced residual levels impact the precision of the dual-satellite orbit and baseline solution, and in conjunction the DD phase ambiguity fixing.

Figure 2.10 (top) displays the ambiguity fixing success rate for one representative day, namely DOY 219 in 2014, for the three EKF orbit solutions. It can be observed that for the first iteration, this success rate improves from 53.2% to 66.8% when using PCV maps, and a further improvement to 87.3% is obtained when using CRV maps as well. The ambiguity fixing by the EKF method thus seems to have a more robust initialization when using CRV maps in conjunction with PCV maps. Moreover, after the first iteration the consistency with KBR observations is improved considerably from 0.93 to 0.52 mm when using PCV maps, and the inclusion of CRV maps even leads to a slightly better consistency of 0.47 mm (Figure 2.10, bottom). Normally ten iterations are set in EKF and convergence can be assured. However after the use CRV maps, typically a few iterations can be saved to reach the eventual convergence (for this representative day eight iterations are sufficient).

Figure 2.11 displays EKF results for the full period. The results in this figure confirm especially the positive impact of CRV maps on the ambiguity fixing. Compared to only using PCV maps, the use of CRV maps results in two further improvements: (1) on average more than 130 additional ambiguities are fixed leading to a final success rate of 95.3%, (2) the fixing rate for the first iteration is greatly increased from 62.3% to 81.7%. It has to be noted that the baseline precision is not improved by CRV maps consistently. For about 40 out of 122 days the KBR validations show a slightly worse solution by about 0.01 mm level. It has to be noted that even the rather strict validation scheme can not detect all wrongly fixed ambiguities, as occasional jumps can be observed in the KBR validation results.

Figure 2.12 depicts the additional DD phase ambiguities that are fixed after using the CRV maps (*+CRV*) compared to using only PCV maps (*+PCV*). It can be seen that indeed more ambiguities are fixed when using CRV maps. Especially for GPS satellites with PRN numbers 1, 11, 14 and 19, new passes of phase observations are identified for which the ambiguities are fixed. At the end of some passes, the ambiguities fixing period is slightly extended. It can be concluded that the use of CRV maps speeds up the ambiguity fixing and in addition also increases the success rate.

2.4.3. External validation

In addition to the internal consistency checks in the previous Section 2.4.2, a number of external validation possibilities exists, which provide more insight in the ab-

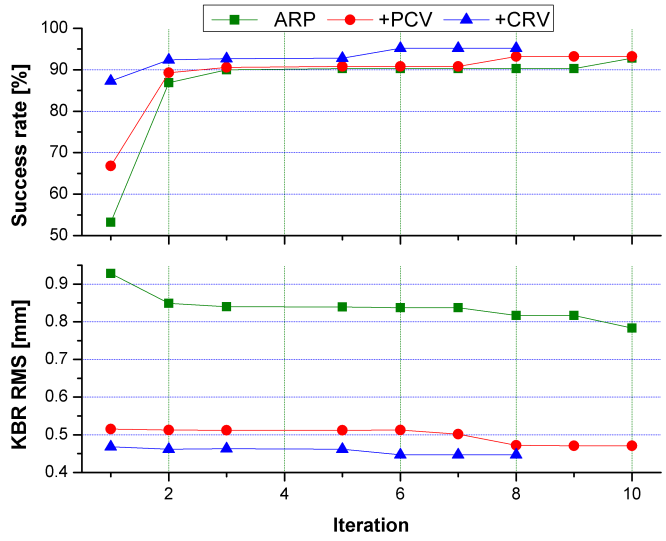

Figure 2.10: The ambiguity fixing success rate (top) and KBR baseline consistency (bottom) as a function of the number of EKF iterations (DOY 219, 2014).

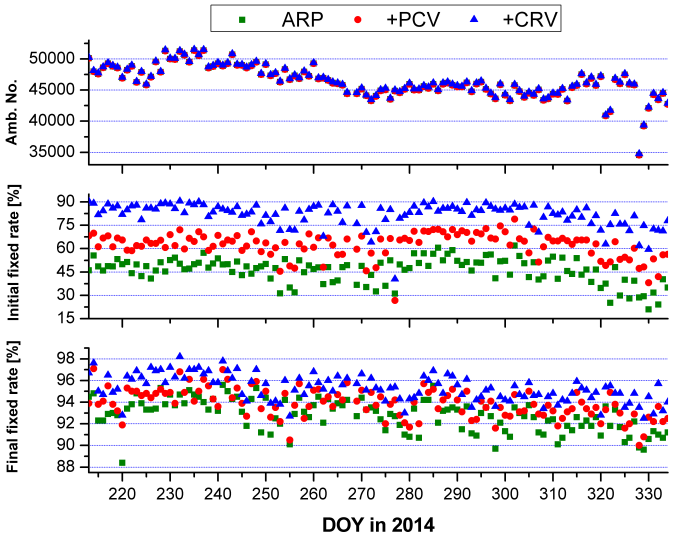

Figure 2.11: Number of daily fixed DD phase ambiguities (top), fixing success rate for the first iteration (middle) and the last iteration (bottom) for the three EKF solutions (DOY: 213-334, 2014).

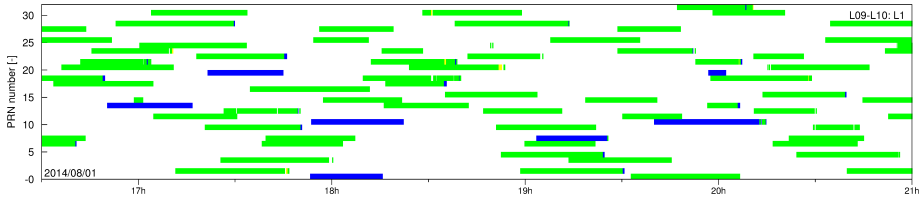

Figure 2.12: Integer ambiguities comparison between two solutions (*+PCV* as reference). Blue: ambiguities only existed in *+CRV* solution; Yellow: ambiguities only existed in *+PCV* solution; Green: same ambiguities existed in both solutions (DOY 213, 2014). (For interpretation of the references to color in this figure legend, the reader is referred to the web version of this article)

solute accuracy of orbit solutions and the impact on this accuracy of the inclusion of consecutive PCV and CRV maps. First, our orbit solutions are compared to those kindly provided by the Jet Propulsion Laboratory (JPL) in Pasadena, CA, USA. It might be argued that such a comparison is in fact not a pure external validation, since the same GPS observations are used for generating the orbit solutions. However, use is made of different software and processing schemes. As such, it is decided to include these comparisons in this section. Furthermore, we have compared our orbit solutions with SLR observations that are not used in the orbit computation itself. Finally, GRACE offers the nice and unique possibility to compare the baseline derived from the orbit solutions with the directly observed distance through the KBR measurements (with a claimed precision of the order of 1 μm). The latter provides especially a validation for the distance in the flight or along-track direction.

It is found that the use of PCV maps slightly enhances the consistency between the reduced-dynamic orbits computed in this research and JPL orbit solutions for all three directions: the RMS about mean is reduced. Moreover, the reduced-dynamic and kinematic orbits are shifted by the PCV maps: the mean offset referring to JPL orbit solutions is changed by a few mm (Table 2.5). It can be seen that the CRV map changes the offset of the of reduced-dynamic orbits in the cross-track direction by around 0.5 cm, which is comparable with the significance of the PCV maps. However, the kinematic orbits are shifted 2-3 cm for both satellites when using the same CRV maps. This result is consistent with the results included in Table 2.3, which confirms that the kinematic orbit solutions are significantly more affected by the CRV maps.

It is important to note that the GRACE orbit solutions computed by the dual-satellite mode of MODK have a slightly worse consistency with the JPL orbit solutions, especially for the along-track direction. It can be seen in Table 2.5 that for both GRACE satellites, the RMS-about-mean of along-track orbit differences increases by about 1.2 cm from single-satellite orbit comparison to dual-satellite orbit comparison. Fixing the ambiguities has a positive impact on the consistency with the KBR observations (see below), which provide predominantly information in the along-track direction.

The results of comparing the different orbit solutions with SLR observations are included in Table 2.6. In principle, the SLR observations offer the opportunity to

Table 2.5: Mean and RMS about mean (cm) of orbit differences between the orbit solutions in this research and JPL orbit solutions for GRACE-A and -B (DOY: 213-334, 2014).

Spacecraft	Pattern	Radial	Along-track	Cross-track
GHOST single satellite reduced-dynamic orbit				
GRACE-A	*ARP*	1.5+/-0.8	-0.2+/-1.3	-0.7+/-1.0
	+PCV	1.4+/-0.8	-0.1+/-1.3	-1.3+/-1.0
	+CRV	1.4+/-0.8	-0.1+/-1.2	-0.6+/-1.0
GRACE-B	*ARP*	1.4+/-0.8	0.4+/-1.4	0.9+/-1.0
	+PCV	1.3+/-0.8	0.4+/-1.3	0.2+/-1.0
	+CRV	1.3+/-0.8	0.4+/-1.3	-0.3+/-1.0
GHOST single satellite kinematic orbit				
GRACE-A	*ARP*	1.6+/-3.5	-0.1+/-2.8	-3.3+/-2.4
	+PCV	1.5+/-3.3	-0.1+/-2.7	-4.6+/-2.3
	+CRV	1.4+/-3.0	-0.1+/-2.5	-1.0+/-2.2
GRACE-B	*ARP*	2.0+/-3.6	0.4+/-2.7	4.0+/-2.3
	+PCV	1.4+/-3.2	0.4+/-2.5	2.9+/-2.1
	+CRV	1.4+/-3.1	0.4+/-2.4	0.1+/-2.1
MODK dual-satellite orbit solution				
GRACE-A	*ARP*	1.5+/-2.1	0.7+/-2.9	-0.5+/-1.5
	+PCV	1.4+/-2.1	0.0+/-2.4	-0.3+/-1.3
	+CRV	1.3+/-2.0	0.1+/-2.2	-0.3+/-1.2
GRACE-B	*ARP*	1.3+/-2.1	1.2+/-2.7	-0.4+/-1.4
	+PCV	1.3+/-2.1	0.6+/-2.5	-0.2+/-1.2
	+CRV	1.3+/-2.0	0.8+/-2.5	-0.3+/-1.2

assess the accuracy of the GPS-based orbit solutions in the direction of the line-of-sight between the SLR ground station and the LEO satellite. In order to eliminate spurious observations, an editing threshold of 30 cm is used, which is an order of magnitude above the RMS of fit levels, and observations below the 10° elevation cutoff angle are excluded. We select the following ten SLR stations in the validation scheme: Yarragadee, Papeete, Wettzell, Mount Stromlo, Herstmonceux, Graz, Greenbelt, Zimmerwald, Hartebeesthoek and Potsdam (note that four of them are located in the southern hemisphere). The exactly same dataset from these stations is applied to the validation of orbits from JPL in this research. The number of used SLR observations during this time span is 8135 for GRACE-A and 7614 for GRACE-B, respectively.

It is shown in Table 2.6 that for all the orbit solutions the RMS of fit of SLR observations does not improve significantly when using PCV maps. These fits are close to the values for the external JPL reduced-dynamic orbit solutions. Note that when PCV maps are included, the kinematic orbit of GRACE-A show slightly decreased SLR residuals. It could be due to the cross-track orbit shift, which also leads to a larger offset compared with the JPL orbits in the cross-track direction. The inclusion of CRV maps hardly improves the fit of SLR observations for reduced-

Table 2.6: Mean and RMS of fit (cm) of SLR observations for the different orbit solutions. The values for the external JPL solutions are included for reference.

Spacecraft	Pattern	RDOD	KIN	MODK
GRACE-A	*ARP*	-0.6+/-2.2	-1.0+/-3.6	-0.4+/-2.8
	+PCV	-0.6+/-2.2	-1.0+/-4.1	-0.6+/-2.6
	+CRV	-0.6+/-2.1	-0.8+/-2.9	-0.6+/-2.5
	JPL	0.4+/-1.8		
GRACE-B	*ARP*	-0.3+/-2.1	-0.7+/-3.6	-0.1+/-2.7
	+PCV	-0.3+/-2.0	-0.4+/-2.9	0.1+/-2.6
	+CRV	-0.3+/-2.0	-0.4+/-2.5	0.0+/-2.5
	JPL	0.6+/-1.9		

dynamic and MODK orbit solutions, but does so for kinematic orbit solutions: from 3.6 to 2.9 cm for GRACE-A, and from 3.6 to 2.5 cm for GRACE-B, respectively. It can be seen that the GRACE dual-satellite orbit solutions obtained with MODK have a slightly worse consistency with the SLR observations than the single-satellite GHOST GRACE orbit solutions. The increase is from 2.1 to 2.5 cm and from 2.0 to 2.5 cm for GRACE-A and -B, respectively. Current results thus seem to show that improved baseline solutions (KBR validated baseline precision, Table 2.7) come with a slightly degraded absolute orbit precision.

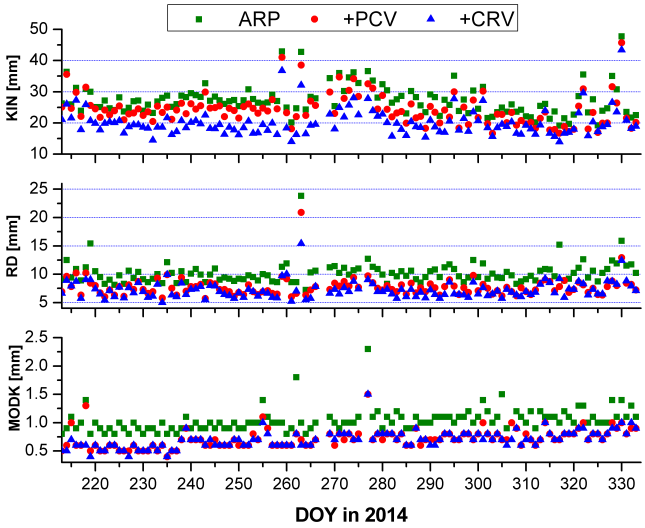

Figure 2.13: KBR validation of undifferenced kinematic orbits(top), undifferenced reduced-dynamic orbits (middle) and double-differenced EKF orbits (bottom) (DOY: 213-334 2014).

Table 2.7: RMS about mean (mm) of differences between KBR observations and the baselines derived from the GRACE-A/B single-satellite reduced-dynamic, kinematic and EKF dual-satellite orbit solutions (DOY: 213-334, 2014).

Pattern	RDOD	KIN	DD baseline
ARP	10.240	27.524	1.170
+PCV	7.732	24.438	0.715
+CRV	7.209	20.189	0.699
JPL	5.939		

As indicated in Figure 2.13, the single-satellite GRACE-A/B orbit solutions have also been compared against the KBR measurements. The largest improvement in consistency between the GHOST GRACE-A/B orbit solutions and the KBR measurements is obtained by using the PCV maps: the RMS about mean is decreased from 10.240 to 7.732 mm and from 27.524 to 24.438 mm for the undifferenced reduced-dynamic and kinematic orbit solutions, respectively. The incremental use of CRV maps further improves the consistency: from 7.732 to 7.209 mm, and from 24.438 to 20.189 mm, for the reduced-dynamic and kinematic orbit solutions, respectively. The consistency for the JPL orbit solutions is included as reference and shows to be superior at a level of 5.939 mm in Table 2.7. However, this last value can be explained by the different methodology employed for the generation of the JPL solutions. This methodology relies on a data preprocessing scheme, which includes carrier-smoothing of code pseudo-range observations. The longer 30-hours data arcs (centered at 12:00 AM) are computed and then smoothed with adjacent orbits to obtain a better 24-hours orbit product. More importantly, single-receiver integer ambiguity resolution using JPL GPS orbit and clock products is applicable in the used GIPSY-OASIS software after May, 2009 (Bertiger et al., 2010). In this research the single-satellite GHOST orbit solutions are based on individual single-satellite POD using 24 hours orbit arcs, without integer ambiguity resolution.

Table 2.7 also includes the validation results for the EKF baseline solutions. The consistency with the KBR observations improves from 1.170 to 0.715 mm when using PCV maps, and improves slightly further to 0.699 mm when also using CRV maps for this four months period in 2014. These results thus also confirm that fixing integer ambiguities leads to a significantly improved consistency with the very high-precision KBR observations.

2.5. Summary

When adopting single-satellite POD strategies that are based on undifferenced GPS observations, the results in this paper confirm the importance of using in-flight calibrated PCV maps, as the maps significantly enhance the phase modeling and lead to lower residual levels. In addition, when using the single-satellite solutions for both GRACE satellites, a better consistency with the KBR observations is obtained. The inclusion of CRV map corrections leads to especially more consistent kinematic

orbit solutions. The biggest impact can be observed for the cross-track direction of the kinematic orbit solutions: systematic mean offsets with respect to reduced-dynamic orbit solutions almost disappeared.

The use of CRV maps is especially beneficial in the presence of cross-talk between multiple switched-on antennas, which was the case for GRACE-B in the selected data period of August-November 2014. The use of the CRV maps does not only lead to more consistent orbit solutions, but also to a significant reduction of frequency-dependent and thus also ionosphere-free combination code residuals.

For dual-satellite POD, where the aim is to achieve the best precision for the baseline which necessitates the resolution of so called DD phase integer ambiguities, both PCV and CRV maps lead to higher ambiguity resolution success rates. In addition, the use of CRV maps improves the efficiency and effectiveness of the iterative EKF. In the first iteration, the use of CRV maps leads to a significantly increased ambiguity fixing rate of 81.7%. After convergence, on the average about 95.3% of the ambiguities are fixed. Moreover, a consistency with KBR observation of better than 0.7 mm is obtained for the whole period. The ambiguity fixing however appears to result in a slightly degraded precision of the absolute orbits. An important topic for future research is to investigate if it is possible to improve not only the baseline precision in a dual-satellite solution strategy, but also the absolute orbit solutions. Data arcs longer than four months or obtained from other periods in the GRACE mission lifetime, could be analyzed to check the stability of the PCV maps and the CRV maps. Other code/phase weighting strategies than uniform weighting are also recommended to be investigated.

The combination of PCV and CRV maps leads in all cases to a - be it slightly - better consistency between GHOST and JPL orbit solutions, SLR observations and KBR measurements. For kinematic orbit solutions, the CRV maps result in an extra improvement of the consistency with the external SLR observations and KBR measurements.

Acknowledgment

The China Scholarship Council (CSC) is gratefully acknowledged for financially supporting part of the work described in this paper. All necessary GRACE L1B data are obtained from the Physical Oceanography Distributed Active Archive Center (PODAAC) of the Jet Propulsion Laboratory (JPL), Pasadena, California. Other data files such as GPS ephemeris/clock products and force model related files, are downloaded from the Center for Orbit Determination in Europe (CODE), Bern, Switzerland, and the NASA Goddard Space Flight Center (GSFC), Greenbelt, Maryland. At last, we would like to specially thank three anonymous reviewers for their insightful comments on the paper.

3

Swarm-A/C Formation Baseline Determination

RQ.2 How is PBD influenced by the in-flight performance of GPS receivers and in conjunction with receiver settings?

This chapter presents the PBD investigation for the Swarm-A/C pendulum formation. In total 30 months of data - from 15 July 2014 to the end of 2016 - are used. The influences of GPS receiver modifications and ionospheric scintillations are assessed.

The impact of GPS receiver modifications and ionospheric activity on Swarm baseline determination

Xinyuan Mao[a], *Pieter Visser*[a], *Jose van den IJssel*[a]

Published in *Acta Astronautica*, 146 (2018) 399–408,
doi:10.1016/j.actaastro.2018.03.009.

3

The European Space Agency (ESA) Swarm mission is a satellite constellation launched on 22 November 2013 aiming at observing the Earth geomagnetic field and its temporal variations. The three identical satellites are equipped with high-precision dual-frequency Global Positioning System (GPS) receivers, which make the constellation an ideal test bed for baseline determination. From October 2014 to August 2016, a number of GPS receiver modifications and a new GPS Receiver Independent Exchange Format (RINEX) converter were implemented. Moreover, the on-board GPS receiver performance has been influenced by the ionospheric scintillations.

The impact of these factors is assessed for baseline determination of the pendulum formation flying Swarm-A and -C satellites. In total 30 months of data - from 15 July 2014 to the end of 2016 - is analyzed. The assessment includes analysis of observation residuals, success rate of GPS carrier phase ambiguity fixing, a consistency check between the so-called kinematic and reduced-dynamic baseline solution, and validations of orbits by comparing with Satellite Laser Ranging (SLR) observations. External baseline solutions from The German Space Operations Center (GSOC) and Astronomisches Institut - Universität Bern (AIUB) are also included in the comparison.

Results indicate that the GPS receiver modifications and RINEX converter changes are effective to improve the baseline determination. This research eventually shows a consistency level of 9.3/4.9/3.0 mm between kinematic and reduced-dynamic baselines in the radial/along-track/cross-track directions. On average 98.3% *of the epochs have kinematic solutions. Consistency between TU Delft and external reduced-dynamic baseline solutions is at a level of 1 mm level in all directions.*

Keywords: Precise baseline determination; Swarm satellite; Ionospheric scintillation; GPS receiver modifications; Antenna patterns

3.1. Introduction

The Swarm mission, launched on 22 November 2013, is the fifth mission of the European Space Agency (ESA) living planet program. With three identical satellites, Swarm aims at unscrambling the Earth geomagnetic field and its temporal variations

(a): Delft University of Technology, The Netherlands

(Friis-Christensen et al., 2006). In its scheduled mission timetable, various maneuvers are made to guarantee a detailed coverage of the Earth (Friis-Christensen et al., 2008), both in spatial and temporal resolution. After the early orbit commissioning phase, the Swarm-A and -C satellites fly in orbital planes with the same inclination, but a difference of 1.5° in right ascension of ascending node and about $0.3^\circ - 0.9^\circ$ in argument of latitude. These differences manifest themselves as a pendulum like relative motion (Friis-Christensen et al., 2006). Swarm-B is flying in a higher and different polar orbit.

A few formation flying satellite missions have been launched in the past years. Their different baseline types enable various research objectives. The in-line formation flying GRACE and its follow-on mission focus on the research of the Earth's gravity field and its variations (Tapley et al., 2004b). The side-by-side flying TanDEM-X/TerraSAR-X mission (baseline of just a few kms) aims at constructing global digital elevation models by the interferometric synthetic aperture radar technique (Krieger et al., 2013). The PRISMA mission intends to investigate rendezvous and docking in space (D'Amico et al., 2013; Persson et al., 2009). Compared to these missions, the Swarm-A and -C formation has a unique pendulum-type baseline. If precisely determined, this baseline could be an ideal test bed for investigating gravity field recovery by making use of baseline perturbations in the cross-track direction (Jäggi et al., 2016).

The three Swarm satellites are equipped with the *RUAG space* dual-frequency, high-precision, eight-channel GPS receivers, which facilitate both single-satellite Precise Orbit Determination (POD) and dual-satellite Precise Baseline Determination (PBD) (Zangerl et al., 2014). The GPS receiver satellite-to-satellite tracking observations are affected by the local environment in which the constellation flies and the GPS signal travels. Much research has proved the significance of using in-flight data derived antenna Phase Center Variation (PCV) and Code Residual Variation (CRV) patterns. Using these patterns for correcting the GPS observations enhances the POD and PBD performance (Allende-Alba and Montenbruck, 2016; Bock et al., 2011; Gu et al., 2017; Van den IJssel et al., 2015; Mao et al., 2017; Montenbruck et al., 2009; Tancredi et al., 2013; Zehentner and Mayer-Gürr, 2016). At present 2 cm precision level is achievable for Swarm POD solutions (Van den IJssel et al., 2015), and 1-2 cm consistency level is obtained between Swarm-A/-C kinematic and reduced-dynamic PBD solutions (Allende-Alba et al., 2017).

Ionospheric scintillations have a big impact on the performance of Swarm GPS receivers and moreover POD (Van den IJssel et al., 2015) and PBD (Allende-Alba and Montenbruck, 2016). Irregular ionospheric plasma bubbles and thunderstorms cause GPS tracking losses near the equator. Strong solar winds will downgrade the GPS receiver tracking capability near the two geomagnetic poles (Buchert et al., 2015; Xiong et al., 2016). To minimize ionospheric influences in these geographical areas and to improve the GPS signal tracking performance, modifications have been made to the Swarm GPS receivers from October 2014 to August 2016, as depicted in Table 3.1. On 11 April 2016, a software issue in the RINEX converter was fixed that caused high noise in the code range observations contained in the Swarm GPS products (https://earth.esa.int/web/guest/news/-/article/swarm-software-issue-in-

rinex-converter-fixed). GPS receiver modifications, especially the improved carrier phase Tracking Loop (TL) bandwidth and increased antenna Field-of-View (FoV), are proved to be effective in improving the POD (Van den IJssel et al., 2016). More importantly, it has been shown that gravity field recovery which relies on kinematic POD solutions, also benefits from the applied GPS receiver modifications (Dahle et al., 2017).

In this research, we focus on analyzing the impact of ionospheric activity and Swarm GPS receiver modifications on PBD. It is crucial for the users of the Swarm GPS data to note the impact of these factors on the data quality in different periods. In total 30 months of the lower pair Swarm-A and -C satellites data (from 15 July 2014, when two GPS receivers started to track 1 Hz data, to the end of 2016) are selected to investigate the influence of the ionospheric activity and GPS data quality. The days without either reference orbits or GPS RINEX files are first excluded, and the days with large maneuvers (7 days for Swarm-A, 1 day for Swarm-C) and data gaps are also not analyzed. An overview of all Swarm satellites maneuvers is available in this report (European Space Research and Technology Centre, 2017).

Table 3.1: Swarm GPS receivers modifications and the RINEX converter change timetable during the entire period.

Date	Modifications
15-07-2014	GPS data rate 0.1 Hz to 1 Hz
21-10-2014	Swarm-A FoV 80° to 83°
22-10-2014	Swarm-B/-C FoV 80° to 83°
01-12-2014	Swarm-C FoV 83° to 86°
13-01-2015	Swarm-C FoV 86° to 88°
06-05-2015	Swarm-A/-B FoV 83° to 88°
06-05-2015	Swarm-C TL L1C+50%,L2W+100%,C1W/C2W+100%
08-10-2015	Swarm-A TL L1C+50%,L2W100%,C1W/C2W+100%
10-10-2015	Swarm-B TL L1C+50%,L2W+100%,C1W/C2W+100%
11-04-2016	New RINEX converter
27-04-2016	Swarm-B code TL to original setting
03-05-2016	Swarm-A code TL to original setting
04-05-2016	Swarm-C code TL to original setting
23-06-2016	Swarm-C phase TL L2W+50% (0.5 Hz to 0.75 Hz)
11-08-2016	Swarm-A phase TL L2W+50% (0.5 Hz to 0.75 Hz)
11-08-2016	Swarm-C phase TL L2W+50% (0.75 Hz to 1.0 Hz)

The Swarm GPS receiver carrier phase observation has tremendously lower noise level than pseudo-range/code observation (Van den IJssel et al., 2015). As a prerequisite of making optimal use of carrier phase in PBD, the so-called Double-Differenced (DD) integer ambiguities should be fixed. However the Swarm GPS receivers experience a mixture of half-cycle and full-cycle ambiguities because of the applied tracking methods (Allende-Alba et al., 2017). It has to be taken into consideration, otherwise only fixing the integer ambiguities as full-cycles significantly

downgrades the PBD (Allende-Alba and Montenbruck, 2016; Jäggi et al., 2016). Swarm lacks an independent baseline validation system, e.g. the K-band ranging system on-board the GRACE twin-satellites. Therefore for Swarm we have to verify the baseline precision by other means. An alternative validation is the consistency check between the reduced-dynamic and the kinematic PBD, which is solely determined by the GPS receiver observation quality (Kroes et al., 2005). The ambiguity fixing success rate is another verification, however it has to be noted that wrongly fixed ambiguities might pass the validation scheme.

This paper is organized as follows. The POD and PBD methodology is outlined in Section 3.2. Special attention is paid to the fixing and validation of the half-cycle integer ambiguities. The POD and PBD is based on an iterative Extended Kalman Filter (EKF), where the GPS observations are treated separately for the two GPS frequencies. The EKF computes the reduced-dynamic POD and then kinematic and reduced-dynamic PBD, where for PBD relative dynamics between two satellites can be additionally constrained. In Section 3.3, the in-flight performance of the GPS receivers is addressed and analyzed. The internal ambiguity fixing success rate, observation residual levels and the consistency of different baseline solutions are checked. POD and PBD solutions in this study are compared with independent Satellite Laser Ranging (SLR) observations. External PBD solutions from The German Space Operations Center (GSOC) (Allende-Alba and Montenbruck, 2016; Allende-Alba et al., 2017) and Astronomisches Institut - Universität Bern (AIUB) (Jäggi et al., 2016) are also used for comparison. Finally, Section 3.4 concludes this paper and proposes a few research perspectives.

3.2. Precise baseline determination methodology

3.2.1. Integer ambiguities fixing and validation

The GPS carrier phase observations offer the most crucial information for computing precise baselines. When constructing the DD observation model between two GPS receivers and two GPS satellite transmitters, a few common errors such as GPS clock and ephemeris errors can almost be eliminated or reduced to a large extent. By fixing as many DD carrier phase integer ambiguities as possible, the EKF is able to fully exploit the carrier phase precision. In this research, the implemented ambiguities fixing algorithm is Least-squares Ambiguity De-correlation Adjustment (LAMBDA), which is proved to be very successful for the determination of static baselines on the ground (Teunissen, 1999) and dynamic baselines in space (Kroes et al., 2005).

It has to be noted that the Swarm GPS receivers experience half-cycle ambiguity, which makes ambiguity fixing more challenging. The half-cycle ambiguity is caused by the fact that the Swarm GPS receiver Numerically Controlled Oscillator (NCO) phase and the derived carrier phase observation may be affected by 180 degrees phase offset for an individual GPS-Swarm pass (Allende-Alba et al., 2017). Allende-Alba and Montenbruck (2016) designed a filter to distinguish between the half-cycle and the full-cycle ambiguities and fixed them separately. In their research, the solution fixing mixed-cycle integer ambiguities obtained 3.9%

more integer ambiguities than the solution fixing all ambiguities as half-cycle values. Besides, in (Allende-Alba et al., 2017) they selected day 29 February 2016 as a test case and the mixed-cycle solution resulted in a slightly better baseline consistency from 5.02 to 4.87 mm in the along-track direction. The cost was 2-2.5 times more processing time. They also corrected all the half-cycle ambiguities to full-cycle values, which contributed much to the ambiguity fixing process. When using the ESA RINEX data in this research, all GPS DD carrier phase ambiguities are fixed as half-cycle values.

To maximize the ambiguity fixing success rate, a subset fixing process is implemented. The LAMBDA algorithm aims at making optimal use of float ambiguities and the associated covariance matrix as computed by the EKF for fixing the ambiguities at integer values (Kroes et al., 2005). The conventional use of the LAMBDA algorithm has a drawback that none of the ambiguities will be accepted for epochs for which one or more of the fixed ambiguities can not pass the statistical testing. To avoid this, a subset selection approach is adopted leading to many more fixed ambiguities (Van Barneveld, 2012).

To begin with, a GPS satellite with the smallest ambiguity variance is selected as the reference. If LAMBDA fails to fix the full set of ambiguities, a subset selection approach will be used. It discards the least likely fixed ambiguities as provided by LAMBDA but fail to pass the ambiguities validations. The subset selection repeats until LAMBDA fixes a smaller subset. The fixed subset ambiguities are then fed into the next EKF iteration to further fix the discarded set of ambiguities. Figure 3.1 depicts the ambiguity fixing process of an epoch. It can be seen that eventually five pairs of ambiguities are fixed after six iterations by using this subset fixing approach, however the G28-G05 pair remains un-fixed. Please note that three of the five fixed ambiguities have odd values, which indicate that they are half-cycle ambiguities. Moreover, a rather strict statistical testing is conducted to check the validity of the fixed ambiguities (Section 3.3.2).

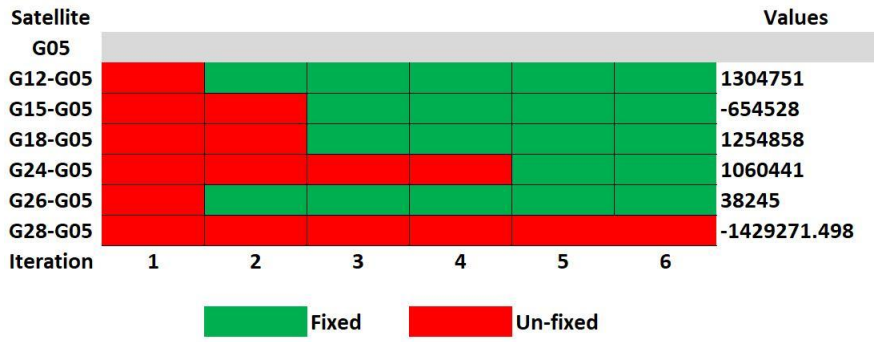

Figure 3.1: The subset ambiguities fixing (on the first GPS frequency) for a representative epoch, 00:30:00 on 17 July 2014 (DOY 198). The horizontal axis represents the consecutive EKF iterations, the vertical axis indicates the pair of GPS satellites for forming the double-differenced ambiguities.

3.2.2. Multiple Orbit Determination using Kalman filtering

This research is accomplished by using a GPS High Precision Orbit Determination Software Tools (GHOST) add-on tool called Multiple Orbit Determination using Kalman filtering (MODK) (Van Barneveld, 2012). GHOST is a precise orbit determination software package developed by GSOC with support from TU Delft (Wermuth et al., 2010).

The satellite dynamic modeling consists of three parts: gravitational forces, non-gravitational forces and empirical accelerations. Empirical accelerations are the estimated parameters to compensate force model errors. In the EKF, the correlation time (τ), the standard deviation of a-priori values (σ_a) and the process noise (σ_p) of empirical accelerations have to be set. The implemented models, used data files and EKF settings are specified in Table 3.2. It can be observed that a comprehensive modeling of gravitational forces is done, including the GOCO03S gravity field model truncated at degree and order 120, ocean tides and 3^{rd}-body perturbations. The modeling of non-gravitational forces is based on a simplified canon-ball modeling of the satellites. Associated modeling errors are compensated by the estimation of atmospheric drag (C_D) and solar radiation (C_R) coefficients, and the estimation of empirical accelerations. Since the Swarm-A and -C satellites are flying in adjacent orbits, it is anticipated that the associated force model errors, which are to be absorbed by the empirical accelerations, are quite similar. Therefore, in PBD differential acceleration constraints are applied that cause the estimated empirical accelerations to be similar as well for both Swarm satellites.

The detailed filtering process in MODK is illustrated in Figure 3.2. MODK includes both a forward and backward filter and iterates until convergence. The EKF first runs from the first epoch to the last epoch of each 24-hours orbit arc with 5 s step. For each epoch, the covariance matrix of the estimated parameters is recorded. The estimated float integer ambiguities and the corresponding covariance matrices are used by the LAMBDA algorithm in order to fix the maximum number of integer ambiguities (subset approach). This process is repeated in the backward direction from the last to the first epoch. Subsequently the estimated integer ambiguities derived from the two directions are compared. In case of consistent values for the forward and backward directions, the ambiguities are considered to be fixed. The EKF smooths both solutions according to the bi-directional covariance matrices recorded at each epoch. In the next iteration, the smoothed orbit and fixed ambiguities are set as input and it is attempted to fix more ambiguities. Iterations are repeated until no new integer ambiguities are fixed.

After the convergence of the reduced-dynamic baseline, a kinematic baseline solution is produced as well using the least squares method. To this aim, the same frequency-dependent GPS observations and fixed integer ambiguities on the two frequencies are used, where one satellite (Swarm-A) is kept fixed at the reduced-dynamic PBD solution. At least 5 observations are required on each frequency to form good geometry. To minimize the influence of wrongly fixed ambiguities and residual outliers, a threshold of 2-sigma of the carrier phase residual standard deviation statistics is set, which results in eliminating around 5% data. A further screening of 3 cm is set to the Root-Mean-Square statistics of the kinematic PBD

Table 3.2: Overview of MODK input template for the baseline determination of Swarm.

Spacecraft model	Canon-ball with cross-section of 1.0 m^2 and varying mass
Gravitational forces	GOCO03S 120×120 (selectable, maximum 250×250) static gravity field, plus linear trends for spherical harmonic degree 2 terms according to IERS2003 (Mayer-Gürr et al., 2012; McCarthy and Petit, 2004) Luni-solar third body perturbations CSR Ocean tides model based on TOPEX and GRACE data (Lyard et al., 2006)
Non-gravitational forces	Atmospheric drag: Jacchia 71 density model (Jacchia, 1977) Solar radiation pressure: conical Earth shadow, Sun flux data
C_D	1 per 24 hr, σ_a =1.3, σ_p =1.0
C_R	1 per 24 hr, σ_a =1.3, σ_p =0.5
Empirical acc.	Radial : τ =600 s, σ_a =5 nm/s², σ_p =1 nm/s² Along-track: τ =600 s, σ_a =15 nm/s², σ_p =3 nm/s² Cross-track: τ =600 s, σ_a =15 nm/s², σ_p =3 nm/s²
Differential empirical acc.	Radial : τ =600 s, σ_a =2 nm/s², σ_p =0.2 nm/s² Along-track: τ =600 s, σ_a =5 nm/s², σ_p =1 nm/s² Cross-track: τ =600 s, σ_a =5 nm/s², σ_p =1 nm/s²
Earth parameters	Leap second data table of TAI-UTC CODE Earth rotation parameters, version 2.0 (Prange et al., 2017)
GPS products	CODE 5s GPS orbits and clocks (Dach et al., 2015) IGS08.atx, the transmitter antenna phase center offsets and variations (Schmid et al., 2016) CODE ionospheric maps (Dach et al., 2016)
GPS data editing	Minimum signal to noise ratio: 5 Minimum cut-off elevation: 0 deg Code editing outliers: 2.0 m Phase editing outliers: 0.02 m
Orbit arc length	24 hours
Antenna pattern	Frequency-dependent phase and code antenna patterns
Ambiguity	Half-cycle Integer ambiguities
Methodology	Iterative Extended Kalman filter
GPS data weighting	For POD: Code/Phase: 0.3/0.003 m For PBD: Code/Phase: 0.5/0.005 m

carrier phase observation residual. It is able to screen out the solutions influenced by large wrongly fixed ambiguities and bad phase observations (Kroes et al., 2005). The kinematic PBD also runs bi-directional and two solutions are averaged according to the epoch-wise covariance matrices from the least squares method.

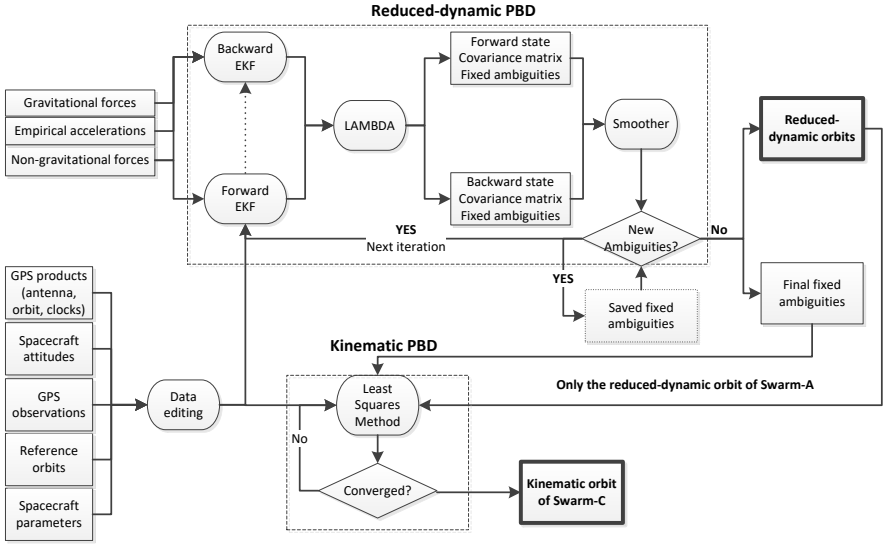

Figure 3.2: Flow chart of the iterative Extended Kalman filter and ambiguities fixing for reduced-dynamic baseline determination, and the Least Squares Method for kinematic baseline determination.

3.3. Results and discussion

3.3.1. GPS data processing

The Swarm Level-1B GPS observations are not recorded at integer seconds and need to be synchronized to exactly the same integer epochs for each Swarm satellite to facilitate the PBD. The approach as outlined in Van den IJssel et al. (2015) is adopted, which synchronizes the different Swarm clocks to within 0.3 μs. A few GPS data editing thresholds are defined for the signal to noise ratio, elevation cut-off angle and code/phase observation detection outliers, as indicated in Table 3.2. This editing scheme is applied for the full Swarm data period. The percentage of remaining data used in this study is shown in Figure 3.3.

Figure 3.3 agrees well with results included in (Van den IJssel et al., 2016). It is found that the number of tracked GPS satellites by each receiver increases with larger antenna FoV and wider signal tracking loop bandwidth. For two satellites, the $80°$ to $88°$ FoV change leads to an increase of the average number from 7.3 to 7.5. In addition, the first tracking loop modification then leads to further increase to 7.7. When this modification was switched back to its original setting on 3 May 2016 and 4

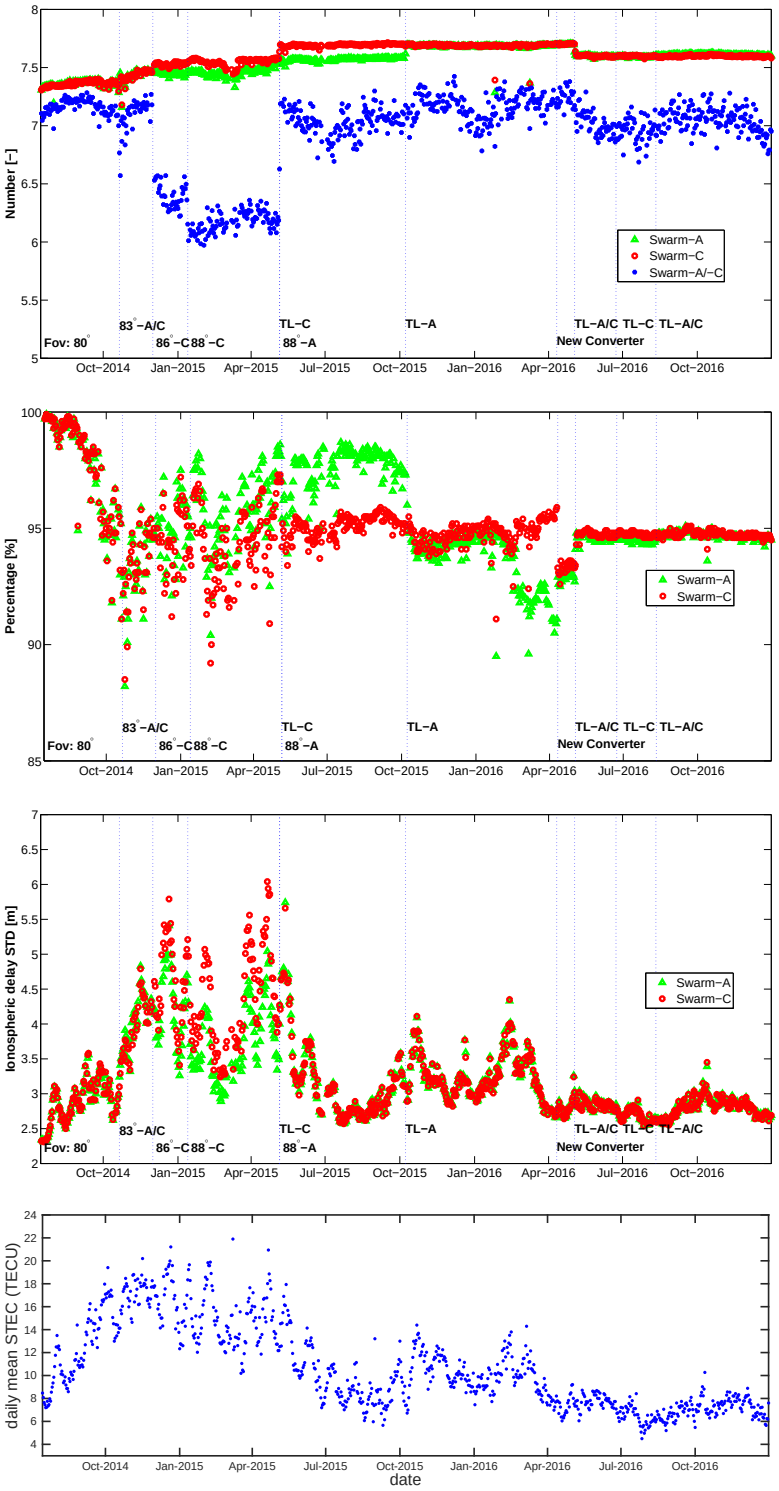

Figure 3.3: From top to bottom: the number of tracked GPS satellites by two GPS receivers, the percentage of used GPS data for two satellites in precise baseline determination, the standard deviation of the un-differenced ionospheric delay estimated in Kalman filter, and the daily mean values of STEC from the Swarm-C ESA level-2 TEC product.

May 2016 for Swarm-A and -C respectively, the number decreased again. However it has to be noted that the FoV changes to Swarm-A and -C are not synchronized: the nominal change always begins with Swarm-C. The number of simultaneously tracked GPS satellites by two receivers is influenced when the two Swarm satellites have different FoVs. The number drops from 7.2 (July to October 2014, the FoVs were $80°$) to merely 6.2 (February to May 2015, the FoV of Swarm-A was $83°$ and -C had $88°$), which leads to fewer available DD integer ambiguities for PBD. When both antennas have the same $88°$ FoV, this number is close to 7.0.

The Swarm GPS receivers are able to track the GPS L1-C/A signal and the encrypted P(Y) signals. Five main ranging observation types are three code/pseudorange observations marked as C1C, C1W and C2W, and two carrier phase observations indicated as L1C and L2W (Gurtner and Estey, 2013). Moreover, we find that the tracked C1C observations show higher noise levels than the C1W data, and it is thus more difficult to fix integer ambiguities for the C1C and L1C code/phase observations combination. Therefore, use will be made of the C1W observations for the code observation on the first GPS frequency for this study.

The GPS observation quality is influenced by the level of ionospheric activity including irregular scintillations, plasma bubbles and storms. Moreover, solar activity approached its 11 years peak level at the end of 2014, which is reflected by the Slant Total Electron Content (STEC) level in Figure 3.3. This effect can be also observed by the EKF estimation of the daily standard deviation of ionospheric delays between a Swarm satellite and the tracked GPS satellites. A larger ionospheric activity level in the winter of 2014 reduces the percentage of kept data from around 99% to below 95% in PBD, reminding that the same data editing scheme as described in Table 3.2 is used for the full analyzed Swarm data period. The first tracking loop modification of Swarm-C improves the number of available GPS observations, but it is found that the additional observations mostly experience larger thermal noise levels. Therefore, approximately 3% more data is eliminated and not used in PBD, which is comparable to the increment of observations due to the receiver modification. It has to be noted that there was a drop of selected data again during 21 February - 10 April, 2016, when the Swarm RINEX converter issue was causing a huge increase in the code observation noise of Swarm-A (Figure 3.4).

Figure 3.4 illustrates the code/phase residual levels on each frequency after the data editing. The carrier phase experiences different residual levels on two frequencies, which are due to the different tracking methods applied for the L2-P(Y) and L1-C/A signals in the Swarm GPS receivers (Allende-Alba et al., 2017). The GPS receiver modifications affect the observation quality in the following aspects:

- the larger FoV slightly increases the code and phase residuals, as reported by Van den IJssel et al. (2016).
- the software issue with the old RINEX converter resulted in larger code residuals, and this was eventually solved on 11 April 2016 when the new RINEX converter was implemented.
- the first tracking loop modification (in May 2014) impacts the phase observations more than the other two modifications (in May 2016 and August 2016,

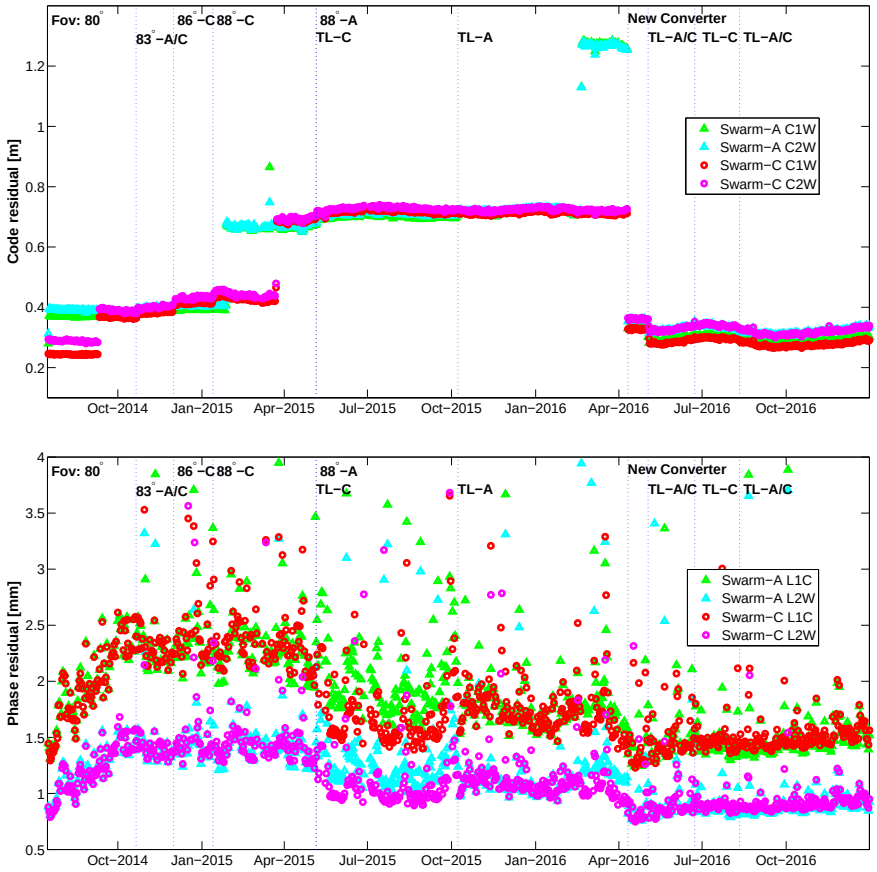

Figure 3.4: The code (top) and phase (bottom) residual levels on each frequency during the entire period.

respectively). When this modification is first implemented on Swarm-C, it experiences clearly lower phase residuals than Swarm-A. This is mostly caused by the significant observation residual reduction near the geomagnetic poles, where the large influence from ionospheric scintillations is reduced (Van den IJssel et al., 2016). This reduction is larger than the slight thermal noise increment of GPS observations due to its widened tracking loop bandwidth. This is consistent with the discussion for Figure 3.3.

- the influence of GPS receiver modifications on code observation is quite limited, because the RINEX converter software issue increases the residual level. Moreover we are using a strict data editing scheme to ensure good PBD environment, the larger-residual code observations are partially neglected in PBD (Figure 3.3).

- the carrier phase residuals are highly determined by the level of ionospheric activity. They fluctuate accordingly when comparing with the STEC trend and the standard deviation of ionospheric delay estimates (Figure 3.3). The activity level is reduced significantly from 2014 to 2016 for both satellites.

After the implementation of new RINEX converter and three GPS receiver tracking loop modifications, the ionospheric activity is also low, therefore both the phase and code residuals have been at low level for 7 months from May to December 2016.

Moreover, PCV and CRV maps have been estimated by the so-called *residual approach* (Jäggi et al., 2009). These maps are used to correct the GPS observations and therefore to enhance the PBD method (Allende-Alba and Montenbruck, 2016; Van Barneveld, 2012). To minimize the disturbance from the RINEX converter issue, four representative months of data (August 2014, November 2014, August 2016 and November 2016) are selected for estimating the antenna maps. Compared with Jäggi et al. (2007) and Allende-Alba et al. (2017) which make use of the differential antenna patterns between two GPS receivers, this research estimates the antenna patterns of two receivers separately. Because the ambiguity fixing is frequency-dependent, the relevant antenna pattern maps are created for each GPS frequency (L_1 and L_2) in single satellite POD. Five iterations are found to be sufficient to first create the PCV maps, then another five iterations are done to further create the CRV maps based on a fixed PCV map. The detailed frequency-dependent PCV and CRV maps of Swarm-A are displayed in Figure 3.5. The maps are defined in a right-handed North-East-Up (NEU) antenna-fixed reference system, for which the North axis coincides with the satellite body-fixed +X axis (0° azimuth), the Up and boresight axis coincides with the -Z axis, and the East axis completes the right-handed system. The Swarm-C GPS receiver experiences nearly identical patterns.

3.3.2. Internal consistency check

Ten representative days from different periods are selected to depict how the iterative approach gradually increases the PBD integer ambiguity fixing success rates in Figure 3.6. In general, 5 iterations are sufficient to converge the PBD. After May 2016, the ambiguity fixing becomes more efficient as the first iteration fixing success rate is higher and eventually more ambiguities can be successfully fixed in fewer iterations. The impact of GPS receiver modifications and ionospheric activities on the integer ambiguities fixing success rate is displayed in Figure 3.7. Here an ambiguity probability test with threshold of 99.9% is adopted. The complete set of validations is described in (Van Barneveld, 2012). It is quite strict to avoid wrongly fixed ambiguities and thus ensure stable kinematic and reduced-dynamic baselines. The best integer ambiguities fixing success rate at around 90% is achieved during 15 July 2014 - 1 September 2014. For this period both the code and the phase residual levels are relatively lower and most of the observations can be used for PBD. After this period, the ambiguity fixing success rate decreases when the code residual noise level increases because of the RINEX converter issue and the phase residual noise level increases because of larger ionospheric activity. The lowest success rate occurs when the code residual noise level for the Swarm-A GPS receiver

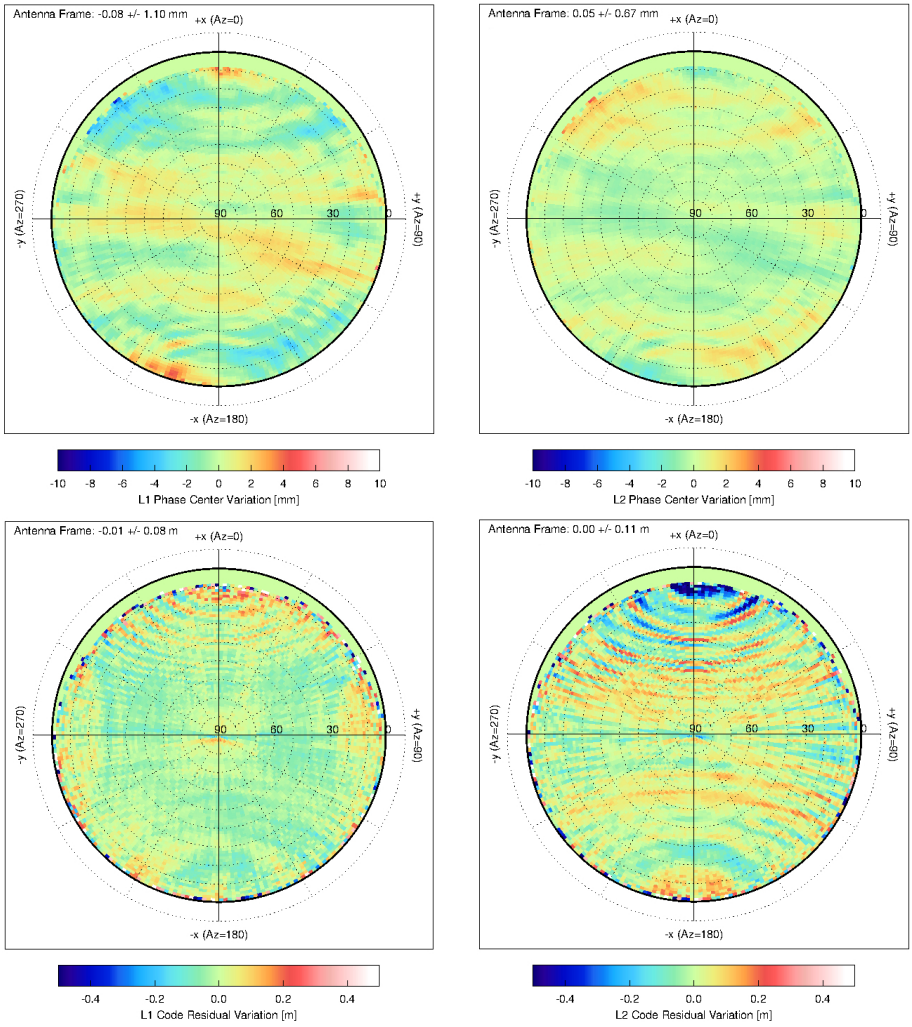

Figure 3.5: The in-flight PCV (top) and CRV (bottom) maps of Swarm-A: L_1 frequency (left) and L_2 frequency (right) in the NEU reference frame (Data: August 2014, November 2014, August 2016, November 2016).

is at a peak near April 2016 (Figure 3.4), although for this period the influence of ionospheric activity is low. This indicates that the code observation noise level is also an important impact factor in fixing the integer ambiguities.

Figure 3.8 displays the global distribution of the Swarm-A carrier phase residuals for the L_1 frequency. The distributions are clearly different for the month of August in 2014 and 2016. For August 2014, much stronger residuals are witnessed near especially the geomagnetic poles. This is highly correlated with ionospheric scintillations. For August 2016, the residual level at the poles is much lower. This

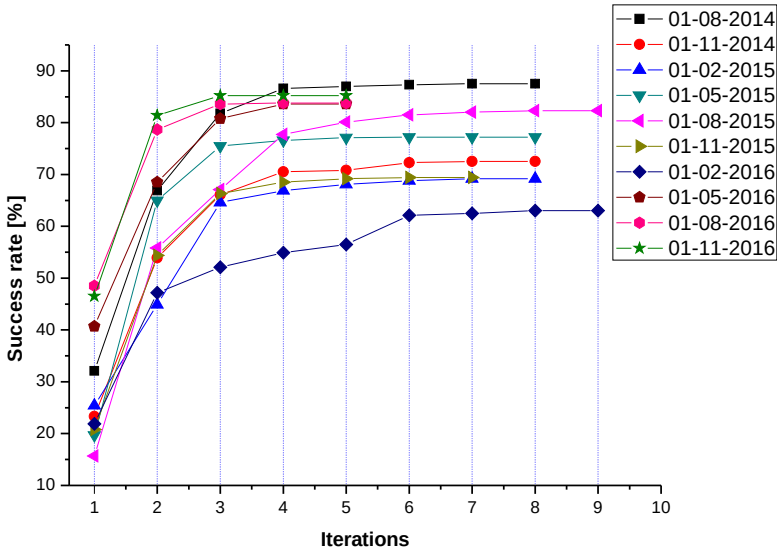

Figure 3.6: Ambiguities fixing success rate against iterations for 10 representative days.

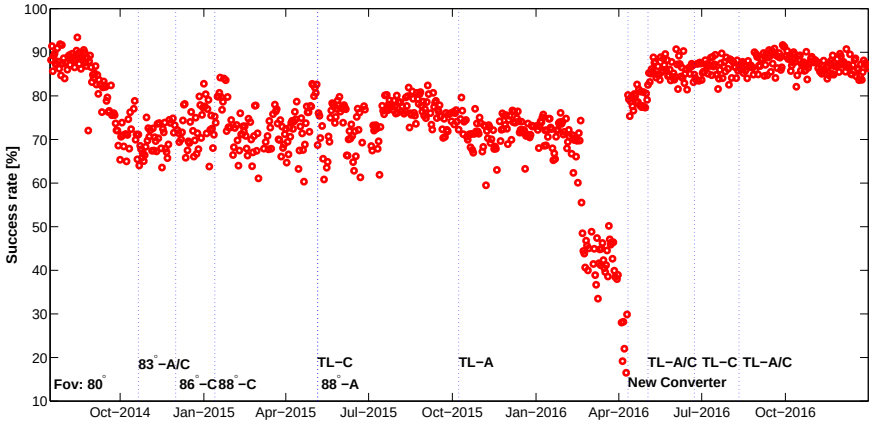

Figure 3.7: Ambiguities fixing success rate during the full period.

can be attributed to two important factors: (1) GPS receiver modifications enhance the tracking performance at the poles, and (2) the ionospheric activity level decreases from 2014 to 2016. However, when comparing the residual levels for middle-latitude areas, the phase residuals slightly increase from 2014 to 2016. This is caused by the increased phase tracking loop bandwidth and antenna FoV which provide more data tracked at lower elevations. These additional observations are

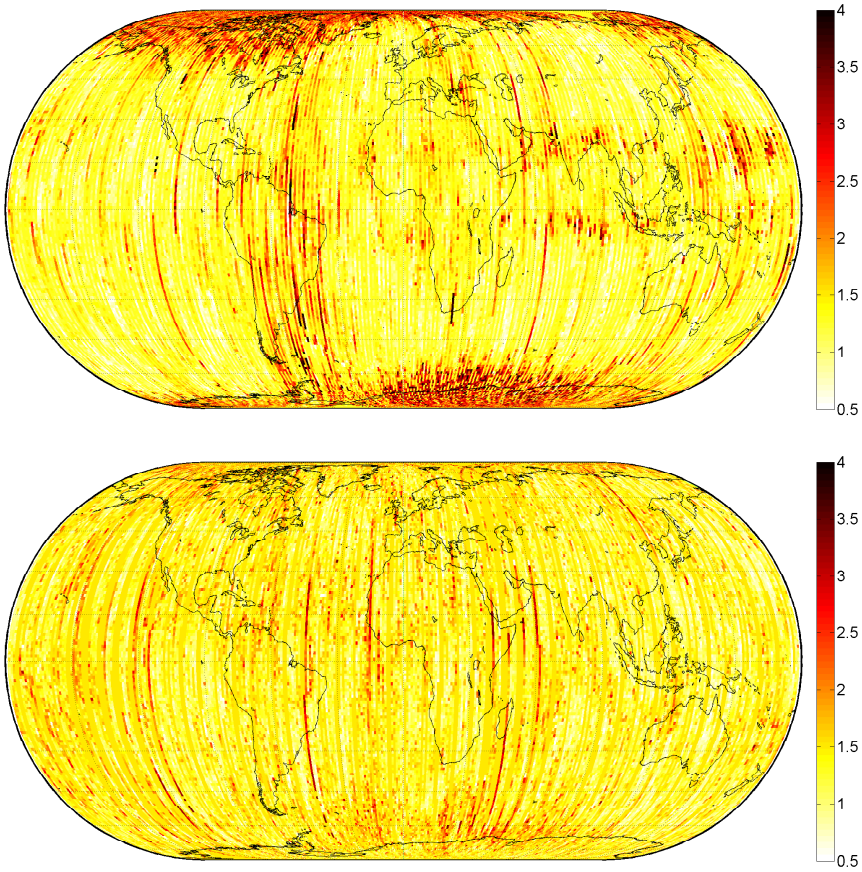

Figure 3.8: The global distribution of the L_1 frequency phase residuals of Swarm-A satellite in August 2014 (top, no tracking loop modifications) and August 2016 (bottom, with tracking loop modifications), unit: [mm].

slightly more noisy.

The consistency between the kinematic and the reduced-dynamic baselines is used to assess the quality of the PBD process (Allende-Alba and Montenbruck, 2016; Jäggi et al., 2016). In this research, both approaches rely on the same GPS observations and fixed integer ambiguities. The kinematic approach solely exploits GPS observations in a batch least-squares filter, while the reduced-dynamic approach uses a Kalman filter that relies on the dynamic modeling of satellites together with the estimation of empirical accelerations. To maximize the availability of kinematic baselines, the adopted approach uses all available fixed integer ambiguities and if not uses the float ambiguities. No kinematic solutions are computed for epochs with fewer than 5 simultaneously tracked GPS satellites by the two Swarm GPS receivers after the 3 cm screening in the kinematic PBD, as mentioned in Section 3.2.

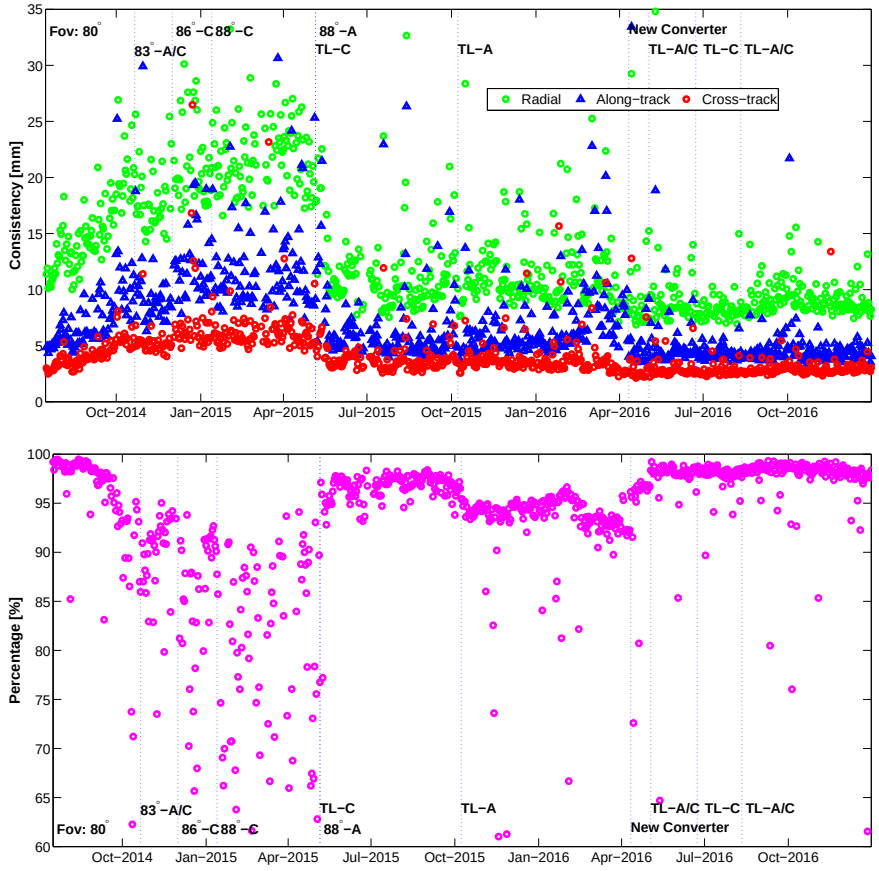

Figure 3.9: Consistency between kinematic and reduced-dynamic baseline solutions in the radial, along-track and cross-track directions (top), and the percentage of epochs covered by the kinematic solution (bottom) for the full data period.

Figure 3.9 depicts the baseline consistency between the kinematic and reduced-dynamic baselines for the full selected period. The consistency is displayed for Radial, Along-track and Cross-track (R/A/C) direction referring to the Swarm-C coordinates. The baseline consistency is the worst for the radial direction, which can be explained by the geometry (i.e. the associated radial dilution of precision) between GPS satellites and GPS receivers. The baseline consistency varies in accordance with the level of carrier phase residual, which is obtained by comparing the modelled carrier phase and the real observations. Lower carrier phase residuals significantly improve the reduced-dynamic and the kinematic PBD. The baseline consistency after implementing the GPS receiver tracking loop modifications and new RINEX converter is at 9.3/4.9/3.0 mm for respectively the R/A/C direction. For around 98.3% of the epochs (5 s time interval), a kinematic baseline solution is available for low ionospheric activity levels. The tracking loop modifications and RINEX

converter correction result not only in improved consistency between kinematic and reduced-dynamic PBD, but also an improved stability of the better consistency level.

3.3.3. Inter-agency comparison

Allende-Alba and Montenbruck (2016) have analyzed the Swarm-A/-C baseline determination for the August 2014 data, which is a month with a relatively low ionospheric activity level. They obtain a kinematic and reduced-dynamic PBD consistency of 40/17/11 mm in the R/A/C directions. In their GHOST baseline determination module, they read one satellite orbit as reference to compute the baseline between two satellites. The mean integer ambiguities fixing success rate achieved by LAMBDA is 93.1%. For the same period, our PBD solutions computed by MODK have better consistency of 14.3/6.6/3.9 mm in the R/A/C directions. The mean ambiguities fixing success rate is 89.7%. Compared to the method in Allende-Alba and Montenbruck (2016) and Jäggi et al. (2016) which rely on the ionosphere-free single-differenced GPS observations, MODK makes use of frequency-dependent GPS observations and ionospheric delay estimates on both frequencies, and therefore obtains better internal consistency between MODK solutions.

Another comparison can be done for the period January 2016, as described in (Allende-Alba et al., 2017). In that paper, two solutions from GSOC and AIUB are compared. GSOC uses the GHOST software package for PBD (marked as *GHOST* in tables). In the research of GSOC, they have created new Swarm RINEX observation files which eliminate the RINEX converter issue on the code observations and all half-cycle ambiguities are corrected to full-cycle values. The AIUB solution is marked as *BSW* which represents the Bernese GNSS software PBD package developed at AIUB. The AIUB baselines are computed in a batch least-squares estimation using DD ionosphere-free GPS observations, and a wide-lane/narrow-lane approach is adopted to fix integer ambiguities (Jäggi et al., 2007). The same batch of corrected GPS RINEX observations (Allende-Alba et al., 2017) is used by AIUB (personal communication with Prof. Adrian Jäggi). However in our research the officially released ESA RINEX files without these corrections, are used. The PBD results for January 2016 data (the first day is excluded due to data gaps) that are available for all three software package solutions, are compared.

Table 3.3: Consistency between kinematic and reduced-dynamic baseline solutions, kinematic baseline availability and ambiguity fixing success rate for different software packages (consistency unit: [mm], period: January 2016).

Solution	*MODK*	*GHOST*	*BSW*
Radial	0.0+/-11.9	1.3+/-17.9	0.7+/-16.1
Along-track	0.0+/-6.2	-0.1+/-6.0	-0.0+/-6.4
Cross-track	-0.1+/-4.0	0.0+/-5.3	-0.1+/-6.7
Availability	94.5%	73.3%	95.7%
Amb. fix.	72.2%	94.0%	N/A

Table 3.3 shows the baseline consistency from different research agencies. In

general three solutions all have very good internal consistency of 11.9 to 17.9 mm in the vertical direction and a few mm in the horizontal direction. The *MODK* solution has the best agreement of 11.9/6.2/4.0 mm (R/A/C) between the kinematic and reduced-dynamic baselines. *MODK* has in total 94.5% epochs with kinematic solutions, which are computed when there are at least 5 GPS satellites are tracked by both receivers. Both the float ambiguities and the fixed integer ambiguities will be used. Compared with that the *GHOST* solution has 21.2% less availability because the kinematic baselines are computed at epochs when all the integer ambiguities are fixed, and also a minimum of 5 GPS satellites are viewed by two GPS receivers. However, it has to be noted that the *MODK* solution fixes 72.2% ambiguities (note that we have more available epochs). This is lower than the 94.0% from the *GHOST* solutions during January-March 2016, which is reported in (Allende-Alba et al., 2017). The most important impact factor is that the *GHOST* solution benefits significantly from the correction of the full cycle ambiguities and the RINEX converter issue which increases the code residuals. Unfortunately the *BSW* wide-lane/narrow-lane ambiguity fixing success rate is not available here.

Table 3.4: Consistency between *MODK* kinematic baseline and reduced-dynamic baseline solutions from different software packages, note that the corrected data is used for all solutions. (unit: [mm], period: 14/15 January 2016).

Solution	Radial	Along-track	Cross-track
MODK	0.1+/-9.0	0.0+/-3.9	-0.1+/-3.1
GHOST	-1.0+/-9.2	1.1+/-6.1	-0.2+/-3.2
BSW	-0.7+/-9.6	0.4+/-6.1	0.1+/-3.2

A new computation is carried out by using two days (14/15 January 2016) of the corrected RINEX files kindly provided by Gerardo Allende-Alba. For the two days, the consistency between *MODK* kinematic and reduced-dynamic baselines is further improved to 9.0/3.9/3.1 mm in the R/A/C directions. More importantly, *MODK* acquires a much higher ambiguities success rate of 97.8% than that of 78.2% when using the un-corrected ESA data (also two days). Other comparisons are done to check the consistency between the *MODK* kinematic baseline and the *GHOST* and *BSW* reduced-dynamic baselines. The *MODK-GHOST* and *MODK-BSW* baseline consistency have good agreement and are close to the *MODK* kinematic and reduce-dynamic baseline consistency (Table 3.4). It indicates that the *MODK* solutions are very consistent with the solutions from the GHOST and the Bernese software packages.

Another comparison is done for the reduced-dynamic baselines. When we use the ESA data, the R/A/C reduced-dynamic baseline comparison is 4.3/4.3/2.1 mm between *MODK* and *GHOST* solutions, and 3.1/4.3/2.5 mm between *MODK* and *BSW* solutions (Table 3.5). However, the *GHOST* and *BSW* solutions have much better agreement of 1.5/1.0/1.4 mm, as they are using the same corrected RINEX files with lower code residuals and full-cycle ambiguities. The lower ambiguities fixing success rate in *MODK* also explains the larger reduced-dynamic baseline dif-

ferences between *MODK* and *GHOST*. However after the use of same corrected RINEX files in MODK, the results of same comparisons are improved to 1 mm level in three directions, as displayed in Table 3.5.

Table 3.5: Inter-agency reduced-dynamic baseline consistency comparison when using different (*MODK* uses ESA data) and same (*MODK* also uses the corrected data) GPS RINEX observations (unit: [mm]).

Solution	Radial	Along-track	Cross-track
ESA data (January 2016)			
MODK-GHOST	0.1+/-4.3	0.6+/-4.3	-0.1+/-2.1
MODK-BSW	-0.2+/-3.1	-0.0+/-4.3	0.0+/-2.5
Corrected data (14/15 January 2016)			
MODK-GHOST	0.2+/-1.5	0.5+/-1.2	-0.0+/-1.1
MODK-BSW	-0.0+/-0.9	-0.1+/-1.0	0.0+/-1.1
GHOST-BSW	-0.3+/-1.5	-0.5+/-1.0	0.1+/-1.4

3.3.4. Satellite laser ranging validation

The availability of SLR observations for the Swarm satellites allows an independent validation of the absolute orbit solutions. The SLR system offers an opportunity to assess the accuracy of the GPS-based orbit solutions in the direction of the line-of-sight between the SLR ground stations and the Swarm satellites. In order to eliminate spurious observations, an editing threshold of 50 cm is used, which is more than an order of magnitude above the RMS of fit levels, and observations below the 10° elevation cutoff angle are excluded. A SLR retro-reflector modeling pattern from German Research Center for Geosciences (GFZ) is included (Neubert et al., 1998). Furthermore seven SLR stations (Kiev, Simeiz, Arequipa, Borowiec, Changchun, San Fernando, Riga) with large mean offsets are excluded. Ultimately, 83.4% and 86.4% of the SLR observations are used for Swarm-A and -C, respectively. Exactly same SLR validation scheme is used for all different orbit solutions. Table 3.6 and Figure 3.10 include the results of comparing the different orbit solutions with the independent SLR observations.

Table 3.6: Mean and RMS of fit of SLR observations for different orbit solutions of MODK. The ESA solutions are included as reference. (unit: [mm], period: July 2014 - December 2016).

Solution	Swarm-A	Swarm-C
PBD	0.6+/-21.4	-0.7+/-20.7
POD	0.7+/-20.5	-0.7+/-20.3
ESA	2.3+/-19.7	0.6+/-20.2
Obs. No.	51234	49823

It can be observed that for the MODK POD orbits the RMS of fit of SLR validation

is quite close to the orbits from ESA. Note that the ESA orbits are also computed at TU Delft using the original GHOST reduced-dynamic POD tool instead of the MODK tool. For the ESA orbit computation, a batch least-squares method is used and the ionosphere-free combination PCV maps are included (Van den IJssel et al., 2015). The SLR validation statistics confirm that MODK provides high-precision orbit solutions. However, for the PBD solutions the RMS of SLR fit deteriorates by only 1 mm for both Swarm-A and -C. Similar result is reported by Kroes et al. (2005); Mao et al. (2017) that the wrongly fixed integer ambiguities reduce the orbit precision. The fixing process can also be easily influenced by the ionospheric activity level between two receivers. More importantly, the code residual level enlarged by errors due to the RINEX converter software issue, also downgrades the float ambiguities estimate accuracy and the subsequent integer ambiguity fixing success rate. There is no such impact on the single-satellite POD which only makes use of float ambiguities.

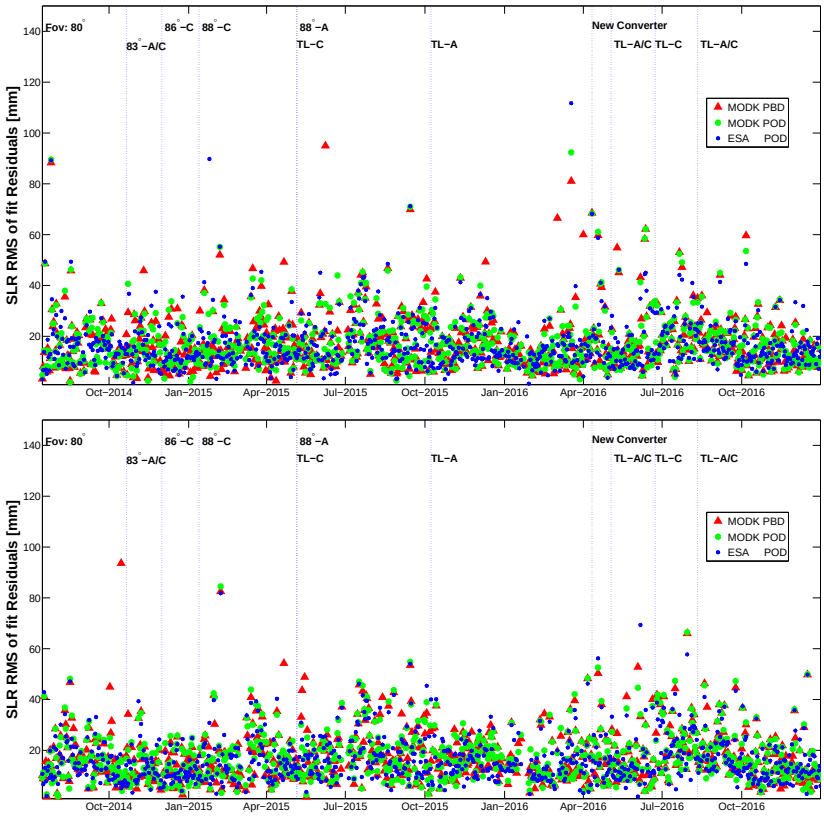

Figure 3.10: The daily RMS of fit of SLR observations for different MODK orbit solutions for Swarm-A (top) and -C (bottom). The ESA solutions are included as reference. (unit: [m], period: July 2014 - December 2016).

Table 3.7: Mean and RMS of fit of SLR observations for different software packages orbit solutions (unit: [mm], period: January-2016).

Software	Solution	Swarm-A	Swarm-C
MODK	PBD	-4.3+/-20.1	-5.1+/-21.1
GHOST	PBD	-3.1+/-19.4	-3.9+/-21.5
BSW	PBD	2.8+/-20.7	2.5+/-22.2
MODK	POD	-3.7+/-19.6	-5.8+/-21.5
ESA	POD	-1.8+/-19.5	-4.5+/-20.6
Obs. No.		910	923

Table 3.7 shows SLR validation is done to different solutions for January 2016 data. Unfortunately the number of laser observations of both satellites is low for this month (most observations are from the first half of this month). It can be clearly seen that after using the acceleration constraints in the PBD of *MODK*, the mean SLR validation difference between two satellites decreases from 2.2 (5.8-3.7) to 0.8 (5.1-4.3) mm. This finding corresponds to similar conclusion in (Allende-Alba et al., 2017) which uses a good tracking SLR station -Yarragadee, Australia- to show the better SLR consistency in mean for PBD orbits than POD orbits. More importantly, there is nearly no precision reduction from the *MODK* POD to PBD orbits. It is mainly due to the fact that January 2016 is a month with lower ionospheric activity, and more importantly the first GPS receiver tracking loop modification further reduces the GPS carrier phase residual level, which is beneficial for the POD and PBD.

3.4. Summary and discussion

Two pendulum formation flying Swarm -A/-C satellites baseline solutions have been generated for a 30 months data period. The solutions are based on an extended Kalman filter with relative empirical accelerations to constrain the dynamics between satellites. The LAMBDA method is used to fix double-differenced carrier phase ambiguities, where it is not required to fix all ambiguities at a certain epoch. It is possible to fix a subset which acquires the maximum of fixed ambiguities. The LAMBDA method makes use of the float ambiguities and the associated covariance matrices from the Kalman filter. A strict and aggressive validation scheme is adopted to test the fixed integer ambiguities. Moreover, in-flight calibrated frequency-dependent antenna phase and code maps are used to correct the GPS observations. The external SLR validation confirms that the orbit determination precision obtained in this study reaches a level comparable with the official ESA orbit solutions.

The ionospheric activity level has a big impact on the integer ambiguity fixing and therefore also the baseline determination. To minimize its impact, a few modifications and a new GPS RINEX converter have been made to the Swarm onboard GPS receivers between 2014 and 2016. These are proved to be effective in many aspects. Firstly, the number of GPS satellites simultaneously tracked by two GPS receivers is influenced by the antenna field of view changes. Larger antenna

field of view improves the number of tracked GPS satellites for single receiver, however similar field of view should be guaranteed to have better geometry, or larger number of simultaneously tracked GPS satellites by two receivers. Secondly, the GPS receiver carrier phase tracking performance is clearly influenced by ionospheric scintillations, therefore the downgraded ionospheric activity from 2014 to 2016 significantly reduces the carrier phase residuals and therefore facilitates the baseline determination. The changes of GPS receiver carrier phase tracking loop bandwidth reduces the carrier phase residuals near the geomagnetic equator and poles, especially the first modification which took place during May-October 2015. In addition, the integer ambiguity fixing is affected by the code observation quality. Fixing the RINEX converter software issue on 11 April 2016 results in much lower code residual level, and acquires a stable 90% ambiguity fixing success rate. Finally, the consistency between the kinematic and the reduced-dynamic baseline is determined by the phase residual level and the software issue in the GPS RINEX converter. After all the changes, this research eventually shows a consistency level of 9.3/4.9/3.0 mm in the radial/along-track/cross-track directions, with 98.3% available kinematic baselines.

An inter-agency comparison is done between this research (Delft University of Technology) and the German Space Operations Center (GSOC) solution and the Astronomisches Institut - Universität Bern (AIUB) solution. The January 2016 data is selected for comparison. Our research achieves the best kinematic and reduced-dynamic baseline consistency of 11.9/6.2/4.0 mm in radial/along-track/cross-track directions. When using the same corrected RINEX files (only 14/15 January 2016 data is available) provided by GSOC, the consistency is further improved to 9.0/3.9/3.1 mm. The correction of the RINEX converter software issue and the correction from half-cycle ambiguities to full-cycle ambiguities indeed help. Reduced-dynamic baselines from different software packages show agreement of 1 mm level in three directions. When comparing our kinematic baselines with the GSOC and AIUB reduced-dynamic baselines, the consistency is close to the consistency between our kinematic and reduced-dynamic solutions. It indicates our baseline solutions agree well with other baseline determination software packages. This precise pendulum Swarm-A and -C kinematic baselines precision level might be very promising for the research to recover the gravity field and its variations.

This research shows that it is important to be aware of the changing quality of the Swarm GPS data, which can be influenced by ionospheric activity and receiver settings. The implemented GPS receiver tracking loop modifications and RINEX converter correction are proved to be working properly to improve the baseline determination between two pendulum formation flying Swarm-A and -C satellites. Future work can be also put on investigating the more dynamic high-low Swarm-B/-A or Swarm-B/-C baselines, for which the baseline determination will be more challenging.

Acknowledgment

The China Scholarship Council (CSC) is gratefully acknowledged for financially supporting part of the work described in this paper. We would like to show our special

gratitude to the European Space Agency (ESA) for sharing the Swarm data products. All necessary Swarm L1B data are obtained from the The Swarm Satellite Constellation Application and Research Facility (SCARF). Other data files such as GPS ephemeris/clock products and force model related files, are downloaded from the Center for Orbit Determination in Europe (CODE), Bern, Switzerland. We indeed appreciate Gerardo Allende-Alba (from The German Space Operations Center) for providing us their baseline solution and two days of the corrected GPS RINEX data, and also Prof. Adrian Jäggi (from Astronomisches Institut - Universität Bern) who provided the AIUB baseline solutions. We also acknowledge two anonymous reviewers for reviewing this paper.

4

Swarm Constellation Baseline Determination

RQ.3 Can we get precise baseline estimates for satellite constellations with long and highly variable baselines?

This chapter introduces the PBD investigation for the whole Swarm constellation which provides three different baselines. Ten 24-hr orbital arcs are selected around the points of closest approach for the high-low satellites. Evaluations are done to check the applicability of PBD methods, particularly for the ambiguity fixing and the consistency between kinematic and reduced-dynamic baseline solutions.

High-dynamic baseline determination for the Swarm constellation

Xinyuan Mao[a], *Pieter Visser*[a], *Jose van den IJssel*[a]

Published in *Aerospace Science and Technology*, 88 (2019) 329-339,
doi:10.1016/j.ast.2019.03.031.

Baseline determination for the European Space Agency Swarm magnetic field mission is investigated. Swarm consists of three identical satellites -A, -B and -C. The Swarm-A and -C form a pendulum formation whose baseline length varies between about 30 and 180 km. Swarm-B flies in a higher orbit, causing its orbital plane to slowly rotate with respect to those of Swarm-A and -C. This special geometry results in short periods when the Swarm-B satellite is adjacent to the other Swarm satellites. Ten 24-hr periods around such close encounters have been selected and the baseline lengths vary between 50 and 3500 km. All Swarm satellites carry high-quality, dual-frequency and identical Global Positioning System receivers not only allowing precise orbit determination of the single Swarm satellites, but also allowing a rigorous assessment of the capability of precise baseline determination between the three satellites. These baselines include the high-dynamic baselines between Swarm-B and the other two Swarm satellites.

For all orbit determinations, use was made of an Iterative Extended Kalman Filter approach, which could run in single-, dual-, and triple-satellite mode. Results showed that resolving the issue of half-cycle carrier phase ambiguities (present in original release of GPS RINEX data) and reducing the code observation noise by the German Space Operations Center converter improved the consistency of reduced-dynamic and kinematic baseline solutions for both the Swarm-A/C pendulum pair and other combinations of Swarm satellites. All modes led to comparable consistencies between the computed orbit solutions and satellite laser ranging observations at a level of 2 cm. In addition, the consistencies with single-satellite ambiguity fixed orbit solutions by the German Space Operations Center are at comparable levels for all the modes, with reduced-dynamic baseline consistency at a level of 1-3 mm for the pendulum Swarm-A/C formation and 3-5 mm for the high-dynamic Swarm-B/A and -B/C satellite pairs in different directions.

Keywords: Precise Baseline Determination, High-dynamic Baseline, Satellite Constellation, Integer Ambiguity, Antenna Pattern

4.1. Introduction

Satellite formations and constellations have been increasingly utilized to fulfill various research objectives (Sabol et al., 2001). Data collected by their on-board in-

(a): Delft University of Technology, The Netherlands

struments offer adequate information to satisfy complex scientific and operational tasks. For instance, two Low Earth Orbiting (LEO) satellites in close formation are used for observing the temporal and spatial variations of Earth's gravity field (Tapley et al., 2004a) or for producing digital elevation maps (Krieger et al., 2007). As a prerequisite for these state-of-the-art applications, satellite orbits and especially also baselines have to be precisely determined, the latter with (sub-)mm level precision. Precise baseline solutions are crucial for *e.g.* interferometric Synthetic Aperture Radar (SAR) missions (Montenbruck et al., 2011) and have the potential benefit of supporting gravity field research (Jäggi et al., 2016).

Formation flying LEO satellites typically make use of high precision, dual-frequency multi-channel GPS receivers for Precise Orbit Determination (POD) (Wu et al., 1991). By forming Double-Differenced (DD) carrier phase observations, common errors are strongly mitigated and so-called integer ambiguities can be resolved (Teunissen, 1999). With the advent of the GRACE mission (Tapley et al., 2004a), it has been proved that Precise Baseline Determination (PBD) at 1-mm level is feasible by fixing DD carrier phase ambiguities (Kroes et al., 2005). Further improvements are obtained by making use of relative dynamics constraints and GPS receiver antenna patterns. Nowadays, sub mm level baseline precision is achievable for in-line or along-track formations like the Gravity Recovery and Climate Experiment (GRACE) mission (Allende-Alba and Montenbruck, 2016; Jäggi et al., 2007; Mao et al., 2017). For a more complex side-by-side or radial/cross-track formation such as the TanDEM-X/TerraSAR-X mission, it is claimed that a precision in each direction of 3-8 mm can be achieved (Montenbruck et al., 2011).

On 22 November 2013, the European Space Agency (ESA) geomagnetic field mission Swarm was launched and soon the three Swarm satellites entered their preferred orbits by a series of dedicated maneuvers (Friis-Christensen et al., 2006). It is an unprecedented three-identical-satellite constellation equipped with the same space-borne instruments. All Swarm satellites fly in near-polar orbits, with Swarm-A/C in a pendulum formation and Swarm-B at a higher altitude (Friis-Christensen et al., 2006). The distance between the Swarm-A and -C satellites is varying between 30 and 180 km. When Swarm-B is in view of the other Swarm satellites, the distance can be as small as about 50 km. For the pendulum part of Swarm, PBD has already been studied in detail, showing that consistencies between reduced-dynamic and kinematic solutions under different in-flight environment can be achieved that are of the order of 5-40 mm in different directions (Allende-Alba et al., 2017; Mao et al., 2018). At present, no successful consistently high-precision high-dynamic PBD research has been done for such kind of constellation.

Obtaining very precise baseline solutions for LEO satellites that do not fly in stable formation is still an open issue. For example, the work described in Van Barneveld (2012) shows that it is not straightforward to achieve precise baseline solutions between the CHAMP and GRACE satellites when these satellites are in view of each other. The CHAMP-GRACE baselines grow easily from hundreds of kms to thousands of kms in one day and these are therefore referred to as high-dynamic baselines. The same applies to the Swarm-B satellite with respect to the Swarm-A and -C satellites. As the baseline - or distance - between two LEO satellites grows,

the number of GPS satellites that are simultaneously in view of two GPS receivers drops, resulting in a smaller number of possible DD combinations. Moreover, LEO satellites experience different perturbing forces when at different altitudes, especially atmospheric drag due to different density levels (Doornbos, 2012).

The three-identical-satellite Swarm constellation will be used as a test bed for high dynamic baseline determination between LEO satellites. The results in Van Barneveld (2012) are based on 24-hr orbital arcs that start and end at midnight, which leads to significantly different CHAMP-GRACE orbital geometries for each arc. Moreover, CHAMP and GRACE carry GPS BlackJack receivers with different performance and also have different antenna installation geometries (Montenbruck et al., 2005). For CHAMP and occasionally for GRACE, also so-called cross-talk signal interference between the POD and radio occultation antenna's took place leading to different multi-path patterns (Mao et al., 2017; Montenbruck and Kroes, 2003). For Swarm, this is not the case. Compared to the work described in Van Barneveld (2012), a different approach is adopted for defining the orbital arcs. A total of 10 days are identified in the period from mid-July to mid-September in 2014 when the Swarm satellites are frequently in view of each other. The time of closest approach is then determined and a 24-hr orbital arc is defined starting 12 hr before and ending 12 hr after this time. This leads to comparable and more stable geometries for each selected orbital arc.

The *RUAG Space* Swarm GPS receiver exhibits half- and full-cycle ambiguities due to the tracking issue with its Numerically Controlled Oscillator (NCO) (Allende-Alba et al., 2017; Zangerl et al., 2014). Systematic 180° phase rotation frequently happens during the tracking process (Montenbruck et al., 2018b). This makes carrier phase integer ambiguity fixing more challenging. Fixing half-cycle ambiguities erroneously to full-cycle will significantly downgrade the baseline solution precision for the lower pair (Allende-Alba and Montenbruck, 2016). This receiver characteristic has thus to be properly dealt with. The German Space Operations Center (GSOC/DLR) has implemented an algorithm to correct the half-cycles into full-cycles by checking a certain bit of each carrier phase tracking record in the raw data (Montenbruck et al., 2018b). In addition, a systematic GPS RINEX converter software issue existed for code observations, leading to larger code noise at the early stage of the Swarm mission and was fixed by ESA on 11 April 2016 (https://earth.esa.int/web/guest/missions/esa-operational-eo-missions/swarm/news/-/article/swarm-software-issue-in-rinex-converter-fixed, last accessed: November 2019). ESA has been re-creating these old Swarm RINEX files with both issues removed (the 8th Swarm Data Quality Workshop, https://earth.esa.int/web/guest/missions/esa-eo-missions/swarm/activities/conferences/8th-data-quality-workshop, last accessed: November 2019). The resulting GPS data lead to significantly more precise single-satellite POD (Montenbruck et al., 2018a) and dual-satellite PBD solutions for the Swarm-A/C formation (Allende-Alba et al., 2017; Mao et al., 2018). Their impacts on the high-low satellite pairs will be investigated in this research.

For the Swarm mission, it is not possible to validate PBD solutions by comparison with independent data coming from for example a K-Band Ranging system as

on board the GRACE twin satellites (Tapley et al., 2004b). A quality check can typically be done by assessing the consistency between kinematic and reduced-dynamic baseline solutions (Allende-Alba and Montenbruck, 2016; Jäggi et al., 2016; Mao et al., 2018). Moreover, external POD and PBD solutions are available and can be used for a quality assessment. An interesting development is single receiver ambiguity fixing, leading to enhanced POD solutions (Bertiger et al., 2010; Montenbruck et al., 2018b). Bertiger et al. (2010) propose a scheme of ambiguity fixing based on the ionosphere-free wide-lane model developed by (Blewitt, 1989), while Montenbruck et al. (2018b) make use of the wide-lane phase bias estimate products provided by (Loyer et al., 2012). Such single-satellite ambiguity fixed POD solutions have been made kindly available by GSOC/DLR for Swarm and will be used for assessing the quality of both POD and PBD orbit solutions in this research (Montenbruck et al., 2018a). Details of the single-satellite ambiguity fixed POD solutions can be found in (Montenbruck et al., 2018b) for the Sentinel-3A satellite, which carries a GPS receiver with similar characteristics when comparing with those flown by Swarm. An external validation of the individual satellite orbit solutions is offered by the availability of Satellite Laser Ranging (SLR) observations, which will form part of the analysis and quality assessments (Degnan, 1993).

The structure of this paper is as follows. Section 4.2 includes a description of the Swarm constellation data selection and corresponding quality assessment. Section 4.3 introduces the kinematic and reduced-dynamic POD and PBD algorithms. Section 4.4 describes results and orbit comparisons for the Swarm constellation. This paper is concluded by Section 4.5, which includes a summary and outlook.

4.2. Observations

4.2.1. Data selection

Representative data have been selected to test PBD for all three Swarm satellites. Table 4.1 includes three selected Keplerian orbital elements for Swarm satellites at a representative epoch. The Swarm-A/C formation flies in two almost identical polar orbits with only 1.5° difference in the right ascension of the ascending node (RAAN). These two satellites form a so-called pendulum formation. During the analyzed period the Swarm-B satellite flies about 50 km higher, which slightly differs with the early designed orbit scheme (Friis-Christensen et al., 2006; Olsen et al., 2006), and the RAAN difference on average is about 10°. Baseline lengths of high-low Swarm satellite pairs thus vary dramatically due to the different orbital planes and altitudes. It is found that the period July-September 2014 includes days for which the Swarm-A/B/C geometry is favorable, *i.e.* all three satellites are in view of each other. During this period, the baseline lengths between the Swarm-B satellite on the one hand and the Swarm-A and -C satellites on the other hand reach a local minimum every 6.1 days.

To evaluate the PBD methods used in this research, a sliding 24-hr orbit arc selection is done. Each selected orbit arc centers around the epoch of minimum distance, see *e.g.* Figure 4.1. The Swarm-A/C formation baseline length varies consistently between 30 and 180 km. For the Swarm-B/A and Swarm-B/C pairs, the

two satellites approach each other from an approximate 3500 km to a minimum of around 50 km. Ten orbit arcs are selected and recorded in Table 4.2. The used GPS ephemeris products are separate 24-hr GPS satellite orbits and 5-sec clock biases files (Dach et al., 2018). Before making use of them, a tool is used to interpolate the adjacent three consecutive 24-hr GPS satellite orbits into 5 seconds and then a merged orbit and clock file is created. The influence of GPS orbit and clock bias gaps crossing midnight is reduced.

Table 4.1: The crucial Keplerian orbital elements determining the relation between Swarm orbital planes during mid-July to mid-September 2014. a represents the semi-major axis, i means the orbit inclination and Ω is the right ascension of the ascending node (Credit: satellite two line elements data is obtained from www.space-track.org).

Satellite	a (km)	i (deg)	Ω (deg)
Swarm-A	6842.06-6840.75	87.35-87.36	197.53-175.66
Swarm-C	6842.05-6840.75	87.35-87.36	198.70-177.03
Swarm-B	6890.98-6890.41	87.75-87.76	206.28-188.59

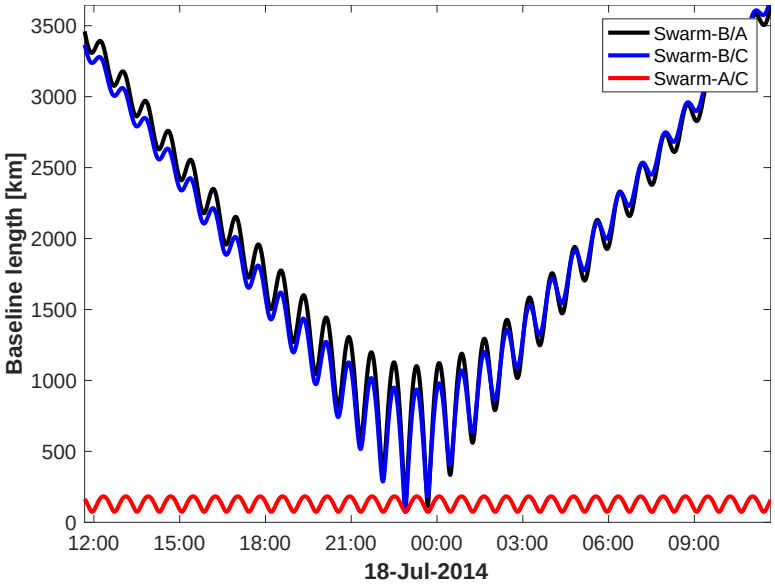

Figure 4.1: Length variations for each Swarm dual-satellite formation during one representative 24-hr orbit arc.

Figure 4.2 shows that the Swarm-A/C pendulum formation has on average > 7 common GPS satellites in view. This number is not yet influenced by the antenna field of view modification and is approximately equal to the number of GPS receiver tracking channels (Mao et al., 2018). For the high-low Swarm satellite pairs, this number drops from 6-8 to 4-6 as the baselines become longer. A low number of

Table 4.2: Ten selected 24-hr orbit arcs for Swarm constellation. Please note that DOY specifies the day of the center of the arc. This DOY number will be used as orbit arc identifier in this research.

Date (YYYY-MM-DD)	DOY	Middle of the arc	Minimum distance (km)
2014-07-17	198	23:40:30	112.57
2014-07-24	205	02:50:40	85.69
2014-07-30	211	06:00:40	82.85
2014-08-05	217	08:23:30	120.39
2014-08-11	223	11:33:00	56.14
2014-08-17	229	13:55:10	51.84
2014-08-23	235	16:17:20	52.51
2014-08-29	241	18:39:10	70.62
2014-09-04	247	20:13:40	58.99
2014-09-10	253	21:47:50	64.91

common GPS satellites in view has a big impact on the achievable PBD precision, especially for kinematic solutions. For high-quality PBD, at least 5 GPS satellites are required to be simultaneously tracked by two GPS receivers (Kroes et al., 2005). If less than 5 GPS satellites are commonly in view, no kinematic PBD solution will be generated for the associated epochs. Reduced-dynamic baseline solutions will then however still be available.

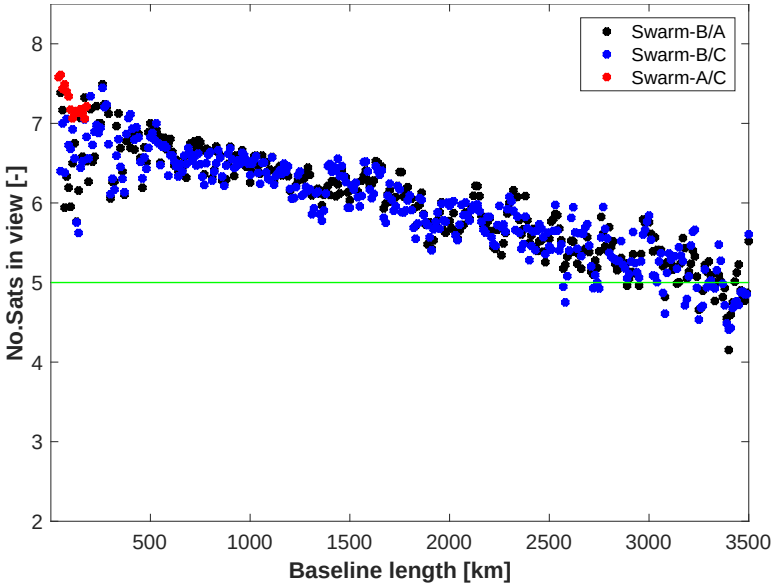

Figure 4.2: The number of GPS satellites simultaneously tracked by two GPS receivers as a function of distance (every 10 kms) for each Swarm dual-satellite formation (analysis for 10 24-hr orbit arcs).

4.2.2. Data quality assessment

GPS code and carrier phase observations are affected by several error sources, including thermal noise and multi-path. For the relevant Swarm data used in this research, the original GPS code observations suffer additionally from systematic errors due to sub optimal RINEX converter software leading to large noise levels. The code noise level has a clear impact on the ambiguity fixing success rate. The original carrier phase observations experience half-cycle ambiguity issues as mentioned above. A new version of Swarm GPS data was kindly provided by GSOC/DLR. For this version, the converter code error was removed and in addition the half-cycle carrier phase ambiguities were corrected to full-cycles.

The quality of in-flight GPS code observations can be assessed by analyzing their multi-path effects by using the multi-path evaluation models that are introduced in (Kroes, 2006; Montenbruck and Kroes, 2003). Thus, the multi-path represents an independent evaluation of misfit caused by the systematic errors from the RINEX converter on the one hand and the code observation noise on the other hand. The Root-Mean-Square (RMS) of multi-path is displayed in Figure 4.3 for Swarm-A as a function of the elevation of the GPS satellites as seen from the GPS receiver antenna installed on the zenith surface of each Swarm satellite. The results displayed in Figure 4.3 hold for 17 July 2014, when the Swarm-A GPS antenna had an antenna field of view of 80° (improved to 88° in October, 2014, (Van den IJssel et al., 2016)). The tracked GPS observations below 10° antenna cut-off angle are obtained by the tracking performance of GPS receiver antenna in its aft direction, as reported by Van den IJssel et al. (2016).

In general, the observation residual level drops with increasing elevation angle, which is in agreement with anticipated noise levels of GPS observations (Montenbruck and Kroes, 2003). Modifications in the new version of data clearly reduce the code noise level. This analysis indicates a reduction from 0.34/0.37 m to 0.18/0.20 m in terms of global RMS for the L_1/L_2 frequencies. Code noise on the L_1 frequency is slightly smaller than on the L_2 frequency. It is anticipated that the ambiguity fixing will improve when using the new batch of data.

Research in (Allende-Alba et al., 2017; Mao et al., 2018) confirms that the GPS observation correction process implemented by GSOC/DLR has a clear impact on the ambiguity fixing process, as also shown in Figure 4.4 in this research. This figure is representative for a triple-satellite PBD (see Section 4.3.1) and displays the ambiguity fixing success rate as a function of the number of iterations completed by the IEKF (with a maximum of 20). In the IEKF procedure, the ambiguities for the pendulum formation Swarm-A/C pair are fixed first (requiring around 6 iterations until convergence), after which as many as possible ambiguities are fixed for the Swarm-B/A and Swarm-B/C pairs. It can be observed that the ambiguity fixing is clearly enhanced by using the new version of the data. For the Swarm-A/C formation, the success rate for the first iteration is improved from 37% to 97%. The final fixing success rate increases from 88% to 98%. For the Swarm-B/A and Swarm-B/C combinations, fixing starts at iteration 8 for the old version of the data and iteration 7 for the new version of the data. It can also be clearly seen that for the starting iteration, the success rate improves from merely 9% and 8% to a much

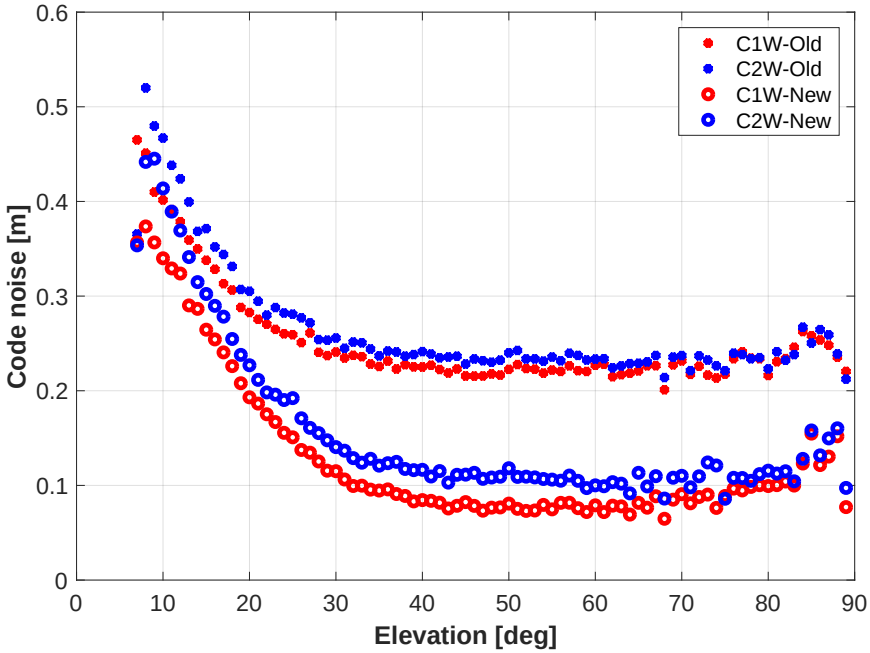

Figure 4.3: RMS of code multi-path as a function of elevation for the GPS L_1 and L_2 frequencies for two versions of Swarm-A GPS receiver RINEX data: *Old* indicates the ESA original file with RINEX converter software issues, *New* indicates the one corrected by GSOC/DLR and used in this research (selected day: DOY 198, 2014).

higher level of 64% and 64% for the Swarm-B/A and Swarm-B/C combinations, respectively. The final success rates reach about 97% and 97%, respectively, which is much higher than 81% and 83% when using the old version of the data.

Swarm dual-satellite PBD (again, please see Section 4.3.1) is done to evaluate the influence of half-cycle *vs.* full-cycle inter ambiguity fixing. As shown in table 4.3, the ambiguity fixing success rate is improved by more than 10% when full-cycle ambiguities are to be fixed. The new version of the data also improves the kinematic and reduced-dynamic baseline consistency, especially for two high-dynamic Swarm-B/A and Swarm-B/C satellite pairs. Therefore, for the remainder of this paper, results will be based on the new version of the data (Section 4.4).

4.3. Methodology

4.3.1. Single-, dual- and triple- POD/PBD

When solely using dual-frequency high-precision GPS tracking data and GPS satellite orbit/clock products, instantaneous satellite positions can be determined at the observation epochs when a sufficient number of GPS satellites is in view. This approach is referred to as kinematic approach (Yunck, 1996) and obviously leads to gaps in the position time series when there are gaps in the GPS observation data

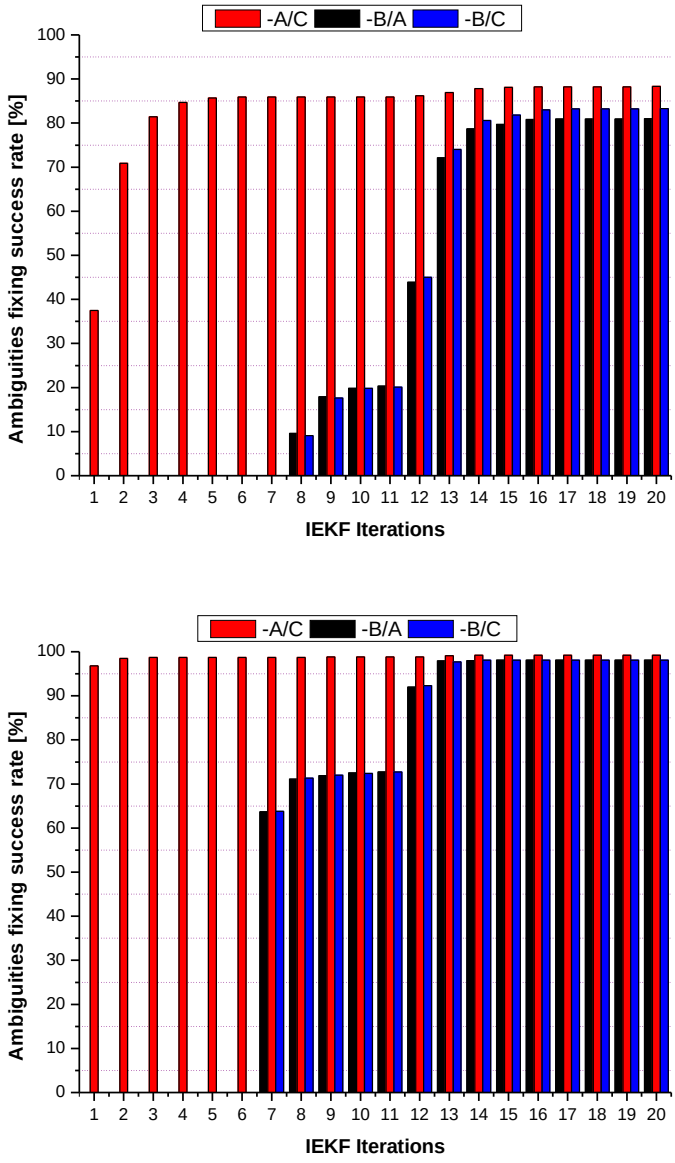

Figure 4.4: Integer ambiguity fixing success rate versus IEKF iterations for the triple-satellite Swarm PBD. Two sets of data, original version (top) and new version with corrections (bottom) are used (selected day: DOY 198, 2014).

or when not enough GPS satellites are in view. Dynamic and reduced-dynamic orbit determination, which include force models to solve equations of motion, result

Table 4.3: Mean of daily RMS differences between kinematic and reduced-dynamic baseline solutions, and ambiguity fixing success rate for Swarm constellation (dual-satellite PBD solutions). Two sets of Swarm GPS RINEX data are used.

Solution	Radial (mm)	Along-track (mm)	Cross-track (mm)	Amb.fix. (%)
		Swarm-A/C		
Half-cycle	15.0	7.8	4.1	86.9
Full-cycle	12.4	5.5	3.6	98.1
		Swarm-B/A		
Half-cycle	24.9	11.2	5.3	84.2
Full-cycle	22.9	9.8	5.6	97.3
		Swarm-B/C		
Half-cycle	24.9	11.4	6.5	83.9
Full-cycle	22.6	10.4	5.7	97.5

in continuous time series of satellite positions (Wu et al., 1991). Force models are typically divided in (1) gravitational force models including the non-spherical gravity field, perturbations from 3^{rd} bodies (Sun and the Moon), and solid-Earth and ocean tides, and (2) non-gravitational force models including the Sun radiation pressure, the Earth albedo pressure, and atmospheric drag. However, the associated models are not perfect, and model errors can be absorbed by so-called empirical accelerations (Montenbruck et al., 2005).

The Multiple Orbit Determination using Kalman filtering (MODK, (Van Barneveld, 2012)) tool is an in-house developed add-on tool to the GPS High Precision Orbit Determination Software Tools (GHOST) (Wermuth et al., 2010). MODK has the capability to provide reduced-dynamic single-, dual- and triple-satellite orbit solutions, where for the dual- and triple-satellite mode ambiguity fixing as well as further kinematic baseline determination can be done. The core of the MODK tool is based on an Iterative Extended Kalman Filter (IEKF) process, where the GPS observations are used and modeled for each frequency, *i.e.* L_1 and L_2 (Mao et al., 2017). A comprehensive description of the MODK tool and underlying method can be found in Chapter 3.3 of (Van Barneveld, 2012).

Compared to single-satellite POD, PBD in case of dual- and triple-satellite orbit determination includes the possibility to constrain differential empirical accelerations, which is especially relevant if two satellites fly in almost identical orbits (as is the case for Swarm-A and -C). This constraining proved to be very beneficial for estimating high-precision baselines for the GRACE tandem and for the Swarm-A/C pendulum formations (Allende-Alba and Montenbruck, 2016; Mao et al., 2018). In this study the frequency-dependent antenna Phase Center Variation (PCV) maps created by so-called *residual approach* are included (Jäggi et al., 2009; Mao et al., 2017). Our proposed Code Residual Variation (CRV) maps are not modelled since the used GSOC/DLR processed data have lower noise levels than the original data.

Besides, no significant signal interference exists for Swarm when comparing with GRACE as described in (Mao et al., 2017).

The MODK tool first computes reduced-dynamic orbit solutions, after which kinematic solutions are generated. The latter are based on the same modeled GPS observations, where use is made of the ambiguity fixing of the reduced-dynamic solution. In order to minimize gaps in the kinematic satellite position time series, all available fixed integer ambiguities and otherwise float ambiguities are used. No kinematic solutions are computed for epochs for which less than 5 GPS satellites are simultaneously in view of each combination of two GPS receivers, or epochs for which the RMS of GPS observation phase residuals is above 5 cm. A Least Squares Method (LSM) is adopted for the kinematic PBD. More detailed information and the data flow chart regarding the kinematic and reduced-dynamic approaches can be found in (Mao et al., 2018). The MODK tool includes the option to define a preferred baseline, *i.e.* a pair of satellites for which the ambiguity fixing is done first, after which the fixing is invoked for the other baselines. For the Swarm triple-satellite PBD, this option is used and the preferred baseline is the one for the pendulum Swarm-A/C satellite pair.

The DD ambiguities are resolved by the Least-squares Ambiguity De-correlation Adjustment (LAMBDA) algorithm (Teunissen, 1999). It has been widely used for different satellite formations PBD (Allende-Alba and Montenbruck, 2016; Kroes et al., 2005; Mao et al., 2017). To maximize the ambiguity fixing success rate, a subset fixing process is implemented. It allows for part of a set of integer ambiguities to be fixed while for the remaining the associated float values are used. This is not a conventional use of the LAMBDA algorithm, which nominally only accepts epochs when the entire set of ambiguities is fixed (Kroes et al., 2005). A strict ambiguity fixing validation scheme is adopted and integrated in the MODK tool (Mao et al., 2017; Verhagen, 2005). Moreover, an additional outlier detection check is included: if the absolute value of GPS carrier phase observation residuals (after fixing) is above 5 cm, the associated ambiguity will be kept at its float value and sent into IEKF for further fixing in the next iterations. It was found that this resulted in a reduced chance of wrongly fixed integer ambiguities and thus a more robust PBD by the IEKF as used by the MODK tool.

4.3.2. Parameter settings

Due to the different orbit altitudes for the Swarm satellites (Table 4.1), especially uncertainties in the modeling of non-gravitational accelerations can be different for Swarm-A and -C on the one hand and Swarm-B on the other hand. This will lead to differences in the estimated empirical accelerations that are used to absorb modeling errors. Figure 4.5 shows typical levels of estimated empirical accelerations for the three Swarm satellites on a representative day. The statistics of them are shown in Table 4.4. The mean of estimates of empirical accelerations represents the level of constant correction to the adopted dynamic models in certain direction. Although for all three Swarm satellites, the values seems to overlap to quite a significant extent, the empirical acceleration differences for the Swarm-A/C pair are significantly smaller than for the other pairs. It can be observed that the empirical

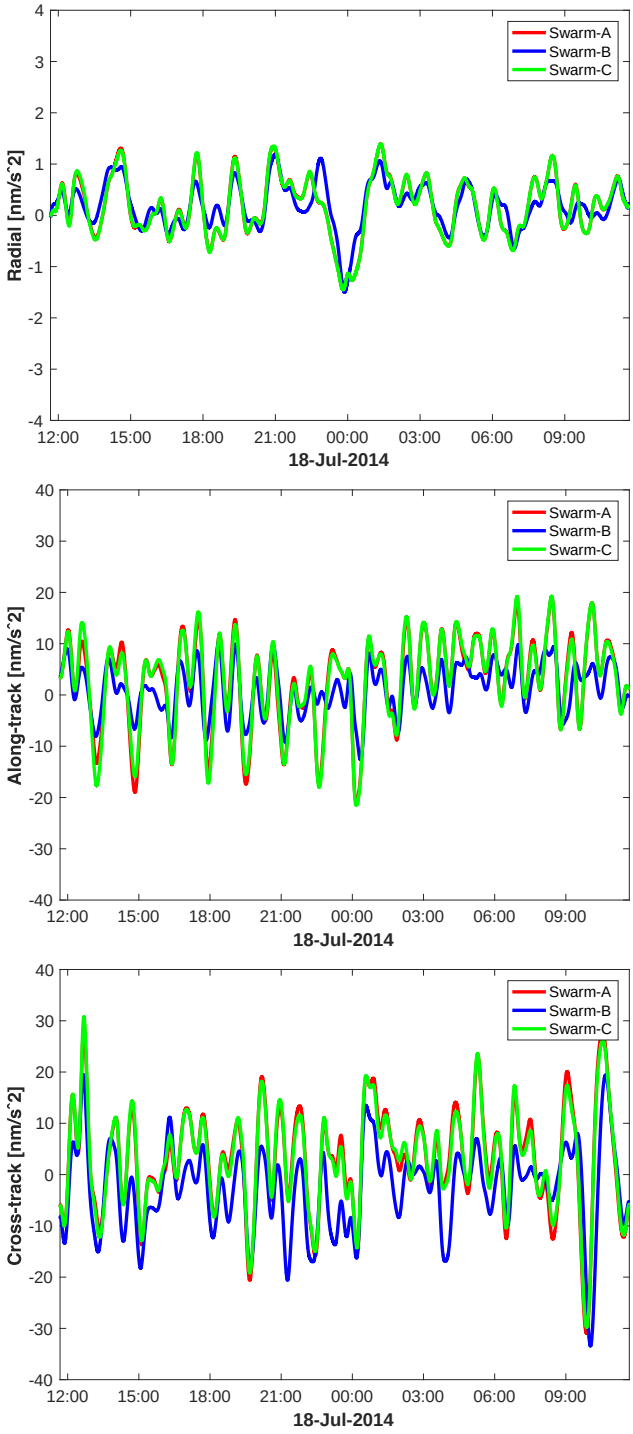

Figure 4.5: Time series of estimated empirical accelerations in the radial (top), along-track (middle) and cross-track (bottom) directions for each Swarm satellite based on triple-satellite PBD. Please note different scales are set for the vertical axes (DOY 198, 2014). Please note that the curves for Swarm-A and -C almost completely overlap.

accelerations (mean and RMS-about-mean) are larger in the along-track direction, which is the direction for which atmospheric drag is predominant, and the cross-track direction, which is the direction for which mis-modeling of solar radiation pressure forces is the largest (also due to the simplified canon ball satellite model that is used by the MODK tool, the scaling factors of the associated non-gravitational forces can not compensate the in-flight perturbations completely (Hackel et al., 2017; Mao et al., 2018)).

Table 4.4: Empirical acceleration estimate statistics for each Swarm satellite and satellite pair (mean and RMS-about-mean, DOY 198, 2014).

Sat/Pair	Radial (nm/s^2)	Along-track (nm/s^2)	Cross-track (nm/s^2)
Swarm-A	0.2 ± 0.6	2.9 ± 8.2	3.2 ± 9.8
Swarm-B	0.2 ± 0.4	1.2 ± 4.6	-2.6 ± 8.2
Swarm-C	0.2 ± 0.6	3.0 ± 8.3	3.2 ± 9.5
Swarm-A/C	0.0 ± 0.0	-0.0 ± 1.1	-0.0 ± 1.2
Swarm-B/A	0.0 ± 0.3	-1.7 ± 5.3	-5.8 ± 6.5
Swarm-B/C	0.0 ± 0.3	-1.7 ± 5.4	-5.8 ± 5.9

The correlation time (τ), standard deviation of a-priori values (σ_a) and process noise (σ_p) of empirical accelerations have been tuned to reflect the typical level for these parameters, both in an absolute and relative sense. The adopted values are included in Table 4.5. It can be seen that the values for the standard deviation for the difference between empirical accelerations is specified to be smaller for the Swarm-A/C pendulum satellite pair, reflecting their similarity of orbit (especially altitude).

Both GPS carrier phase and code observations are used by MODK to produce orbit solutions. The carrier phase weight is set inversely proportional to its claimed noise level, which is 3 mm for each frequency in POD and 5 mm in PBD as in that case single-differences are used. The same force models and standards are used as specified in (Mao et al., 2018).

Table 4.5: Empirical acceleration parameter settings in three directions (radial/along-track/cross-track) for each Swarm satellite and each pair of satellites in IEKF. The correlation time τ is equal to 600 s.

Sat/Pair	σ_a (nm/s^2)	σ_p (nm/s^2)
Swarm-A	5/15/15	1/3/3
Swarm-B	5/15/15	1/3/3
Swarm-C	5/15/15	1/3/3
Swarm-A/C	2/5/5	0.2/1/1
Swarm-B/A	5/15/15	1/3/3
Swarm-B/C	5/15/15	1/3/3

4.4. Results and discussion

This section includes the results of the Swarm precise orbit and baseline determination for the selected 10 orbit arcs. The single-satellite ambiguity fixed GSOC/DLR kinematic and reduced-dynamic POD solutions serve as reference both for the absolute and baseline solutions, where the latter is referred to as the GSOC/DLR Differential POD or DPOD solution. Results for both dual-satellite (Section 4.4.2) and triple-satellite (Section 4.4.3) PBD will be provided and discussed, followed by SLR validation (Section 4.4.4). However, this section starts with a brief result regarding the detection of GPS observation outliers.

4.4.1. GPS data outliers

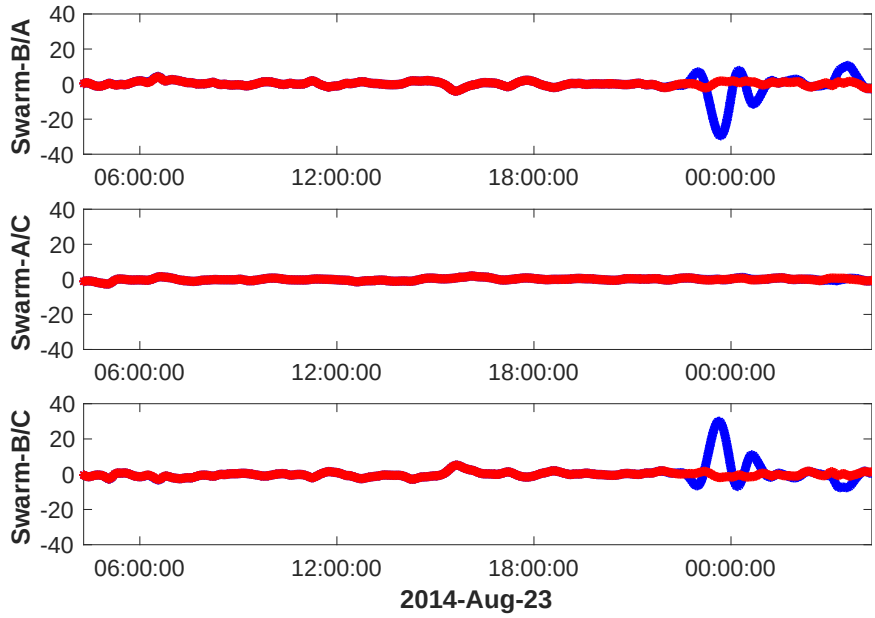

Figure 4.6: Consistency (unit:cm) between triple-satellite Swarm baseline solutions and baselines derived from the reference GSOC/DLR orbits in the along-track direction, both for including (blue) and excluding (red) the identified G04 outliers (22:50 to 23:50, on 23 August 2014). The consistency is included for the Swarm-B/A (top), Swarm-A/C (middle) and Swarm-B/C (bottom) satellite pairs.

GPS observation outliers are in principle detected automatically by the MODK tool (Section 4.2.2). It is important to report that for a few GPS satellite tracking passes very large observation residuals were obtained, *i.e.* after the automated outlier detection. This resulted in an unstable IEKF process. Therefore, these observations were excluded manually. To be precise, the following passes were eliminated: GPS Block IIA G04 for Swarm-B from 22:50 to 23:50 on 23 August 2014 (DOY 235) and GPS Block IIR-M G17 for Swarm-A from 23:50 on 04 September (DOY 247) to 00:50 on 05 September 2014. Block IIA GPS satellites are sometimes in eclipse

affecting their yaw attitude motion (Montenbruck et al., 2015). The outliers for 23 August can be attributed to G04 being in eclipse. The cause for the outliers during the other pass might be the inconsistency of GPS satellite clock corrections spanning midnight. The impact of removing the outlying pass is shown for 23 August 2014 in Figure 4.6. It can be seen that the impact of the outlying pass reaches a level of 20 centimeters. The eliminated data accounts for less than 0.5% of all GPS available observations. It has to be noted that for PBD the relevant GPS tracking passes are excluded for all three satellites when forming DD combinations.

4.4.2. Dual-satellite PBD

Three dual-satellite PBD solutions can be obtained for Swarm. For each possible pair of Swarm satellites, selected parameter settings are included in Table 4.5. An ephemeris comparison is done for each satellite between its MODK dual-satellite PBD solution and external GSOC/DLR solutions (Table 4.6). As for reduced-dynamic POD, two edges of each orbit often show large inconsistency when comparing with adjacent orbits. These edge effects will be exaggerated by differentiating two GSOC/DLR orbits directly. Therefore two 15 min edges of each MODK or GSOC/DLR orbit are neglected for all baseline comparisons in this research, namely 23-hr baseline comparisons are done instead of 24-hr. An example is shown in Figure 4.7 for 5 August 2014 (DOY 217), which indicates that the edge effects cause clearly larger inconsistency between two solutions. Therefore these influence will be excluded for the following ephemeris comparisons.

In general the different reduced-dynamic orbit solutions show a good level of consistency: the RMS-about-mean of orbit differences is about 5-7 mm for the radial and cross-track directions. For the along-track direction, this is around 12 mm level, which corresponds to a larger dynamic modeling difference between two institutes. Moreover, the comparison shows mean orbit differences of about 2-5 mm in the radial and cross-track directions. They again indicate the differences between the satellite cannon-ball model used in this research and the panel box-wing macro-model used in (Montenbruck et al., 2018a). The mean of differences in the radial direction can be attributed to the missing Earth albedo modeling in this research. More sophisticated dynamic modeling of satellite is beneficial for POD and PBD (Calabia and Jin, 2016; Hackel et al., 2017), however it goes beyond the scope of this research.

Results of the ephemeris comparisons in terms of baseline are displayed in Table 4.7. It has to be noted that the GSOC/DLR solutions are provided from midnight to midnight, which differs with the 24-hr arc in this research. The comparisons have been done for both the reduced-dynamic and kinematic MODK baseline solutions. It can be observed that the mean of baseline differences is very small, typically below 1 mm for the radial and cross-track directions, and below 2.5 mm for the along-track direction. It is clear that common single-satellite orbit errors are canceled to a large extent when forming baselines, *cf.* Table 4.6. For the reduced-dynamic solutions, a 1-3 mm level consistency is obtained for the Swarm-A/C baseline. This is slightly worse than the level of consistency as reported in (Mao et al., 2018), in which only a comparison for the Swarm-A/C pair was done and the GSOC/DLR baselines

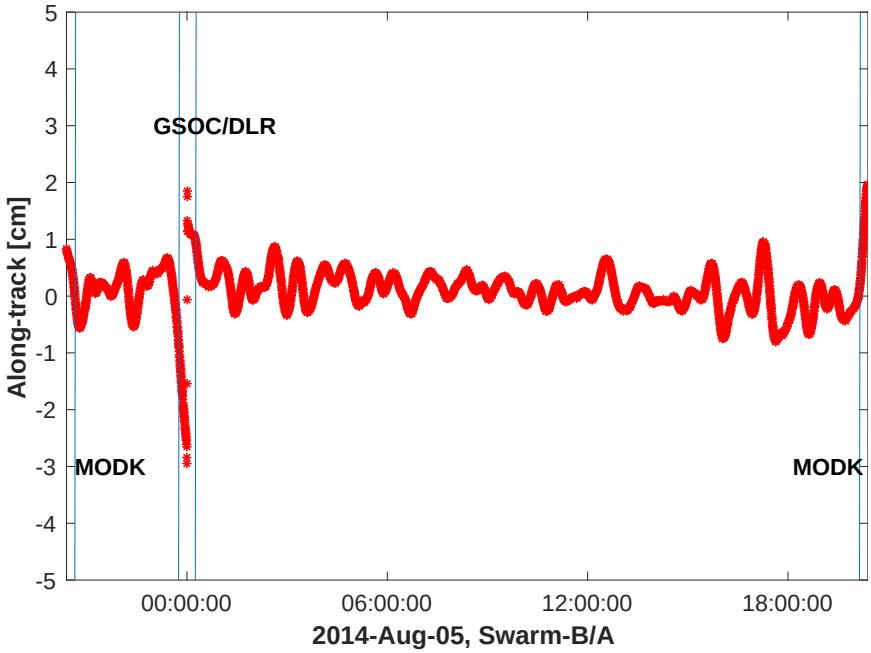

Figure 4.7: Ephemeris comparison between MODK reduced-dynamic solution and GSOC/DLR single receiver ambiguity fixed reduced-dynamic orbits in along-track direction for the Swarm-B/A baseline (DOY 217, 2014).

Table 4.6: Ephemeris comparison between different dual-satellite reduced-dynamic MODK baseline solutions and GSOC/DLR single receiver ambiguity fixed reduced-dynamic orbits (mean and RMS-about-mean, 10 orbit arcs).

Satellite	PBD solution	Radial (mm)	Along-track (mm)	Cross-track (mm)
Swarm-A	Swarm-A/C	4.8 ± 6.0	-2.8 ± 12.8	1.4 ± 7.1
	Swarm-B/A	4.9 ± 6.0	-2.7 ± 12.4	3.1 ± 7.1
Swarm-B	Swarm-B/A	5.0 ± 5.3	-0.7 ± 11.1	3.3 ± 6.7
	Swarm-B/C	5.0 ± 5.4	-0.4 ± 11.5	3.2 ± 7.1
Swarm-C	Swarm-A/C	4.7 ± 5.9	-1.3 ± 12.8	1.3 ± 7.2
	Swarm-B/C	4.8 ± 5.7	-0.4 ± 12.1	2.9 ± 7.1

were also DD ambiguity fixed solutions. Mao et al. (2018) selected a more quiet ionospheric activity period (January 2016) for comparison. Stronger ionospheric activities bring more challenging issues for precise baseline determination (Tancredi et al., 2015). For the other two reduced-dynamic baselines, larger differences are obtained, which is due to the less favorable geometry between the associated two satellites.

For the kinematic baselines, the consistency between the MODK and the reference GSOC/DLR orbit solutions is worse (Table 4.7). The consistency level is comparable to the consistency between the MODK reduced-dynamic and kinematic orbit solutions (Table 4.3). The consistency for Swarm-A/C is better than for Swarm-B/A and Swarm-B/C, which can be attributed to the less favorable geometry when these satellites are at larger distances. Kinematic solutions will not be computed when less than 5 GPS satellites are in view by two Swarm satellites, therefore the percentage of epochs with available kinematic solutions drops as the distance gets longer for satellite pairs. Another comparison is done between baselines derived from GSOC/DLR kinematic and reduced-dynamic DPOD solutions. It is interesting to observe that for the GSOC/DLR kinematic baseline comparison, a similar level of consistency is obtained for all three baselines, thus including Swarm-A/C. The MODK kinematic baselines display better consistency with the GSOC/DLR DPOD reduced-dynamic reference orbits than the associated GSOC/DLR DPOD kinematic orbits, even for Swarm-B/A and Swarm-B/C formations for which the lengths are varying up to 3500 km. This can be explained by considering that in single-satellite POD, no advantage can be taken of *e.g.* constraining relative dynamics, as are done for Swarm-A/C with the MODK tool. Nevertheless, the GSOC/DLR kinematic solutions for the high-dynamic satellite pairs have around 10% higher availability than the MODK solutions.

Table 4.7: Comparison between different MODK baseline solutions (dual-satellite PBD) and baselines derived from the GSOC/DLR DPOD reduced-dynamic reference orbits (mean and RMS-about-mean, 10 orbit arcs), another comparison is done between the GSOC/DLR DPOD kinematic and reduced-dynamic reference orbits. The percentage of epochs with available kinematic solutions is also shown.

Solution	Radial (mm)	Along-track (mm)	Cross-track (mm)	Perc. (%)
MODK Reduced-dynamic				
Swarm-A/C	-0.0 ± 1.6	2.1 ± 2.9	-0.1 ± 1.4	100
Swarm-B/A	0.7 ± 4.7	1.6 ± 6.7	0.2 ± 3.5	100
Swarm-B/C	-0.2 ± 2.9	0.7 ± 4.3	-0.2 ± 3.0	100
MODK Kinematic				
Swarm-A/C	-0.1 ± 11.9	2.2 ± 5.7	-0.1 ± 3.5	97.7
Swarm-B/A	-0.2 ± 22.8	2.0 ± 12.0	0.4 ± 6.3	80.2
Swarm-B/C	0.9 ± 21.3	0.3 ± 10.0	-0.4 ± 5.9	81.3
DLR DPOD Kinematic				
Swarm-A/C	0.2 ± 21.2	0.1 ± 8.3	-0.1 ± 6.3	93.7
Swarm-B/A	-0.1 ± 25.0	1.0 ± 11.6	0.0 ± 7.6	91.7
Swarm-B/C	0.2 ± 25.4	-1.0 ± 11.6	-0.1 ± 7.6	91.8

Table 4.8: Comparison between MODK kinematic and reduced-dynamic baseline solutions, and ambiguity fixing success rate for dual- and triple-satellite PBD (mean of RMS-about-mean statistics of 10 orbit arcs).

Solution	Radial (mm)	Along-track (mm)	Cross-track (mm)	Amb.fix. (%)
		Swarm-A/C		
Dual-	12.4	5.5	3.6	98.1
Triple-	13.9	6.4	4.0	98.4
		Swarm-B/A		
Dual-	22.9	9.8	5.6	97.3
Triple-	23.4	10.0	5.8	97.3
		Swarm-B/C		
Dual-	22.6	10.4	5.7	97.5
Triple-	23.5	10.4	5.9	97.4

4.4.3. Triple-satellite PBD

When comparing the kinematic and reduced-dynamic baseline consistency obtained by dual-satellite and triple-satellite PBD, respectively, slightly downgraded consistency can be seen for the triple-satellite case in Table 4.8. Table 4.9 shows the direct comparison between satellite orbits computed using the triple-satellite PBD mode and the GSOC/DLR single-satellite reference orbit solutions. This in general also corresponds to the results in Table 4.6. The results indicate that by including a third Swarm satellite leading to high-dynamic baselines does not significantly degrade the baselines solution for the Swarm-A/C pendulum pair.

Table 4.9: Comparison between the Swarm triple-satellite reduced-dynamic PBD orbits of each satellite and the reference GSOC/DLR reduced-dynamic orbit (mean and RMS-about-mean, 10 orbit arcs).

Solution	Radial (mm)	Along-track (mm)	Cross-track (mm)
Swarm-A	4.8 ± 5.7	-2.7 ± 12.0	3.8 ± 7.2
Swarm-B	4.9 ± 5.4	-0.6 ± 11.6	3.9 ± 7.1
Swarm-C	4.7 ± 5.7	-0.5 ± 12.3	3.6 ± 7.3

Table 4.10 shows the results of comparison between Swarm triple-satellite PBD solutions and baselines derived from the reference GSOC/DLR orbits. When comparing with dual-satellite mode, in general around 2.6% less kinematic solutions are created for Swarm-A/C baseline due to more data editing for three satellites. Compared to the dual-satellite mode, more single-differenced combinations have to be established and pass the data editing because of the involvement of Swarm-B (Van Barneveld, 2012). It is found that the single-differenced clock offset editing

- highly determined by the relative ionospheric changes between two satellites - is the dominant impact factor which discards more than 1% data for each satellite. However for especially Swarm-B/A baseline a slight improvement of 1% is obtained, which can be attributed to more kinematic solutions passing the residual assessment. Dual-satellite PBD mode lacks constraint from the third satellite, therefore more solutions at larger distance will fail to pass this test. The baseline consistency between the MODK kinematic solutions and the reference solutions is similar compared to the result for dual-satellite PBD (Table 4.7), which corresponds to the results in Tables 4.8 and 4.9. Nevertheless, for the triple-satellite PBD, the reduced-dynamic baseline solutions, especially baselines involving Swarm-A, have slightly better agreement with the GSOC/DLR orbits. For the Swarm-A/C pair an improvement from 1.6/2.9/1.4 to 1.5/2.6/1.4 mm is obtained, for the Swarm-B/A pair 4.7/6.7/3.5 to 3.3/4.7/3.3 mm, and for the Swarm-B/C pair a slight degradation from 2.9/4.3/3.0 to 3.1/4.6/3.1 mm. It will be assessed in Section 4.4.4 if the absolute orbit solutions are influenced by the triple-satellite PBD.

Table 4.10: Comparison between different MODK baseline solutions (triple-satellite PBD) and the baselines derived from the reduced-dynamic GSOC/DLR reference orbits (mean and RMS-about-mean, 10 days). The percentage of epochs with available kinematic solutions is also shown.

Solution	Radial (mm)	Along-track (mm)	Cross-track (mm)	Perc. (%)
MODK Reduced-dynamic				
Swarm-A/C	-0.1 ± 1.5	2.2 ± 2.6	-0.1 ± 1.4	100
Swarm-B/A	0.6 ± 3.3	1.5 ± 4.7	0.1 ± 3.3	100
Swarm-B/C	-0.2 ± 3.1	0.7 ± 4.6	-0.2 ± 3.1	100
MODK Kinematic				
Swarm-A/C	-0.0 ± 13.0	2.2 ± 6.2	-0.1 ± 3.8	95.1
Swarm-B/A	-0.6 ± 22.2	2.3 ± 10.0	0.5 ± 6.2	81.5
Swarm-B/C	1.1 ± 22.5	0.1 ± 10.8	-0.6 ± 6.3	81.2

Figure 4.8 depicts a one day comparison between two kinematic solutions and the GSOC/DLR-derived reduced-dynamic baseline solution for three satellite pairs. It shows periodic peaks, especially for the Swarm-A/C pair whose baseline length is varying between 30 to 180 km. They fly simultaneously over two poles with the smallest distance. However, they also experience the worst consistency in the polar areas. Allende-Alba et al. (2017); Van den IJssel et al. (2015); Mao et al. (2018) all report that ionospheric activities clearly deteriorate the POD and PBD solutions above two geomagnetic poles. The ionospheric activity became stronger as the 11-year solar cycle was approaching its peak at the end of 2014.

Figure 4.9 takes one example and shows the baseline consistency between the MODK kinematic and reduced-dynamic solutions as a function of the distance between two associated satellites for a representative day. This consistency is displayed for each individual direction, where the direction is defined by the local-

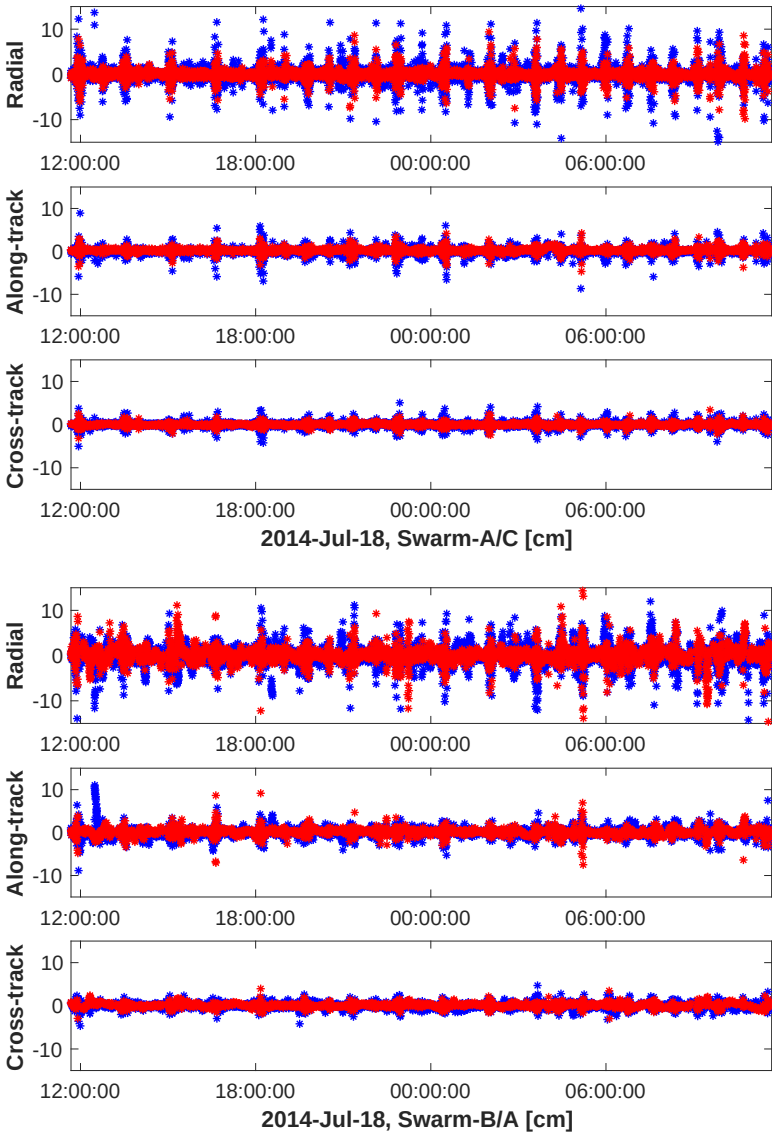

Figure 4.8: Ephemeris comparison (unit:cm) for the GSOC/DLR(blue) and MODK(red) kinematic baselines for the Swarm-A/C (top), Swarm-B/A(bottom) satellite pairs, the GSOC/DLR DPOD reduced-dynamic baselines are set as reference (DOY 198, 2014). The comparison for Swarm-B/C pair is similar with Swarm-B/A pair.

horizontal, local-vertical reference frame (*i.e.* radial, along-track and cross-track direction) of a reference satellite (Swarm-A for Swarm-B/A and Swarm-A/C formations, and Swarm-B for Swarm-B/C formation). Baseline consistency for the radial

direction is the worst, which can be explained by geometry, *i.e.* the largest component of Geometric Dilution Of Precision (GDOP) is in this direction.

Figure 4.9 also shows that the availability of kinematic solutions drops when the distance between the two associated satellites increases. As shown in Figure 4.2, the number of simultaneously tracked GPS satellites by two on-board GPS receivers drops when the distance increases. Eventually, there will not be sufficient satellites simultaneously in view to compute a kinematic baseline solution. Apparently the spatial geometry for the more dynamic Swarm-B/A and Swarm-B/C pairs deteriorates more quickly. In general the Swarm-B/A and Swarm-B/C satellite pairs have only 81.5% and 81.2% of epochs with kinematic solutions, respectively, compared to 95.1% for the Swarm-A/C satellite pair (see Table 4.10). It can be observed in Figure 4.9 that the consistency between kinematic and reduced-dynamic baselines solutions become slightly worse with increasing distance. The consistency statistics are shown in Table 4.10, which indicate that 13.0/6.2/3.8 mm is achievable for the Swarm-A/C satellite pair in respectively the radial, along-track and cross-track directions. For the Swarm-B/A satellite pair, a degraded consistency level of 22.2/10.0/6.2 is obtained, similar to the Swarm-B/C satellite pair.

4.4.4. Satellite laser ranging

The availability of SLR observations for the Swarm constellation allows for an independent validation of orbit solutions in the line-of-sight direction between the SLR ground stations and each LEO satellite (Pearlman et al., 2002). An editing threshold of 30 cm is applied, which is more than an order of magnitude above the RMS of fit levels. In addition, observations below a 10° elevation cut-off angle are excluded to eliminate observations with relatively large atmospheric delay correction errors. An SLR retro-reflector correction map from the German Research Center for Geosciences (GFZ) is included (Neubert et al., 1998). Furthermore, four SLR stations (Arequipa, Hartebeest, Kiev, Simeiz) with large mean offsets are excluded for the Swarm SLR validations. Eventually $76.5\%(649/848)$, $80.2\%(1385/1726)$ and $75.3\%(510/677)$ of the SLR observations are used for orbit validation of Swarm-A, -B and -C respectively (Table 4.11).

It can be observed that for the MODK POD single-satellite orbits the RMS-about-mean of fit of SLR validation is quite close to the reference ESA reduced-dynamic Precise Science Orbits (PSO) (Van den IJssel et al., 2015). In general, a consistency level (RMS-about-mean) of around 20 mm is achieved for the three Swarm satellites. The best performance is obtained for Swarm-B, which flies at the highest altitude. The best accuracy is found for the GSOC/DLR single-receiver ambiguity fixed solutions. Similar to the analysis in (Kroes, 2006; Van Barneveld, 2012), the dual-satellite PBD results in slightly worse SLR consistency levels. Note that for the Swarm-B satellite, the consistency improves for the Swarm-B/C PBD, but not for the Swarm-B/A PBD solution. For the Swarm triple-satellite MODK PBD solution, similar levels are obtained. This indicates good consistency between dual-satellite and triple-satellite modes of MODK.

The Swarm-A/C satellites fly in formation with a baseline below 180 km. Therefore it is possible that an SLR station switches between these two Swarm satellites

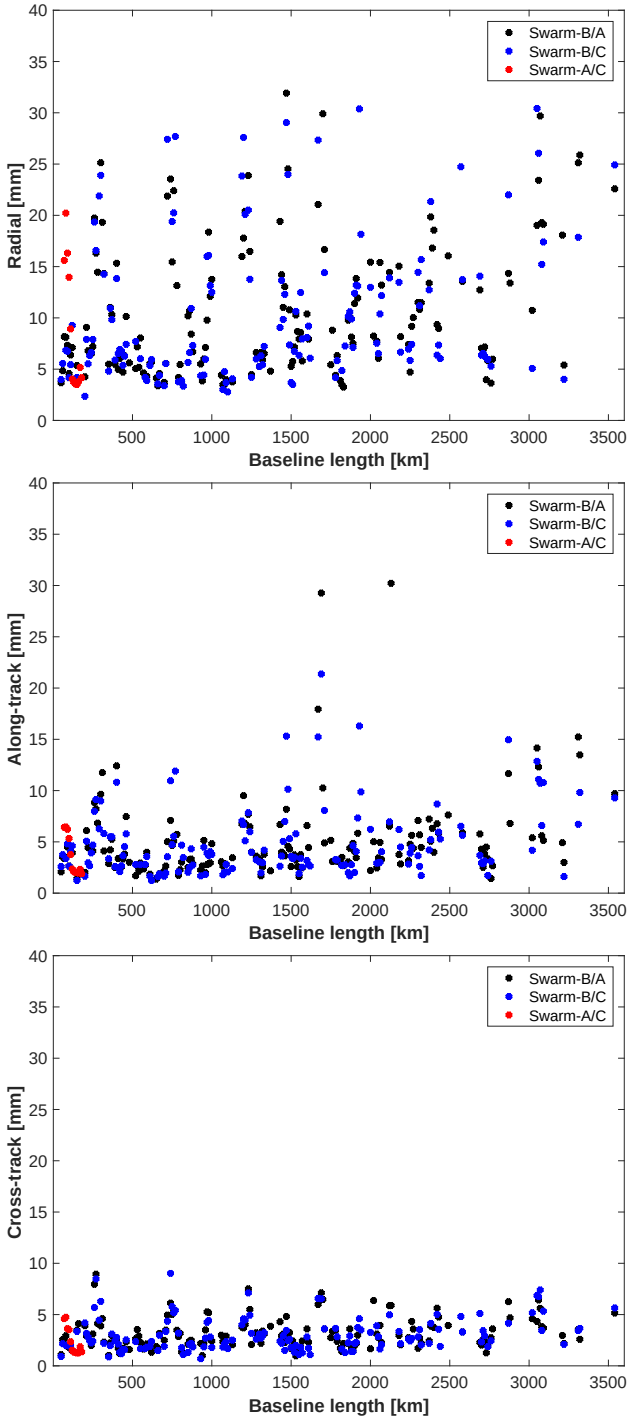

Figure 4.9: RMS of differences between kinematic and reduced-dynamic solutions as a function of distance (every 10 kms) in the radial (top), along-track (middle) and cross-track (bottom) directions for the three Swarm baselines (DOY 198, 2014).

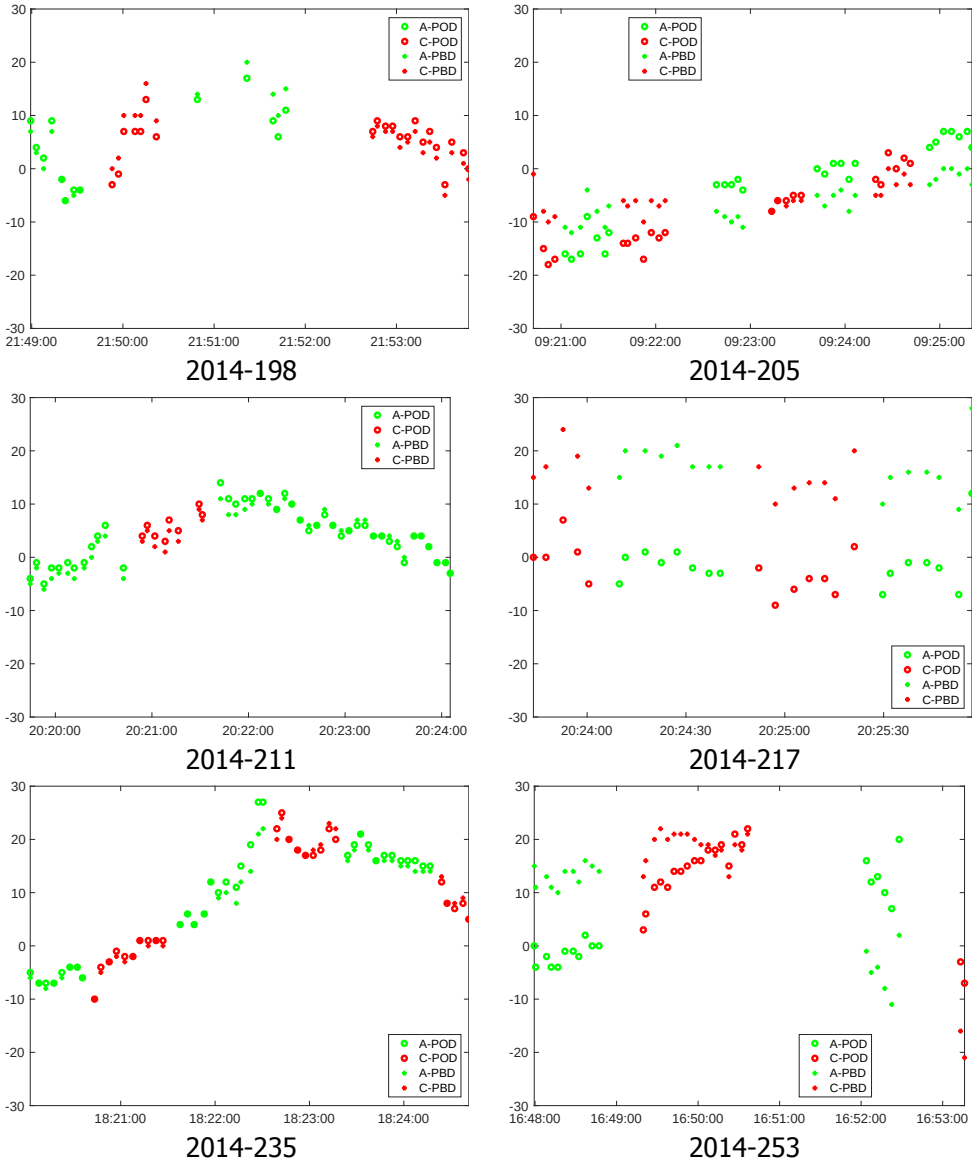

Figure 4.10: SLR validations (unit:mm) for the SWARM-A/C single-satellite POD (reference) and dual-satellite PBD orbit solutions by using the well-performing Yarragadee station in Australia. Six tracking passes with more than 27 points are selected. For each pass the DOY in 2014 is indicated.

Table 4.11: Mean and RMS-about-mean of fit of SLR observations for different reduced-dynamic orbit solutions for the 10 selected orbit arcs.

Solution	Swarm-A (mm)	Swarm-B (mm)	Swarm-C (mm)
ESA	1.5 ± 18.4	-2.8 ± 14.7	1.9 ± 21.0
GSOC/DLR	1.1 ± 17.5	1.0 ± 11.1	1.6 ± 21.2
POD	-1.1 ± 20.8	-4.0 ± 14.1	0.8 ± 21.6
PBD Swarm-A/C	-0.7 ± 21.0	NA	0.7 ± 22.1
PBD Swarm-B/A	-0.8 ± 19.2	-2.2 ± 14.3	NA
PBD Swarm-B/C	NA	-3.7 ± 12.7	1.1 ± 22.3
PBD Swarm-A/B/C	-0.9 ± 19.7	-3.5 ± 12.9	1.3 ± 22.2
No.	649	1385	510

during one overpass. This offers an additional opportunity to assess the consistency in terms of time series between the two different orbit solutions and the SLR observations. The Yarragadee station in Australia offers the largest number of such overpasses and is therefore selected for this analysis.

When tracking the Swarm-A and C satellites, normally the Yarragadee tracking switches happen 1 to 6 times during the satellite overpass, which typically has a duration of only a few minutes. Figure 4.10 shows that for DOY 205 in 2014, the SLR residuals are better aligned in time when using the Swarm-A/C dual-satellite PBD solution. For other passes displayed in Figure 4.10, consistency is minimally at the same level for the PBD solutions as compared to the POD solutions. This result agrees well with results reported in (Allende-Alba et al., 2017) and also similar analysis for the TanDEM-X/TerraSAR-X formation as reported in (Arnold et al., 2018).

Another assessment is done to check the alignment of Swarm-A/C satellites based on the Swarm-B/A and Swarm-B/C PBD on DOY 205 in 2014. Good alignment is also obtained. This demonstrates the benefits of relative dynamics constraints between the higher Swarm-B and either of the lower Swarm satellites. The standard deviations of Swarm-A/C satellite SLR validation residuals for this orbit pass are 7.78, 3.36, 3.12 and 2.48 mm for the single-satellite POD, Swarm-A/C dual-satellite PBD, triple-satellite PBD and the Swarm-A/C baseline based on the Swarm-B/A and Swarm-B/C PBD, respectively. A smaller standard deviation represents better alignment between two satellite orbits. Clearly the alignments for the latter three solutions are very close and are better than the single-satellite POD orbits. The PBD seems to improve the SLR consistency between the Swarm-A and -C satellites for this day.

4.5. Conclusions and recommendations

The three-satellite Swarm constellation has been used as test bed for Swarm dual- and triple-satellite orbit determination, where two of the satellites are flying in formation and the third one flies in a different orbit. Thus, in addition to relatively slowly varying baselines, also fast changing or high-dynamic baselines are included

in the tests. Three different Swarm satellite pairs and thus baselines can be defined: the pendulum baseline (Swarm-A/C) and two high-low baselines (Swarm-B/A and Swarm-B/C), where the high-low baselines can typically be formed during limited periods every 6.1 days. For the latter, the baseline varies from 50 km to 3500 km for orbital arcs with a duration of 24-hr centered around the time of closest approach. Precise Baseline Determination (PBD) for Swarm involving the Swarm-B satellite is challenging because of different levels of dynamic force modeling uncertainty, where it is expected that this is different for Swarm-A and -C. An Iterative Extended Kalman Filter (IEKF) in combination with subset ambiguity fixing is used to compute reduced-dynamic PBD solutions for Swarm. Kinematic PBD solutions are then obtained by using the fixed ambiguities obtained from the reduced-dynamic solutions.

Results show that the GPS receiver RINEX converter and half-cycle to full-cycle ambiguities corrections are very beneficial for PBD. The Swarm reduced-dynamic baseline comparisons with external orbits from the German Space Operations Center (GSOC/DLR) show good baseline consistency at a level of only 1-3 mm for the pendulum Swarm-A/C satellite pair. For the other two pairs, a consistency at a level of 3-5 mm is achieved for different directions. The overall MODK kinematic baseline consistences with its reduced-dynamic baseline are at a level of 13/6/4 mm for Swarm-A/C and a level of 23/11/7 mm for the other two pairs (radial/along-track/cross-track). They are better than the internal consistences between two GSOC/DLR solutions and again indicate the benefits of constraining relative dynamics and fixing Double-Difference (DD) carrier phase ambiguities. However it has to be noted that these consistencies deteriorate when baselines increase.

The research in this paper has shown that triple-satellite PBD including high-dynamic baselines leads to comparable performance in terms of kinematic/reduced-dynamic baseline consistencies and SLR observation fits as dual-satellite PBD. The inclusion of high-dynamic baselines does thus not degrade the quality of the orbit solutions as was the case in *e.g.* Van Barneveld (2012). Compared to single-satellite POD, it was shown that a better Swarm-A/C consistency can be obtained in the time series of SLR observation residuals.

It has also been shown that the consistency between kinematic and reduced-dynamic baseline solutions deteriorates with growing distance, which can be explained to a large extent by a less favorable geometry. A possibility for improvement might be to combine the single-satellite ambiguity fixed method with the PBD ambiguity fixing method used in this paper. This is a nice topic for future research. The single-satellite ambiguity fixed solutions lead to lower kinematic/reduced-dynamic consistency levels at short distance, but might suffer less from a deteriorated geometry for longer distances.

Acknowledgments

The China Scholarship Council (CSC) is gratefully acknowledged for financially supporting part of the work described in this paper. We would like to show our special gratitude to the European Space Agency (ESA) for sharing the Swarm data products. We also very much thank Dr. Oliver Montenbruck from The German Space Oper-

ations Center for providing the single-receiver ambiguity fixed orbit solutions and the new version GPS RINEX data. We also acknowledge two anonymous reviewers for reviewing this paper.

5

CHAMP/GRACE Constellation Baseline Determination

RQ.4 Can we have reliable PBD solutions for satellite constellations comprised of different satellite missions?

This chapter presents the PBD investigation for the complex CHAMP/GRACE constellation. It provides the most dynamic baselines and demands the investigations into many impact factors for a period of three months (March to May, 2005). The CHAMP satellite arouses many new questions due to its significantly different GPS receiver performance and stronger in-flight perturbations.

Absolute and relative orbit determination for the CHAMP/GRACE constellation

Xinyuan Mao[a], *Pieter Visser*[a], *Jose van den IJssel*[a]

Published in *Advances in Space Research*, 63/12 (2019) 3796-3816,
doi:10.1016/j.asr.2019.02.030.

Precise orbit determination was investigated for a satellite constellation comprised of two different missions, the CHAllenging Minisatellite Payload (CHAMP) satellite and the Gravity Recovery And Climate Experiment (GRACE) twin satellites. The orbital planes of these two missions aligned closely during March to May 2005, allowing precise baseline determinations between the associated three satellites based on their onboard BlackJack Global Positioning System (GPS) receivers. The GRACE-A/B satellites fly in tandem formation with a baseline of around 220 km, whereas the baselines between CHAMP and the GRACE tandem vary from about 110 to 7500 km during 24-h orbital arcs centered around the points of closest approaches. A number of factors had to be dealt with for orbit determinations, including the cross-talk between the CHAMP GPS main navigation and occultation antennas, the different levels of non-gravitational accelerations, and the rapidly changing geometry that complicates the fixing of integer ambiguities for the GPS carrier-phase observations.

Quality assessments of the orbit solutions were based on comparisons with Satellite Laser Ranging (SLR) observations, best orbit solutions had a precision of typically 1.7-2.3 cm. Consistency checks between reduced-dynamic and kinematic orbit solutions were done. For the GRACE baselines, the reduced-dynamic/kinematic baseline consistency was typically better than 1 cm, with an ambiguity fixing success rate of around 94%. The agreement with the K-Band Ranging (KBR) measurements was about 0.6 mm. For the CHAMP/GRACE pairs, the reduced-dynamic/kinematic baseline consistency varied from 0.5 to 2.5 cm, where better consistency was obtained for shorter arcs.

Keywords: Precise Orbit Determination; Precise Baseline Determination; High-dynamic Baseline; Satellite Constellation; Integer Ambiguity; Antenna Pattern

5.1. Introduction

Precise Orbit Determination (POD) is a prerequisite for many Low Earth Orbit (LEO) satellites for meeting their mission objectives. Often, absolute orbit precision levels of a few cm are required (Vetter, 2007). Nowadays, the Global Positioning System (GPS) becomes the prime system for cm-level POD of LEO satellites (Wu et al., 1991). In addition, formation flying missions like the tandem GRACE and

(a): Delft University of Technology, The Netherlands

the bistatic TerraSAR-X/TanDEM-X have shown the capability of GPS-based mm-level Precise Baseline Determination (PBD) (Kroes et al., 2005; Montenbruck et al., 2011), where the best precision is obtained after fixing the integer ambiguities of Double-Differenced (DD) carrier-phase observations (Teunissen, 1999). For GRACE, a PBD precision level of better than 1 mm has been achieved. In addition, few mm precision levels have been claimed for the TerraSAR-X/TanDEM-X satellites (Allende-Alba and Montenbruck, 2016). The Swarm constellation has been used as a test bed for also PBD, where two of the three identical Swarm satellites fly in a pendulum formation (Friis-Christensen et al., 2008). It has been shown that great care has to be taken with GPS observation pre-processing, characterizing carrier-phase center and code residual variations, estimating and constraining (relative) empirical accelerations that absorb force model errors and orbital arc length, and fixing DD integer carrier-phase cycle ambiguities (Allende-Alba et al., 2017; Mao et al., 2018). In general, the present PBD research focus mostly on satellite formations with relatively stable baselines between hundreds of meters up to 220 km (GRACE).

At present many space projects call for the implementation of more complex constellations to fulfill corresponding mission requirements and PBD for those satellites might support their mission objectives (Sabol et al., 2001). The European Copernicus Program has been building a constellation comprised of diverse satellites functioning in different orbits until the end of the next decade (Butler et al., 2014). One of its composed sub-missions, Sentinel-1, will consist of two or even four satellites flying in formation to provide continuous global radar imaging observations (Torres et al., 2012). By the end of 2018, an Iridium-next constellation will be completed with 66 functioning satellites. A simulation shows its capacity of making use of their GPS-based orbits for recovering large-scale gravity variations and especially for tracking large scale movement of water mass (Gunter et al., 2011). Moreover, the next generation gravity field recovery satellite mission will probably consist of two separate formations operating in different orbital planes (Elsaka et al., 2014). These space missions flying in large constellations definitely require more robust absolute and relative orbit reconstructions, for which the POD and PBD methods need to be further investigated.

Van Barneveld (2012) initiated an innovative research for a complex constellation comprised of the CHAMP (Reigber et al., 2002b) and the GRACE twin satellites (Tapley et al., 2004a). After the launch of CHAMP on 15 July 2000 and GRACE on 17 March 2002, a favorable geometry existed in the first half of 2005 when the two orbital planes were closely aligned. In this period, the CHAMP and GRACE satellites regularly closely approached each other allowing to serve as an ideal test bed for assessing the performance of POD and PBD methods. The GRACE formation baseline length was always varying around 220 km, whereas each CHAMP/GRACE baseline length varied rapidly from 110 to more than 7500 km in a 24-h period around the point of closest approach. Nonetheless, Van Barneveld (2012) showed that it is very challenging to have a completely correct carrier-phase integer cycle ambiguity fixing. In fact, the precision of PBD solutions often significantly deteriorated because of wrongly fixed ambiguities, particularly for the ground-based PBD which experienced more challenging disturbances such as troposphere (Blewitt, 1989). The

work presented in this study builds on the work initiated by Van Barneveld (2012). It is assessed if PBD solutions can be enhanced by considering the following modifications based on the implementation outlined by Van Barneveld (2012):

- A different approach is adopted to select orbital arcs. The CHAMP satellite and the GRACE twin satellites baseline lengths reach a local minimum in every 2.7 days in the favorable time period. The epoch of the closest approach - or encounter - is determined and then a 24-h orbital arc is defined starting 12 hr before and ending 12 hr after. This differs with Van Barneveld (2012) in which orbital arcs started and ended at midnight and thus resulted in significantly different constellation geometries. In fact, also the impact of the length of the orbital arc on the reliability of DD carrier-phase ambiguity fixing and associated precision of baseline solutions is assessed. Typically, 24-h arcs are used in GPS-based POD and PBD, but due to the rapidly changing geometry for the CHAMP/GRACE baselines, it is interesting to assess the impact of the arc length which has been varied from 2 to 24 hr.

- The so-called Code Residual Variation (CRV) patterns are applied to correct GPS code observations (Mao et al., 2017). The need of using antenna Phase Center Variation (PCV) patterns in both POD (Haines et al., 2004; Van den IJssel et al., 2015; Jäggi et al., 2009) and PBD (Allende-Alba and Montenbruck, 2016; Mao et al., 2017) has been well demonstrated for many satellite missions. In addition to these PCV patterns, CRV patterns were found to further improve POD and PBD when GPS signal cross-talk and large multi-path existed on the GPS main navigation antenna of the trailing GRACE satellite (Mao et al., 2017). During the selected period, the CHAMP satellite had kept its space-borne GPS occultation antenna activated and therefore signal interference occurred on the main antenna. No GPS antenna code patterns were applied in Van Barneveld (2012).

- The GRACE DD carrier-phase ambiguities are fixed before introducing the DD carrier-phase observations between the CHAMP and GRACE satellites. The so-called empirical accelerations that absorb GRACE force model errors can be more heavily constrained in a relative sense than for the CHAMP/GRACE combinations leading to more reliable DD ambiguity fixing. These then serve as prior information to compute the CHAMP/GRACE baselines. For the CHAMP/GRACE baselines, both solutions with and without ambiguity fixing (the latter referred to as *float* solution), are generated. In the *float* solution, the GRACE solution will then not be influenced by the additional CHAMP-relevant ambiguity resolution. In Van Barneveld (2012) no float solution was computed. As stated above, Van Barneveld (2012) showed that especially wrongly-fixed integer ambiguities affect the precision of both GRACE and CHAMP/GRACE baselines. In this research, the comparison between two solutions will show the detailed impact of CHAMP/GRACE baseline ambiguity fixing on the GRACE baseline.

This research selects 30 24-h orbital arcs from March to May 2005, or the period

indexed by Day-Of-Year (DOY): 061-152. Each orbital arc provides one relatively stable GRACE baseline and two highly variable baselines, *i.e.* CHAMP/GRACE-A and CHAMP/GRACE-B. The quality of POD and PBD solutions will be assessed by comparison with independent Satellite Laser Ranging (SLR) observations (Degnan, 1993) and, for GRACE, also K-Band Ranging (KBR) system (Tapley et al., 2004b). In addition, quality assessments will be done by comparison with external orbit solutions and by comparing kinematic with reduced-dynamic POD and PBD solutions (Allende-Alba and Montenbruck, 2016; Mao et al., 2018).

This study is organized as follows. Section 5.2 introduces the selected satellite constellation and observational data, including a quality assessment of the latter. Section 5.3 briefly presents the kinematic and reduced-dynamic PBD methods and associated parameterizations. Section 5.4 includes the assessment of GPS observations processing and antenna CRV patterns. PBD is done for each dual-satellite pair and the triple-satellite constellation. Moreover, the results of quality assessments are discussed. In Section 5.5 conclusions and future recommendations are made resulting from this research.

5.2. Satellite constellation

As outlined in the previous Section, a constellation is formed by selecting CHAMP and the two GRACE satellites. For this constellation, 30 orbital 24-h arcs are selected during which CHAMP closely approaches the GRACE tandem. This section includes a quality assessment of the associated GPS data.

5.2.1. Orbital arc selection

The CHAMP and GRACE satellites were initially deployed into different polar orbits, which aligned closely in April 2005. In this period, the difference between the CHAMP and GRACE altitudes is around 110 km on the average and the alignment of the orbital planes follows from the adjacent values for the inclination and right ascension of ascending node (see Table 5.1 for the relevant Keplerian orbital elements). The lower CHAMP satellite experiences stronger non-gravitational perturbations than GRACE mostly due to the denser neutral thermosphere along its in-flight direction (Doornbos, 2012). The best alignment of the orbital planes occurs on 7 April 2005.

Table 5.1: Three selected Keplerian orbital elements for the CHAMP and GRACE satellites during March-May 2005. a represents the semi-major axis, I the orbit inclination and $RAAN$ the right ascension of the ascending node (Credit: satellite two line elements data are obtained from www.space-track.org).

Satellite	a [km]	I [deg]	$RAAN$ [deg]
GRACE-A	6849.3-6848.3	89.0	211.4-199.5
GRACE-B	6849.3-6848.3	89.0	211.4-199.5
CHAMP	6739.9-6734.4	87.2	221.1-185.4

The altitude difference leads to an orbital period difference of around 2.2 min. Therefore, CHAMP will have a closest approach with the GRACE twin satellites ap-

proximately every 2.7 days. Eventually 35 24-h orbital arcs can be selected based on these orbit encounters (Table 5.2). Please note that the orbital arc indexed by DOY 096 is excluded because of maneuvers by GRACE-B, DOYs 061, 064, 074 and 077 are excluded due to large gaps in the GPS data of at least one of the three satellites. A representative orbital arc is illustrated in Figure 5.1. It can be clearly seen that the GRACE baseline is maintained at a value of around 220 km. Two CHAMP/GRACE baseline lengths vary dramatically from 110 to 7500 km in a 12-h period close to the encounter.

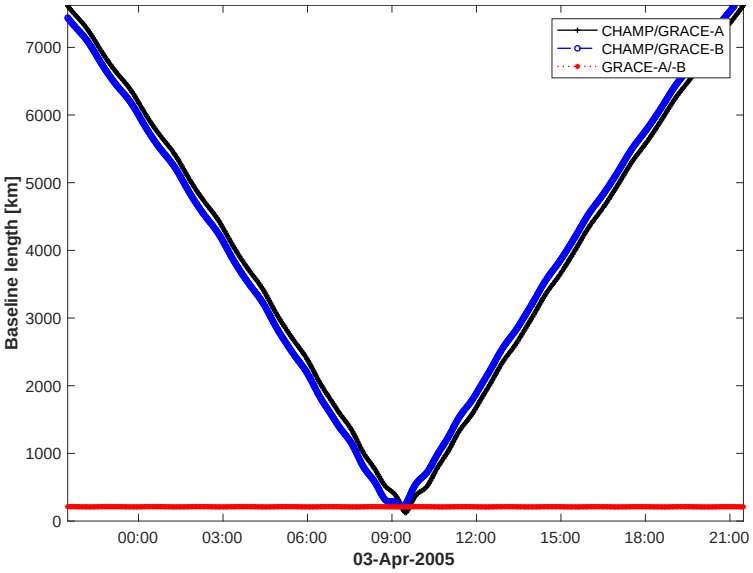

Figure 5.1: Baseline length variations for each dual-satellite pair during a representative 24-h orbital arc (DOY 093, 2005). The GRACE baseline has been stabilized at around 220 km, the two CHAMP/GRACE baselines are rapidly changing from 110 to 7500 km in 24 hours.

5.2.2. Data quality assessment

Figure 5.2 shows the number of GPS satellites that are simultaneously tracked by each satellite pair. For a dual-satellite PBD, a minimum of 5 GPS satellites is required that are simultaneously in view (Kroes, 2006). The GRACE pair shares on average 7 satellites that are in view simultaneously. For the high-low CHAMP/GRACE satellite pairs this number drops rapidly as the baseline lengths increase. Surprisingly, for the CHAMP/GRACE-A satellite pair this number is larger than that for the GRACE tandem when the distance is smaller than 500 km. This is because the CHAMP GPS receiver tracks GPS satellites down to lower elevations than GRACE-B resulting in more DD carrier-phase combinations. It is noted that the number for the CHAMP/GRACE-A pair is nearly always larger than CHAMP/GRACE-B, which again is due to the lower elevation cut-off angle for GRACE-A than for GRACE-B. A smaller number of possible DD carrier-phase combinations results in a larger Geometric Dilution Of

Table 5.2: Thirty-five identified 24-h orbital arcs for the CHAMP/GRACE constellation. Please note that DOY specifies the day of the middle epoch of each orbital arc. This DOY number will be used as orbital arc identifier in this research (the 5 orbital arcs marked by * are excluded).

Date (YYYY-MM-DD)	DOY	Middle of the arc	Minimum distance (km)
2005-03-02	061	13:37:30	235.97*
2005-03-05	064	05:09:30	208.80*
2005-03-07	066	21:27:00	122.47
2005-03-10	069	13:44:00	191.49
2005-03-13	072	05:16:00	183.20
2005-03-15	074	21:32:20	195.28*
2005-03-18	077	13:03:50	132.32*
2005-03-21	080	04:35:30	119.71
2005-03-23	082	20:06:40	102.98
2005-03-26	085	11:37:40	121.40
2005-03-29	088	03:07:50	171.49
2005-03-31	090	18:00:10	220.47
2005-04-03	093	09:29:00	121.92
2005-04-06	096	00:26:20	205.76*
2005-04-08	098	15:50:10	126.39
2005-04-11	101	06:42:50	123.35
2005-04-13	103	21:31:50	167.06
2005-04-16	106	12:17:40	197.76
2005-04-19	109	03:01:40	201.95
2005-04-21	111	17:45:00	176.84
2005-04-24	114	08:28:00	135.27
2005-04-26	116	23:10:50	129.65
2005-04-29	119	13:53:40	218.93
2005-05-02	122	03:52:00	225.44
2005-05-04	124	18:34:20	111.55
2005-05-07	127	08:31:30	219.99
2005-05-09	129	23:13:20	172.97
2005-05-12	132	13:09:50	130.90
2005-05-15	135	03:06:20	153.27
2005-05-17	137	17:02:20	208.57
2005-05-20	140	06:58:10	151.70
2005-05-22	142	20:53:50	139.24
2005-05-25	145	10:49:30	121.03
2005-05-28	148	00:44:50	227.62
2005-05-30	150	13:54:30	205.15

Precision (GDOP) negatively affecting the quality of PBD solutions. The combination of Figure 5.1 and 5.2 reveals that PBD for longer CHAMP/GRACE baselines will be more challenging than shorter baselines, since with increasing baseline lengths less and less GPS satellites are simultaneously in view. It can be also observed that for time instances less than 5 hr away from the point of closest approach (thus arc length of around 10 hr), on the average more than 5 GPS satellites are in view

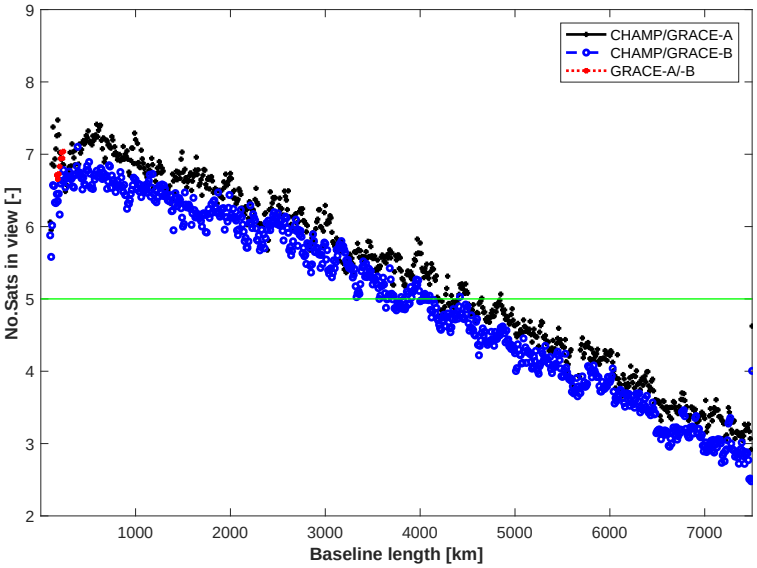

Figure 5.2: The number of GPS satellites simultaneously tracked by two space-borne GPS receivers as a function of distance (every 10 km) for each dual-satellite pair (analysis for 30 24-h orbital arcs).

simultaneously.

As stated in Section 5.1, the application of PCV and CRV maps are essential to fully exploit the precision of GPS observations for POD and PBD. The GPS antenna PCV patterns are created for each individual satellite using the *Residual Approach* method (Jäggi et al., 2009). The use of PCV maps has been widely recognized as standard processing step for satellite POD. In addition, GPS code observations can also be affected by various random and systematic error sources, *e.g.* thermal noise and multipath. The CHAMP GPS main navigation receiver suffers from significant superposition of the direct signal with interfering signals taking a different signal path, referred to as *cross-talk* (Ho et al., 2012; Montenbruck and Kroes, 2003). A GPS data quality assessment has been done based on the methods outlined in (Kroes, 2006). Figure 5.3 displays estimated code noise levels for the CHAMP and GRACE GPS receivers as a function of elevation. The CHAMP and GRACE-A GPS receivers experience larger patterns at lower elevations, where the collected GPS signal will be influenced more by the ionosphere. Besides, for particularly the L_2 frequency, it can be observed that an irregular pattern exists for CHAMP. This agrees with Montenbruck and Kroes (2003) who reported pronounced code patterns for the aft-looking hemisphere of the navigation antenna. The *cross-talk* was found to impact the P_2 code observations more than the P_1 code observations. This cross-talk signal interference is due to the activated occultation antenna and characterizing the associated impact is expected to improve POD and PBD solutions. A similar phenomenon occurred during the later phases of the GRACE mission lifetime, but not during the selected period for the research described in this study. For the

CHAMP/GRACE POD and PBD solutions of this research, GPS antenna CRV patterns were derived and implemented (Section 5.4).

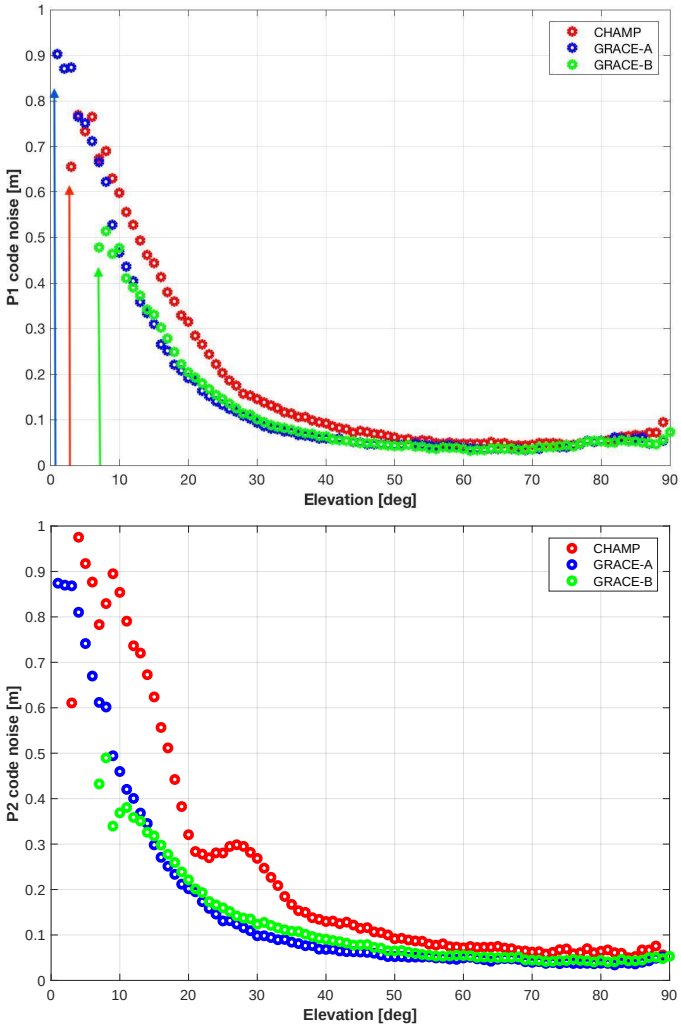

Figure 5.3: Root-Mean-Square (RMS) of code residuals (mostly multi-path effect, interference, systematic errors, etc.) as a function of elevation for the GPS L_1 (top) and L_2 (bottom) frequencies for the associated GPS receiver RINEX data (selected day: DOY 091, 2005).

5.3. Precise baseline determination

This research makes use of the GPS High Precision Orbit Determination Software Tools (GHOST) add-on tool called Multiple Orbit Determination using Kalman filtering (MODK) (Van Barneveld, 2012; Wermuth et al., 2010). The MODK tool relies on

an Iterative Extended Kalman Filter (IEKF) and allows the so-called subset ambiguity fixing. MODK is also capable of providing a kinematic baseline solution in addition to the reduced-dynamic baseline solution produced by the IEKF (Mao et al., 2018). Another GHOST software module - KInematic Point Positioning (KIPP) - is used for computing single-satellite kinematic orbit solutions for comparison purposes.

The primary MODK module output consists of reduced-dynamic POD and PBD solutions based on an IEKF, where both gravitational and non-gravitational force models are employed. Force model errors are compensated by the estimation of so-called empirical accelerations. Since the CHAMP and GRACE satellites fly at different altitudes, the level of - especially non-gravitational - force model errors is different. The empirical accelerations are defined in the local-horizontal, local-vertical reference frame, *i.e.* they act in the radial, along-track and cross-track direction, and are defined as first-order Gauss-Markov processes (Bierman, 2006). These are characterized by a correlation time (τ), standard deviation of a-priori values (σ_a) and process noise (σ_p). These parameters are to be set according to predicted force model error level for each satellite.

In addition, it is possible to not only set these parameters for absolute, but also relative empirical accelerations. This has been proved to be very beneficial for estimating the empirical accelerations for the GRACE satellites, since they fly almost identical orbits and it is fair to assume that their orbit determination suffer from similar force model errors. It has been demonstrated that constraining the relative empirical accelerations results in improved GRACE and Swarm-A/C baseline solutions (Mao et al., 2017, 2018). For this research, it was found by trial and error that for τ a value of 600 s works well. Values for the other parameters, dynamic models and data sets are included in Table 5.4.

Table 5.3: Overview of dynamic models, data sets and IEKF parameter settings employed in the MODK PBD package for the CHAMP/GRACE constellation.

Spacecraft model	500 kg canon-ball with cross-section of 1.0 m^2 for GRACE and 0.5 m^2 for CHAMP
Gravitational forces	GOCO03S 120×120 (selectable, maximum 250×250) static gravity field, plus linear trends for spherical harmonic degree 2 terms according to IERS2003 (Mayer-Gürr et al., 2012; McCarthy and Petit, 2004) Luni-solar third body perturbations CSR Ocean tides model based on TOPEX/GRACE data (FES2004 as reference) (Lyard et al., 2006)
Non-gravitational forces	Atmospheric drag: Jacchia 71 density model (Jacchia, 1972) Solar radiation pressure: Conical Earth shadow, Sun flux data
Earth parameters	Leap second data table of TAI-UTC CODE Earth rotation parameters, version 2.0 (Dach et al., 2009)
GPS products	CODE 5s GPS final products and clocks (Dach et al., 2018) IGS transmitter antenna phase center offsets and variations (Schmid et al., 2016) CODE global ionosphere maps (also P1-P2 differential code bias for GPS satellites) (Schaer, 1999)
Antenna patterns	Frequency-dependent PCV and CRV patterns (Mao et al., 2017)
Orbit arc length	2 to 24 hr (selectable with an interval: 2 hr)

Reference orbits	GRACE: Jet Propulsion Laboratory (JPL) L1B orbit products (Bertiger et al., 2002), CHAMP: reduced-dynamic POD orbit computed by MODK
Attitude data	GRACE: JPL L1B (Case et al., 2002), CHAMP: GeoForschungsZentrum (GFZ) ISDC (Reigber et al., 2002b)
GPS observations	GRACE: JPL L1B, CHAMP: GFZ ISDC
IEKF iterations	Maximum: 15
GPS data weighting	Code/Carrier-phase: 0.5/0.004 m
Amb. Resolution	LAMBDA subset fixing (Teunissen, 1999; Van Barneveld, 2012)
Amb. Validation (Verhagen, 2005)	Probability test : 99.9% Integer test: 5% Discrimination test: 5 Widelane test: 5%, 0.2 cycles Ionosphere free test: 5%, 0.01 m
GPS data editing Zero-difference	Minimum SNR (signal to noise ratio): 5 Minimum cut-off elevation : 0 ° Ionospheric delay change threshold : 2.0 m Ionosphere-free (IF) code editing outliers : 1.0 m IF carrier-phase editing outliers : 0.015 m
C_D Zero-difference	1 per 24 hr, GRACE: σ_a =2.3, σ_p =1.0, CHAMP: σ_a =4.5, σ_p =1.0
C_R Zero-difference	1 per 24 hr, GRACE: σ_a =1.3, σ_p =1.0, CHAMP: σ_a =1.6, σ_p =1.0
Empirical acc. (τ =600 s unit: nm/s^2)	Radial : σ_a =10, GRACE: σ_p =2, CHAMP: σ_p =4 Along-track: σ_a =40, GRACE: σ_p =8, CHAMP: σ_p =16 Cross-track: σ_a =20, GRACE: σ_p =4, CHAMP: σ_p =8
Ionospheric delay Clock offset	τ =10 s, σ_a =100 m, σ_p =1 m τ =100 s, σ_a =500 m, σ_p =500 m

Single-difference settings	GRACE-A/B	CHAMP/GRACE
Ionospheric delay change threshold	0.5 m	2.5 m
IF code editing outlier	1.0 m	5.0 m
IF carrier-phase editing outlier	0.02 m	0.20 m
C_D	σ_p =0.1	σ_p =1.0
C_R	σ_p =0.1	σ_p =1.0
Empirical acc. (τ =600 s unit: nm/s^2)	Radial: σ_a = 5 , σ_p =0.1 Along-track: σ_a = 30 , σ_p =1 Cross-track: σ_a = 10 , σ_p =0.3	σ_a = 50 , σ_p =10 σ_a = 300 , σ_p =100 σ_a = 100 , σ_p =30
GPS data weighting: code/carrier-phase	0.7/0.002 m	0.7/4000 m
Ionospheric delay (τ =10 s)	σ_p =10 m	σ_p =10 m
Clock offset (τ =100 s)	σ_p =5000 m	σ_p =5000 m

For the CHAMP orbit, relatively large non-gravitational force model errors are to be absorbed by the empirical accelerations, especially in the along-track direction, for which atmospheric drag dominates. As mentioned above, the empirical accelerations for the two GRACE satellites are constrained such that they more or less take identical values: the differences between these accelerations have values of 0.1, 1.0, and 0.3 nm/s^2 for the process noise σ_p in three directions. The associated values for the CHAMP/GRACE satellite pair combinations is two orders of magnitude larger to make sure the GRACE POD and PBD solutions are not adversely affected.

The CHAMP and GRACE GPS receiver carrier-phase observations typically have a

precision at the mm-level, compared to dm for the code observations (Montenbruck and Kroes, 2003). When using GPS code and carrier-phase observations in the PBD, the latter should be exploited with higher weight. For the CHAMP and GRACE single-satellite POD the precision level is set at 0.5 m for the code and 4 mm for the carrier-phase observations, comparable to the actual noise levels (see *e.g.* Figure 5.3), leading to a ratio of 125. When constructing the DD combination between two GPS satellites and two GPS receivers, DD carrier-phase integer ambiguities can be resolved for each GPS frequency, and most common errors such as GPS clock and ephemeris errors are eliminated to the maximal extent. For the single-difference combination the code/carrier-phase weight ratio for GRACE tandem is set as 350 (0.7/0.002 m) to facilitate its pre-constrained ambiguity resolution, whilst for CHAMP/GRACE a much smaller ratio is set (0.7/4000 m, Table 5.4) to minimize the influence of more challenging CHAMP/GRACE carrier-phase ambiguity fixing on GRACE baseline determination.

The so called Least-squares Ambiguity De-correlation Adjustment (LAMBDA) is selected for ambiguity resolution (Teunissen, 1999). It has been used to determine baseline solutions for several satellite missions (Allende-Alba and Montenbruck, 2016; Kroes et al., 2005). To maximize the ambiguity fixing success rate, a subset fixing process is implemented. It allows to fix only those integer ambiguities that pass several tests (Verhagen, 2005). This is a modification of the conventional use of LAMBDA which only accepts epochs when the entire set of ambiguities pass the tests (Van Barneveld, 2012). Unfixed ambiguities are retained at their float values, but might be fixed in next iterations (provided the IEKF did not yet converge). An extra test was included that results in keeping the float values if one (or more) of the GPS carrier-phase observation residuals that contribute to the DD is (are) above 5 cm.

As mentioned above, MODK has the capability to provide a second baseline solution, referred to as kinematic. To generate this solution, the position of one of the satellites is kept fixed (and thus its absolute position is in fact a reduced-dynamic solution), but the position of the other satellites is then derived kinematically from the GPS observations including the integer ambiguity fixes that were made in the generation of the reduced-dynamic PBD. Kinematic baseline solutions are only generated if at least 5 GPS satellites are in common view of the reference and other satellite for each possible combination pair. Also here an additional test is employed: epochs for which the RMS of GPS observation residuals after kinematic PBD is above 5 cm will be excluded. The kinematic baseline acts as an internal consistency check for the reduced-dynamic PBD. For detailed information regarding the differences between the kinematic and reduced-dynamic approaches please see Mao et al. (2018).

5.4. Results and discussions

Before discussing single-, dual-, and triple-satellite POD and PBD solutions and associated consistency checks (Sections 5.4.2 and 5.4.3), attention is paid to the impact of processing GPS code observations and correcting them by introducing CRV maps (Section 5.4.1). Validation of POD and PBD solutions by comparison

with SLR observations is addressed in Section 5.4.4. This Section is concluded by an analysis of the impact of the arc length (Section 5.4.5).

5.4.1. GPS observations processing

The tracking channels of the BlackJack main navigation GPS receiver are allocated in sets of three to track C/A, P_1 (on the first frequency) and P_2 (on the second frequency) code observations accompanied by the corresponding C/A, L_1, and L_2 carrier-phase observations. This research only makes use of the dual-frequency P-code and the associated carrier-phase measurements. It has to be noted that for the CHAMP GPS receiver a small percentage of rather adverse carrier-phase outliers are identified (Montenbruck and Kroes, 2003). Its unfavorable impact on PBD has to be minimized. Figure 5.4 presents the time series of CHAMP single-satellite POD carrier-phase residuals on the first frequency for DOY 101. Irregular residual outliers exist frequently even after the default data processing scheme. To get rid of these outliers, the setting for the data editing item *ionosphere-free combination carrier-phase editing outliers* (as stated in Table 5.4) is realized to be extremely important. This item is described by the following equations,

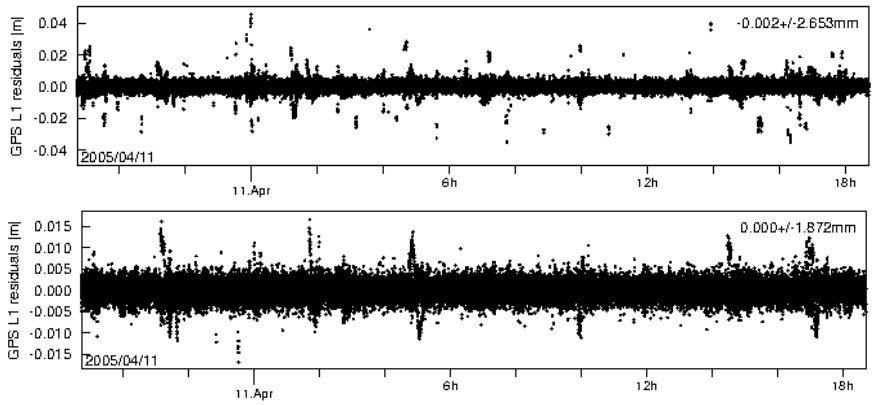

Figure 5.4: The CHAMP GPS receiver carrier-phase residuals on the first frequency for the old (top) and new (bottom) data processing schemes (Orbit arc DOY 101 2005, please note the difference in scale between top and bottom plots).

$$\frac{1}{n-1}\sum_{i=1}^{n}\left\{\left[R_{IF}^{obs}(t_i)-R_{IF}^{mod}(t_i,\mathbf{r})\right]-\left[R_{IF}^{obs}(t_{i-1})-R_{IF}^{mod}(t_{i-1},\mathbf{r})\right]\right\}^2 \leq \sigma_{res}^2$$

$$R_{IF}=\frac{f_1^2R_{f_1}-f_2^2R_{f_2}}{f_1^2-f_2^2} \tag{5.1}$$

where, R is the carrier-phase converted range computed either by the IF combination or on each frequency (f_1=1575.42 MHz and f_2=1227.60 MHz). It can be modeled (mod) based on the reference coordinates of the LEOs (**r**) and the corresponding GPS satellites at certain epochs (t_i). The modeled range will be compared with the real observed value (obs) to obtain the modeling residuals. The mean of the residual change between two adjacent epochs for n GPS satellite measurements is required to pass a certain threshold σ_{res}, otherwise the associated GPS measurements will be excluded for the following POD steps. The original threshold is set as 0.05 m, which accepts 92.6%, 98.0% and 90.9% data for the GRACE-A, GRACE-B and CHAMP POD respectively for the selected 30 orbital arcs. A reduction from 0.05 to 0.015 m results into 1.3%, 0.7% and 0.5% less data passing the data processing scheme for the associated satellites (Table 5.5, indexed by *Old* and *New*).

Figure 5.4 displays that the new processing scheme screens out most of the existing outliers. This change is found to be of great importance to improve the overall POD and PBD performance. Table 5.5 displays the residual level statistics comparison between the *Old* (0.05 m) and *New* (0.015 m) sets of data. The carrier-phase residual statistics on the first frequency is significantly reduced by 0.9, 0.6 and 1.5 mm for GRACE-A, GRACE-B and CHAMP satellites, respectively. Reduction for the other frequency is however less pronounced. Smaller carrier-phase residuals are considerably beneficial for the PBD performance (Mao et al., 2018). Therefore the *New* scheme has been adopted for the following research.

Table 5.5: The RMS of GPS observation residuals and the percentage of used GPS observations in the MODK single-satellite POD mode. Three sets of data are displayed: $-Old$ represents the data set using the old data processing scheme and $-New$ means the new one, CRV means the results by including the antenna CRV patterns. For all the solutions PCV patterns are included (statistics for 30 orbital arcs).

Satellite	Solution	P1	P2	L1	L2	Perc.
		Code		Carrier-phase		
		[m]	[m]	[mm]	[mm]	[%]
GRACE-A	Old	0.21	0.22	2.85	1.73	92.60
	New	0.20	0.21	1.94	1.17	91.26
	+CRV	0.20	0.20	1.94	1.18	91.26
GRACE-B	Old	0.17	0.17	2.41	1.46	97.96
	New	0.17	0.17	1.77	1.08	97.29
	+CRV	0.17	0.15	1.77	1.08	97.29
CHAMP	Old	0.23	0.29	3.46	2.12	90.93
	New	0.23	0.29	2.00	1.24	90.44
	+CRV	0.23	0.19	2.03	1.24	91.90

The CHAMP and GRACE satellites are equipped with different generation JPL BlackJack GPS receivers leading to different performance. Figure 5.5 shows the CHAMP GPS antenna CRV patterns created for this research, note that the creation of them is only based on single-satellite POD with MODK. The patterns clearly depict the signal interference on the rear side of the CHAMP GPS navigation antenna, which is close to the GPS occultation antenna (see Figure 3 in (Montenbruck and Kroes,

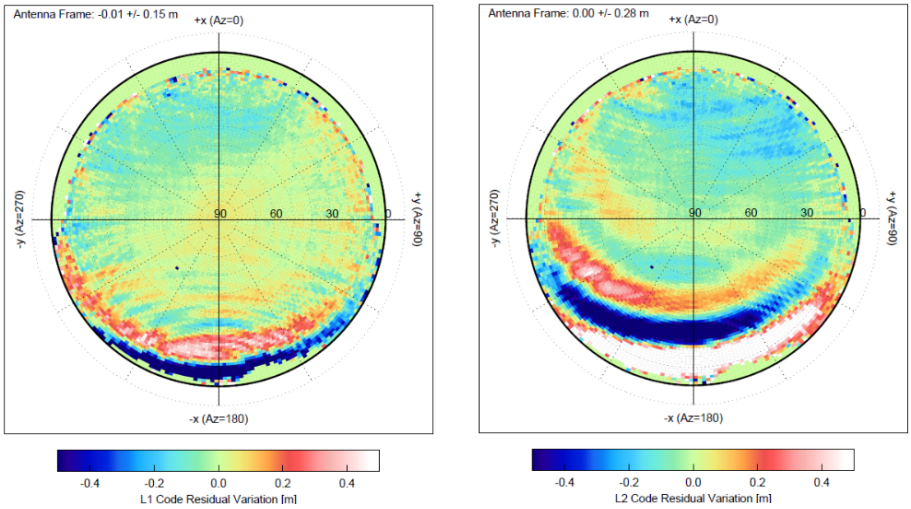

Figure 5.5: The CHAMP GPS receiver code residual variation patterns on the first (left) and the second (right) GPS frequency in the antenna-fixed reference system, for which the North axis coincides with the satellite body-fixed +X axis (0° azimuth), the Up and bore-sight axis coincides with the -Z axis, and the East axis completes the right-handed system. The April 2005 (DOY 091-120) data were used for generating the CRV maps.

2003)). The CRV patterns reach a level of nearly 1 m on especially the GPS L_2 frequency. This level is much above the L_2 wavelength and will thus impact the ambiguity fixing for DD carrier-phase combinations that include CHAMP. No similar interference patterns are observed for the two GRACE satellites during this period, see *e.g.* (Mao et al., 2017).

Table 5.5 displays statistics for the GPS observation residuals obtained by first excluding (indicated as *New*) and then including CRV maps (indicated as *+CRV*). The implementation of CRV patterns significantly reduces the RMS of the CHAMP code residuals on the second frequency from 29 to 19 cm. This also agrees with Mao et al. (2017) presenting similar analysis for GRACE-B satellite during when its radio occultation was activated. A similar but smaller effect of 1-2 cm reduction can be seen for the two GRACE satellites. The RMS of the carrier-phase residuals slightly increases on the first GPS frequency for CHAMP when including the CRV maps, which increases the percentage of GPS observations passing data editing process from 90.4% to 91.9%. Changes to both GRACE satellites are hardly visible since only less than 0.01% of GPS observations is influenced.

Another assessment is done to evaluate the impact of CRV patterns on the DD ambiguity fixing for a typical 24-h arc dual-satellite PBD, as displayed in Figure 5.6. The top part of this Figure shows that the GRACE CRV patterns slightly increase the ambiguity fixing success rate by 0.5%, indicated by the sparse blue stripes at edges of a few tracking passes. Thus especially for DD carrier-phase combinations that include observations at the begin and end of tracking passes at low elevations the ambiguity fixing success rate is increased. This corresponds to the conclusions

in (Mao et al., 2017) for GRACE-only PBD. The impact for CHAMP is bigger: its CRV patterns change the values of many fixed integers (the red stripes), also lead to extra fixed integer ambiguities (blue stripes), but also causes some integer ambiguities not to be fixed (yellow stripes). However, in total around 5% more ambiguities are fixed. Changes predominantly occur when the GRACE and CHAMP satellites are further away from the point of closest approach (distance typically larger than 1000 km). Although several stringent ambiguity tests were done (as Table 5.4 describes), including a 99.9% probability test (Verhagen, 2005), it was found that several DD ambiguities are likely wrongly fixed. Attention to this will be paid in the next Sections.

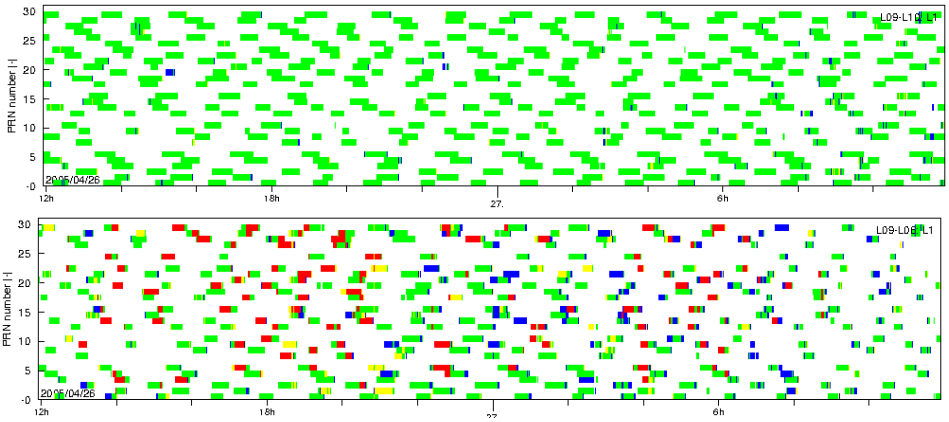

Figure 5.6: The fixed ambiguities comparison between the solution with and without GPS receiver antenna CRV patterns for the GRACE-A/B (top) and the CHAMP/GRACE-A (bottom) baselines, only the result for the first frequency is shown. Green: the same integers, Red: different integers, Yellow: fixed integers that exist in the solution using only antenna PCV patterns, Blue: newly fixed integers that only exist in the solution additionally including antenna CRV patterns (DOY 116, 2005).

5.4.2. Dual-satellite PBD

MODK is capable of running orbit determinations in different modes, *i.e.* single- (see Section 5.4.1), dual- and triple-satellite. In this section first dual-satellite POD and PBD is addressed, followed by triple-satellite POD and PBD in Section 5.4.3. As mentioned above, PBD for the close GRACE formation benefits from constraining the differences between empirical accelerations since they fly almost identical orbits, and enhances the ambiguity fixing success rate. Moreover, its onboard KBR instrument provides the data for an independent validation of the GPS-derived baseline at μm precision level. The dual-satellite PBD approach is used as well for the two CHAMP/GRACE satellite pair combinations. However, for these combinations the differences between the estimated empirical accelerations are very loosely constrained. Unfortunately, for these baselines no independent validation can be done as for GRACE with KBR observations. For these baselines, quality assessment will be based on comparisons with other external PBD and POD solutions (Allende-Alba and Montenbruck, 2016; Jäggi et al., 2016), and in this case the *KIPP* orbits will

be used. In addition, a consistency check will be included by comparison with the earlier mentioned MODK kinematic PBD solutions.

Table 5.6: Consistency between MODK dual-satellite reduced-dynamic and kinematic baseline solutions (RMS) for the radial, along-track, cross-track and line-of-sight direction. Two reduced-dynamic baseline solutions were obtained, one with (*Integer*) and one without (*Float*) ambiguity fixing. In addition, the consistency between MODK float baseline solutions and baselines derived from single-satellite kinematic POD using the GHOST *KIPP* module was assessed. The ambiguity success rate (Amb.), percentage of epochs covered by kinematic PBD solutions (Ava.), and consistency with KBR observations (for GRACE) are indicated as well. The values hold for the selected 30 24-h arcs.

Solution Unit	Radial [mm]	Along-track [mm]	Cross-track [mm]	Line-of-sight [mm]	Amb. [%]	Ava. [%]	KBR [mm]
GRACE-A/B							
Float	6.88	3.89	1.87	3.91	NA	92.40	3.00
Integer	7.60	3.08	2.17	3.11	94.56	92.49	0.64
KIPP	30.80	23.15	20.55	23.34	NA	99.33	NA
CHAMP/GRACE-A							
Float	24.31	18.56	5.56	17.79	NA	61.42	NA
Integer	23.49	14.12	6.32	11.76	80.02	62.00	NA
KIPP	41.44	37.48	24.81	34.14	NA	98.65	NA
CHAMP/GRACE-B							
Float	24.24	19.08	5.64	17.83	NA	57.36	NA
Integer	22.62	13.60	6.25	10.68	85.61	57.36	NA
KIPP	43.72	38.14	33.87	35.50	NA	98.59	NA

Table 5.6 shows the baseline consistency between the kinematic and reduced-dynamic solutions for each possible satellite pair. For the GRACE tandem, baseline consistency is obtained at a level of 7.6/3.1/2.2 mm in the radial/along-track/cross-track directions for the ambiguity fixed solution. The consistency is thus displayed in the local-horizontal, local-vertical reference frame, where for baselines the radial, along-track and cross-track direction of a reference satellite is taken (GRACE-A for GRACE-A/B and CHAMP/GRACE-A satellite pair, and GRACE-B for CHAMP/GRACE-B pair). The worst consistency is obtained for the radial direction, which results from the geometry, *i.e.* a large value for the Radial Dilution Of Precision (RDOP). As expected, for the line-of-sight (pointing from the reference satellite to the other satellite) direction, the value is almost identical to the value for the along-track direction. Fixing the ambiguities, clearly significantly improves the consistency with the KBR down to a level of 0.64 mm compared to 3.00 mm for the *Float* solution, which agrees well with precision levels achieved by different PBD software (Allende-Alba and Montenbruck, 2016; Jäggi et al., 2007; Kang et al., 2006).

Note that ambiguity fixing will generally increase the carrier-phase residuals for two satellites, since the fixing allows less freedom for the ambiguities to accommodate the carrier-phase observations and in additions wrongly-fixed integer ambiguities probably occasionally occur (Van Barneveld, 2012). In this research,

the RMS-of-fit of carrier-phase residuals for two satellites slightly increased from 1.95/1.82 (L_1, GRACE-A/B) and 1.18/1.10 mm (L_2) to 1.97/1.84 and 1.19/1.12 mm respectively. Incorrectly fixed ambiguities are expected to deteriorate the kinematic baseline precision. As discussed in Section 5.3, the kinematic baseline is the subtraction between the reduced-dynamic orbit of a reference satellite and the kinematic orbit of the other satellite, all computations are done in the MODK module. This differs with the *KIPP* solution, which is the subtraction of two independent kinematic orbits computed by the KIPP module of the GHOST software package. The reduced-dynamic PBD is influenced to a much smaller extent due to its inherent smoothing capacity. It can be seen from Table 5.6 that for the GRACE tandem the ambiguity fixing slightly deteriorates the baseline consistency in the radial and cross-track directions by 0.7 and 0.3 mm, respectively. Nevertheless the baseline consistency is improved by 0.8 mm in the along-track direction, where the GRACE baseline geometry and thus the fixed ambiguities align.

For the CHAMP/GRACE-A PBD solution, the kinematic and reduced-dynamic baseline consistency is changed from a level of 24.3/18.6/5.6 to 23.5/14.1/6.3 mm after ambiguity fixing. A clear improvement of 4.5 mm is seen in the along-track direction, only small deterioration exists for the cross-track direction. Improvement in the line-of-sight direction is more profound, showing a change from 17.8 to 11.8 mm. The result for the CHAMP/GRACE-B pair is similar. In fact, the dominating geometric component for the CHAMP/GRACE satellite pairs for 24-h arcs aligns in the along-track direction since two orbital planes were aligned closely. A smaller component will be in the radial direction due to the orbital altitude difference of around 110 km (Table 5.1). The ambiguity fixing again improves the consistency in the radial and along-track directions. For the CHAMP/GRACE pairs Van Barneveld (2012) did an additional analysis of full-set ambiguity fixing in LAMBDA, showing that only $1-2\%$ epochs experience successful full-set ambiguity fixing. In this research the subset ambiguity fixing acquires again a much higher proportion of 80.0% and 85.6% for CHAMP/GRACE-A and CHAMP/GRACE-B, respectively. The latter satellite pair benefits further from the better GRACE-B GPS measurements (Table 5.5). It will be shown in Section 5.4.5 that there is also a strong dependency of the consistency on the arc length. For longer arc lengths the CHAMP/GRACE baselines grow rapidly leading to a less favorable geometry with a reduced number of GPS satellites in common view (see also Figure 5.2). The next step should be enhancing the CHAMP/GRACE PBD with more strict triple-satellite dynamic constraints and make use of the more reliable GRACE ambiguity fixing as much as possible.

The baselines derived from the single-satellite kinematic POD *KIPP* have been compared with the *Float* MODK reduced-dynamic baseline solutions as well. The *KIPP*-based baselines are available for $98.6-99.3\%$ of the epochs, much higher than for the MODK PBD solutions. In fact, during the selected period both versions of the BlackJack GPS receivers are tracking a large number (around 8) of GPS satellites, which results in this high availability for single-satellite POD. This differs significantly with MODK PBD which requires to have at least 5 GPS satellites in common view by two GPS receivers. However, the associated *KIPP* baseline consistency with the MODK PBD solutions is much worse, clearly showing the benefit of adopting

a dual-satellite *vs.* single-satellite POD approach. PBD has the benefit of using DD carrier-phase observations and, particular for GRACE, the use of constraints for limiting the differences between estimated empirical accelerations (see Figure 5.7, in the next Section, where for GRACE-A and -B indeed almost identical values are obtained in an MODK triple-satellite solution).

5.4.3. Triple-satellite PBD

In a next step, MODK is used to generate PBD solutions for the full CHAMP/GRACE constellation in one go, *i.e.* by triple-satellite POD and PBD. First, PBD solutions are obtained without ambiguity fixing (again referred to as *Float*). Second, solutions are produced for which DD ambiguities are fixed for all GRACE/CHAMP satellite pairs (*Integer*). The triple-satellite PBD offers the possibility to define a so-called preferred baseline and then assess if this leads to improved solutions for the other baselines. Since the GRACE baseline can be determined with high precision by GPS, it can be investigated if the CHAMP/GRACE baselines and in conjunction the CHAMP absolute orbit solution can benefit from this. In a first step, the MODK IEKF estimates the GRACE baselines until the DD ambiguity fixing has converged (typically requiring 5-6 iterations). After this, the two CHAMP/GRACE baselines are included as well and a new DD integer ambiguity fixing is done (including the GRACE-A/B DD ones). The crucial question is if this new ambiguity fixing can be done correctly and indeed improved baseline and absolute CHAMP (and GRACE) positions can be obtained. The first attempts reported in Van Barneveld (2012) show that the risk of incorrectly fixing the ambiguities and thereby decreasing the quality of the orbit and PBD solutions is high. Therefore, a third MODK triple-satellite solution is done by freezing the GRACE-related DD ambiguities obtained in the first step and not fixing the DD ambiguities for CHAMP/GRACE combinations, referred to as *GAB-pref*.

When comparing the results for the MODK dual- and triple-satellite PBD solutions, it can be seen that the consistency between the reduced-dynamic and kinematic baseline solutions in general hardly changes when the third satellite is introduced (Table 5.6 and Table 5.7). For the GRACE *Float* solution, the baseline consistency slightly deteriorates from 6.9/3.9/1.9 to 7.0/4.0/1.9 mm when CHAMP is introduced. Also a deterioration of 0.1 mm for the line-of-sight is obtained. These are caused by the fact that the availability of GRACE kinematic baselines is reduced by around 1.6%. Actually the additional data editing after including the third satellite eliminates around 1.5% GRACE GPS observations extra before the PBD computation. The kinematic baseline availability reductions for CHAMP/GRACE-A and CHAMP/GRACE-B are only 0.2% and 0.7%, indicating that more kinematic solutions could pass the 5 cm GPS residuals criterion (Section 5.3) even after the exclusion of more GPS data. The inclusion of the lower flying CHAMP satellite and the more relaxed relative dynamic constraints between CHAMP and GRACE thus do not improve the baseline consistency for all *Float* baselines. The impact of stringent and relaxed constraints on the differences between estimated GRACE and CHAMP empirical accelerations can be clearly seen in Figure 5.7. Moreover, it is clear that including the CHAMP satellite relevant ambiguity fixing negatively affects the GRACE DD ambi-

Table 5.7: Consistency between MODK triple-satellite reduced-dynamic and kinematic baseline solutions (RMS) for the radial, along-track, cross-track and line-of-sight direction. Three reduced-dynamic baseline solutions were obtained adopting different handling of the DD carrier-phase ambiguities (see main text for details), referred to as *Integer*, *Float* and *GAB-pref*. In addition, the consistency between MODK float baseline solutions and baselines derived from single-satellite kinematic POD using the GHOST *KIPP* module was assessed. The ambiguity success rate (Amb.), percentage of epochs covered by kinematic PBD solutions (Ava.), and consistency with KBR observations (for GRACE) are indicated as well. The values hold for the selected 30 24-h arcs.

Solution Unit	Radial [mm]	Along-track [mm]	Cross-track [mm]	Line-of-sight [mm]	Amb. [%]	Ava. [%]	KBR [mm]
			GRACE-A/B				
Float	6.95	4.00	1.90	4.02	NA	90.84	3.22
GAB-pref	7.70	3.18	2.21	3.21	93.89	90.91	0.63
Integer	8.29	3.31	2.29	3.34	93.70	90.91	0.66
KIPP	30.82	23.23	20.55	23.36	NA	99.33	NA
			CHAMP/GRACE-A				
Float	24.08	18.63	5.51	17.40	NA	61.19	NA
GAB-pref	24.14	18.50	5.49	17.31	NA	61.17	NA
Integer	23.61	13.96	6.57	11.45	82.92	61.05	NA
KIPP	41.47	37.92	24.91	34.53	NA	98.65	NA
			CHAMP/GRACE-B				
Float	23.91	18.22	5.56	16.98	NA	56.61	NA
GAB-pref	24.07	18.02	5.63	16.76	NA	56.61	NA
Integer	25.02	15.16	6.69	11.96	86.67	56.47	NA
KIPP	43.89	38.89	28.87	36.13	NA	98.60	NA

guity fixing. The baseline precision displays a slightly worse level for the RMS of differences with the KBR observations from 0.63 to 0.66 mm (in comparison with 0.64 mm in Table 5.6 for the dual-satellite PBD).

Compared to the *Float* and *GAB-pref* solutions, the third MODK triple-satellite approach *Integer* results in a significantly improved consistency in the line-of-sight between the reduced-dynamic and kinematic baseline solutions for the two CHAMP/GRACE satellite pairs. This corresponds to the conclusions drawn from Table 5.6. Please note that when comparing with the MODK GRACE dual-satellite ambiguity fixed solution, the kinematic and reduced-dynamic baseline consistency for the *Integer* solution is worse (0.7/0.2/0.1 mm for the radial, along-track and cross-track directions) and around 0.9% fewer integer ambiguities are fixed. Small changes again result from additional data editing to take into account the lower CHAMP satellite (Table 5.4). It has to be noted that in comparison with Van Barneveld (2012) the adverse influence of CHAMP/GRACE ambiguity fixing for the GRACE PBD is hardly visible in this research. The newly implemented modifications as introduced in Section 5.1 obtain more stable POD and PBD performance for each of the satellites or satellite pairs.

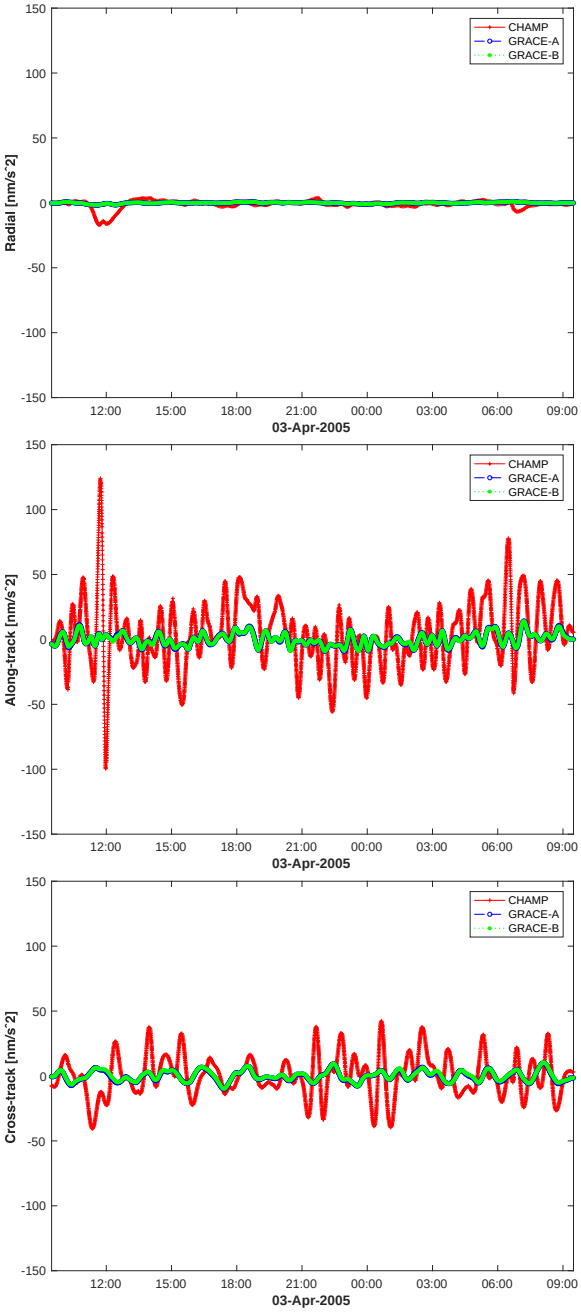

Figure 5.7: Time series of estimated empirical accelerations in the radial (top), along-track (middle) and cross-track (bottom) directions for each satellite based on triple-satellite PBD (no ambiguity fixing) for a typical day (DOY 093, 2005). Same scales are set for the vertical axes. Please note that the curves for GRACE-A and -B almost completely overlap.

5.4.4. Satellite laser ranging validation

SLR observations for three satellites allow an independent validation of MODK GPS-based orbits in the line-of-sight direction between each SLR ground station and a LEO satellite (Pearlman et al., 2002). To get rid of occasionally poor quality tracking observations, an editing threshold of 30 cm - which is more than an order of magnitude above the RMS of fit levels - is used. Observations below 10° elevation angle are also excluded to eliminate observations that are relatively more affected by atmospheric delay. The SLR retro-reflector modeling pattern from GFZ is included as corrections (Neubert et al., 1998). Table 5.8 shows that 93.1%, 92.5% and 93.8% of the SLR observations are used for the orbit validations for GRACE-A, GRACE-B and CHAMP, respectively. In total 22 SLR stations are included in the validations. The reference orbits of GRACE are obtained from JPL, for which use was made of so-called single receiver ambiguity fixing (Bertiger et al., 2010).

Table 5.8: Mean and standard deviation of SLR observations for different orbit solutions for the 30 24-h arcs (unit: [mm]). Please note that all solutions identified by Single, Dual and Triple were obtained by using MODK.

Satellite	GRACE-A	GRACE-B	CHAMP
JPL	-3.1 ± 14.3	-1.9 ± 16.5	NA
Single	-5.1 ± 15.2	-3.3 ± 18.8	-7.4 ± 23.5
Dual:GRACE	-5.1 ± 14.9	-3.6 ± 17.9	NA
Dual:CHAMP/GRA	-4.7 ± 16.7	NA	-8.2 ± 23.7
Dual:CHAMP/GRB	NA	-0.7 ± 22.3	-8.7 ± 23.2
Triple:Float	-5.4 ± 15.0	-3.4 ± 18.5	-7.4 ± 24.0
Triple:GAB-pref	-5.2 ± 15.1	-3.3 ± 18.4	-7.8 ± 23.8
Triple:Integer	-5.7 ± 17.2	-3.2 ± 18.8	-7.3 ± 23.2
Nr.SLR Obs.	3031(93.1%)	2937(92.5%)	2921(93.8%)

For the single-satellite MODK and external orbit solutions, the mean of the SLR observation residuals is in general at the level of a few mm , where the RMS varies between 14 and 24 mm (Table 5.8). For GRACE, the best consistency is obtained for the JPL orbits, which - as mentioned above - make use of single receiver ambiguity fixing. In the mean time, single receiver ambiguity fixing and more sophisticated non-gravitational force modeling have been tested and implemented in several GHOST modules (Hackel et al., 2017; Montenbruck et al., 2018b). However they are not yet applied to MODK.

It is clear to see that the SLR consistency improves for the MODK dual-satellite GRACE orbit solutions (0.3 to 0.9 mm reduction in the standard deviation). The correlations between the daily RMS of empirical accelerations for two GRACE satellites are analyzed for the single-satellite POD solutions and the dual-satellite PBD solutions. The correlations significantly increase from $0.945/0.999/0.980$ to $1.000/0.999/0.991$ in the radial, along-track and cross-track directions, respectively. The precision of the GRACE orbits thus benefits from their joint estimation, the ambiguity fixing and the use of constraints for the differences between the empirical

accelerations.

For the two MODK triple-satellite solutions (*Float* and *GAB-Pref*), SLR consistency levels become slightly better (between 0.1 and 0.4 mm) than the single-satellite orbits for the GRACE satellites. However, slight GRACE satellites orbit precision reductions for especially GRACE-A are seen for the MODK triple-satellite solution where all ambiguities are fixed (*Integer*). This agrees with the conclusions in Van Barneveld (2012) that fixing all integer ambiguities will downgrade the GRACE-A orbit precision. It has to be noted that in this research no reduction of precision is seen for the GRACE-B orbit and the CHAMP orbit precision is even improved by 0.3 mm, whilst Van Barneveld (2012) reported downgraded orbit precision for all three satellites in comparison with the single-satellite solutions (3.4, 6.7 and 4.2 mm for GRACE-A, GRACE-B and CHAMP respectively). The dual-satellite CHAMP/GRB integer ambiguity fixing also slightly improves the CHAMP orbit. However, the *Dual:CHAMP/GRA* solution slightly deteriorates the CHAMP orbit. For both MODK CHAMP/GRACE dual-satellite orbit solutions, the SLR consistency deteriorates for the GRACE satellites. They indicate the existence of wrongly-fixed integer ambiguities for particularly the CHAMP/GRACE satellite pairs, which is a very interesting point for further research.

For some SLR passes, an interesting extra validation can be done for GRACE. For these passes, the associated SLR tracking station is switching between the GRACE-A and -B satellites and it is interesting to see if time series of remaining SLR observation residuals are continuous or display jumps. To this aim, all tracking passes by the high-quality Yarragadee station in Australia are selected. In the selected period, this station collected 547 and 632 observations for GRACE-A and -B satellites. The SLR validation residuals for two satellite orbits are displayed in Figure 5.8. It can be seen that in general two satellite orbits align slightly better in the GRACE-A/B dual-satellite PBD solution. Figure 5.10 shows three representative tracking passes on DOY 093, 101 and 109. When tracking the GRACE-A/B formation, normally the tracking of Yarragadee station switches 1-6 times during one satellite overpass that lasts for a few minutes. For these three days, smaller jumps occur at the switching times for the dual-satellite solutions. To a lesser extent this is the case for the other selected days as well. The GRACE-A/B orbit alignment assessment for the triple-satellite PBD is similar. Thus, this is an indication that the PBD seems to improve the consistency between the GRACE-A and -B orbit solutions. These results agree well with Allende-Alba et al. (2017) and Arnold et al. (2018) who report similar conclusions for the Swarm-A/C and TerraSAR-X/TanDEM-X formations, respectively.

Further assessment is done to check the alignment of GRACE-A/B satellites based on the CHAMP/GRACE-A and CHAMP/GRACE-B PBD solutions. Surprisingly better alignment can be also obtained for a few days, as Figure 5.9 displays. However when comparing with Figure 5.8 more unstable days exist: Table 5.8 shows worse RMS of fits for the GRACE-A and GRACE-B orbits for the two associated CHAMP/GRACE PBD solutions. This means the CHAMP satellite occasionally constrains the GRACE orbits through dual-satellite PBD however it does not necessarily always improve the other satellite orbit due to its more in-flight perturbations and problematic data quality. This however implies that the use of a high-quality satel-

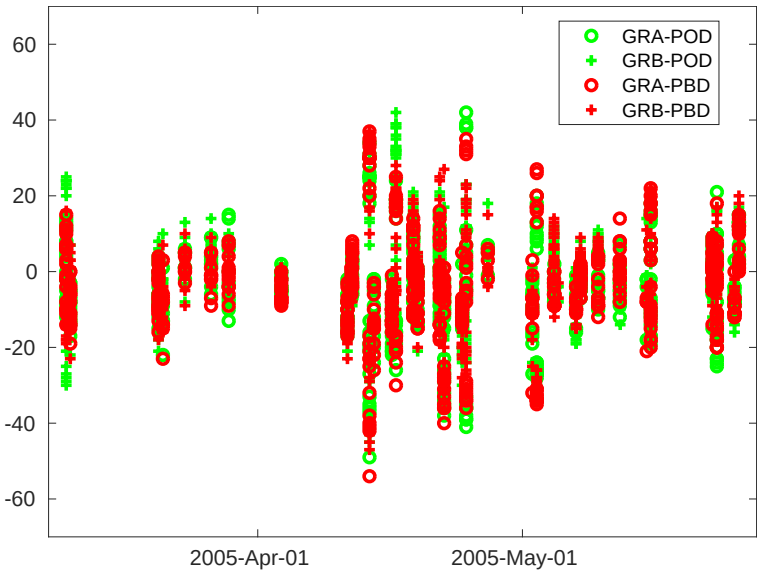

Figure 5.8: SLR observation residuals (unit:mm) for the GRACE-A/B MODK single-satellite POD and dual-satellite PBD orbit solutions for all passes of the Yarragadee station in Australia. The RMS of all green marks (reference) is 13.2 mm, the RMS of all red marks is 13.0 mm.

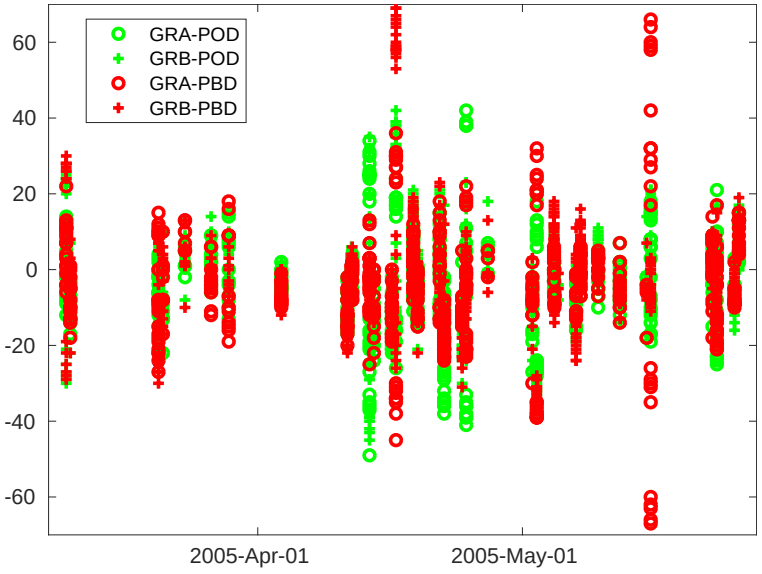

Figure 5.9: SLR observation residuals (unit:mm) for the GRACE-A/B MODK single-satellite POD and GRACE-A/B orbits obtained from CHAMP/GRACE-A and CHAMP/GRACE-B PBD orbit solutions for all passes of the Yarragadee station in Australia. The RMS of all green marks (reference) is 13.2 mm, the RMS of all red marks is 15.3 mm.

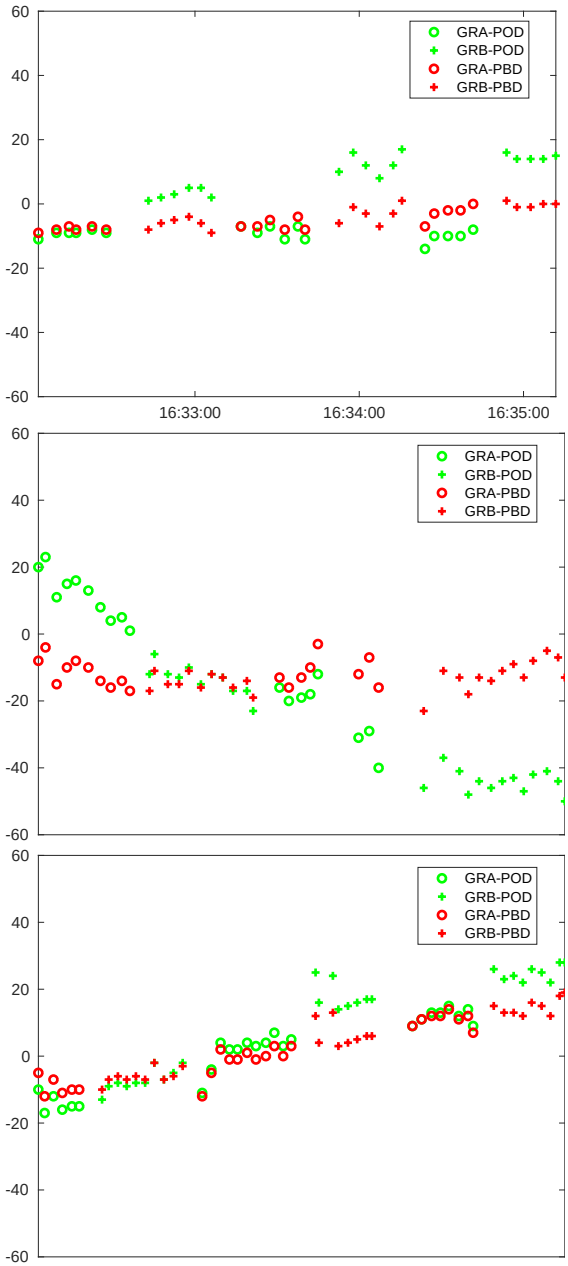

Figure 5.10: SLR observation residuals (unit:mm) for the GRACE-A/B MODK single-satellite POD and dual-satellite PBD orbit solutions for three representative passes (top: DOY 093; middle: DOY 101; bottom: DOY 109) of the Yarragadee station in Australia. For each pass the DOY in 2005 is indicated.

lite as the third satellite might be more beneficial for all satellites.

5.4.5. Orbital arc length analysis

Figure 5.11 displays the baseline consistency between the kinematic and reduced-dynamic solutions as a function of distance for DOY 093, 2005. The CHAMP/GRACE baseline consistency deteriorates rapidly as the length of baseline grows and the availability of kinematic solution also drops correspondingly. Therefore, it is interesting to assess the impact of selecting shorter periods around the point of closest approach between CHAMP and the GRACE satellites. MODK triple-satellite PBD solutions have been produced for arc lengths from 2 to 24 hr, *i.e.* between 1 and 12 hr from the point of closest approach (all within the selected 30 24-h periods specified in Table 5.2). For all arc lengths, the triple-satellite *GAB-pref* and *Integer* solutions were produced. Figure 5.12 clearly reveals the impact of increasing the arc length for all 30 orbital arcs: the line-of-sight baseline consistency deteriorates for longer CHAMP/GRACE arcs however not for the stable GRACE baseline. The integer ambiguity fixing for both CHAMP/GRACE baselines significantly improves the agreement between the kinematic and reduced-dynamic solutions, however it is found that the GRACE integer ambiguity fixing might be also perturbed occasionally by CHAMP (in this research, only the 10 hours GRACE-A/B PBD on DOY 111 is influenced).

Figure 5.13 displays the statistics of the kinematic and reduced-dynamic baseline consistency as a function of maximum orbital arc length for two MODK triple-satellite solutions, *GAB-pref* and *Integer*. The orbit arc has a significant impact on the PBD performance, for instance the consistency in the radial direction worsens by a factor of 2 when the arc is increased from 2 to 24 hours. It can be seen again that the baseline consistency for the *Integer* solution is in general worse than for the *GAB-pref* solution for the cross-track directions. However, clearly better consistency is obtained for the radial and along-track directions. The only difference between two solutions is the fixing of CHAMP/GRACE DD integer ambiguities. A similar conclusion is drawn based for the GRACE baseline results displayed in Table 5.6. Thus, results indicate that the ambiguity fixing will enhance the baseline solution in the radial, along-track and line-of-sight direction, but slightly deteriorate the cross-track direction.

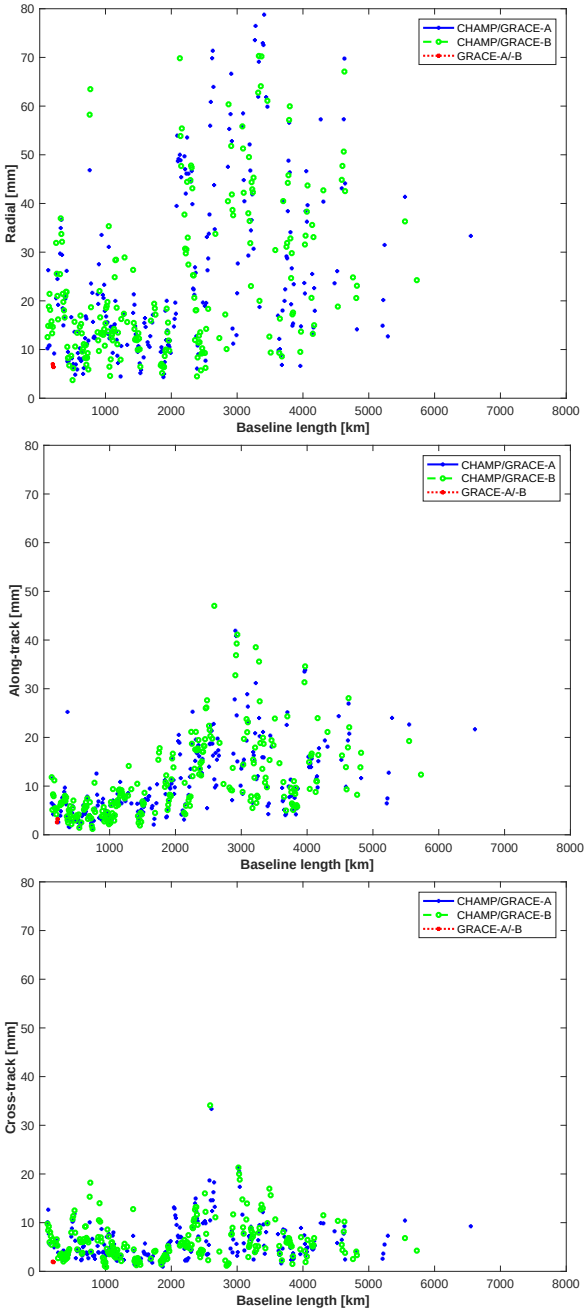

Figure 5.11: RMS of differences between MODK triple-satellite kinematic and reduced-dynamic solutions as a function of distance (in steps of 10 km) in the radial (left), along-track (middle) and cross-track (right) directions for the three baselines (DOY 093, 2005).

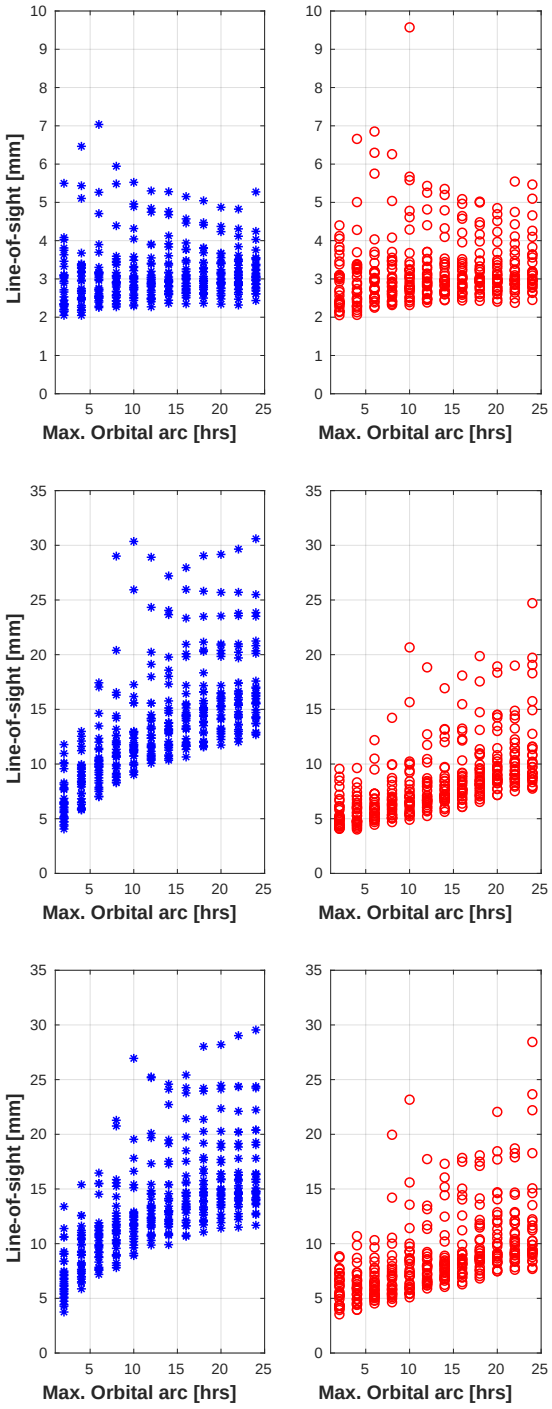

Figure 5.12: RMS of MODK triple-satellite kinematic and reduced-dynamic baseline solution differences in the line-of-sight direction for the *GAB-pref* and *Integer* approaches, as a function of the maximum orbital arc length for all 30 arcs of the GRACE-A/B (top), CHAMP/GRACE-A (middle) and CHAMP/GRACE-B (bottom) satellite pairs. Note that different axis scales are used for GRACE-A/B and the other two baselines. For each direction, the *GAB-pref* solution is displayed on the left as blue stars, and the *Integer* solution on the right as red circles.

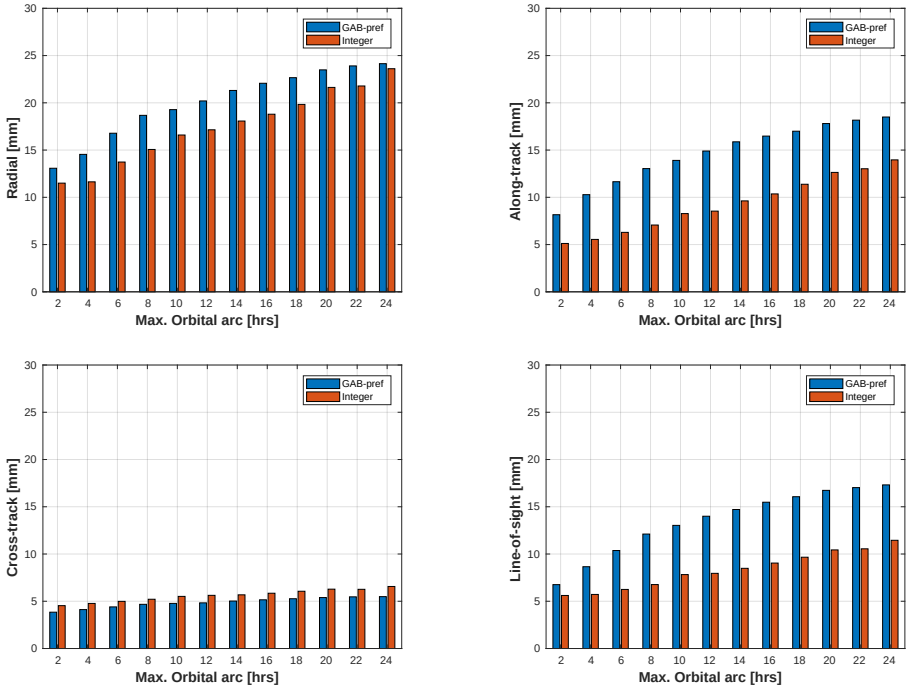

Figure 5.13: RMS of MODK triple-satellite kinematic and reduced-dynamic baseline differences for the *Integer* and the *GAB-pref* approaches as a function of the maximum orbital arc length in the radial (top-left), along-track (top-right), cross-track (bottom-left) and line-of-sight (bottom-right) directions for the CHAMP/GRACE-A baseline. Similar results are obtained for the CHAMP/GRACE-B baseline.

5.5. Summary and outlook

This study investigates a challenging satellite constellation formed by the CHAMP satellite and the GRACE twin satellites. Two different types of satellite baselines are available: one stable tandem baseline (GRACE-A/B) and two high-dynamic high-low baselines (CHAMP/GRACE-A and CHAMP/GRACE-B). Each selected 24-h CHAMP/GRACE orbital arc has a baseline length ranging from 110 to 7500 km. The GRACE satellites on the one hand and the CHAMP satellite on the other hand show quite different levels of non-gravitational force model uncertainties. This makes the triple-satellite Precise Baseline Determination (PBD) more challenging. An iterative extended Kalman filter and a subset ambiguities fixing strategy are conducted for the reduced-dynamic PBD, whereas a kinematic PBD solution can be generated by using the fixed integer ambiguities and satellite coordinates obtained from the reduced-dynamic solutions. The MODK module allows different strategies for ambiguity fixing, namely no fixing at all *float*, full integer ambiguity fixing *Integer*, and only fixing the GRACE DD ambiguities *GAB-pref*.

Compared with Van Barneveld (2012) who initially proposed this research case, a few innovations were made that led to improvements. First, orbital arcs (thirty in total) were selected that center around the point of closed approach between the GRACE and CHAMP satellites (occurring every 2.7 days). This approach leads to a more homogeneous observation geometry for the investigated arcs and allows to better study the possibility of PBD as a function of baseline length. The GPS data processing scheme has also been carefully tailored for especially editing out spurious carrier-phase observations. In addition, Code Residual Variation (CRV) maps are generated to correct GPS code observations. These maps mitigate the effect of so-called cross-talk between the CHAMP GPS POD and radio occultation antennas. The single-, dual- and triple-satellite PBDs are done based on either float or fixed integer ambiguities. It can be also done such that the GRACE baseline is first computed based on fixed integer ambiguities, and then subsequently fix the CHAMP/GRACE DD carrier-phase ambiguities. By this approach, the influence of the more challenging CHAMP/GRACE ambiguity fixing could be assessed. Furthermore, the sensitivity of PBD precision to arc length (and thus baseline length) was assessed by generating solutions for different orbital arcs ranging from 2 to 24 hrs.

The above mentioned changes have resulted in improved PBD solutions for the high-dynamic GRACE/CHAMP constellation in comparison with Van Barneveld (2012). As for the more stable GRACE baseline, the consistency between its kinematic and reduced-dynamic solutions are at a level of 8.3/3.3/2.3 mm (radial/along-track/cross-track). The ambiguity fixing success rate reaches 93.7% and the K-Band Ranging (KBR) system proves a baseline precision at a level of 0.6 mm. The baseline consistency for the CHAMP/GRACE-A baseline are at a level of 23.6/14.0/6.6 mm due to rapidly changing and less favorable geometry, which is also shown by the rapidly deteriorating CHAMP/GRACE consistency with arc length or baseline length. The result for the CHAMP/GRACE-B baseline is similar. The consistency of PBD orbit solutions with Satellite Laser Ranging (SLR) observations is at the level of a few cm, 17.2, 18.8 and 23.2 mm RMS of fit for GRACE-A, GRACE-B, and CHAMP, respectively. Compared to the single-satellite Precise Orbit Determination (POD) solutions, the

CHAMP orbit precision slightly improved by 0.3 mm. No improvement was obtained for the GRACE-B orbit solution, and the SLR RMS-of-fit deteriorated by 2.0 mm for GRACE-A. Finally, SLR passes for which the laser station is alternating between the two GRACE satellites were used to show improved consistency between the orbits of the GRACE satellites. The Yarragadee SLR station was selected to this aim. Results show that indeed a better agreement for the orbit solutions is obtained when using dual- or triple-satellite PBD solutions. It was shown that also the inclusion of the CHAMP satellite in the constellation occasionally helps to improve the GRACE-A/B orbit alignment, nevertheless it is not as effective as the dual-satellite GRACE PBD. The results also show that more robust and precise PBD results are obtained for the high-dynamic baselines as compared to the initial work done by Van Barneveld (2012). Despite the significantly improved high-dynamic baseline determinations, results indicate there is still room for improvement. Possibly, results can be further enhanced by revisiting and enhancing the ambiguity fixing method, which now fully relies on the LAMBDA method. Moreover, it will be interesting to assess if precise high-dynamic baseline solutions can indeed support improved observation of gravity by space-borne GPS receivers.

Acknowledgment

The China Scholarship Council (CSC) is gratefully acknowledged for financially supporting part of the work described in this paper. We would like to show our special gratitude to the Jet Propulsion Laboratory (JPL) for providing the GRACE data products, German Research Centre for Geosciences (GFZ) for providing the CHAMP data products, Center for Orbit Determination in Europe (CODE) for providing the IGS and Ionosphere products and The Crustal Dynamics Data Information System (CDDIS) for providing the Satellite Laser Ranging observations (Noll, 2010). The DLR German Space Operations Centre (GSOC) kindly provided the GHOST software. We also acknowledge two anonymous reviewers for reviewing this paper.

6

Conclusions and Recommendations

6.1. Conclusions

Several recent formation flying space missions in LEO require POD and PBD products. The primary objective of the research described in this dissertation was to further build up the methods for determining reliable satellite orbits not only for formations with stable baseline lengths, but also for constellations with rapidly varying baseline lengths. The six satellites selected for this research carry with different GPS receivers (CHAMP and GRACE tandem: the JPL BlackJack series GPS receiver, different performance; Swarm three-satellite constellation: *RUAG Space* GPS receiver) and their (relative) orbits are perturbed differently by gravitational and non-gravitational forces. Especially rapidly varying baseline lengths (or a rapidly changing satellite geometry) make PBD more challenging. For the selected satellite combinations, first reduced-dynamic solutions are computed with the GHOST MODK software based on an IEKF and the LAMBDA method is used to fix DD carrier-phase ambiguities, where a subset fixing algorithm is adopted. Second, kinematic solutions are obtained using the integer ambiguities fixed in the reduced-dynamic approach. For triple-satellite constellations, it is possible to define a so-called preferred satellite pair for which the baseline is determined first followed by the other baselines. The results in this dissertation show that successful implementations have been done for single-, dual- and triple-satellite orbit determinations in order to address the research questions defined in Chapter 1.

RQ.1 What is the impact of GPS receiver antenna patterns on orbit determination precision, not only regarding GPS carrier-phase, but also code observations?

In Chapter 2, POD and PBD was investigated for the GRACE tandem formation in which the GRACE-B satellite experiences cross-talk between its multiple switched-on GPS antennas in the selected data period of August to November 2014. Results confirm the importance of using in-flight calibrated PCV patterns and also CRV patterns for both single- and dual-satellite POD and PBD. The antenna patterns enhance both GPS carrier-phase and code observations modeling accuracy. For single satellite, the inclusion of CRV maps results in more consistent kinematic POD orbit solutions particularly in the cross-track direction. Moreover for DPOD solutions, a better consistency with KBR observations is obtained.

For dual-satellite PBD, a higher success rate of DD carrier-phase integer ambiguity fixing is achieved by using not only PCV but also CRV maps. Moreover, the use of CRV maps improves the efficiency and effectiveness of the implemented IEKF, since the ambiguity fixing success rate is significantly increased for the first iteration. After convergence, on the average about 95.3% of the ambiguities are fixed. In addition, the baseline consistency with KBR observations turned out to be better than 0.7 mm for the selected data period. Also, the combination of PCV and CRV maps leads to better internal consistency between kinematic and reduced-dynamic orbit and baseline solutions, smaller differences with orbit solutions by JPL, and smaller SLR validation residuals.

RQ.2 How is PBD influenced by the in-flight performance of GPS receivers and in conjunction with receiver settings?

In Chapter 3, the Swarm-A/C satellite pair flying in pendulum formation (Sharifi et al., 2007) is used as test platform. It is found that the ionospheric activity level and high levels of code noise influence the quality of the single-satellite POD (Van den IJssel et al., 2016). In order to mitigate these effects, onboard GPS software settings were modified and a correction to the RINEX converter was implemented. For the research described in this dissertation, a 30-months data period from July 2014 to the end of 2016 was selected. The selection of this period allowed to study the impact of the modifications and corrections for low to high levels of ionospheric activity. In addition, attention was paid to tuning the data (pre)processing including outlier detection, to optimizing parameter settings, and to tuning the several LAMBDA tests. For the associated POD and PBD, use was made of frequency-dependent PCV and CRV antenna maps.

The GPS receiver modifications and updated post-facto data processing were found to be effective in many aspects. First, part of the modifications included an increased GPS receiver antenna field of view angle which resulted in the tracking of more GPS satellites and a more precise single-satellite POD. However, this increased field of view was not applied simultaneously for all Swarm GPS receivers which then caused a reduction of the number of satellites in common view and a less favorable geometry for PBD. Second, ionospheric scintillation is an important cause

for degrading the precision of carrier-phase observations. A decreased ionospheric activity level from 2014 to 2016 significantly reduced the carrier-phase residuals and in conjunction resulted in an increased quality of the PBD solutions. Third, a few GPS receiver carrier-phase tracking loop bandwidth modifications were implemented. In principle, a widening of the bandwidth increases the noise level, but it also increases the robustness of the tracking loop resulting in less loss of signal lock. It was found that the level of carrier-phase residuals was reduced particularly near the geomagnetic equator and poles, where stronger ionospheric scintillations exist and lead to more noisy GPS observations. Fourth, the RINEX software converter update and the correction of half-cycle ambiguities to full-cycle ambiguities improve the integer ambiguity fixing success rate to more than 90%, which significantly enhanced the PBD.

POD and PBD solutions obtained with the MODK IEKF were compared with external solutions kindly provided by GSOC/DLR and AIUB. The same sets of GPS measurements - after the implementations of all mentioned modifications for two days in 2016 (Jan 14/15) - are used. The MODK POD and PBD solutions display the best consistency level between kinematic and reduced-dynamic baseline solutions (9/4/3 mm in the radial/along-track/cross-track directions, with 98.3% of the epochs covered). The consistency of the MODK reduced-dynamic baselines solutions with external PBD solutions is of the order of around 1 mm for all directions. The consistency of kinematic and reduced-dynamic orbit solutions reach similar levels for the MODK and external PBD solutions (below 1 cm for the cross-track and along-track directions, and between 1 and 2 cm for the radial direction). The SLR validation confirms that the the MODK POD precision reaches a level that is comparable with the external orbit solutions.

RQ.3 Can we get precise baseline estimates for satellite constellations with long and highly variable baselines?

In Chapter 4, the Swarm triple-identical-satellite constellation has been used as test bed for single-, dual-, and triple-satellite POD and PBD. To this aim, a data period covering July-September 2014 was selected. PBD for two high-dynamic high-low satellite baselines (Swarm-B/A and Swarm-B/C) is investigated and for the relatively more slowly varying Swarm-A/C baseline. Ten 24-hr orbital arcs centered around the time of closest approach between Swarm-B and the other two satellites were selected. The high-dynamic high-low baselines vary from 50 to 3500 km for a duration of 12-hr around the close encounter. The different dynamic force modeling uncertainties make it more challenging to conduct POD and PBD for the associated satellites. In addition, it is possible to define a so-called preferred baseline. For example, the DD carrier-phase integer ambiguities can be fixed first for the Swarm-A/C satellites and after this for the other two pairs.

Results show again that half-cycle to full-cycle ambiguities corrections and the GPS receiver RINEX software converter that is used to convert the original GPS data

into RINEX data improve the precision of the high-dynamic high-low baseline PBD. The triple-satellite PBD performs comparably in terms of kinematic and reduced-dynamic baseline consistencies and SLR observation fits as compared to the dual-satellite PBD. The inclusion of high-dynamic baselines does not degrade the quality of the orbit solutions. Compared to single-satellite POD, it is shown that a better Swarm-A and -B satellite orbit agreement can be obtained with independent SLR observations, unfortunately it was not the case for Swarm-C. An interesting result is the improved consistency of time series of SLR residuals when conducting PBD: for SLR stations that switch between the two satellites (especially many passes are available for Yarragadee, Australia) of an overflying pair (Swarm-A and -C), the jumps between SLR residuals sometime become smaller when the SLR tracking switches from one satellite to the other.

In addition, the consistency between MODK Swarm reduced-dynamic baselines and those derived from GSOC/DLR single-receiver ambiguity fixed orbit solutions reaches a of 3-5 mm for the Swarm-B/A and Swarm-B/C satellite pairs, and around 1-3 mm level for the more stable Swarm-A/C baseline. The consistency between the kinematic and reduced-dynamic baseline solutions is at a level of 13/6/4 mm for Swarm-A/C and a level of 23/11/7 mm for the other two pairs (radial/along-track/cross-track). These consistency levels are better than the consistency between the associated two GSOC/DLR solutions for which a single-satellite POD with the integer ambiguity fixing is used. This shows the benefit of using a PBD approach and it was found that especially the possibility to constrain the relative uncertainty of dynamic force models (i.e. specify correlations between the associated empirical accelerations) increases the success rate of fixing DD carrier-phase ambiguities and improves the precision of the PBD solutions. Results confirm that the precision of the Swarm-B/A and Swarm-B/C baselines is not as good as for the Swarm-A/C baseline because of less favorable geometry and stronger relative dynamics.

RQ.4 Can we have reliable PBD solutions for satellite constellations comprised of different satellite missions?

PBD for a more challenging constellation comprised of the CHAMP satellite and the GRACE twin satellites was addressed in Chapter 5. PBD for this constellation was initiated by Van Barneveld (2012) however the orbit precision for each satellite was significantly downgraded. This necessitated further investigation into the PBD methods. The baselines for the CHAMP/GRACE satellite pairs vary stronger than for the Swarm-B/A and Swarm-B/C pairs, again making high-precision baseline determination more challenging. As for Swarm, 24-hr orbit arcs around the point of closest approach were selected, during which CHAMP/GRACE baselines typically ranged from 100 to 7500 km. Besides, the CHAMP satellite flies in a significantly stronger atmospheric drag environment than the GRACE satellites. This is not the case for Swarm-B, which flies in more quiet in-flight environment than Swarm-A and -C. The CHAMP GPS receiver also displays more sophisticated antenna pat-

terns than other associated satellites in this dissertation. For the CHAMP/GRACE constellation, thirty orbital arcs were selected based on the repeating encounters of CHAMP satellite and the GRACE twin satellites every 2.7 days. The MODK module allowed different strategies for ambiguity fixing, namely no fixing at all, subset, and full integer ambiguity fixing. The DD carrier-phase integer ambiguities can be fixed first for the GRACE satellites and after this for the CHAMP/GRACE pairs.

Compared to the work described in (Van Barneveld, 2012), a few updates and improvements were proposed and implemented. The choice for centering orbit arcs around the point of closest approach (as also done for the Swarm constellation in Chapter 4) proved to result in improved CHAMP/GRACE baseline solutions. This also allowed to investigate the quality of baseline solutions as a function of distance between two satellites. In addition, a more strict observation carrier-phase outlier detection and observation was found to be very important for PBD. Moreover, CRV patterns eliminate much of the impact of cross-talk between the CHAMP GPS POD and radio occultation antennas. The consistency between GRACE kinematic and reduced-dynamic solutions is at a level of 8/3/2 mm (radial/along-track/cross-track). The ambiguity fixing success rate reaches a level of 93.7% and the KBR observations confirm a baseline precision at a level of 0.6 mm. The baseline consistency for the more rapidly varying CHAMP/GRACE baselines is at a level of 25/15/7 mm. This kinematic/reduced-dynamic consistency deteriorates when the baseline lengths increase from 2 to 24 hrs.

The Yarragadee SLR station in Australia also provided many passes where it switched tracking between the GRACE-A and -B satellites during their overflights. Also for GRACE, adopting a PBD approach leads to smaller or almost absent jumps in the time series of SLR residuals for those passes. An interesting result is that occasionally these jumps are reduced as well when CHAMP is used to compute dual-satellite PBD solutions with first the GRACE-A satellite and second the GRACE-B satellite. However, in general including the CHAMP satellite in multiple-satellite PBD with GRACE does not lead to improved baseline solutions. Validation by comparison with SLR observations indicates that the orbit precision levels for the three satellites (GRACE-A, GRACE-B and CHAMP) is at the level of a few cm: the SLR residual RMS is equal to 17.2, 18.8 and 23.2 mm, respectively. When comparing with their single-satellite POD solutions, the CHAMP orbit precision is slightly improved by 0.3 mm, but no improvement is seen for the GRACE-B orbit, whilst the GRACE-A orbit precision deteriorated by 2.0 mm. However, significant improvements were achieved as compared to the initial work done by Van Barneveld (2012).

6.2. Recommendations

The research in this dissertation focused on improved and more robust absolute and relative orbit determination for satellite constellations. All research questions have been addressed and answers have been provided. However, the obtained results also show that further work can be done. The recommendations emanating from the research are outlined below.

1. **GPS data (pre)processing**

Tracking observations by GNSS, including GPS, are affected by many factors. On their way from the transmitter to the receiver antenna, GNSS signals are affected by the ionosphere and for ground based receivers also the troposphere. In addition, observations can be affected by multipath and cross-talk in case multiple antennas are switched on. For carrier-phase observations, the associated signals enter the receiver antenna at different locations, which can be taken into account by PCV maps. For code observations, multipath and cross-talk can be mitigated by the use of CRV maps.

One of the first issues addressed is GPS receiver antenna patterns. It was confirmed that PCV maps obtained from inflight data result in better POD and PBD solutions. In addition, the use of CRV maps proved to enhance POD and PBD results and in particular lead to a better initialization of DD carrier-phase ambiguity fixing. The implementation chosen for this research includes the estimation of frequency-dependent carrier-phase and code antenna maps for all 6 selected satellites. The conventional approach was to produce PCV maps for ionosphere-free carrier-phase observations, both for a single satellite and differentially for a pair of satellites (Allende-Alba and Montenbruck, 2016; Jäggi et al., 2009). It has to be noted that the frequency dependent maps derived in this research (Chapters 2 and 3) might be absorbing other effects than phase center variations or multipath. For some of the obtained maps, the map on the GPS L_1 frequency seems to be for a significant part of mirror image of the map on the GPS L_2 frequency. Nevertheless, these maps do improve the POD and PBD performance. An interesting point for further research is to find a way to ascertain that the maps really represent the frequency dependent phase center and/or code azimuth/elevation dependent observation deviations. It might be also an interesting topic to investigate antenna pattern recovery based on single-frequency POD process.

Results in this dissertation confirm that different GPS receivers, even when originating from the same BlackJack series, perform differently for different satellites (Montenbruck and Kroes, 2003). These different behaviors impact among others DD carrier-phase integer ambiguity fixing. Results in Chapters 4 and 5 show that the removal of only a small percentage of GPS outlying observations can already significantly improve the PBD performance. Thus, careful outlier detection is crucial for a successful PBD. An example is the successful modification of the *ionosphere-free combination phase editing threshold* introduced and discussed in Chapter 5. In addition, results in Chapters 3 and 4 confirm the significance of making use of the several Swarm GPS receiver and RINEX converter updates: the associated data were kindly provided by GSOC/DLR. An important correction concerned the elimination of half-cycle carrier-phase ambiguities and resolve them into full ones. A relatively recent development concerns the production of so-called single-receiver ambiguity fixed POD solutions (Bertiger et al., 2010; Montenbruck et al., 2018a). A very interesting idea for further research is to integrate this single-satellite ambiguity fixing in precise baseline determination for satellite formations and constella-

tions. One possibility might be to use the single-satellite ambiguity fixes to initialize DD carrier-phase integer ambiguities and still use the single-satellite ambiguities when no double difference carrier-phase observations can be formed or when the LAMBDA tests indicate the DD ambiguity can not be fixed with sufficient reliability.

The LEO missions used for this research have had long mission periods: 10 years for CHAMP, 15 years for GRACE, and Swarm has already flown successfully for 5 years (status November 2018) with many more years expected to come. During such extended mission periods, often several updates and modifications are implemented for various instruments, including the GPS receivers. It is recommended to properly document such updates and modifications, and publish PCV (and if so required CRV) maps for the user community, possibly as part of the IGS. As shown in this dissertation, such PCV and CRV maps are essential for fully exploiting the GPS tracking data for POD and PBD.

Data weighting is also an essential factor that determines the quality of POD and PBD solutions. Constants weights have been used for both the carrier-phase and code observations in the POD and PBD MODK implementations. The reason for this constant weighting was to facilitate DD carrier-phase ambiguity fixing in connection with limitations of the MODK software. Other weighting schemes that more reflect the real quality of GPS tracking observations, for example elevation dependent weighting or weights that depend on the Signal-to-Noise Ratio (SNR), might enhance the quality of POD and PBD solutions. An interesting prospect is the development of multi-GNSS space-borne receivers, where the noise levels of carrier-phase and code observations might/will be different for the different contributing global navigation satellite systems.

2. **Ambiguity fixing and checking**

An existing challenge for PBD is integer ambiguity fixing and checking, especially for long and rapidly changing baselines. Correct DD carrier-phase ambiguity fixing is a prerequisite for achieving a sub-mm level baseline precision for e.g. the GRACE, which flies in a stable formation with slowly changing baseline. For more rapidly varying baselines, mm-level precision is hard to achieve. The research described in this dissertation has shown that is not straightforward to properly fix ambiguities with the LAMBDA method. Several tests are used for determining if a certain ambiguity is properly fixed. Such tests depend on observation weighting, the set of estimated parameters, and constraints for and between these parameters (e.g. constraints for limiting the differences between the GRACE-A and GRACE-B empirical accelerations). An interesting point for further research is the inclusion of space-borne accelerometer observations (if available, such as for CHAMP and GRACE) in the POD and PBD (see e.g. Van Helleputte and Visser (2008)). This will reduce the need for estimating empirical accelerations and/or allow heavier constraints, leading to different properties of the covariance matrix used by the LAMBDA method. It needs to be investigated if this will result in a more robust and

reliable ambiguity fixing and in conjunction more precise PBD solutions.

The current MODK implementation (status November 2018) relies on the LAMBDA method for ambiguity fixing. It is recommended to investigate if the LAMBDA-based ambiguity fixing can be enhanced, (partly) replaced and/or combined with other ambiguity fixing methods (wide-line/narrow-lane, bootstrapping, etc.). Especially when space-borne multi-GNSS receivers are going to be used, with different weights for observations from different GNSS, different ambiguity fixing schemes might become essential.

Checking if ambiguities are properly fixed is a challenging issue. For the LAMBDA method, this checking relies for a large part on the characteristic of the parameter estimation method (covariance matrix). Odijk and Teunissen (2008) refer to a promising method where the so-called Ambiguity Dilution Of Positioning (ADOP) is used for terrestrial applications. This is a scalar measure that can be used to infer the strength of the GNSS model for ambiguity resolution, and it can be applied to estimate the contribution of various GNSS model factors. Therefore, it might be very interesting to assess if a similar approach can be adopted for satellite POD and PBD.

3. **Multi-GNSS receivers**

In the above, a number of recommendations related to the possible future development of space-borne multi-GNSS receivers has already been formulated. Four Global Navigation Satellite Systems are available today (status November 2018), including the US GPS, Russian GLONASS, Chinese BeiDou, and the European Galileo systems. Multi-GNSS receivers, if equipped with a sufficient number of channels, will result in larger numbers of GPS satellites tracked by the LEO receivers. Especially for longer baselines, this will significantly enhance the geometry for PBD. It is recommended to further investigate the possible benefits of such receivers for PBD of satellite formations and constellations. Interesting aspects can be investigated concerning the acquisition of tracking observations on more than two frequencies, observation weighting for the different GNSS, enhanced ionospheric modeling.

4. **POD and PBD for other satellite constellations**

For the research described in this dissertation, POD and PBD was limited to formations and constellations consisting of two or three satellites. The MODK software tool is in principle designed and structured such that POD and PBD for larger formations and constellations is possible. In theory, this number can be infinite, but it has not been assessed yet if MODK can indeed properly handle POD and PBD for constellations consisting of more than three satellites. An example of an interesting constellation that can be defined is the combination of Swarm and GRACE

Follow-On (altogether) 5 satellites. Considering the development of the Iridium-next constellation, that will consist of 66 LEO satellites, much larger constellations will be available for POD and PBD. In the future, a large number of small satellites equipped with relatively high-quality GNSS receivers might become available. Interesting GNSS receiver developments include NovAtel's OEM4-G2L, Septentrio's PolaRx2 and JAXA's Nec Toshiba Space Systems (Montenbruck et al., 2006). These receivers have already been flown onboard small satellites and have the potential for not only real time navigation, but also precise post-facto positioning. POD and PBD for constellations consisting of more LEO satellites requires the development of more efficient and robust methods. Possibly, a LEO disk can be defined for which a full network solution is to be produced.

Last but not least, a fundamental question is how existing and possible future scientific research and applications can be (better) supported by POD and PBD of formations and constellations of - possible massive numbers of - LEO satellites.

One application will be mentioned here and that concerns the observation of Earth's time variable gravity (Gunter et al., 2011), which could also be a big impact on orbit determination (Schrama, 2018). The GRACE mission has shown the great potential of observing this Earth's time variable gravity by precisely observing the baseline between two tandem LEO satellites at a distance of about 220 km. The baseline variations are observed directly by the KBR instrument with a precision at the μm-level. Tracking by GNSS allows a precision of just better than 1 mm, which is orders of magnitude above the KBR precision level. However, more complicated formations and constellations offer more viewing directions as compared to the 1-dimensional, along-track viewing direction offered by the KBR instrument (Sharifi et al., 2007). It is interesting to explore how well gravity can be observed if 3-dimensional PBD is possible for large numbers of LEO satellites with a wide variety in baseline lengths and variations.

References

Allende-Alba, G., Montenbruck, O., 2016. Robust and precise baseline determination of distributed spacecraft in LEO. Advances in Space Research 57, 46–63. doi:10.1016/j.asr.2015.09.034.

Allende-Alba, G., Montenbruck, O., Jäggi, A., Arnold, D., Zangerl, F., 2017. Reduced-dynamic and kinematic baseline determination for the Swarm mission. GPS Solutions 21, 1275–1284. doi:10.1007/s10291-017-0611-z.

Arnold, D., Montenbruck, O., Hackel, S., Sośnica, K., 2018. Satellite laser ranging to low Earth orbiters: orbit and network validation. Journal of Geodesy (2018). doi:10.1007/s00190-018-1140-4.

Bertiger, W., Bar-Sever, Y., Bettadpur, S., Dunn, C., Haines, B., Kruizinga, G., Kuang, D., Nandi, S., Romans, L., Watkins, M., et al., 2002. GRACE: millimeters and microns in orbit, in: ION-GPS 2002, Portland, OR, USA, Sept. 24-27.

Bertiger, W., Desai, S.D., Haines, B., Harvey, N., Moore, A.W., Owen, S., Weiss, J.P., 2010. Single receiver phase ambiguity resolution with GPS data. Journal of Geodesy 84, 327–337. doi:10.1007/s00190-010-0371-9.

Bettadpur, S., 2012. GRACE product specification document (CSR-GR-03-02, Rev 4.6). Technical Report. Center for Space Research, The University of Texas at Austin.

Bierman, G.J., 2006. Factorization methods for discrete sequential estimation. Courier Corporation, ISBN: 0486449815, 9780486449814.

Birmingham, W., Miller, B., Stein, W., 1983. Experimental results of using the gps for Landsat 4 onboard navigation. Navigation 30, 244–251. doi:10.1002/j.2161-4296.1983.tb00843.x.

Blewitt, G., 1989. Carrier phase ambiguity resolution for the Global Positioning System applied to geodetic baselines up to 2000 km. Journal of Geophysical Research: Solid Earth 94, 10187–10203. doi:10.1029/JB094iB08p10187.

Bock, H., Jäggi, A., Meyer, U., Dach, R., Beutler, G., 2011. Impact of GPS antenna phase center variations on precise orbits of the GOCE satellite. Advances in Space Research 47, 1885–1893. doi:10.1016/j.asr.2011.01.017.

Buchert, S., Zangerl, F., Sust, M., André, M., Eriksson, A., Wahlund, J.E., Opgenoorth, H., 2015. SWARM observations of equatorial electron densities and topside GPS track losses. Geophysical Research Letters 42, 2088–2092. doi:10.1002/2015GL063121.

Butler, D., et al., 2014. Earth observation enters next phase. Nature 508, 160–161.

Calabia, A., Jin, S., 2016. Assessment of conservative force models from GRACE accelerometers and precise orbit determination. Aerospace Science and Technology 49, 80–87. doi:10.1016/j.ast.2015.11.034.

Carpenter, J.R., Bishop, R.H., 1996. Flight data results of estimate fusion for spacecraft rendezvous navigation from shuttle mission STS-69. Technical Report. NAS 1.26:201484; NASA-CR-201484.

Case, K., Kruizinga, G., Wu, S., 2002. GRACE level 1B data product user handbook. JPL Publication D-22027 .

Cerri, L., Berthias, J., Bertiger, W., Haines, B., Lemoine, F., Mercier, F., Ries, J., Willis, P., Zelensky, N., Ziebart, M., 2010. Precision orbit determination standards for the Jason series of altimeter missions. Marine Geodesy 33, 379–418. doi:10.1016/j.asr.2010.05.007.

Dach, R., Brockmann, E., Schaer, S., Beutler, G., Meindl, M., Prange, L., Bock, H., Jäggi, A., Ostini, L., 2009. GNSS processing at CODE: status report. Journal of Geodesy 83, 353–365. doi:10.1007/s00190-008-0281-2.

Dach, R., Schaer, S., Arnold, D., Orliac, E., Prange, L., Susnik, A., Villiger, A., Jäggi, A., 2016. CODE final product series for the IGS. Technical Report. Astronomical Institute, University of Bern. doi:10.7892/boris.75876.

Dach, R., Schaer, S., Arnold, D., Prange, L., Sidorov, D., Stebler, P., Villiger, A., Jäggi, A., 2018. CODE final product series for the IGS. Technical Report. Astronomical Institute, University of Bern. doi:10.7892/boris.75876.3.

Dach, R., Schaer, S., Lutz, S., Meindl, M., Bock, H., Orliac, E., Prange, L., Thaller, D., Mervart, L., Jäggi, A., et al., 2015. Center for Orbit Determination In Europe: IGS Technical Report 2014. Technical Report. Astronomical Institute, University of Bern.

Dahle, C., Arnold, D., Jäggi, A., 2017. Impact of tracking loop settings of the Swarm GPS receiver on gravity field recovery. Advances in Space Research 59, 2843–2854. doi:10.1016/j.asr.2017.03.003.

D'Amico, S., Ardaens, J.S., De Florio, S., 2013. Autonomous formation flying based on GPS — PRISMA flight results. Acta Astronautica 82, 69–79. doi:10.1016/j.actaastro.2012.04.033.

Degnan, J.J., 1993. Millimeter accuracy satellite laser ranging: a review, in: Contributions of space geodesy to geodynamics: technology. Wiley Online Library, pp. 133–162. doi:10.1029/GD025p0133.

Doornbos, E., 2012. Thermospheric density and wind determination from satellite dynamics. Ph.D. thesis. Delft University of Technology, ISBN: 978-3-642-44264-3.

Dow, J.M., Neilan, R.E., Rizos, C., 2009. The international GNSS service in a changing landscape of global navigation satellite systems. Journal of Geodesy 83, 191–198. doi:10.1007/s00190-008-0300-3.

Drinkwater, M.R., Haagmans, R., Muzi, D., Popescu, A., Floberghagen, R., Kern, M., Fehringer, M., 2006. The GOCE gravity mission: ESA's first core Earth explorer, in: Proceedings of the 3rd international GOCE user workshop, European Space Agency, Noordwijk, The Netherlands. pp. 6–8.

Elsaka, B., Raimondo, J.C., Brieden, P., Reubelt, T., Kusche, J., Flechtner, F., Pour, S.I., Sneeuw, N., Müller, J., 2014. Comparing seven candidate mission configurations for temporal gravity field retrieval through full-scale numerical simulation. Journal of Geodesy 88, 31–43. doi:10.1007/s00190-013-0665-9.

European Space Research and Technology Centre, 2017. Swarm Spacecraft Anomalies And Manoeuvers History (till 31 May 2017, PE-RP-ESA-PLSO-0591). Technical Report. European Space Agency.

Flechtner, F., Morton, P., Watkins, M., Webb, F., 2014. Status of the GRACE follow-on mission, in: Gravity, geoid and height systems. Springer, ISBN: 978-3-319-10836-0, pp. 117–121.

Friis-Christensen, E., Lühr, H., Hulot, G., 2006. Swarm: A constellation to study the Earth's magnetic field. Earth Planets Space 58, 351–358. doi:10.1186/BF03351933.

Friis-Christensen, E., Lühr, H., Knudsen, D., Haagmans, R., 2008. Swarm–an Earth observation mission investigating geospace. Advances in Space Research 41, 210–216. doi:10.1016/j.asr.2006.10.008.

Garcia, M., Montenbruck, O., 2007. TerraSAR-X/TanDEM-X GPS antenna phase center analysis and results. Technical Report. German Space Operations Center.

Goodman, J.L., 2006. History of space shuttle rendezvous and proximity operations. Journal of Spacecraft and Rockets 43, 944–959. doi:10.2514/1.19653.

Gu, D., Ju, B., Liu, J., Tu, J., 2017. Enhanced GPS-based GRACE baseline determination by using a new strategy for ambiguity resolution and relative phase center variation corrections. Acta Astronautica 138, 176–184. doi:10.1016/j.actaastro.2017.05.022.

Gunter, B., Encamagao, J., Ditmar, P., Klees, R., Van Barneveld, P., Visser, P., 2011. Deriving global time-variable gravity from precise orbits of the iridium next constellation. Advances in the Astronautical Sciences 142.

Gurtner, W., Estey, L., 2013. RINEX - The Receiver Independent Exchange Format (Version 3.02). Technical Report. International GNSS Service (IGS), RINEX Working Group and Radio Technical Commission for Maritime Services Special Committee 104 (RTCM-SC104).

Hackel, S., Montenbruck, O., Steigenberger, P., Balss, U., Gisinger, C., Eineder, M., 2017. Model improvements and validation of TerraSAR-X precise orbit determination. Journal of Geodesy 91, 547–562. doi:10.1007/s00190-016-0982-x.

Haines, B., Bar-Sever, Y., Bertiger, W., Desai, S., Willis, P., 2004. One-centimeter orbit determination for Jason-1: new GPS-based strategies. Marine Geodesy 27, 299–318. doi:10.1080/01490410490465300.

Hajj, G.A., Romans, L.J., 1998. Ionospheric electron density profiles obtained with the Global Positioning System: Results from the GPS/MET experiment. Radio Science 33, 175–190.

Ho, S.p., Hunt, D., Steiner, A.K., Mannucci, A.J., Kirchengast, G., Gleisner, H., Heise, S., Engeln, A., Marquardt, C., Sokolovskiy, S., et al., 2012. Reproducibility of GPS radio occultation data for climate monitoring: Profile-to-profile inter-comparison of CHAMP climate records 2002 to 2008 from six data centers. Journal of Geophysical Research: Atmospheres 117. doi:10.1029/2012JD017665.

Van den IJssel, J., Encarnação, J., Doornbos, E., Visser, P., 2015. Precise science orbits for the Swarm satellite constellation. Advances in Space Research 56, 1042–1055. doi:10.1016/j.asr.2015.06.002.

Van den IJssel, J., Forte, B., Montenbruck, O., 2016. Impact of Swarm GPS receiver updates on POD performance. Earth Planets Space 68, 1–17. doi:10.1186/s40623-016-0459-4.

Van den IJssel, J., Visser, P., Rodriguez, E.P., 2003. CHAMP precise orbit determination using GPS data. Advances in Space Research 31, 1889–1895. doi:10.1016/S0273-1177(03)00161-3.

Jacchia, L., 1972. Atmospheric models in the region from 110 to 2000 km. Caspar International Reference Atmosphere (CIRA) 1972 , 227–340.

Jacchia, L.G., 1977. Thermospheric temperature, density, and composition: new models. SAO special report 375.

Jäggi, A., 2007. Pseudo-stochastic orbit modelling of low Earth satellites using the Global Positioning System. volume 73. Schweizerische Geodätische Kommission/Swiss Geodetic Commission.

Jäggi, A., Dach, R., Montenbruck, O., Hugentobler, U., Bock, H., Beutler, G., 2009. Phase center modeling for LEO GPS receiver antennas and its impact on precise orbit determination. Journal of Geodesy 83, 1145–1162. doi:10.1007/s00190-009-0333-2.

Jäggi, A., Dahle, C., Arnold, D., Bock, H., Meyer, U., Beutler, G., Van den IJssel, J., 2016. Swarm kinematic orbits and gravity fields from 18 months of GPS data. Advances in Space Research 57, 218–233. doi:10.1016/j.asr.2015.10.035.

Jäggi, A., Hugentobler, U., Bock, H., Beutler, G., 2007. Precise orbit determination for GRACE using undifferenced or doubly differenced GPS data. Advances in Space Research 39, 1612–1619. doi:10.1016/j.asr.2007.03.012.

Kang, Z., Nagel, P., Pastor, R., 2003. Precise orbit determination for GRACE. Advances in Space Research 31, 1875–1881. doi:10.1016/S0273-1177(03)00159-5.

Kang, Z., Tapley, B., Bettadpur, S., Ries, J., Nagel, P., Pastor, R., 2006. Precise orbit determination for the GRACE mission using only GPS data. Journal of Geodesy 80, 322–331. doi:10.1007/s00190-006-0073-5.

Kaplan, E., Hegarty, C., 2005. Understanding GPS: principles and applications. Artech house, ISBN 10: 1580538940 ISBN 13: 9781580538947.

Krieger, G., Moreira, A., Fiedler, H., Hajnsek, I., Werner, M., Younis, M., Zink, M., 2007. TanDEM-X: A satellite formation for high-resolution SAR interferometry. IEEE Transactions on Geoscience and Remote Sensing 45, 3317–3341. doi:10.1109/TGRS.2007.900693.

Krieger, G., Zink, M., Bachmann, M., Bräutigam, B., Schulze, D., Martone, M., Rizzoli, P., Steinbrecher, U., Antony, J.W., De Zan, F., et al., 2013. TanDEM-X: A radar interferometer with two formation-flying satellites. Acta Astronautica 89, 83–98. doi:10.1016/j.actaastro.2013.03.008.

Kroes, R., 2006. Precise relative positioning of formation flying spacecraft using GPS. Ph.D. thesis. Delft University of Technology, ISBN: 90-8559-150-3,.

Kroes, R., Montenbruck, O., Bertiger, W., Visser, P., 2005. Precise GRACE baseline determination using GPS. GPS Solutions 9, 21–31. doi:10.1007/s10291-004-0123-5.

Kuang, D., Bar-Sever, Y., Bertiger, W., Desai, S., Haines, B., Iijima, B., Kruizinga, G., Meehan, T., Romans, L., 2001. Precise orbit determination for CHAMP using gps data from BlackJack receiver, in: ION National Technical Meeting 2001, Long Beach, CA, USA.

Loiselet, M., Stricker, N., Menard, Y., Luntama, J., 2000. GRAS-Metop's GPS-based atmospheric sounder. ESA bulletin 102, 38–44.

Loyer, S., Perosanz, F., Mercier, F., Capdeville, H., Marty, J.C., 2012. Zero-difference GPS ambiguity resolution at CNES-CLS IGS analysis center. Journal of Geodesy 86, 991. doi:10.1007/s00190-012-0559-2.

Lyard, F., Lefevre, F., Letellier, T., Francis, O., 2006. Modelling the global ocean tides: modern insights from FES2004. Ocean Dynam. 56, 394–415. doi:10.1007/s10236-006-0086-x.

Mao, X., Visser, P., Van den IJssel, J., 2017. Impact of GPS antenna phase center and code residual variation maps on orbit and baseline determination of GRACE. Advances in Space Research 59, 2987–3002. doi:10.1016/j.asr.2017.03.019.

Mao, X., Visser, P., Van den IJssel, J., 2018. The impact of GPS receiver modifications and ionospheric activity on Swarm baseline determination. Acta Astronautica 146, 399–408. doi:10.1016/j.actaastro.2018.03.009.

Mao, X., Visser, P., Van den IJssel, J., 2019a. Absolute and relative orbit determination for the CHAMP/GRACE constellation. Advances in Space Research 63, 3796–3816. doi:10.1016/j.asr.2019.02.030.

Mao, X., Visser, P., van den IJssel, J., 2019b. High-dynamic baseline determination for the Swarm constellation. Aerospace Science and Technology 88, 329–339. doi:10.1016/j.ast.2019.03.031.

March, G., Doornbos, E., Visser, P., 2018. High-fidelity geometry models for improving the consistency of CHAMP, GRACE, GOCE and Swarm thermospheric density data sets. Advances in Space Research 63, 213–238. doi:10.1016/j.asr.2018.07.009.

Marradi, L., Banfi, E., Mambretti, A., 2001. The Lagrange receiver: design and in-flight demonstration. Proceedings of NAVITECH , 10–12.

Mayer-Gürr, T., Rieser, D., Höck, E., Schuh, W.D., Krasbutter, I., Kusche, J., Maier, A., Krauss, S., Hausleitner, W., Baur, O., et al., 2012. The new combined satellite only model GOCO03s, in: presented at International Symposium on Gravity, Geoid and Height Systems GGHS 2012, Venice, Italy, last-accessed: Dec-2018. URL: https://www.bgu.tum.de/iapg/forschung/schwerefeld/goco/.

McCarthy, D.D., Petit, G., 2004. IERS conventions (2003). Technical Report. International Earth Rotation And Reference Systems Service (IERS) (Germany), 2004.

McDonald, K.D., 2002. The modernization of GPS: plans, new capabilities and the future relationship to Galileo. Journal of Global Positioning Systems 1.

Montenbruck, O., Garcia-Fernandez, M., Williams, J., 2006. Performance comparison of semicodeless GPS receivers for LEO satellites. GPS Solutions 10, 249–261. doi:101007/s10291-006-0025-9.

Montenbruck, O., Garcia-Fernandez, M., Yoon, Y., Schön, S., Jäggi, A., 2009. Antenna phase center calibration for precise positioning of LEO satellites. GPS Solutions 13, 23–34. doi:10.1007/s10291-008-0094-z.

Montenbruck, O., Gill, E., 2012. Satellite orbits: models, methods and applications. Springer Science & Business Media, ISBN10: 3642583512, ISBN13: 9783642583513.

Montenbruck, O., Hackel, S., van den IJssel, J., Arnold, D., 2018a. Reduced dynamic and kinematic precise orbit determination for the Swarm mission from 4 years of GPS tracking. GPS Solutions 22. doi:10.1007/s10291-018-0746-6.

Montenbruck, O., Hackel, S., Jäggi, A., 2018b. Precise orbit determination of the Sentinel-3A altimetry satellite using ambiguity-fixed GPS carrier phase observations. Journal of Geodesy 92, 711–726. doi:10.1007/s00190-017-1090-2.

Montenbruck, O., Kroes, R., 2003. In-flight performance analysis of the CHAMP BlackJack GPS Receiver. GPS Solutions 7, 74–86. doi:10.1007/s10291-003-0055-5.

Montenbruck, O., Schmid, R., Mercier, F., Steigenberger, P., Noll, C., Fatkulin, R., Kogure, S., Ganeshan, A.S., 2015. GNSS satellite geometry and attitude models. Advances in Space Research 56, 1015–1029. doi:10.1016/j.asr.2015.06.019.

Montenbruck, O., Van Helleputte, T., Kroes, R., Gill, E., 2005. Reduced dynamic orbit determination using GPS code and carrier measurements. Aerospace Science and Technology 9, 261–271. doi:10.1016/j.ast.2005.01.003.

Montenbruck, O., Wermuth, M., Kahle, R., 2011. GPS based relative navigation for the TanDEM-X mission-first flight results. Navigation 58, 293–304. doi:10.1002/j.2161-4296.2011.tb02587.x.

Moreira, A., Krieger, G., Hajnsek, I., Hounam, D., Werner, M., Riegger, S., Settelmeyer, E., 2004. TanDEM-X: a TerraSAR-X add-on satellite for single-pass SAR interferometry, in: Geoscience and Remote Sensing Symposium, 2004. IGARSS'04. Proceedings. 2004 IEEE International, IEEE. pp. 1000–1003.

Neubert, R., Grunwaldt, L., Neubert, J., 1998. The retro-reflector for the CHAMP satellite: Final design and realization, in: Proceedings of the 11th International Workshop on Laser Ranging, pp. 260–270. URL: http://ilrs.gsfc.nasa.gov/docs/rra_champ.pdf.

Noll, C.E., 2010. The crustal dynamics data information system: A resource to support scientific analysis using space geodesy. Advances in Space Research 45, 1421–1440. doi:10.1016/j.asr.2010.01.018.

Odijk, D., Teunissen, P., 2008. ADOP in closed form for a hierarchy of multi-frequency single-baseline GNSS models. Journal of Geodesy 82, 473. doi:10.1007/s00190-007-0197-2.

Olsen, N., Haagmans, R., Sabaka, T.J., Kuvshinov, A., Maus, S., Purucker, M.E., Rother, M., Lesur, V., Mandea, M., 2006. The Swarm End-to-End mission simulator study: A demonstration of separating the various contributions to Earth's magnetic field using synthetic data. Earth Planets Space 58, 359–370. doi:10.1186/BF03351934.

Pearlman, M.R., Degnan, J.J., Bosworth, J., 2002. The international laser ranging service. Advances in Space Research 30, 135–143. doi:10.1016/S0273-1177(02)00277-6.

Persson, S., Veldman, S., Bodin, P., 2009. PRISMA-a formation flying project in implementation phase. Acta Astronautica 65, 1360–1374. doi:10.1016/j.actaastro.2009.03.067.

Peter, H., Jäggi, A., Fernández, J., Escobar, D., Ayuga, F., Arnold, D., Wermuth, M., Hackel, S., Otten, M., Simons, W., et al., 2017. Sentinel-1a–first precise orbit determination results. Advances in Space Research 60, 879–892. doi:10.1016/j.asr.2017.05.034.

Pinard, D., Reynaud, S., Delpy, P., Strandmoe, S.E., 2007. Accurate and autonomous navigation for the ATV. Aerospace Science and Technology 11, 490–498. doi:10.1016/j.ast.2007.02.009.

Prange, L., Orliac, E., Dach, R., Arnold, D., Beutler, G., Schaer, S., Jäggi, A., 2017. CODÉs five-system orbit and clock solution—the challenges of multi-GNSS data analysis. Journal of Geodesy 91, 345–360. doi:10.1007/s00190-016-0968-8.

Reigber, C., Balmino, G., Schwintzer, P., Biancale, R., Bode, A., Lemoine, J.M., König, R., Loyer, S., Neumayer, H., Marty, J.C., et al., 2002a. A high-quality global gravity field model from CHAMP GPS tracking data and accelerometry (EIGEN-1S). Geophysical Research Letters 29, 37–1. doi:10.1029/2002GL015064.

Reigber, C., Lühr, H., Schwintzer, P., 2002b. CHAMP mission status. Advances in Space Research 30, 129–134. doi:10.1016/S0273-1177(02)00276-4.

Roselló, J., Silvestrin, P., Risueño, G.L., Weigand, R., Perelló, J., Heim, J., Tejerina, I., 2010. AGGA-4: Core device for GNSS space receivers of this decade, in: Satellite Navigation Technologies and European Workshop on GNSS Signals and Signal Processing (NAVITEC), 2010 5th ESA Workshop on, IEEE. pp. 1–8.

Rothacher, M., 2001. Comparison of absolute and relative antenna phase center variations. GPS Solutions 4, 55–60. doi:10.1007/PL00012867.

Rothacher, M., Schmid, R., 2006. ANTEX: The antenna exchange format version 1.3. Technical Report. IGS Central Bureau.

Sabol, C., Burns, R., McLaughlin, C.A., 2001. Satellite formation flying design and evolution. Journal of spacecraft and rockets 38, 270–278. doi:10.2514/2.3681.

Schaer, S., 1999. Mapping and predicting the Earth's ionosphere using the Global Positioning System. volume 59. Société helvétique des sciences naturelles. Commission géodésique, Institut für Geodäsie und Photogrammetrie, Eidg. Technische Hochschule Zürich.

Schmid, R., Dach, R., Collilieux, X., Jäggi, A., Schmitz, M., Dilssner, F., 2016. Absolute IGS antenna phase center model igs08.atx: status and potential improvements. Journal of Geodesy 90, 343–364. doi:10.1007/s00190-015-0876-3.

Schmid, R., Rothacher, M., 2003. Estimation of elevation-dependent satellite antenna phase center variations of GPS satellites. Journal of Geodesy 77, 440–446. doi:10.1007/s00190-003-0339-0.

Schrama, E., 2018. Precision orbit determination performance for CryoSat-2. Advances in Space Research 61, 235–247. doi:10.1016/j.asr.2017.11.001.

Schutz, B., Tapley, B., Abusali, P., Rim, H., 1994. Dynamic orbit determination using GPS measurements from TOPEX/POSEIDON. Geophysical Research Letters 21, 2179–2182. doi:10.1029/94GL01040.

Schutz, B., Tapley, B., Born, G.H., 2004. Statistical orbit determination. Elsevier, ISBN:0-12-683630-2.

Sharifi, M., Sneeuw, N., Keller, W., 2007. Gravity recovery capability of four generic satellite formations, in: Proc. Symp. Gravity Field of the Earth, General Command of Mapping, pp. 211–216.

Sheard, B., Heinzel, G., Danzmann, K., Shaddock, D., Klipstein, W., Folkner, W., 2012. Intersatellite laser ranging instrument for the GRACE follow-on mission. Journal of Geodesy 86, 1083–1095. doi:10.1007/s00190-012-0566-3.

Tancredi, U., Allende-Alba, G., Renga, A., Montenbruck, O., Grassi, M., 2015. Relative positioning of spacecraft in intense ionospheric conditions by GPS. Aerospace Science and Technology 43, 191–198. doi:10.1016/j.ast.2015.02.020.

Tancredi, U., Renga, A., Grassi, M., 2013. Validation on flight data of a closed-loop approach for GPS-based relative navigation of LEO satellites. Acta Astronautica 86, 126–135. doi:10.1016/j.actaastro.2013.01.005.

Tapley, B.D., Bettadpur, S., Ries, J.C., Thompson, P.F., Watkins, M.M., 2004a. GRACE measurements of mass variability in the Earth system. Science 305, 503–505. doi:10.1126/science.1099192.

Tapley, B.D., Bettadpur, S., Watkins, M., Reigber, C., 2004b. The gravity recovery and climate experiment: Mission overview and early results. Geophysical Research Letters 31, L0960. doi:10.1029/2004GL019920.

Tapley, B.D., Ries, J., Davis, G., Eanes, R., Schutz, B., Shum, C., Watkins, M., Marshall, J., Nerem, R., Putney, B., et al., 1994. Precision orbit determination for TOPEX/POSEIDON. Journal of Geophysical Research: Oceans 99, 24383–24404. doi:10.1029/94JC01645.

Teunissen, P.J., 1999. An optimality property of the integer least-squares estimator. Journal of Geodesy 73, 587–593. doi:10.1007/s001900050269.

Teunissen, P.J.G., 1995. The least-squares ambiguity decorrelation adjustment: a method for fast GPS integer ambiguity estimation. Journal of Geodesy 70, 65–82. doi:10.1007/BF00863419.

Torres, R., Snoeij, P., Geudtner, D., Bibby, D., Davidson, M., Attema, E., Potin, P., Rommen, B., Floury, N., Brown, M., et al., 2012. GMES Sentinel-1 mission. Remote Sensing of Environment 120, 9–24. doi:10.1016/j.rse.2011.05.028.

Van Barneveld, P.W.L., 2012. Orbit determination of satellite formations. Ph.D. thesis. Delft University of Technology, ISBN: 9778-94-6191-546-7.

Van Helleputte, T., Visser, P., 2008. GPS based orbit determination using accelerometer data. Aerospace Science and Technology 12, 478–484. doi:10.1016/j.ast.2007.11.002.

Verhagen, S., 2005. The GNSS integer ambiguities: estimation and validation. Ph.D. thesis. Delft University of Technology, ISBN: 90-804147-4-3.

Vetter, J.R., 2007. Fifty years of orbit determination. Johns Hopkins APL technical digest 27, 239.

Visser, P.N.A.M., Van den IJssel, J., Van Helleputte, T., Bock, H., Jäggi, A., Beutler, G., Švehla, D., Hugentobler, U., Heinze, M., 2009. Orbit determination for the GOCE satellite. Advances in Space Research 43, 760–768. doi:10.1016/j.asr.2008.09.016.

Visser, P.N.A.M., Rummel, R., Balmino, G., Sünkel, H., Johannessen, J., Aguirre, M., Woodworth, P., Le Provost, C., Tscherning, G., Sabadini, R., 2002. The European Earth explorer mission GOCE: impact for the geosciences. Geodynamics Series 29, 95–107. doi:10.1002/9781118670101.ch6.

Visser, P.N.A.M., Van den IJssel, J., 2003. Aiming at a 1-cm Orbit for Low Earth Orbiters: Reduced-Dynamic and Kinematic Precise Orbit Determination. Space science reviews 108, 27–36. doi:10.1023/A:1026253328154.

Wermuth, M., Montenbruck, O., Van Helleputte, T., 2010. GPS high precision orbit determination software tools (GHOST), in: Proceedings of 4th International Conference on Astrodynamics Tools and Techniques, Madrid, ESA WPP-308, pp. 3–6.

Wickert, J., Beyerle, G., König, R., Heise, S., Grunwaldt, L., Michalak, G., Reigber, C., Schmidt, T., 2005. GPS radio occultation with CHAMP and GRACE: A first look at a new and promising satellite configuration for global atmospheric sounding 23, 653–658.

Willis, P., Fagard, H., Ferrage, P., Lemoine, F.G., Noll, C.E., Noomen, R., Otten, M., Ries, J.C., Rothacher, M., Soudarin, L., et al., 2010. The international DORIS service (IDS): toward maturity. Advances in Space Research 45, 1408–1420. doi:10.1016/j.asr.2009.11.018.

Witkowski, M., Massmann, F., 2014. Status GRACE Mission Operations, in: Proceedings of the GSTM (GRACE Science Team Meeting), Potsdam, Germany, Sept. 29-Oct. 2.

Wu, S.C., Yunck, T.P., Thornton, C.L., 1991. Reduced-dynamic technique for precise orbit determination of low Earth satellites. Journal of Guidance, Control, and Dynamics 14, 24–30. doi:10.2514/3.20600.

Xiong, C., Stolle, C., Lühr, H., 2016. The Swarm satellite loss of GPS signal and its relation to ionospheric plasma irregularities. Space Weather 14, 563–577. doi:10.1002/2016SW001439.

Yunck, T., Bertiger, W., Wu, S., Bar-Sever, Y., Christensen, E., Haines, B., Lichten, S., Muellerschoen, R., Vigue, Y., Willis, P., 1994. First assessment of GPS-based reduced dynamic orbit determination on TOPEX/Poseidon. Geophysical Research Letters 21, 541–544. doi:10.1029/94GL00010.

Yunck, T.P., 1996. Orbit determination. Progress in Astronautics and Aeronautics 164, 559–592. doi:10.2514/5.9781600866395.0559.0592.

Zangerl, F., Griesauer, F., Sust, M., Montenbruck, O., Buchert, S., Garcia, A., 2014. SWARM GPS precise orbit determination receiver initial in-orbit performance evaluation. Proceedings of the 27th International Technical Meeting of the Satellite Division of the Institute of Navigation (ION-GNSS+-2014), Tampa, Florida , 1459–1468.

Zehentner, N., Mayer-Gürr, T., 2016. Precise orbit determination based on raw GPS measurements. Journal of Geodesy 90, 275–286. doi:10.1007/s00190-015-0872-7.

Zin, A., Landenna, S., Conti, A., Marradi, L., Di Raimondo, M., 2007. ENEIDE: An experiment of a spaceborne, L1/L2 integrated GPS/WAAS/EGNOS receiver. Microgravity Science and Technology 19, 54–59. doi:10.1007/BF02919453.

List of Publications

Peer reviewed publications

4. **Xinyuan Mao**, Pieter Visser, Jose van den IJssel, *Absolute and relative orbit determination for the CHAMP/GRACE constellation*, Advances in Space Research, **63/12** (2019) 3796-3816, doi: 10.1016/j.asr.2019.02.030.

3. **Xinyuan Mao**, Pieter Visser, Jose van den IJssel, *High-dynamic baseline determination for the Swarm constellation*, Aerospace Science and Technology, **88** (2019), 329-339, doi: 10.1016/j.ast.2019.03.031.

2. **Xinyuan Mao**, Pieter Visser, Jose van den IJssel, *The impact of GPS receiver modifications and ionospheric activity on Swarm baseline determination*, Acta Astronautica, **146** (2018), 399-408, doi: 10.1016/j.actaastro.2018.03.009.

1. **Xinyuan Mao**, Pieter Visser, Jose van den IJssel, *Impact of GPS antenna phase center and code residual variation maps on orbit and baseline determination of GRACE*, Advances in Space Research, **59/12** (2017), 2987-3002, doi: 10.1016/j.asr.2017.03.019.

Conference contributions

8. **Xinyuan Mao**, Pieter Visser, Jose van den IJssel, *Absolute and Relative Orbit Determination for the CHAMP-GRACE Constellation*, COSPAR 2018 42nd ASSEMBLY, Pasadena, USA, July 14-22, 2018 (presentation).

7. Adrian Jäggi, Ulrich Meyer, Lucas Schreiter, Veerle Sterken, Christoph Dahle, Daniel Arnold, Joao de Teixeira da Encarncao, Pieter Visser, Jose van den IJssel, **Xinyuan Mao**, Elisabetta Iorfida, Ales Bezdek, Josef Sebera, Torsten Mayer-Gürr, Norbert Zehentner, C.k. Shum, Christina Lück, Roloef Rietbroek, Jürgen Kusche, *Assessment of individual and combined gravity field solutions from Swarm GPS data and mitigation of systematic errors*, 20th EGU general assembly, Vienna, Austria, April 4-13, 2018 (co-author abstract).

6. Joao de Teixeira da Encarncao, Pieter Visser, Eelco Doornbos, Jose van den IJssel, **Xinyuan Mao**, Elisabetta Iorfida, Daniel Arnold, Adrian Jäggi, Ulrich Meyer, Ales Bezdek, Josef Sebera, Jaroslav Klokocnik, Matthias Ellmer, Torsten Mayer-Gürr, Norbert Zehentner, Junyi Guo, Peter Luk, C.K. Shum, Yu Zhang, *Signal contents of combined monthly gravity field models derived from Swarm GPS data*, 20th EGU general assembly, Vienna, Austria, April 4-13, 2018 (co-author abstract).

5. Norbert Zehentner, Matthias Ellmer, Torsten Mayer-Gürr, Daniel Arnold, Ulrich Meyer, Adrian Jäggi, **Xinyuan Mao**, Jose van den IJssel, Eelco Doornboos, Pieter Visser, Elisabetta Iorfida, Ales Bezdek, Josef Sebera, Jaroslav Klokocnik, Junyi Guo, C.K. Shum, Joao de Teixeira da Encarncao, *Investigation of GNSS-derived baselines for gravity field recovery*, 20th EGU general assembly, Vienna, Austria, April 4-13, 2018 (co-author abstract).

4. **Xinyuan Mao**, Pieter Visser, Jose van den IJssel, *The impact of GPS receiver modifications and ionospheric activity on Swarm baseline determination*, Swarm 7th data quality workshop, Delft, Netherlands, October 24-27, 2017 (presentation).

3. **Xinyuan Mao**, Pieter Visser, Jose van den IJssel, *Impact of Swarm GPS receiver modifications on baseline determination*, Fourth Swarm science meeting, Banff, Canada, March 20-24, 2017 (poster).

2. **Xinyuan Mao**, Pieter Visser, Jose van den IJssel, Eelco Doornbos, *Swarm absolute and relative orbit determination*, ESA living planet symposium, Prague, Czech Republic, May 9-13, 2016 (poster).

1. **Xinyuan Mao**, Pieter Visser, Jose van den IJssel, *The application of in-flight antenna pattern corrections to GPS-based baseline determination for formation flying GRACE*, International workshop on satellite constellations and formation flying, Delft, Netherlands, June 8-10, 2015 (presentation).

Curriculum Vitæ

Xinyuan MAO

1989 Born in Zhumadian, China.

Education

2006–2010 Beijing Institute of Technology, Beijing, China
Undergraduate in Engineering
Aeronautical & Astronautical Science & Technology

2010–2010 Samara State Aerospace University, Samara, Russia
Visiting student
Aerospace Science and Technology

2010–2013 Beijing Institute of Technology, Beijing, China
M.Sc. in Engineering
Aeronautical & Astronautical Science & Technology

2013-2018 Delft University of Technology, Delft, The Netherlands
Ph.D.
Astrodynamics and Space Missions
Dissertation: Absolute and relative orbit determination for satellite constellations
Promotor: Prof. dr. ir. P.N.A.M. Visser
Copromotor: Dr. ir. J.A.A. van den IJssel